Study on Hydraulic Characteristics of Debris Flow Breakers and Sabo Dams with a Flap

A dissertation submitted in partial fulfillment for the requirement

Doctoral Degree in Civil and Earth Resources Engineering

by

Yeonjoong KIM

Supervised by Prof. Hajime NAKAGAWA

Disaster Prevention Research Institute

River Disaster Prevention Systems Laboratory

Department of Civil and Earth Resources Engineering

Kyoto University

Japan

September 2013

Abstract

Sediment-related disasters caused by localized torrential downpours, earthquakes, volcanic eruptions, etc. occur frequently every year, and they account for nearly half of the total human casualties from natural disasters. A sediment-related disaster is not as large as an earthquake, flood, storm surge or tsunami, but its threat to human lives is very high because it can occur at multiple locations simultaneously. The occurrence of sediment-related disasters, such as debris flows, landslides, and slope failures have been increasing every year due to the various impacts of surface water flows. These flows are caused by glacier melting and heavy rainfall due to the changing global climate and environment (i.e. global warming), as well as urbanization (paving a road with asphalt), rapid forest development in mountainous areas (deforestation), increasing population density, and so on. Furthermore, these disasters frequently lead to the large-scale destruction of infrastructures or individual properties and cause psychological harm or human death (or physical harm). However, we are dealing with natural disasters, and humans cannot always control natural disasters. Therefore, it is important to mitigate damage by establishing effective structural and non-structural measures.

Sabo dams (structural measures) are one of the effective structural countermeasures for debris flow control. In recent years, many researchers have been carrying out experiments regarding the efficient function of sabo dams, which have a great impact on the ecology and landscape. Such dams are also surcharged with the impulsive forces of the debris flow, as the typical feature of the longitudinal section of a debris flow shows that the front part of the flow is very important and complex where there is an accumulation of large boulders. It is important to control or dampen the energy of the front part of a debris flow for the safety of the downstream area because the destructive power of a debris flow is much greater than that of the clear fluid. Therefore, in order to reduce the sediment-related disaster caused by debris flows, it is necessary to investigate the mechanism of debris flows regarding various sabo dams.

This dissertation aims to characterize the type of permeable dam regarding the change in pore water pressure and flow patterns by debris-flow breaker, identifying the underlying processes and mechanisms, and developing numerical models to simulate the dynamic feedback process. In addition, a new, closed-type, impermeable sabo dam with a flap is proposed and identifies the underlying processes and mechanisms to reduce the coarser particle of debris flows through the experimental study. Under these objectives, this research concentrates on the flow pattern, travel length of debris, impact force and deposition process due to the various

shapes of a sabo dam.

The main function of a debris-flow breaker is effectively stopping a debris flow front part. These structures have an advantage not only to dampen the energy of the frontal part of a debris flow, but also to create a suitable narrow or wider area that is cost-efficient, simply designed, and easily repaired and maintained. However, the mechanism of the debris-flow breaker has not been explained clearly yet by the researchers. Therefore, in this study, to clarify the mechanism of these structures, fundamental experiment and numerical simulation are conducted to investigate the characteristics of the breaker. The experiments were carried out in the fixed bed condition, in which the debris flow depositions (due to the change in pore water pressure at the debris-flow breaker) were analyzed. A numerical simulation for debris-flow breaker was developed and analyzed the mechanism and interaction between the opening and blocking areas of breaker. The simulated results of the travel length and the deposit thickness are in good agreement with the experimental results. In addition, the ranges of the debris-flow breaker parameters such as opening and blocking sizes for the design of structural elements of debris-flow breaker are evaluated.

The objectives of this study are to analyze the function of the proposed closed-type dam with flap, then to compare the vertical pressure distribution with other types of available dams, and finally, to determine the empirical coefficients of the hydrodynamic and solid collision model. Laboratory experiments were conducted to analyze the improved functions of the proposed dam. In the experiments, the total pressure associated with major debris flows was recorded in real time by a system consisting of four dynamic pressure sensors installed on different types of dams. The results from experimental data clearly show that the closed-flap dam has advantages of capturing the front of debris flow with large boulders and effectively controlling the total pressure due to reflection compared to a closed-type dam without a flap. Furthermore, the empirical coefficients of hydrodynamic and solid collision models were proposed and compared with available coefficients.

Keywords*: debris flow, structural measure, debris-flow breaker, flap structure*

Acknowledgements

I would never have been able to finish my dissertation without the guidance of my committee members, help from friends, and support from my family and wife.

I would like to express my deep and sincere gratitude to my supervisor, Professor Dr. Hajime Nakagawa, Disaster Prevention Research Institute (DPRI), Kyoto University, for his excellent guidance, caring, patience, and providing me with an excellent atmosphere for doing research.

I am deeply grateful to my dissertation reviewers, Professor Dr. Masaharu Fujita and Associate Professor Dr. Kenji Kawaike, DPRI, Kyoto University, for their valuable comments and suggestions to refine the dissertation.

I am also grateful to other faculty members, Assistant Professor Dr. Hao Zhang, Assistant Professor Dr. Hideaki Mizutani, Dr. Hiroshi Teraguchi, Dr. Badri Bhakta Shrestha, Dr. Woo-dong Lee, Dr. Myoung-kyu Kim and Mr. Bhattarai Pawan Kumar for their guidance, suggestions in all aspects of my study.

I am greatly indebted to many teachers in the past, Professor Dr. Jung-sung Yoon (Inje University, Korea), Professor Dr. Dong-soo Hur (Gyeongsang National University, Korea) and Dr. Sun-bong Woo for getting me interested in each and every topic of water resource engineering and coming to Japan.

I am also indebted to my all colleagues of River Disaster Prevention System, DPRI, Kyoto University for their kind cooperation and unforgettable friendship. I am especially grateful to Dr. Dong-keun Lee, Dr. Ram Krishna Regmi, Mr. Amir Reza Mansoori, Mr. Seung-soo Lee, Mr. Nam-gyun Kim, Mr. Dong-woo Ko, Mr. Ogura Masatoshi, Mr. Kitaguchi Osamu, Mr. Hiratsuka Shunsuke, Mr. Tanaka Nanahiro and Mr. Oomoto Taku. Also I want to thank to Ms. Sugimura Natsuyo and Ms. Himuro Tomoko, who helped me every time I need a hand.

I thank all the professors and friends in the Research Center for Fluvial and Costal Disaster, Disaster Prevention Research Institute of Kyoto University, who have made my academic experience rich and memorable. I would like to thank Mr. Fujihara, Ms. Kitagawa, Mr. Tatsumi, Mr. Nishimura, Mr. Yoshida and all the staffs in Ujigawa Open Laboratory, Disaster Prevention

Research Institute of Kyoto University for their support in routine administrative process and experiment.

I gratefully acknowledge the financial support of the Monbukagakusho (Ministry of Education, Culture, Sports, Science and Technology, Japan) and Kyoto University Global COE Program (GCOE-ARS).

I wish to express my grateful to my family and my wife's family for their encouragement and praying for me throughout the course of this study. All the time they gave me the feeling of doing something special. Actually, it is priceless knowing that somebody is proud of what you are doing.

Last but not least, my sincere gratitude to my darling, So-jeong, for her persistent love, continuous support, enormous patience, and for accepting me as I am, and to Yeeun our little angel.

"Faithfulness makes all things possible"

Table of Contents

Abstract i

1. Introduction……. 1

1.1 General……... 1

1.2 Types of Debris Flow...…..…… 7

1.3 Preventive Measures for Debris flow…….…… 7

1.4 Literature Review: a Brief Overview…...……... 15

1.4.1 Debris Flow Control by a Sabo Dam...……... 15

1.4.2 Debris Flow Impact Model……....… 18

1.5 Objectives of the Research…..……... 20

1.6 Outlines of the Dissertation….……... 21

References

2. Hydraulic Model Test on Debris-Flow Breaker…..……... 29

2.1 General……...…… 29

2.2 Experimental Set-up for Debris-flow Breaker……..….…… 33

2.2.1 Description of Hydraulic Model...……..…… 33

2.2.2 Experimental Conditions…….…… 36

2.2.3 Sediment Properties……. 37

2.2.4 Measurement Techniques…….……... 39

2.3 Experimental Results ……. 41

2.3.1 Deposition Process.....……...……... 41

2.3.2 Deposition Process for Different Configuration of Breaker……... 45

2.3.3 Travel Length……..…… 61

2.3.4 Discharges and Sediment concentration……..... 63

2.4 Summary…….…….…….. 64

References

3. Numerical Simulation and Verification on Debris-Flow Breaker……..... 67

3.1 General……...…… 67

3.2 Pore Water Pressure on the Debris-flow Breaker……...…… 69

3.3 Governing Equations……...……...…… 72

3.3.1 Momentum Conservation Equations……... 74

3.3.2 Constitutive Equations and Bottom Shear Stress…… 76

3.3.3 Erosion and Deposition Velocity Equations…… 79

3.4 Solution Methods…….....……...…… 82

3.5 Boundary Conditions……...……...…… 85

3.6 Contents of Numerical Simulation……..……...…… 86

3.7 Numerical Results ……. 88

3.7.1 Discharges and Sediment Concentration…..……... 88

3.7.2 Deposition Process (without Debris-flow Breaker)..…….. 89

3.7.3 Deposition Process for Different Configuration of Breaker.....…..…….. 93

3.7.4 Deposit Thickness at the Debris-Flow Breaker……... 96

3.8 Verification and Discussions for Debris-Flow Breaker……..... 99

3.8.1 Discharges and Sediment Concentration…..……... 99

3.8.2 Comparison of γ Coefficient……... 101

3.8.3 Deposit Thickness at the Debris-Flow Breaker……... 104

3.8.4 Travel Length……...……... 109

3.8.5 Relationship of Reduction Rate……... 111

3.9 Summary…….……..…….. 115

References

4. Hydraulic Model Test on Closed-Type Sabo Dam with a Flap……...… 119

4.1 General……...…… 119

4.2 Debris Flow Impact Model…….……... 124

4.3 Experimental Set-up for Sabo Dam with a Flap...…….…… 126

4.3.1 Experiment for Hydraulic Characteristic……..……..…… 126

4.3.2 Experiment for Debris Flow……...…….…… 128

4.3.3 Experimental Conditions…..……...…….…… 129

4.3.4 Sediment Properties……. 132

4.3.5 Measurement Techniques…….……... 133

4.4 Results and Discussions……. 136

4.4.1 Comparison of Flow Profile near the Dam…..……..…… 136

4.4.2 Flow Pattern……...…….…… 140

4.4.3 Mass Ratio and Median Grain Diameter……. 144

4.4.4 Vertical Distribution of Total Pressure……... 147

4.4.5 Force Behaviour of Debris Flow……..... 149

4.4.6 Impact Pressure and Velocity……..……..... 150

4.4.7 Impact Model of Debris Flow…….……..... 152

4.5 Summary……..…….…….. 154

References

5. General Conclusions and Recommendations..... 159

5.1 General…...…… 159

5.2 Conclusions..…….. 160

5.2.1 Debris-Flow Breaker……...……...…….…… 160

5.2.2 Closed-Type Sabo Dam with a Flap…… 161

5.3 Recommendations for Future Researches……..… 162

List of Figures……. 164

List of Photos……...……... 169

List of Tables……..... 171

IMFORMATION OF AUTHOR……... 173

REFEREED JOURNAL ARTICLES……... 174

CHAPTER 1

INTRODUCTION

1.1 General

Sediment-related disasters caused by localized torrential downpours, earthquakes, volcanic eruption, and so on occur frequently every year, and they account for nearly half of the total human casualties from natural disasters. A sediment disaster is not as large as an earthquake, flood, storm surge or tsunami, but its threat to human lives is very high because it can occur at multiple locations simultaneously (Kim et al. 2013a, 2013b). The occurrence of sediment-related disasters, i.e., debris flow, landslide, and slope failure have been increasing every year due to the various impacts of surface water flows. These flows are caused by glacier melting and heavy rainfall due to the changing global climate and environment (i.e. global warming) as well as urbanization (e.g., paving a road with asphalt), rapid forest development in mountainous areas (e.g., deforestation), increasing population density and so on. Furthermore, these disasters frequently lead to the large-scale destruction of infrastructure or individual properties and cause psychological harm or human death (or physical harm). However, we are dealing with natural disasters, and humans cannot always control natural disasters.

Debris flow is one of the oldest sediment disasters in the world. The definition of debris flows has already been mentioned by many previous researchers. One clear definition is that of Takahashi (2007): Debris flow is a mixture sediment and water flowing as if it was a continuous fluid driven by gravity, and it attains great mobility due to the enlarged void space saturated with water or slurry. Likewise, debris flow is composed of many types of sediment, including

large boulders (i.e. debris), wood, water, and so on. Debris flow occur when masses of poorly sorted sediment, agitated and saturated with water, surge down a slope in response to gravitational attraction (Iverson et al. 1997). Therefore, it usually begins from the upstream in a mountainous area. Photo 1.1 shows a debris flow event in Caraballeda, Venezuela in December 1999 caused by heavy rainfall. Debris flow scars along Quebrada San Julián; Rio Naiguatá drains across an alluvial fan in a newly widened channel at Naiguatá. Photos 1.2 and 1.3 illustrte a slope failure and a landslide disaster which occurred in Japan.

One of the important characteristics of debris flow is its high velocity (i.e. the speed gradually increases due to the gravity and steep bed slope) in comparison to other types of fluid, as well as the front part of the flow where large boulders accumulate, lasting for a few seconds, and the following part, which lasts longer and looks like a mud flow with gradually decreasing discharge. In addition to causing significant morphological changes along riverbeds and mountain slopes, these flows are frequently reported to have brought about extensive property damage and loss of life (Takahashi 1991, Hunt 1994, Huang and Garcia 1997, Nakagawa et al. 2002a, Shrestha et al. 2008, and Kim et al. 2012a, 2012b). Furthermore, they lead to variation of surface condition (i.e. erosion or deposition) when the mass of earth debris and other materials are transported by floods downstream. Debris flow can be classified into three types (i.e. stony debris flow, turbulent-mud type debris flow, and viscous debris flow).

Okuda et al. (1977) from DPRI (Disaster Prevention Research Institute of Kyoto University, Japan) succeeded in taking photos of debris flow occurring at Kamikamihorizawa, Nagano

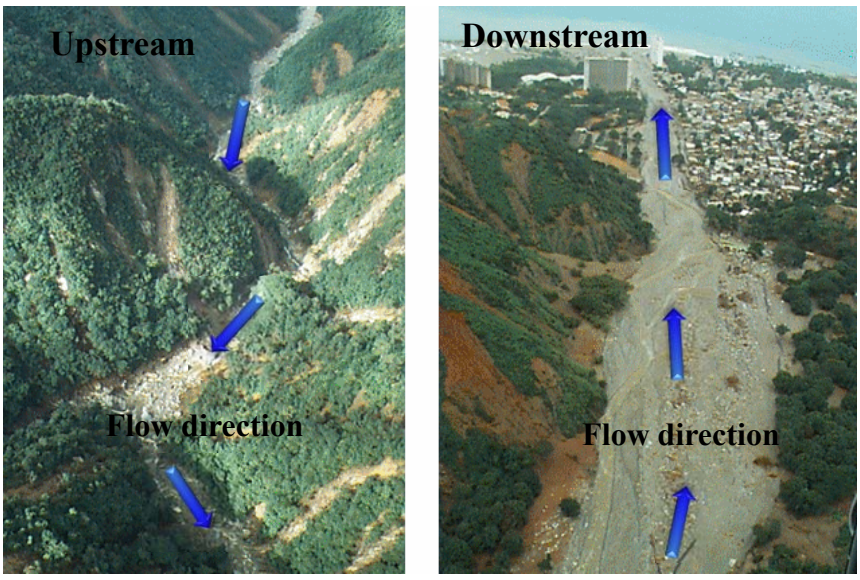

(Photo Courtesy: USGS, December, 1999)

Photo 1.1 Debris flow event at Caraballeda, Venezuela

Prefecture, Japan in 1976. This research confirmed that in stony debris flow the biggest stones accumulate at the front part and the forefront contains little water. Turbulent-mud debris flow, even though it contains many large boulders, is mainly comprised of fine ash, and the behaviours of the flow are different from those of stony debris flow. Viscous debris flow is defined as the flow of a dispersion of coarser particles in a dense slurry, the concentration of coarser particles in the slurry is more than 50 % by volume (Takahashi 2007). The characteristics of debris flow differ largely depending on the type, size and sediment concentration that they contain. Nakagawa et al. (2003) determined that the criteria for each type depend on the equilibrium of sediment concentration with the slope of surface flow. The three types of debris flow are shown in Photo 1.4.

(Photo Courtesy: MLIT, Japan, July, 1997)

Photo 1.2 Slope failure event at Minamata, Kumamoto Prefecture, Japan

(Photograph by: Yeonjoong KIM, June 2012)

Photo 1.3 Deep-seated Landslide event at Mt. Akatani, Nara Prefecture, Japan

(a) Stony debris flow (source: Okuda et al, 1977)

(b) Mud debris flow (Photo Courtesy: MLIT, Japan, July 2-3, 1985)

(c) Viscous debris flow (source: http://www.dpri.kyoto-u.ac.jp)

Photo 1.4 Types of debris flow

The phenomenon of debris flow as the agent which forms alluvial cones in the mouths of mountain canyons has attracted the attention of physiography for more than a century. This is a phenomenon in which soil and boulders on a hillside or in a riverbed are carried downward quickly under the influence of prolonged or torrential rainfall. Although the flow velocity differs depending on the scale of debris flow, it sometimes exceeds several m/sec, thereby destroying homes and farmland in an instant. Debris flows are also of concern to engineers who are responsible for human life and property. Although various kinds of countermeasures have been invented, debris flow is still one of the most threatening natural phenomena in some regions of the world (Takahashi 1981). Usually we have a general idea that debris flow disasters occur in high mountainous areas, far away from modern cities. However, recently such disasters have occurred at multiple locations simultaneously between high mountainous areas and low mountain areas in urban areas. The debris flow disaster that occurred at Mt. Umeyon in downtown Seoul, Korea in 2011 is shown in Photo 1.5. Therefore, understanding the phenomenon and mechanism of debris flow is very important in order to manage sediment disasters in river basins and prevent downstream hazards by establishing various effective preventative measures.

In Japan, 54 % of the total human casualties and persons missing on account of natural disasters during the 31-year period from 1967 to 1997 were due to sediment disasters alone. In the case of sediment disasters, it is very difficult to implement preventive works at every location, because such locations would be virtually countless. In addition, we have general knowledge that debris flow disasters occur in high mountainous areas, far away from modern

(Photo courtesy: ohmynews)

Photo 1.5 Debris flow disaster event at Mt. Umeyon in downtown Seoul

cities. Thus, sabo structures have been installed to prevent damages in mountainous areas. However, a total of 12.1 million people are threatened by sediment-related disasters in Japan. Thus, the introduction of progressive technology is needed for preventive measures. However, debris flow can occur at multiple locations simultaneously between high mountainous areas and low mountain area in urban areas. Therefore, it is important to mitigate damage by establishing effective structural and non-structural measures. Figure 1.1 shows the number of occurrences of debris flow, landslide and slope failure disasters from 1991 to 2012 in Japan. Figure 1.2 shows the death toll due to sediment-related disasters from 2004 to 2011.

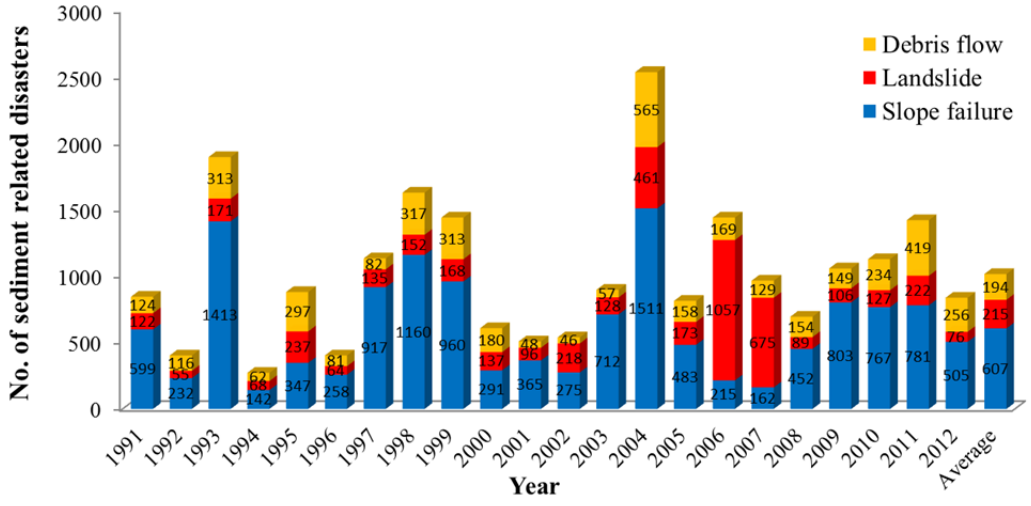

Figure 1.1 Number of sediment-related disasters (Data source: MLIT, Japan)

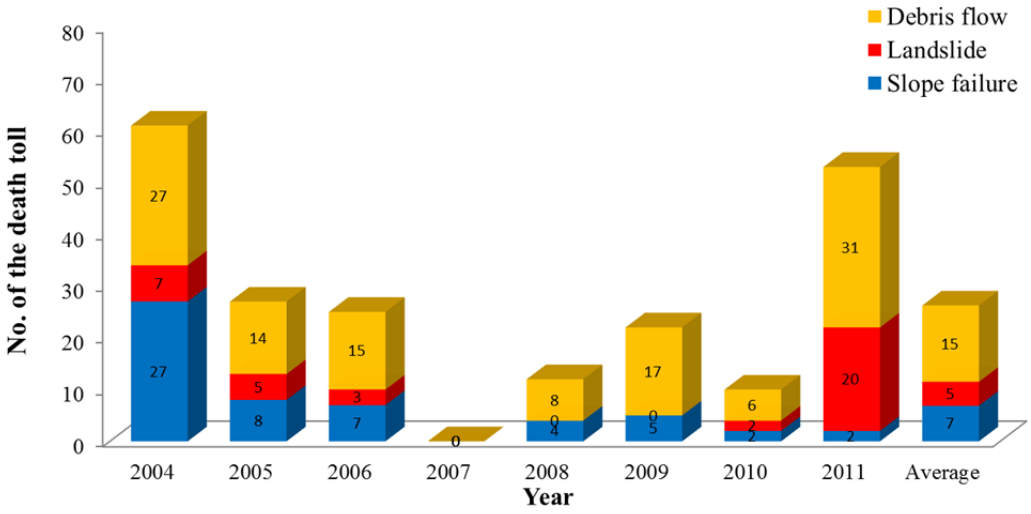

Figure 1.2 Death toll due to sediment-related disasters (Data source: MLIT, Japan)

Every year, nearly 1,000 sediment-related disasters occur. Relatively few occurrences of debris flow disasters are recorded i.e., an average of about 194 (19 % of the total number) sediment disasters. But if debris flow occurs, the potential for damage is huge i.e., an average of 15 human deaths (56 % of the average death toll). Therefore, debris flow disasters are more life-threatening than other sediment-related disasters.

1.2 Types of Debris flow

Debris flow occurs in a variety of forms depending on the conditions of the site and the factors contributing to their occurrence. A number of types by contributing factors have been published by Ikeya (1989), Nakagawa et al. (2002a), Takahashi (2007), Shrestha (2009) and others. Debris flow can be divided into various types by the contributing factors.

- **Sediment gradient:** This type occurs if the accumulated sediment concentration in a river bed exceeds the gradient made by the bed load transport of sediment.
- **Slope failure:** This type of debris flow occurs due to the failure of a slope directly.
- **Natural dam collapse:** This type occurs due to the collapse of a natural dam formed by landslides in a river or stream.
- **Landslide:** This type occurs due to the liquefaction of soils.
- **Volcanic activity:** This type occurs due to volcanic activity or volcano-induced earthquakes and consists of fine-grained rapidly flowing debris.
- **Avalanche:** This is a rapid flow of snow down a slope. These are typically triggered in a starting zone by a mechanical failure in the snowpack when the forces on the snow exceed its strength but sometimes only with gradual widening. These flows move downstream with boulders or debris and then gradually develop into debris flow.

1.3 Preventive Measures for Debris Flow

Natural disasters can strike without notice at any time anywhere. Today, advances in science and technology have brought us many benefits for mitigating the damage. However, they still require development because it is impossible to protect from the all disasters by means of countermeasures. However, we can minimize the risk of damages using structural and non-structural measures.

Countermeasures designed to mitigate debris flow disasters can be classified as structural (i.e. hard countermeasure) and non-structural (i.e. soft countermeasure) measures. In Europe, Japan, the U.S.A., South Korea and other countries, structural and non-structural measures have been widely used for mitigation of sediment related disasters. Sabo dams (i.e. check dams) are commonly used and are the most effective structural measure for protecting properties and lives from sediment-related disasters. The concept of the sabo dam proposed about 70 years ago in Japan and was discussed based on qualitative recognition (Nishimoto 2011). In mountain areas, where debris torrents might have catastrophic and dramatic impact, check dams (i.e. called debris dams or Sabo dams) can be used to reduce the impact torrents (Chanson 2004). Sediment-related disasters occur in a very extensive area from a headwater area to downstream cities. Events like the ones which occurred in Mie prefecture, Japan in September 2012 demonstrate the effectiveness of a sabo structure in mitigating the damage in downstream area (outlined by the yellow dotted line) as shown in Photo 1.6. But it sometimes is counterproductive for the ecosystem or the equilibrium of sediment mass. Therefore we must structural measures effectively. The literal translation of sabo in Japanese is sand arrestation, sand erosion control or sediment control.

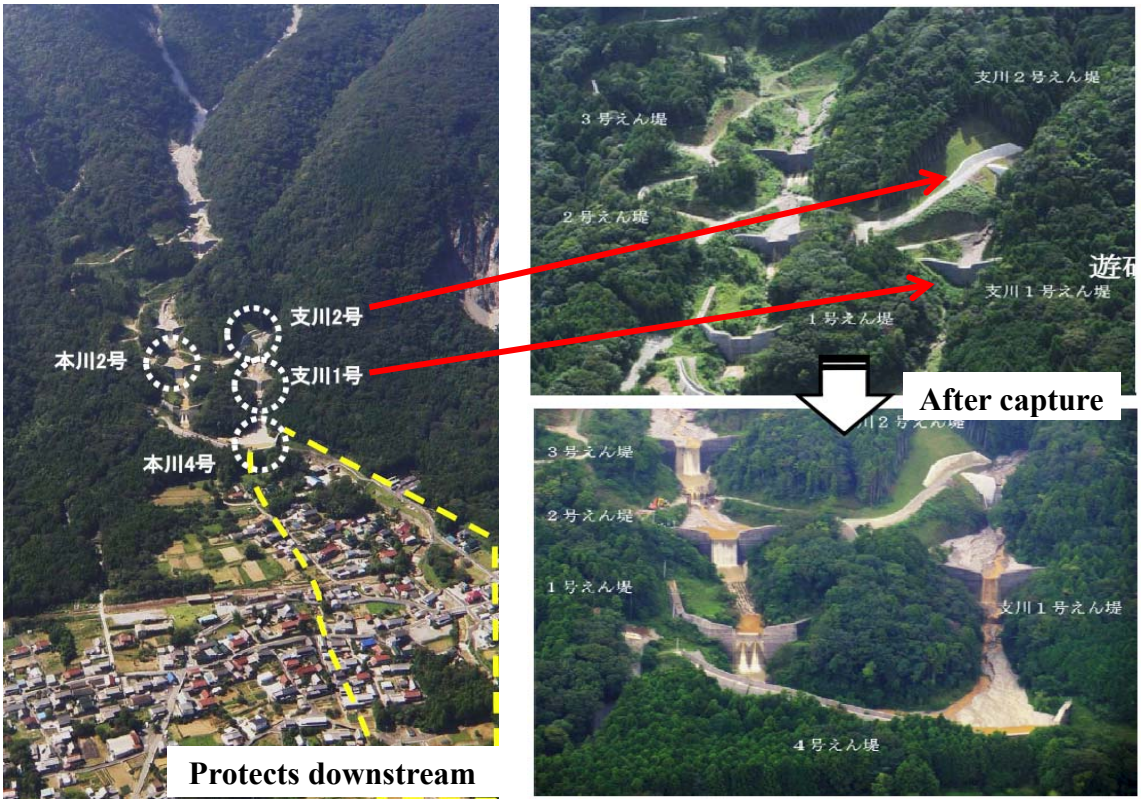

Debris flow event at Mie Prefecture, Japan 2012 (Photo Courtesy: MLIT)

Photo 1.6 Effectiveness of sabo structure

As mentioned above, in order to protect people and properties from sediment-related disasters, two types of preventive measures are taken; structural measures such as check dams, sabo structures, levees, training channels, and so on; and non-structural measures such as warning and evacuation systems and restricting and controlling new residential land development in areas vulnerable to sediment-related disasters.

1) Structural measures

Many researchers have tried to improve structural measures for mitigating damages through field observations, laboratory experiments and numerical simulation. Structural measures can be classified into two types: those in areas where debris flows occur and those in areas subject to such flow and deposition (Mizuyama 2008). To judge the optimal types of structural measures, an understanding of the behaviour and mechanism of debris flow is needed because the characteristics of debris flow can change depending on the geographic environment of the event zone, types of debris flow and contributing factors.

In general, debris flow control structures can be divided into two basic types: open and closed. Open control structures are designed primarily to constrain the flow of a channelized debris flow; closed control structures are designed primarily to contain a channelized debris flow. The features of both types are described briefly below.

Sabo dams are one of the most effective structural measures for the debris flow. Sabo structures are designed to stop the occurrence of debris flow. But a single structure cannot capture all of the debris from one event. The debris capture capacity of one sabo structure is very small in comparison to the total volume of debris flow. But these structures are active

(a) Closed dam (typical type) in France
(Source: http://commons.wikimedia.org/wiki/File)

(b) Closed dam (typical type) in Japan
(Source: http://staff.civil.uq.edu.au)

Photo 1.7 Closed dam

debris flow mitigation measures which may affect the initiation, transport, or deposition of debris flows and can therefore change the event's magnitude and frequency characteristics. The term debris flow dam is used to describe both consolidation dams and sediment retention structures. The former is generally a closed type structure as shown in Photo 1.7. It is designed to elevate the torrent bed, to fix and to stabilize the bottom profile, and primarily to contain a channelized debris flow. The latter type of structure is commonly an open structure (e.g., grid dam, beam dam, slit dam, ring net, debris-flow breaker and so on) designed to trap medium to large size debris (e.g., rocks, boulders, driftwood, debris and so on).

The open type of dam allows harmless sediment to flow downstream normally, thereby preventing riverside and coast erosion. In the case of floods, it controls downstream hazardous

(a) Front view (b) Top view

(Source: http://staff.civil.uq.edu.au/h.chanson/sabo.html)

Photo 1.8 Slit dam (open type) at Mt. Fuji, Japan

(a) Tubular grid dam at Gifu Prefecture, Japan (Shrestha et al. 2008)

(b) Screen dam at Gangwon-do, Korea (Source: http://www.hkbs.co.kr)

Photo 1.9 Grid (permeable structure) dams

sediment in the same manner as ordinary sabo dams. Some slits in a dam can function as fish ways, aiming at harmony with the ecosystem. In particular, open type check dams such as grid or slit type check dams are being adopted more often for debris flow control because they are more compatible with the natural environment than the conventional wall-like closed type dams (Mizuyama and Mizuno 1997). But it is necessary to accurately estimate the hydrograph of debris flow or the debris flow discharge passing rate according to the configuration of structures. Photo 1.8 shows a slit dam on the western slope of Mt. Fuji, Japan. The system includes a flat, wide flood plain area to store large material and a slit check dam downstream. The slit check dam is 104 m wide and 7 m high; photo (a) shows the front view, and photo (b) shows the view from the right bank on 1 Nov. 2001.

(a) Flexible ring net barriers
(Source: http://www.geobrugg.com)

(b) Debris-flow breaker in Japan
(Photo Courtesy: Murao H.)

Photo 1.10 Drain-off structure

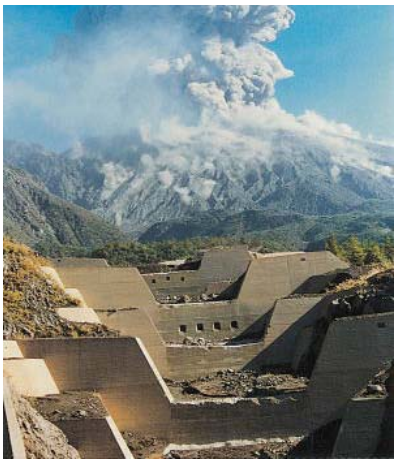

(a) The Nojiri River sabo dam
(Photo Courtesy: MLIT)

(b) The Mt. Umeyon sabo dam after debris flow event
(Photo Courtesy: Yonhapnews)

Photo 1.11 Series of sabo dams (Combination type)

Permeable structure dams are designed to trap small to medium-sized debris. Photo 1.9 shows tubular grid dams and screen dams as permeable structure; photo (a) shows tubular grid dams constructed to prevent downstream sediment disasters due to debris flow at the Hirayu River, Gifu Prefecture, Japan, while photo (b) shows a screen (or beam) dam in Gangwon-do, Korea. Photo 1.10 shows drain-off water structures. These structures have advantages compared to traditional concrete structures in that they are light, flexible and easily installed, as well as cost-efficient, simply designed, and easily repaired and maintained. Photo (a) shows a flexible ring net barrier, and photo (b) shows a debris-flow breaker in the Kamikami-Horisawa Valley of Mt. Yakedake, Japan. In addition, various types of structures are being used to protect people and properties from debris flow disasters. Photo 1.11 shows a series of sabo dams (combination type). These plans should consider the relationships between the location of each dam, the capacity of sediment volume, and other parameters. Therefore, selecting types and arrangement of dams, one should consider the function of each dam carefully.

The function of a sabo dam is to temporarily store excess sediment in the upstream pocket of the sabo dam and reduce the discharge safely. In general, the objectives of sabo training may be summarized as:

- To capture flowing sediment. The river bed rises as the flowing sediment is captured.
- To secure the ridges of mountains and prevent the hillside from collapsing due to the rising river bed.
- To lessen the slope of the river bed and prevent erosion of river beds and banks.
- To prevent the movement of unstable sediment accumulated on the river bed.
- After the sabo dam is filled up, it functions as a sediment runoff control facility.

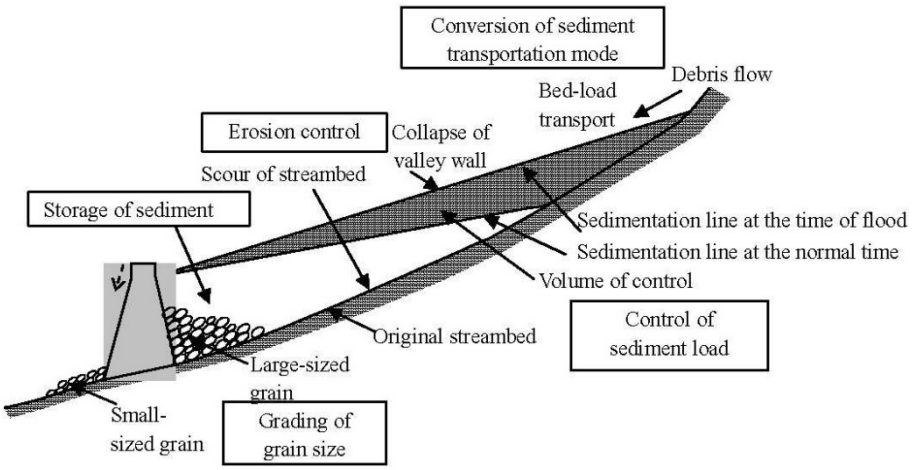

Figure 1.3 Functions of a sabo dam

Figure 1.3 shows the various functions of a sabo dam (MLIT 2011). The capacity of a sabo dam to control sediment is determined by the sediment storage capacity between the stable slope and the temporary slope of accumulated sediments. In recent years, there have been a lot of research on the efficient functioning of sabo dams, and it is still very much a work in progress. If newer sabo dams are designed, they will capture the sediment discharge from debris flow more effectively. Therefore, we should continue to strive to mitigate damages.

2) Non-structural measures

To establish so-called non-structural or soft countermeasures for debris flow hazards, it is essential to delineate the hazardous zone for a potential debris flow at the debouchment of a ravine. Because the natural and man-made features of the areas and the scale and properties of debris flows are different from place to place, data from actual experiences sometimes contribute to the issues (Takahashi and Tsujimoto 1984).

Preventing the occurrence of disasters by controlling the mechanical and incidental factors through the installation of structural works is the most basic approach to disaster prevention. However, the rage of nature sometimes strikes unexpectedly. Because it is extremely difficult to determine the disaster site and the occurrence time in advance, complete prevention of sediment disasters is virtually impossible even today, when society has access to highly advanced technologies. Structural measures are very useful for mitigating the damages, but they cannot protect from all damages resulting from sediment-related disasters. Therefore, we try to make effective use of structural and non-structural measures to mitigate the damages wisely. But the non-structural measures are not built in a day, so we must recognize the importance of disaster prevention in our lives and pay close attention to the messages from previous disasters.

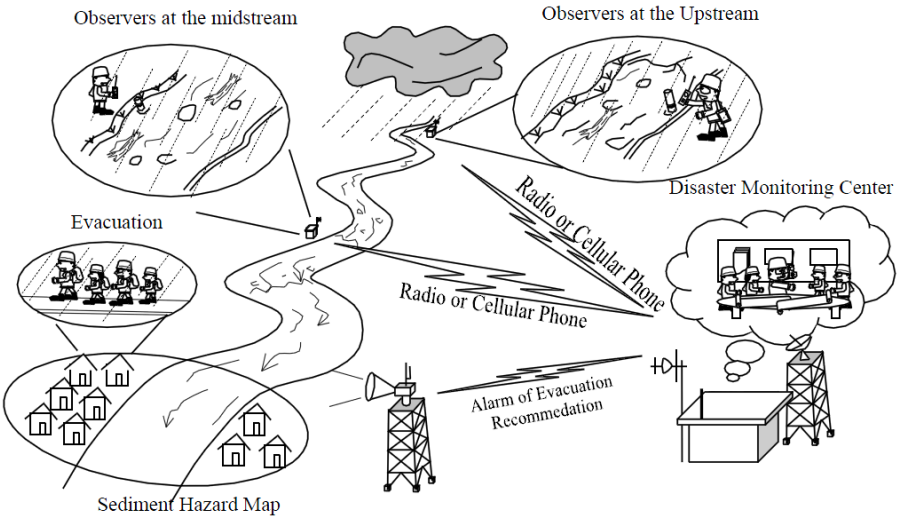

Figure 1.4 Warning and evacuation system (MLIT, Japan)

There are three types of non-structural measures against sediment disasters (i) development of warning and evacuation systems, (ii) restriction of land use in areas at risk for sediment disasters, (iii) preparation and publication of hazard maps with public involvement (MLIT 2004). A sediment disaster warning and evacuation system must be based on monitoring and observation of sediment disasters or rainfall forecasts. Figure 1.4 shows examples of the operation of a sediment disaster warning and evacuation system. In order to operate warning and evacuation system, it is necessary to build the staffing and organization required for collecting sediment disaster information and carrying out the suitable operation.

Natural hazard has been defined as the probability of occurrence of a potentially damaging phenomenon within a specified period of time and within a given area (Varnes 1984). Hazard maps are indicative risk maps for large flood events and useful only for knowing where not to be during extremely heavy rainfall. For local governments, these debris flow hazard maps can be used for localized emergency response (i.e. evacuation and access routes, road closures, siting of key rescue facilities) and for urban planning. Figure 1.5 shows the designation of a hazard area and preventive measures between the degrees of risk.

Systematic analyses of comprehensive structural and non-structural countermeasures to prevent debris flow disasters are very important. Both methods are very useful for mitigating damages, but we must consider many parameters because it is tightly linked to our lives. Especially when deciding on the type of check dam to use, one must pay attention to the environment of the basin. In addition, one should thoroughly investigate the cause of the accident after an event for the growth and development of disaster prevention.

(a) Steep slope failure (b) Landslide (c) Debris flow

Yellow zone: Sediment-related disaster hazard area

Red zone: Special sediment-related disaster hazard area

Figure 1.5 Designation of hazard areas and preventive measures (MLIT, Japan)

1.4 Literature Review: a Brief Overview

1.4.1 Debris Flow Control by a Sabo Dam

A sabo dam (i.e. check dam) is commonly used and is the most effective structural measure for protecting properties and lives; they can effectively dampen or mitigate the damage from sediment-related disasters. Many structures of this type have been constructed in mountainous areas. The concept of the sabo dam was proposed about 70 years ago in Japan and was discussed based on qualitative recognition (Nishimoto, 2011). Usually, sediment control structures temporarily store the excess sediment in the upstream pocket of the sabo dam and reduce the discharge or energy of a debris flow along a river channel or ravine safely, thereby controlling the surface erosion that usually occurs in upstream areas. In recent years the sabo structure has made much progress; in particular, open type check dams (e.g. grid type or slit type check dams) have become increasingly more popular than closed type check dams from the viewpoint of comprehensive sediment management in the river basin and river environment. But there are still many problems that must be solved because the mechanism of debris flow is very complex. Therefore, a lot of researches are being carried out to improve the function of sabo dams based on field observations, laboratory experiments (i.e. large and small scales) and numerical simulations.

Field observations, laboratory experiments and numerical studies on debris flow control by various types of dam are reported in many sources. First, Honda and Egashira (1997), Takahashi et al. (2001a), Nakagawa et al. (2002b), Satofuka and Mizuyama (2005), Nakatani et al. (2008), Shrestha et al. (2008), Osti and Egashira (2008), Niwa et al. (2009), Suzuki et al. (2009) and others have conducted research regarding the closed type dam, which is the most common type. Second, among open types of dam many researchers have investigated both the grid type dam, such as Ashida and Takahashi (1980), Mizuyama et al. (1995), Seto et al. (1998), Mizuno et al. (2000), Takahashi et al. (2000, 2001c), Sato et al. (2001), Miyazawa et al. (2003), Gotoh et al. (2006), Satofuka and Mizuyama (2006), Takahara and Matsumura (2008), Horiuchi et al. (2011), Yoshida et al. (2011) and others, and the slit type dam, such as Watanabe et al. (1980), Ikeya and Uehara (1980), Johnson et al. (1989), Mizuyama et al. (1989, 1999, 2000), Nishikawa et al, (1999), Mizuno et al. (2001), Takahashi et al. (2001b), Fukuda et al. (2002), Mizuno et al, (2002), Lien (2003) and others. Ohkubo et al. (1997), Masuda et al. (2002), Hasegawa et al. (2004), Shima et al. (2011), and Kim et al (2013) explained the function of series of sabo dam with various types. Nakagawa et al. (1994, 1995, 2001), Ozaki et al. (1998), Doi et al. (2000), Gotoh et al. (2002), Simizu and Osada (2008), Katatani and Yamada (2006), Shibuya et al.

(2010, 2011), and Shrestha et al. (2011) have performed analyses of the capturing of driftwood. Furthermore, the locations of check dams in a river channel are also very important for effective debris flow control. The numerical studies of Wang (2001) have revealed that the optimum positions for grid dam installation are where debris flow arrives at its most developed stage.

Many researchers have also investigated debris flow control by type of impermeable dams. In particular, Takahashi et al. (2001a) proposed a method for calculating the effect of a closed type check dam. This method uses the relationship between dam height and riverbed height upstream of the dam to determine whether materials will pass over a closed dam. This method was used by Nakagawa et al. (2002b), and Satofuka and Mizuyama (2005) for the evaluation of the effectiveness of closed dam using a one-dimensional model in order to reduce debris flow disasters. Bovolin and Mizuno (2000) carried out an experiment to clarify the effectiveness of permeable and non-permeable check dams in reducing discharge and sediment concentration in case of a mudflow.

Many research studies are being carried out to discover the benefits of permeable dams. The sediment control function of the slit type check dam has been mainly discussed with reference to its use in the case of bed load transport (Mizuyama et al. 1990, Okubo et al. 1997, Fujita et al. (1998, 2001), Armanini and Larcher 2001, Busnelli et al. 2001, Masuda et al. 2002). Watanabe et al. (1980) has shown that the spacing of the posts has an effect on the trapping capacity of a slit dam and a screen dam. When the relative spacing is $l_o / d_{max} < 2.0$, where l_o is the spacing of the posts and d_{max} is the maximum diameter of the debris flow, the research indicated that the volume of the debris flow could be reduced by 50% ~ 70% during peak times, but the total volume of debris flow cannot be reduced. The above studies validated the effectiveness of open-type dams in the prevention of debris flows. Mizuno et al. (2001) presented the mudflow control function of slit or conduit type check dams. Previous research works had not focused on the sediment control function of the slit type check dam in the case of debris flow. However, Nakatani et al. (2008) tried to simulate debris flow trapping by slit dams based on the narrowing river width between upstream and downstream calculation points. Thus, further studies on debris flow control functions of slit type check dams are very important.

Ashida and Takahashi (1980) conducted experimental studies on the debris flow control of grid type sabo dams; through experiments they defined the hydraulic function of a grid dam regarding the suitable spacing between columns for effective capturing of debris flow as $L_g/d_{max} = 1.5 \sim 2$ (L_g= span of open space and d_{max}= maximum diameter of particle). Ashida et al. (1987) investigated the mechanism of debris flow control using two types of grid dams (i.e.

zigzag and square grid dams). In this study the relation among pass rates of sediment through grid dams, sediment particle sizes and opening lengths of grids was proposed, and is used to evaluate the pass rate of sediment for the boundary condition of the numerical model. Mizuyama et al. (1995) and Mizuyama and Mizuno (1997) clarified the function of capturing sediment by the grid dam effectively. The blockage phenomenon is regarded as a stochastic process, and a new stochastic model of blockage of a grid dam by large boulders in a debris flow is proposed by Takahashi et al. (2001c). Recently, Satofuka and Mizuyama (2006) developed a growing rate formula to calculate debris flow capture by a grid dam. Likewise, many researchers have conducted laboratory experiments and numerical simulations regarding the mechanism of capturing sediment for transmittance.

Among permeable dams, the number of debris-flow breaker (i.e. breaker) and ring-net structures are increasing these days. These structures have the advantage of not only reducing velocity but also creating suitable narrow or wider area, and they are cost-efficient, simply designed, and easily repaired and maintained due to the rapidly changing pressure through the opening area. The debris-flow breaker was installed nearly 30 years ago, and is designed to check the boulder dam. In order to clarify the mechanism of debris-flow breakers, monitoring and field surveys were conducted by Izumi et al. (1982) and Kurihara et al. (1987) at Mt. Fuji, as well as by Kiyono et al. (1986), Imai et al. (1989) and Nisimoto et al. (1994) at Mt. Yake-dake. More recently, Gonda (2009) proposed a mechanism of debris-flow breaker for a 1-D numerical simulation. Kim et al. (2012a, 2012b) estimated the optimum condition for the parameters of the debris-flow breaker using a 2-D numerical simulation. A new type of debris flow mitigation measure, the flexible ring net barriers are expected to capture the debris flow efficiently and can reduce the maximum impact forces through long braking distances and flexible deforming structures. Field measurements and numerical simulations were carried out to clarify the mechanism by DeNatale et al. (1999), Volkwein (2005) and Chiba et al. (2011).

Most of the above models can analyse the debris flow control function of check dams to some extent. However, the investigation of the debris flow deposition process in areas upstream of check dams have not yet been focused upon by previous researchers. In the area upstream of a check dam, sediment concentration of debris flow becomes maximum sediment concentration due to the existence of the check dam, and we cannot ignore the effect of static pressures in a numerical model. The constitutive equations and deposition velocity equation are very important in calculating debris flow deposition in the area upstream of a check dam. Therefore, it is necessary to study the deposition process of debris flow in areas upstream of a check dam in order to reduce sediment disasters in the river basin. It is also necessary to study the erosion

process of deposited sediment upstream of a check dam to investigate the flushing out of deposited sediment upstream of check dams by a normal scale flood flow.

1.4.2 Debris Flow Impact Model

Debris flow impact models were suggested for calculating the external force. But it is very difficult to estimate the applied force due to the impact collision because the debris flow is composed of many kinds of sediment sizes and fractions, which makes it difficult to estimate actual contact area. Furthermore, the debris flow is characterized by the front part of the flow (i.e. very complex), where large boulders accumulate, lasting for a few seconds; the following part, which lasts longer, looks like a mud flow with gradually decreasing discharge. The force behaviour of debris flow can be classified into three stages: impact forces due to the impact collision at first, then both the dynamic and static forces condition, and finally the static force condition. The total force of debris flow consists of hydrostatic force, hydrodynamic force, and the impact force due to boulders entrained in the flow, and these three types of forces usually occur simultaneously. Among these forces, impact force has huge destructive power. Therefore, many researchers have tried to clarify the impact force to estimate the exact force.

A lot of research is being carried out to clarify the impact force of debris flow based on field observation, laboratory experiments (large and small scales) and numerical simulations. A few field experiments have been carried out, such as those of Okuda et al. (1978), Suwa and Okuda (1983), and Hu et al. (2011). A-part from those, Hu et al. (2011) reported an in-situ test of debris flow impact at Jiangjia Ravine, and introduces a simple approach to separating the two components of the impact force. In his paper, preliminary analyses were made to produce the relationships of mean velocity to hydrodynamic pressure, and hydrodynamic pressure to grain impact loading from the measurement data. Okuda et al. (1978) indicated the characteristics of debris flows from field observations (i.e. the forefront of the debris flow looks like a bore and the depth suddenly becomes large from virtually no preceding flow, and the biggest stones accumulate at the front and the forefront contains little water). Field measurements performed at Mt. Yakedake (Suwa and Okuda. 1983) show that impact forces consist of two distinct parts: fluid dynamic pressures up to 10 kN/m^2 and collisional forces of single boulders up to 10^2~10^4 kN/m^2.

Many small scale laboratory experiments have been performed in order to develop theoretical models for the calculation of impact force (Kim et al. 2012c, 2013a, 2013b, 2013c). Mizuyama (1979) separated the impulsive force of debris flow into the fluid force and the boulder impact force. In his paper, the impulsive force on a vertical sabo dam was described

using fluid theories, and the theory of complete sphere elasticity was assumed so that the impulsive force of the boulders could be derived. Scheidl et al. (2012) analyse the impact forces of granular and viscous debris flow and discuss the observations of single, short time impacts of large particles, significantly exceeding the peak pressure values. However, there have been very few studies that discuss how debris flow is influenced by the shape of a sabo dam. Shieh et al. (2008) designed a new form of sabo dam by changing the geometric shape of the upstream dam surface to reduce the impulsive force of the debris flow, with enhanced stability and reduced concrete mass being the anticipated outcomes. Their study showed that the curved dam experienced less impact force than other dams under the same debris flow conditions, demonstrating the importance of curved geometry for a well-designed sabo dam. Huang et al. (2007) applied the theory of elastic collision to find a boulder collision impact model for four types of dam. Recently, Shibuya et al. (2012) presented the load of debris flow with woody debris for the open type steel frame check dam structure. Likewise, the understanding of the behaviour and mechanism of debris flow and the study of preventive measures are very important in order to manage sediment disasters in river basins and prevent the downstream hazards.

The destructive power of debris flow consists of surface pressure due to fluid-phase slurry thrusting, and point-wise loading due to coarser solid particle collision. The fluid pressure, including hydrostatic and hydrodynamic components, strongly depends on fluid density, flow depth, velocity and impact angle, while the solid loading depends on the velocity and size of the largest boulder, as well as the geometry and properties of the structures subject to collision (Hu et al. 2011). To estimate the impact force of debris flow against barriers, several models exist. However, it is difficult to determine the impact force due to the diversity of substances composing the debris flow, i.e. water, mixtures of granular and fine particles in water and boulders. So far, the impact force of debris flow has been mainly described using two different models which can be classified as hydraulic and solid collision models. The hydraulic models are further separated into hydrostatic and hydrodynamic models. Based on observations and theoretical consideration, different models have been developed for estimation of debris flow impact force.

- **Hydrostatic Model**

The hydrostatic models by Lichtenhahn (1973) and Armanini (1997) are useful because they require only the approaching depth of debris flow to calculate pressure. For simplicity, the value of P_{max} is often estimated, for preliminary dam design purposes, assuming the approach depth of debris flow equal to height of dam.

- **Hydrodynamic Model**

The hydrodynamic formulas are based on the impulse theorem. The phenomenon of debris flow impact against an obstacle has been analysed in scientific literature; many empirical and non-empirical relations can in fact be found for the calculation of dynamic thrust. Zhang (1993) and Bugnion et al. (2011) are estimated the empirical coefficients by field measurement. Canelli et al. (2012), and Watanabe and Ikeya (1981) proposed that the force of empirical value changes with flow material; for clear water it has been found to be between 1 and 2, and for bentonite 2.0, as well as a value of 1.5 by Hungr et al. (1984). Besides, when designing a sabo dam in Japan, the fluid load formulas proposed by Yamamoto et al. (1998) are usually used.

- **Solid collision Model**

Conventional contact mechanics are mainly concerned with static contact, although they have been extended to approximate solutions when impact is involved. For spheroidal surfaces, Hertz theory is used to obtain the force deformation relation needed to calculate the duration of impact and the maximum indentation. Hertz theory predicts the stress distribution in the contact zone between two bodies having a surface of revolution. It also allows us to calculate the normal and shear stress distribution inside the solid. Mizuyama (1979) calculated the impact load between sabo structure and boulders due to the elastic properties of the sphere materials.

1.5 Objectives of the Research

This study aims at characterizing of the type of permeable dam regarding change in pore water pressure and flow patterns by debris-flow breaker, identifying the underlying processes and mechanisms, and developing numerical models to simulate the dynamic feedback process. Besides, as a type of impermeable dam, a new closed-type sabo dam with flap is proposed and identified the underlying processes and mechanisms by the experimental study. Under these objectives, this research concentrates on the flow pattern, travel length of debris, impact force and deposition process due to the various shapes of a sabo dam. The main objectives of this study are summarized as follows.

- To clarify the mechanism of debris-flow breaker, fundamental experiment and numerical simulation are conducted to investigate the characteristics of the breaker. In addition, a design methodology based on change in pore water pressure on the breaker during separation of water from the debris flow is developed and the ranges of the debris-flow breaker parameters such as opening and blocking sizes for the design of structural elements

of debris-flow breaker are evaluated.

- To investigate various parameters for the proposed new type of sabo dam with a flap such as flow profile near the dam, flow pattern, captured or overflowed to input mass ratio of debris with median grain diameter, vertical distribution of total pressure, force behaviour of debris flow, and finally, estimate the coefficients of the impact model based on experimental study.

1.6 Outlines of the Dissertation

This dissertation, firstly, concerns the analysis of hydraulic characteristics of debris-flow breaker and concentrates on the understanding of the mechanism and hydraulic phenomenon by physical and numerical modeling. The dissertation also consists of the experimental analysis regarding the superiority of proposed new type of sabo dam with flap structure in comparison to traditional sabo dam based on the hydraulic characteristics.

The present dissertation consisting of five chapters is organized as follows.

Chapter 1 presents the motivation and the objectives of this study, together with a brief introduction of the types of debris flow, preventive measures for debris flow disasters, debris flow impact model, and the contents of the dissertation.

Chapter 2 presents the hydraulic model test of the debris-flow breaker structure consisting experimental setup, experimental condition and experimental results. In the first part of this chapter, the flume geometry, the measured parameters, adopted measurement techniques and the characteristics of sediment material used in the experiments are described. On the final part, the studied characteristics of deposition and erosion on the debris-flow breaker (which are obtained from the measuring system) due to the change in pore water pressure and the respective experimental results are elaborated. The results from the measurements of flow and sediment discharges, sediment concentration, flow pattern, travel length, and deposit thickness on the debris-flow breaker are also presented. These are later used to validate the numerical model described in detail in Chapter 3.

Chapter 3 provides a detailed description of the numerical simulation which was developed to analyze the flow interaction between opening and blocking size of the debris-flow breaker as

well as the characteristics of the deposition process of debris flow under various parameters (i.e. bed sediments and opening and blocking size of the debris-flow breaker). For numerical analysis, a new numerical model based on an existing depth-wise averaged 2-D model that can analyze the hydraulic phenomena of the debris-flow breaker was developed using momentum conservation equations for change in pressure at the debris-flow breaker. To validate the newly developed 2-D numerical model, the results of hydraulic model test (from chapter 2) are compared with the results of the numerical calculation. Also, using the newly developed numerical model, the dynamic mechanism by the interaction of pressure at the debris-flow breaker (which is not defined by the hydraulic model test) was studied.

Chapter 4 describes the hydraulic model test for proposed new type of dams with flap structure to analyse the working principle and respective hydraulic mechanisms. The result shows that the proposed dam is far better in terms of hydraulic functioning than the traditional vertical sabo-dams. This chapter also includes the results consisting of the empirical coefficients of the hydrodynamic and solid collision models and their comparison with the prevailing coefficients. To elaborate the above results, a detailed description of the debris flow impact model, the procedure of experimental set-up for the experiment, experimental conditions, and measurement techniques of different parameters are also incorporated in this chapter.

Finally, in Chapter 5, the main findings and conclusions about the characteristics of debris-flow breaker structure and closed-type sabo dam with a flap structure are summarized. Various outstanding issues are identified and recommendations for future research are also described.

References

1) Armanini A. 1997, On the dynamic impact of debris flows. *In: Armanini A, Masanori M (eds) Recent developments on debris flows,* lecture notes in earth sciences, Springer, Berlin, pp. 208-226.
2) Armanini A. and Larcher M. 2001, Rational criterion for designing opening of slit-check dam. *Journal of Hydraulic Engineering, ASCE,* Vol. 127, No. 2, pp. 94–104.
3) Ashida K. and Takahashi T. 1980, Study on debris flow control, hydraulic function of grid type open dam. *Annuals of the Disaster Prevention Research Institute, Kyoto University,* No. 23 B-2, pp. 433-441. (in Japanese with English Synopsis)
4) Ashida K., Egashira S., Kurita M. and Aramaki H. 1987, Debris flow control by grid dams. *Annuals of the Disaster Prevention Research Institute, Kyoto University,* No. 30 B-2, pp.441-456. (in Japanese with English Synopsis)

5) Bovolin V. and Mizuno H. 2000, Experimental study on the effect of a check dam against mudflow. *Debris-Flow Hazards Mitigation:* Mechanics, Prediction, and Assessment, Wieczorek & Naeser (eds), pp. 573-578.
6) Bugnion L., McArdell B.W., Bartelt P. and Wendeler C. 2011, Measurements of hillslope debris flow impact pressure on obstacles. *Landsildes (2012)* 9, pp. 179-187.
7) Busnelli M. M., Stelling G. S. and Larcher M. 2001, Numerical morphological modeling of open-check dams. *Journal of Hydraulic Engineering, ASCE,* Vol. 127, No. 2, pp. 105-114.
8) Canelli L., Ferrero A.M., Migliazza M. and Segalini A. 2012, Debris flow risk mitigation by the means of rigid and flexible barriers-experimental tests and impact analysis. *Nat. Hazards Earth Syst. Sci.,* 12, pp. 1693-1699.
9) Chanson H. 2004, Sabo check dams-mountain protection systems in Japan. *Intl. J. River Basin Management,* Vol. 2, No. 4, pp. 301-307.
10) Chiba M., Sakaguchi T., Shimojo K., Imura T. and Bugnion L. 2011, Effect of flexible protection on slope failure. *Journal of the Japan Society of Erosion Control Engineering,* Vol. 64, No. 1, pp. 25-29. (in Japanese with English Abstract)
11) DeNatale J. S., Iverson R. M., Major J. J., LaHusen R.G., Fliegel G. L. and Duffy J. D. 1999, Experimental Testing of flexible barriers for containment of debris flows. *Open-file report* 99-205.
12) Doi, Y, Minami N., Yamada T. and Amada T. 2000, Experimental analysis of woody debris trapping by impermeable type sabo dam, filled with sediment, -woody debris carried by debris flow-. *Journal of the Japan Society of Erosion Control Engineering,* Vol. 52, No. 6, pp. 49-55. (in Japanese)
13) Fujita M., Mizuyama T. and Musashi Y. 1998, Functions of sabo dams with horizontal slit. *Annual Journal of Hydraulic Engineering, JSCE,* Vol. 42, pp. 931-936. (in Japanese)
14) Fujita M., Mizuyama T. and Musashi Y. 2001, Sediment runoff control by a series of sabo dams. *Annual Journal of Hydraulic Engineering, JSCE,* Vol. 45, pp. 697-702. (in Japanese)
15) Fukuda K., Matsumoto K., Taniguchi K., Tsubakishita Y., Shimizu M. and Mizuyama T. 2002, Research of sediment control by slit sabo dam during floods. *Journal of the Japan Society of Erosion Control Engineering,* Vol. 54, No. 6, pp. 25-34. (in Japanese with English Abstract)
16) Gonda Y. 2009, Function of a debris-flow brake. *International Journal of Erosion Control Engineering,* Vol. 2, No. 1, pp. 15-21.
17) Gotoh H., Sakai T. and Hayashi M. 2002, Lagrangian model of drift-timbers induced flood by using moving particle semi-implicit model. *Journal of Hydroscience and Hydraulic Engineering, JSCE,* Vol. 20, No. 1, pp. 95-102.
18) Gotoh H., Harada E., Sakai T. and Goda K. 2006, Numerical simulation of blocking process of grid-type dam by debris flow. *Annual Journal of Hydraulic Engineering, JSCE,* Vol. 50, pp. 739-744. (in Japanese)
19) Hasegawa Y., Oda A., Mizuyama T., Izumi I. and Abe H. 2004, Evaluation of the function of slit dams through hydraulic model experiments. *Internationals Symposium Interpraevent,* riva/trient, pp. 107-118.
20) Honda N. and Egashira S. 1997, Prediction of debris flow characteristics in mountainous torrents, *Proceedings of First Conference on Debris-Flow Hazards Mitigation: Mechanics, Prediction, and Assessment, California, ASCE,* pp. 707-716.
21) Horiuchi S., Tabata S., Ono S., Itoh T. and Mizuyama T. 2011, Experimental study on runoff control for sediment passing through upper parts of a grid type high dam. *Journal of the Japan Society of Erosion Control Engineering,* Vol. 64, No. 1, pp. 11-16. (in Japanese with English Abstract)
22) Hu K., Wei F., and Li Y. 2011, Real-time measurement and preliminary analysis of debris-flow impact force at Jiangjia ravine, *China. Earth Surface Process and Landforms* 36, pp. 1268-1278.

23) Huang X. and Garcia M. H. 1997, A perturbation solution for Bingham-plastic mudflows. *Journal of Hydraulic Engineering, ASCE,* Vol. 123, No. 11, pp. 986-994.
24) Huang H.P., Yang K.C., and Lai S.W. 2007, Impact force of debris flow on filter dam. *Geophysical Research European Geosciences Union,* Vol. 9, 03218.
25) Hungr O., Morgan G.C., and Kellerhals R. 1984, Quantitative analysis of debris torrent hazards for design of remedial measures. *Canadian Geotech. J.,* 21, pp. 663-677.
26) Hunt B. 1994, Newtonian fluid mechanics treatment of debris flows and avalanches. *Journal of Hydraulic Engineering, ASCE,* Vol. 120, No. 12, pp. 1350-1363.
27) Imai K., Miyamoto N. and Mizuyama T. 1989, Test of a debris-flow breaker at the Kamikamihori Valley, Mt. Yakedake (Part-2). *Journal of the Japan Society of Erosion Control Engineering,* Vol. 42, No. 2, pp. 16-20. (in Japanese)
28) Ikeya H. and Uehara S. 1980, Experimental study about the sediment control of slit sabo dam, *Journal of the Japan Society of Erosion Control Engineering,* Vol. 32, No. 3, pp. 37-44. (in Japanese)
29) Ikeya H. 1989, Debris flow and its countermeasures in Japan. *Bulletin of the International Association of Engineering Geology,* pp. 15-33.
30) Iverson R.M. 1997, The physics of debris flows. Reviews of Geophysics, Vol.35, Issue 3, pp. 245-296.
31) Izumi I., Watanabe M., Takemura T. and Mizuyama Y. 1982, Test of a bottom infiltration screen in Ohsawa Fam, Mt. Fuji. *Journal of the Japan Society of Erosion Control Engineering,* Vol. 34, No. 3, pp. 45-50. (in Japanese)
32) Johnson P.A., and Richard H.M. 1989, Slit dam design for debris flow mitigation. *Journal of Hydraulic Engineering, ASCE,* Vol. 115, No. 9, pp. 1293-1296.
33) Katatani M. and Yamada T. 2006, Study on new type slit dam development for reduction of slit blockade by drift woods. *Journal of the Japan Society of Erosion Control Engineering,* Vol. 59, No. 3, pp. 23-31. (in Japanese with English Abstract)
34) Kim N., Nakagawa H., Kawaike K. and Zhang H. 2013, A study on debris flow deposition by the arrangement of sabo dam. *Annual Journal of Japan Society of Civil Engineering, JSCE,* Vol. 69, No. 4, pp. 97-102.
35) Kim Y., Nakagawa H., Kawaike K. and Zhang H. 2012a, Numerical analysis of debris flow deposition on breaker structure. *Annual Journal of Japan Society of Civil Engineering, JSCE,* Vol. 68, No. 4, pp. 1-6.
36) Kim Y., Nakagawa H., Kawaike K. and Zhang H. 2012b, Numerical and experimental study on debris-flow breaker. *Annuals of the Disaster Prevention Research Institute, Kyoto University,* No. 55 B, pp. 471-481.
37) Kim Y., Nakagawa H., Kawaike K., and Zhang H. 2012c, An experimental study on impact force for verification of 3D debris flow model. *31st Japan Society for Natural Disaster Science annual meeting*, pp.159-160.
38) Kim Y., Nakagawa H., Kawaike K., and Zhang H. 2013a, Study on the function of closed-type sabo dam with a flap by debris flow. *12th international Symposium on River Sedimentation, ISRS.* (in printing)
39) Kim Y., Nakagawa H., Kawaike K. and Zhang H. 2013b, Study on characteristic analysis of closed-type sabo dam with a flap due to dynamic force of debris flow. *Annuals of the Disaster Prevention Research Institute, Kyoto University,* No. 56 B. (In printing)
40) Kim, Y., Nakagawa, H., Kawaike, K., and Zhang, H. 2013c, Study on impact force of debris flow due to variable of check dam shape. *Journal of Disaster Research,* Vol.8, No.1, pp.195-196.
41) Kiyono M., Miyakoshi H., Uehara S. and Mizuyama T. 1986, Test of a debrisflow braker in Valley Kamikami, Mt. Yake-dake. *Journal of the Japan Society of Erosion Control Engineering,* Vol. 39, No. 3, pp. 15-19. (in Japanese)

42) Kurihara J., Hukujawa M. and Iwata Y. 1987, The report on mud flows occurred at Osawa River, Mt. Fuji and the function of the screen dam (prompt report). *Journal of the Japan Society of Erosion Control Engineering,* Vol. 40, No. 3, pp. 23-28. (in Japanese with English Abstract)
43) Lichtenhahn C. 1973, Die Berechnung von Sperren in Beton und Eisenbeton. *In: Kolloquium über Wildbachsperren, Mitteilungen der Forstlichen Bundesanstalt Wien,* Vol. 102, pp. 91-127.
44) Lien H.P. 2003, Design of slit dams for controlling stony debris flows. *International Journal of Sediment Research,* Vol. 18, No. 1, pp. 74-87.
45) Masuda S., Mizuyama T., Fujita M., Abe H., Oda A. and Otsuki H. 2002, Fundamental study about sediment runoff control by a series of slit sabo dam. *Journal of the Japan Society of Erosion Control Engineering,* Vol. 54, No. 6, pp. 39-42. (in Japanese)
46) Miyazawa N., Tanishima T., Sunada K. and Oishi S. 2003, Debris-flow capturing effect of grid type steel-made sabo dam using 3D distinct element method. *Proceedings of the Third Conference on Debris-Flow Hazards Mitigation: Mechanics,* Prediction, and Assessment, Switzerland, Rotterdam, pp. 527-538.
47) Mizuno H., Mizuyama T., Minami N. and Kuraoka S. 2000, Analysis of simulating debris flow captured by permeable type dam using distinct element method. *Journal of the Japan Society of Erosion Control Engineering,* Vol. 52, No. 6, pp. 4-11. (in Japanese)
48) Mizuno H., Bovolin V. and Minami N. 2001, Study on effectiveness of reducing peak discharge of muddy debris flow with open type dams. *Journal of the Japan Society of Erosion Control Engineering,* Vol. 53, No. 6, pp. 45-54. (in Japanese with English Abstract)
49) Mizuno H., Bovolin V. and Nakano M. 2002, Study on forecasting hydrograph of mudflow passing through a slit dam. *Journal of the Japan Society of Erosion Control Engineering,* Vol. 54, No. 5, pp. 3-11. (in Japanese with English Abstract)
50) Mizuyama T. 1979, Computational method and some considerations on impulsive force of debris flow acting on sabo dams. *Journal of the Japan Society of Erosion Control Engineering,* 112, pp. 40-43 (in Japanese)
51) Mizuyama T., Abe S. and Yajima S. 1989, Discharge coefficient and depositional shape of slit type sabo dam. *Journal of the Japan Society of Erosion Control Engineering,* Vol. 42, No. 4, pp. 28-30. (in Japanese)
52) Mizuyama T., Abe S., Yajima S. and Ido K. 1990, Application of a two-dimensional river bed routing method to slit sabo dams. *Journal of the Japan Society of Erosion Control Engineering,* Vol. 42, No. 5, pp. 21-28. (in Japanese)
53) Mizuyama T., Kobashi S. and Mizuno H. 1995, Control of passing sediment with grid type dam. *Journal of the Japan Society of Erosion Control Engineering,* Vol. 47, No. 5, pp.8-13. (in Japanese with English Abstract)
54) Mizuyama T. and Mizuno H. 1997, Prediction of debris flow hydrographs passing through grid type control structures. *Proceedings of First Conference on Debris-Flow Hazards Mitigation: Mechanics,* Prediction, and Assessment, California, ASCE, pp. 74-82.
55) Mizuyama T., Ougi Y. and Abe S. 1999, Experiments on debris flow control dams with gates. *Journal of the Japan Society of Erosion Control Engineering,* Vol. 52, No. 4, pp. 39-41. (in Japanese)
56) Mizuyama T. and Oda A. 2000, Sediment control with a slit sabo dam in a debris flow torrent. *Journal of the Japan Society of Erosion Control Engineering,* Vol. 52, No. 6, pp. 56-60. (in Japanese)
57) Mizuyama T. 2008, Structural countermeasures for debris flow disaster. *International Journal of Erosion Control Engineering,* Vol. 1, No. 2, pp. 38-43.
58) National Institute for Land and Infrastructure Management, Japan. 2011, Management of sediment-related risks. *Associated program on flood management.*

59) Nakagawa H., Takahashi T. and Ikeguchi M. 1994, Driftwood behavior by overland flood flows. *Journal of Hydroscience and Hydraulic Engineering, JSCE,* Vol. 12, No. 2, pp. 31-39.
60) Nakagawa H., Inoue K., Ikeguchi M. and Tsubono T. 1995, Behavior of driftwood and the process of its damming up. *Journal of Hydroscience and Hydraulic Engineering. JSCE,* Vol. 13, No. 2, pp. 55-67.
61) Nakagawa H. and Takahashi T. 2001, Behavior of driftwood debouched from the ohno river into the bay of beppu during the 1990 flood. *Journal of Hydroscience and Hydraulic Engineering, JSCE,* Vol. 45, pp. 913-936.
62) Nakagawa H., Satofuka Y. and Takahama J. 2002a, Water Induced Hazard – I. *Sub Text Book,* M. Sc. in Water Resources Engineering, Institute of Engineering, Nepal
63) Nakagawa H., Takahashi T., Satofuka, Y. and Kawaike, K. 2002b, Evaluation of efficiency of sabo facilities by means of numerical simulation methods. *Annual Journal of Hydraulic Engineering, JSCE,* Vol. 46, pp. 665-670. (in Japanese)
64) Nakagawa H., Takahashi T., Satofuka Y. and Kawaike K. 2003, Numerical simulation of sediment disasters caused by heavy rainfall in Camuri Grande basin, Venezuela 1999, *Proceedings of the Third Conference on Debris-Flow Hazards Mitigation: Mechanics,* Prediction, and Assessment, Switzerland, Rotterdam, pp. 671-682.
65) Nakatani K., Wada T., Satofuka Y. and Mizuyama T. 2008, Development of "Kanko 2D (Ver.2.00)," a user-friendly one- and two-dimensional debris flow simulator equipped with a graphical user interface. *International Journal of Erosion Control Engineering,* Vol. 1, No. 2, pp. 62-72. (in Japanese with English Abstract)
66) Nishikawa S., Wada H., Tajima H., Mizuyama T. and Oda A. 1999, Sediment trap reliability of the semi-open slit sabo dam installed in debris flow prone torrents. *Journal of the Japan Society of Erosion Control Engineering,* Vol. 52, No. 4, pp. 42-44. (in Japanese)
67) Nishimoto H. 2011, Discussion on the transition of idea about sediment control effect functioned by check dam. *Journal of the Japan Society of Erosion Control Engineering,* Vol. 64, No. 4, pp. 46-51. (in Japanese with English Abstract)
68) Nisimoto H., Ishikura K., Mizuyama T. and Santosa U.B. 1994, Behavior of a debris-flow on the debris-flow breaker at Mount Yake-dake. *Journal of the Japan Society of Erosion Control Engineering,* Vol. 46, No. 6, pp. 21-24. (in Japanese)
69) Niwa S., Ohno R., Yoshimatsu H. and Kashiyama K. 2009, Debris flow simulation based on stabilized FEM in penetration type sabo dam. *Journal of the Japan Society of Erosion Control Engineering,* Vol. 62, No. 1, pp. 11-22. (in Japanese with English Abstract).
70) Okubo S., Mizuyama T., Kaba M. and Ido K. 1997, Sediment control by a series of slit-sabo dams. *Journal of the Japan Society of Erosion Control Engineering,* Vol. 50, No. 2, pp.14-19. (in Japanese with English Abstract)
71) Okuda S., Suwa H., Okuunishi K., Nakano M. and Yokoyama K. 1977, Synthetic Observation on Debris flow, Part 3. Observation at valley Kamikamihorizawa of Mt. Yakedake in 1976. *Annuals of the Disaster Prevention Research Institute, Kyoto University,* No. 21 B-1, pp. 277-296. (in Japanese with English Synopsis)
72) Okuda S, Suwa H, Okunishi K, Yokoyama K, Nakano M, Ogawa K, and Hamana S. 1978, Synthetic observation on debris flow (part 4) observation in 1977, *Disaster Prevention Research Institute Annals 21,* Vol. 1, pp. 277-296. (in Japanese with English synopsis)
73) Osti R. and Egashira S. 2008, Method to improve the mitigative effectiveness of a series of check dams against debris flows. *Hydrological Processes, Wiley InterScience,* Vol. 22, pp. 4986-4996.
74) Ozaki Y., Kamogawa Y., Mizuyama T., Kasai S. and Shima J. 1998, A debris flow with woody debris trapped by a steel-pipe gridded sabo dam. *Journal of the Japan Society of Erosion Control Engineering,* Vol. 51, No. 2, pp. 39-44. (in Japanese)

75) Sato K., Uehara S., Mizuyama T. and Kasai S. 2001, Structral behavior of open type steel dam hit by stony debris flow. *Journal of the Japan Society of Erosion Control Engineering,* Vol. 53, No. 6, pp. 61-65. (in Japanese)
76) Satofuka Y. and Mizuyama T. 2005, Numerical simulation on a debris flow in a mountainous river with a sabo dam. *Journal of the Japan Society of Erosion Control Engineering,* Vol. 58, No. 1, pp. 14-19. (in Japanese with English Abstract)
77) Satofuka Y. and Mizuyama T. 2006, Numerical simulation on debris flow control by a grid dam. *The 6th Japan-Taiwan Joint Seminar on Natural Hazard Mitigation.* (in CD-ROM)
78) Scheidl C., Chiari M., Kaitna R., Müllegger M., Karawtschuk A., Zimmermann T., and Proske D. 2012, Analysisng Debris-Flow Impact Models, Based on a Small Scale Modelling Approach. *Surv Geophys (2013)* 34, pp. 121-140.
79) Seto T., Kasai S., Yamaguchi K. and Mizuyama T. 1998, State of stony debris flow by the open type steel pipe gridded sabo dam. *Journal of the Japan Society of Erosion Control Engineering,* Vol. 51, No. 3, pp. 19-26. (in Japanese with English Abstract)
80) Shieh C.L., Ting C.H., and Pan H.W. 2008, Impulsive force of debris flow on a curved dam. *International Journal of Sediment Research 23,* pp. 149-158.
81) Shimizu Y. and Osada K. 2008, Numerical simulation on the driftwood behavior in open-channel flows by using distinct element method. *The Eighth International Conference on Hydro-Science and Engineering,* Nagoya, Japan.
82) Shibuya H., Katsuki S., Ohsumi H., Ishikawa N. and Mizuyama T. 2010, Experimental study on wood debris trap performance of drift wood capturing structure. *Journal of the Japan Society of Erosion Control Engineering,* Vol. 63, No. 3, pp. 34-41. (in Japanese with English Abstract)
83) Shibuya H., Katsuki S., Ohsumi H. and Ishikawa N. 2011, 3D-DEM simulation on trap performance of drift wood capturing structure. *Journal of the Japan Society of Erosion Control Engineering,* Vol. 63, No. 6, pp. 13-22. (in Japanese with English Abstract)
84) Shibuya H., Katsuki S., KokuryoH., Ohsumi H., and Ishikawa N. 2012, Experimental study of load for steel frame check dam caused by debris flow with woody debris. *Journal of the Japan Society of Erosion Control Engineering,* Vol. 65, No. 1, pp. 54-61 (in Japanese with English Abstract)
85) Shima J., Katade R., Takahashi K., Katsuki S. and Ishikawa N. 2011, Probabilistic evaluation on rock capturing performance of series check dam system. *Journal of the Japan Society of Erosion Control Engineering,* Vol. 64, No. 4, pp. 15-24. (in Japanese with English Abstract)
86) Shrestha B.B., Nakagawa H., Kawaike K. and Yasuyuki B. 2008, Numerical simulation on debris flow deposition and erosion processes upstream of a check dam with experimental verification. *Annuals of the Disaster Prevention Research Institute, Kyoto University,* No. 51B, pp. 613-624.
87) Shrestha B. B. 2009, Study on mitigation measures against debris flow disasters with driftwood. Ph.D. Dissertation, *Department of Civil and Earth Resources Engineering, Kyoto University.*
88) Shrestha B.B., Nakagawa H., Kawaike K., BaBa Y. and Zhang H. 2011, Numerical and experimental analysis on deposition process of debris flow with driftwood on the fan. *Journal of Hydroscience and Hydraulic Engineering,* Vol. 29, No. 1, pp. 15-32.
89) Suwa H., and Okuda S. 1983, Deposition of debris flow on a fan surface, Mt. Yakedake, *Japan. Z.* Geo-morph, Vol. 46, pp. 79-101.
90) Suzuki T., Hotta N. and Miyamoto K. 2009, Numerical simulation method of debris flow introducing the non-entrainment erosion rate equation, at the transition point of the riverbed gradient or the channel width and in the area of sabo dam. *Journal of the Japan Society of Erosion Control Engineering,* Vol. 62, No. 3, pp. 14-22. (in Japanese with English Abstract)

91) Takahashi T. and Tsujimoto H. 1984, Numerical simulation of flooding and deposition of debris flow. *Annuals of the Disaster Prevention Research Institute, Kyoto University,* No. 27 B-2, pp. 467-485. (in Japanese with English Synopsis)
92) Takahashi T. 1981, Debris flow, *Annual Review of Fluid Mechanics,* Vol. 13, pp. 57-77.
93) Takahashi T. 1991, Debris flow, Monograph Series of IAHR, *Balkema,* pp. 1-165.
94) Takahashi T., Nakagawa H., Satofuka Y. and Wang H. 2000, Stochastic model of blocking for a grid type dam by large boulders in a debris flow. *Annuals of the Disaster Prevention Research Institute, Kyoto University,* No. 43 B-2, pp. 287-294. (in Japanese with English Synopsis)
95) Takahashi T., Nakagawa H., Satofuka Y. and Kawaike, K. 2001a, Flood and sediment disasters triggered by 1999 rainfall in Venezuela. *A river restoration plan for an alluvial fan, Journal of Natural Disaster Science,* Vol. 23, No. 2, pp. 65-82.
96) Takahashi T., Nakagawa H., Satofuka T. and Wang H. 2001b, Simulation of debris flow deposition by open-type sabo dam. *Annuals of the Disaster Prevention Research Institute, Kyoto University,* No. 44 B-2, pp. 185-191. (in Japanese with English Synopsis)
97) Takahashi T., Nakagawa H., Satofuka Y. and Wang H. 2001c, Stochastic model of blocking for a grid type dam by large boulders in a debris flow. *Annual Journal of Hydraulic Engineering, JSCE,* Vol. 45, pp. 703-708. (in Japanese with English Abstract)
98) Takahara T. and Matsumura K. 2008, Experimental study of the sediment trap effect of steel grid type sabo dam. *Journal of the Japan Society of Erosion Control Engineering,* Vol. 1, No. 2, pp. 73-78.
99) Takahashi T. 2007, Debris flow: Mechanics, Prediction and Countermeasures. *Taylor & Francis/Balkema,* pp. 1-448.
100) Varnes D. J. 1984, Landslide hazard zonation: a review of principles and practice. *United Nations Educational,* Scientific and Cultural Organization. pp. 1-63.
101) Volkwein A. 2005, Numerical simulation of flexible rockfall protection systems. *Proc. Computing in Civil Engineering, ASCE,* pp. 1-11.
102) Wang H. 2001, Study of function and performance designing of grid type sabo-dam. Ph.D. Dissertation, *Department of Civil and Earth Resources Engineering, Kyoto University.* (in Japanese)
103) Watanabe M., Mizuyama T. and Uehara S. 1980, Review of debris flow countermeasure facilities, *Journal of the Japan Society of Erosion Control Engineering,* Vol. 32, No. 4, pp. 40-45. (in Japanese)
104) Watanabe M., and Ikeya H. 1981, Investigation and analysis of volcanic mud flows on Mt Sakurajima, Japan. *Erosion and Sediment Transport Measurement (Proceedings of the Florence Symposium). IAHS Publ.* No. 133, pp. 245-256.
105) Yamamoto A., Yamamoto S., Toriihara M., and Hirama K. 1998, Impact Load on Sabo Dam due to Debris flow. *Journal of the Japan Society of Erosion Control Engineering,* Vo1. 51, No. 2, pp. 22-30. (in Japanese with English Abstract)
106) Yoshida K., Yamaguchi M. and Mizuyama T. 2011, Field survey on the capture of debris flow with steel open sabo dam. *Journal of the Japan Society of Erosion Control Engineering,* Vol. 63, No. 5, pp. 43-46. (in Japanese)
107) Zhang S. 1993, A Comprehensive Approach to the Observation and Prevention of Debris flow in China. *Natural Hazards 7,* pp. 1-23.

CHAPTER 2

HYDRAULIC MODEL TEST ON DEBRIS-FLOW BREAKER

2.1 General

In recent years, many researches have been carrying out experiments regarding the efficient function of sabo dams, which have a great impact on ecology and the landscape. Such dams are also surcharged with the impulsive forces of the debris flows. The front part of the flow is very important and complex in the case of debris flow where there is an accumulation of large boulders. It is important to reduce or decelerate the velocity of the front part of a debris flow for the safety of the downstream area because the destructive power of a debris flow is much greater than that of the clear fluid. Photo 2.1 shows the debris-flow breakers.

(a) After removal of the July 21, 1985 debris flow deposits and the construction of sidewall reinforcements

(b)Boulder deposits of the July 21, 1985 debris flow trapped on the breaker (Photo taken July 22, 1985)

Photo 2.1 Debris-flow breaker (Suwa et al. 2009)

Usually, sediment control structures temporarily stores the excess sediment in the upstream pockets of the sabo dam and reduce the discharge safely. The capacity of a sabo dam to control sediment is determined by the sediment storage capacity between the stable slope and the

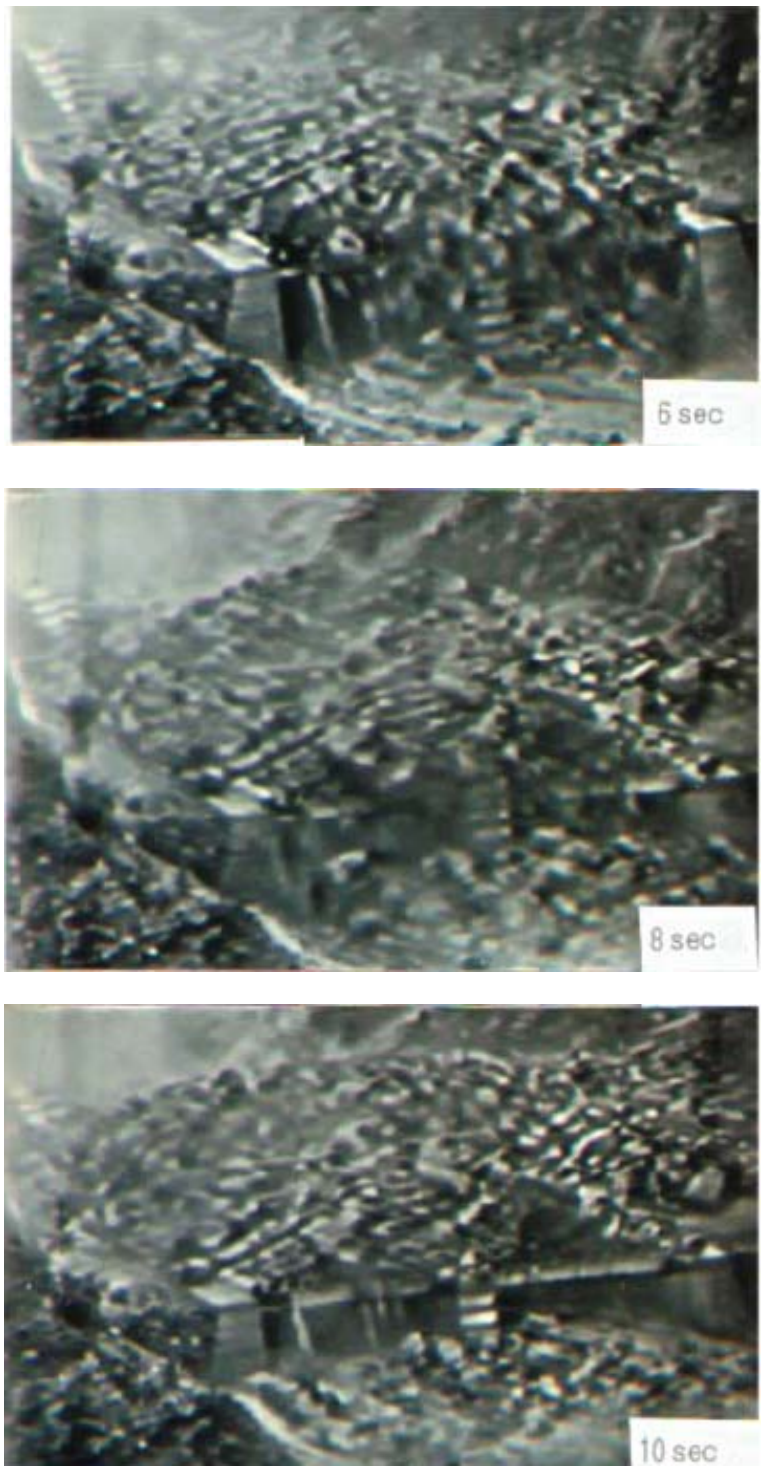

(Source: Mizuyama 2008)

Photo 2.2 Debris-flow breaker stopping the front portion of a debris flow

temporary slope of accumulated sediments. Therefore, a sabo dam should control the increasing amount of sediment discharge due to the gradual acceleration of debris flow. Debris-flow breakers are designed to reduce the debris flow velocity. By slowing and depositing the surge front of the debris flow, the downstream reaches the stream channels and settlement areas which are exposed to considerable dynamic impact. Photo 2.2 shows the videotaped footage showing the debris-flow breaker effectively stopping a debris flow front (Mizuyama 2008). In an array of different debris flow mitigation structures, debris-flow breakers are almost in the upstream position. The debris-flow breaker should retain at least the volume of surge wave. Numerous functional structures with modern sediment management systems could be installed downstream of the breakers.

Debris-flow breakers have advantages in not only reducing the velocity, but also in creating a suitable narrow or wider area that is cost-efficient, simply designed, and easily repaired and maintained, if their size and location are well planned before construction, as shown in Photo 2.3. The features in photo (a) show the sediment deposited on a debris-flow breaker being removed after the debris flow event to prepare for the next debris flow, while photo (b) shows the easiness of constructing a narrow area (ICHARM 2008). Using the debris-flow breaker upstream of a sabo dam could be more effective in controlling sediment discharge than not using a debris-flow breaker at all (Kim et al. 2012a, 2012b). Likewise, the debris-flow breakers are very useful in many other ways.

To judge the optimal parameters of debris-flow breakers, an understanding of the behavior and mechanism of debris flows is needed because the characteristics of debris flows would change due to the geographic environment of the occurrence area and types of debris flows from the contributing factors. Thus, the mechanism between the opening size and blocking size (a physical factor with the greatest influence) under the bed sediments should be analyzed to

(a) Repair the debris for the next debris flow (b) Narrow area

Photo 2.3 Advantages of debris-flow breaker

understand clearly the hydraulic characteristics of the debris-flow breaker.

The open check dam restoration technique has been developed since the second half of the 20th century. A great variety of slightly different devices has been designed and has been tested on empirically based rules. The debris-flow breaker was installed nearly 30 years ago, and was designed to check the boulder dam. In order to clarify the mechanism of debris-flow breakers, monitoring and field surveys were conducted by Izumi et al. (1982) and Kurihara et al. (1987) at Mt. Fuji, as well as by Kiyono et al. (1986), Imai et al. (1989) and Nisimoto et al. (1994) at Mt. Yake-dake. In addition, Fiebiger (1997) discussed the various types of structures of debris flow countermeasures and their functions. Watanabe et al. (1980) has shown that the spacing of the posts has an effect on the trapping capacity of a slit dam and a screen dam. When the relative spacing is $l_o / d_{max} < 2.0$, where l_o is the spacing of the posts and d_{max} is the maximum diameter of the debris flow, the research indicated that the volume of the debris flow could be reduced by 50% - 70% during peak times, but the total volume of debris flow cannot be reduced. The above studies validated the effectiveness of open-type dams in the prevention of debris flows. They only considered the relative spacing factor in designing the spacing of open-type dams. In addition, many research studies are being carried out to clarify the mechanism for the type of open dam (i.e. slit and grid dams).

The debris-flow breaker (i.e. breaker) is designed to check the boulder dam. The mechanism is that the boulders in the dam lose their buoyancy as soon as the dam arrives at and gets on the board. Namely, it is thought that two phenomena occur when a debris flow crosses the breaker: the pore (mud) water drains through the opening area of the breaker and the pore water pressure near the breaker changes (Gonda 2009). Drainage of the pore water through the breaker increases the sediment concentration of the debris flow increasing the bottom shear stress of the debris flow. Because the breaker is open to the air, the pore water pressure of the debris flow near the breaker decreases instantaneously. As stated above, the debris-flow breaker is one of the open type check dams. However, the debris-flow breaker has a different mechanism in comparison to other open type dams, and the mechanism of the debris-flow breaker structure has not been well explained. Therefore, the objectives of this study are to confirm the mechanism of the debris-flow breaker, to clarify the change in pore water pressure at the breaker, and to evaluate the parameters of the breaker for the design of its structural elements.

Chapter 2 describes the laboratory experiments performed during this research. In addition, an overview of the flume geometry, the measured parameters the measurement techniques, and

the characteristics of sediment material used in the experiments are described. A methodology is proposed to assess the suitability of a variable breaker size and change the pore water pressure on the breaker according to separation of the water between the blocking and opening sizes. The results from the measurements of flow and sediment discharges, sediment concentration, flow pattern, travel length, and deposit depth on the debris-flow breaker are shown. These were used to validate the numerical model described in detail in Chapter 3.

2.2 Experimental Set-up for Debris-Flow Breaker

To clarify the characteristics of debris flows under the three bed sediments, as well as to detect the functions of debris-flow breakers, the experiments were conducted in a flume located at the Ujigawa Open Laboratory (UOL) of the Disaster Prevention Research Institute (DPRI), Kyoto University, Kyoto, Japan.

2.2.1 Description of Hydraulic Model

A schematic view of the experimental setup is shown in Figure 2.1. The flume was composed of two parts between the upstream and downstream. The debris flow experimental facility consists of a 500 cm long horizontal smooth flume with a rectangular section 10 cm wide and 14 cm high at the upstream section of the flume. One side of the wall is made of

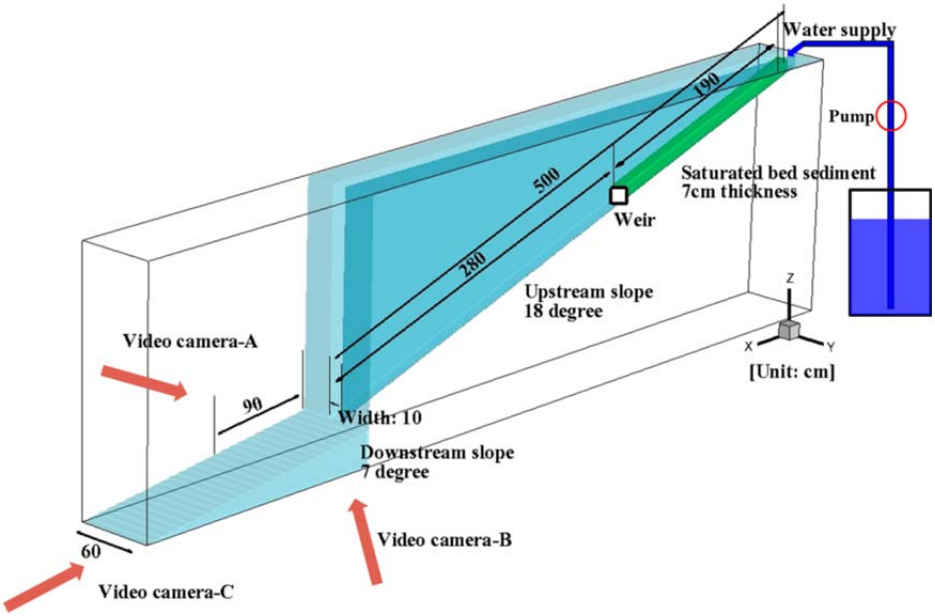

Figure 2.1 Sketch of experimental setup

transparent glass and the other side is opaque, made of PVC. The slope of the flume can be controlled freely using the fixed pulley. The downstream flume is a 200 cm long horizontal smooth flume with a rectangular section 60 cm wide, 20 cm high and has a flat bottom. Both sides of the walls are made of transparent glass, and the slope of the flume can be controlled freely. The slopes of the flumes are set at 18º in the upstream and 7º in the downstream. The experimental facility and its different parts (upstream and downstream) are illustrated in Photo 2.4.

Debris flow is produced by supplying a constant water discharge of 300 cm^3/sec for 10 sec from the upstream end of the flume. Details of the experimental setup for generation of the debris flow are shown in Photo 2.5. Debris flow velocity, the radius of the boulder, and approaching height are very important factors to discuss in the characteristics of debris flows. Each experiment used three different generation methods. Itoh et al. (2011) explained the generation methods of debris flow as follows:

A) Type- NL: Natural landslide dam break
B) Type-U: Sediment and water is supplied steadily in the upstream end of the channel.
C) Type-QS: Bed sediment is set on the bed in an upstream reach of the channel, saturating the upstream sediment with water, and supplying the input discharge from upstream.

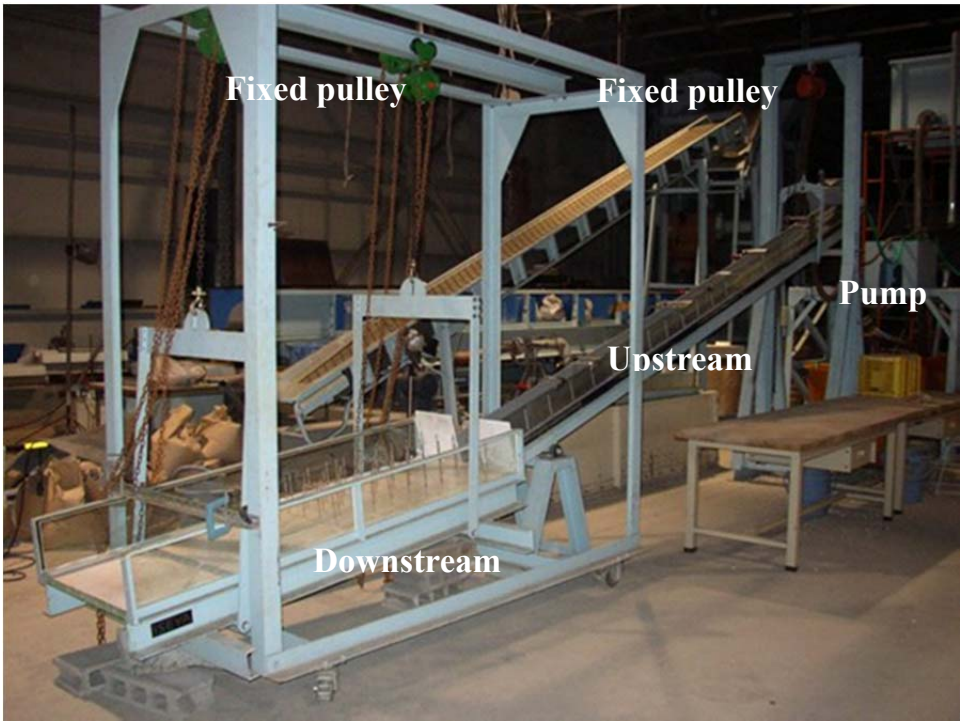

Photo 2.4 Experimental flume

(a) Generation (b) Water supply system

Photo 2.5 Experimental flume for debris flow generation

In most studies, type-U has been used for debris flow generation. In this study, the phenomenon of the debris flow is approximated by the type-QS generation method. As the generation type is QS, the sediment composition and degree of saturation might not be uniform throughout the sediment layer. In addition, the standard size of the boulder cannot be measured when a debris flow hits the obstacle. Therefore, the experiments were repeated several times under identical conditions. Debris flows produced in the experiments are the stony type of debris flows and the largest particles are accumulated in the forefront.

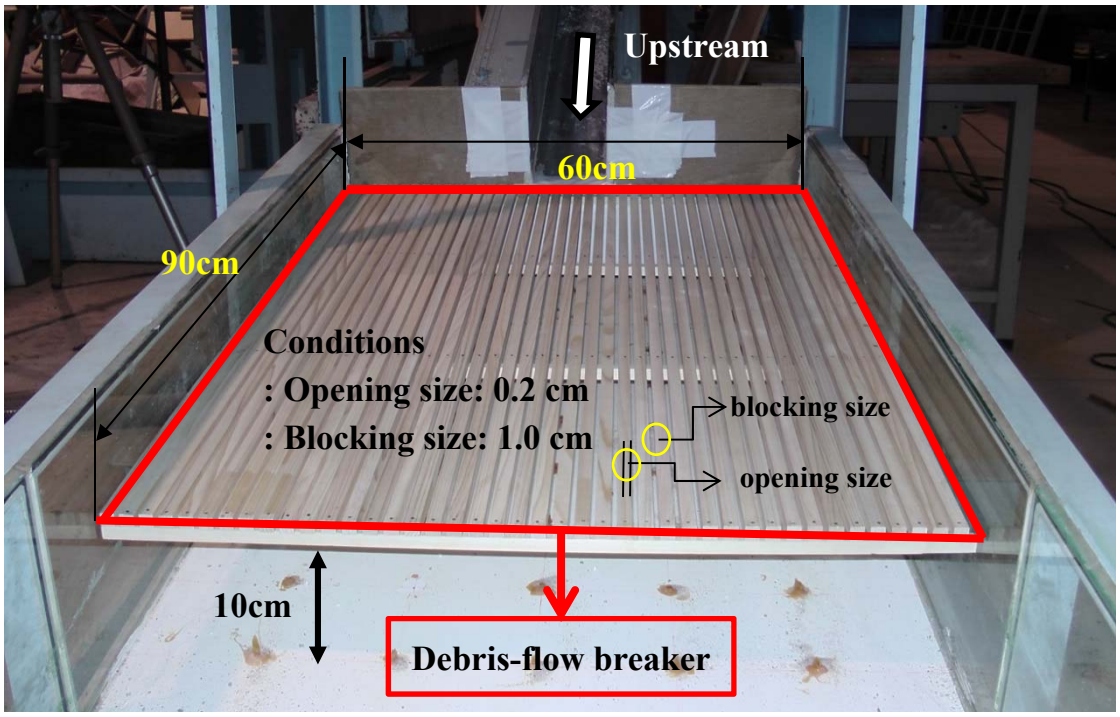

Photo 2.6 Installation of debris-flow breaker

2.2.2 Experimental Conditions

The debris-flow breaker has two parameters i.e. the opening and blocking area. The pore water pressure can be changed by the opening area. To confirm the relationship of the parameters of the breaker, the experiments were conducted with various conditions under the three bed sediments.

Photo 2.6 shows the installation of the debris-flow breaker in the downstream flume. The debris-flow breakers are made of wood, and the parameters are 90 cm long and 60 cm wide. These structures have opening (l_o = 0.2, 0.4, and 0.6 cm) and blocking (l_b = 1, 3, and 6 cm) sizes. Figure 2.2 shows the definition of the breaker properties and conditions. Table 2.1 shows the experimental conditions. The definition of case number is that the first number denotes the blocking size, the second number denotes the opening size, and the letter denotes the sediment

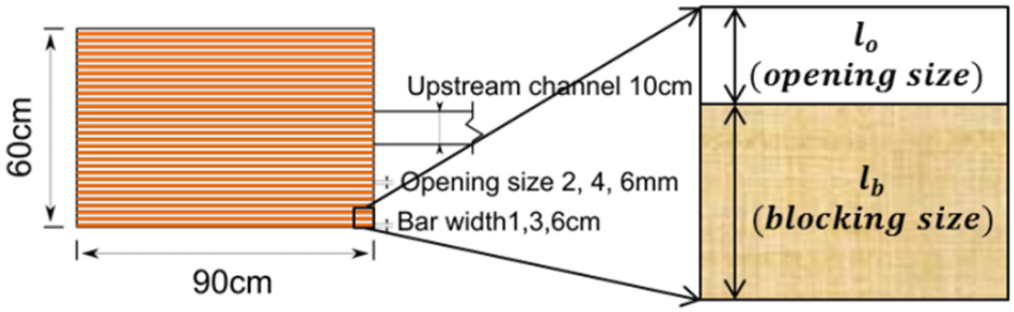

Figure 2.2 Definition of breaker properties

Table 2.1 Properties of bed sediment material (size unit: cm)

	Bed sediment	*Upstream*	*Downstream*	*Blocking size*	*Opening size*
Case-0-0.0-A,B,C	A, B, C	18º	7º	×	×
Case-1-0.2-A,B,C				1.0	0.2
Case-1-0.4-A,B,C					0.4
Case-1-0.6-A,B,C					0.6
Case-3-0.2-A,B,C				3.0	0.2
Case-3-0.4-A,B,C					0.4
Case-3-0.6-A,B,C					0.6
Case-6-0.2-A,B,C				6.0	0.2
Case-6-0.4-A,B,C					0.4
Case-6-0.6-A,B,C					0.6
Case-0-0.0-B (5º)	B	18º	5º	0.0	0.0
Case-1-0.2-B (5º)				1.0	0.2

used. The slopes of the flumes are set at 18º in the upstream and 7º in the downstream. The experiments were experimented for the debris-flow breaker in the downstream using 31 conditions. The debris-flow breaker was installed in the downstream flume, which has a depth of 10 cm with a 7º slope in the downstream from the bottom. The reason for having the depth is that the fine sediments and water will drop through the opening area of the breaker.

2.2.3 Sediment Properties

To generate the stony debris flow, various materials can be used, mixing sediment with gravel and silica sands. For the sediments used in the experiments, silica sands (S1, S2, S3, S4, S5, and S6) and gravel (G1) are mixed in equal proportion by weight to prepare bed sediment-A. Silica sands (S1, S2, S3, S4, S5, and S6) in proportion (1.6, 1.5, 1, 1, 1, and 0.7) and gravel (G1) in (1.7) by weight are mixed to prepare bed sediment-B. Silica sands (S1, S2, S3, S4, S5, and S6) in proportion (2.6, 1.7, 0.7, 0.7, 0.7, and 0.6) and gravel (G1) in (2.0) by weight are mixed to prepare the bed sediment-C. Table 2.2 and Figure 2.3 show each of the sediments of median grain diameters and mixing ratio, and Figure 2.4 shows particle size distributions of the prepared material for bed sediment-A, bed sediment-B, and bed sediment-C. The bed sediments have an angle of repose, $\tan\phi=0.7$, and sediment density, $\sigma=2.65$ g/cm^3, and are saturated with water. Debris flow is produced by supplying a constant water discharge of 300 cm^3/sec for 10 sec from the upstream end of the flume.

Table 2.2 Mixing ratio of bed sediment material

Type		*Gravel*	*S1*	*S2*	*S3*	*S4*	*S5*	*S6*
D_{50} (mm)		10.00	4.26	2.56	1.85	0.94	0.67	0.29
S-A		1	1	1	1	1	1	1
S-B	Ratio	1.7	1.6	1.5	1	1	1	0.7
S-C		2.0	2.6	1.7	0.7	0.7	0.7	0.6

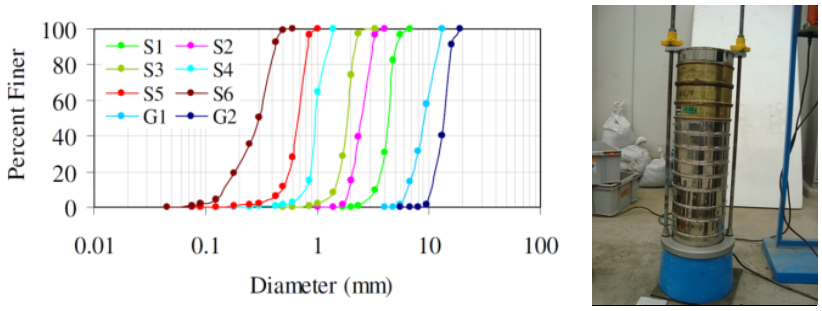

Figure 2.3 Particle size distributions of silica sands and gravels

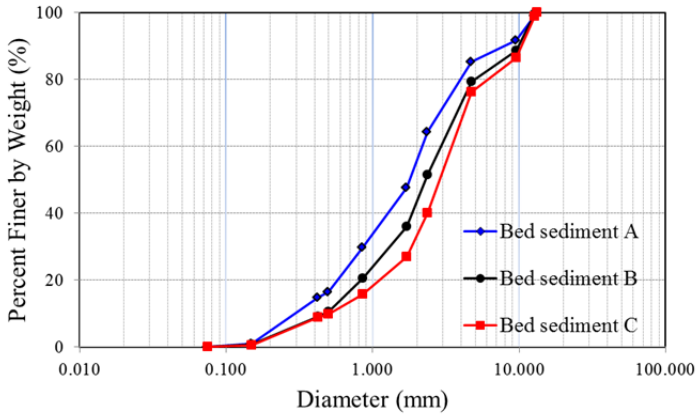

Figure 2.4 Particle size distributions of bed sediments

Properties of sediment material are shown in Table 2.3. The parameters were calculated which are d_{50} and d_{95} by the particle size distributions and the geometric standard deviation (σ_g) using the following equation :

$$\sigma_g = 0.5\left(\frac{d_{84}}{d_{50}} + \frac{d_{50}}{d_{16}}\right) \tag{2.1}$$

The sediment of porosity (k_d) is a term that is used to describe an important physical property of most materials. The porosity of a material is determined by measuring the amount of void space inside, and determining what percentage of the total volume of the material is made up of void space. The porosity was estimated for the three bed sediments due to the experiments. The total porosity is defined as follows:

$$k_d = \frac{pore\ \ volume}{total\ \ bulk\ \ volume} \tag{2.2}$$

Table 2.3 Properties of bed sediment material

	D_{50} (mm)	D_{95} (mm)	σ_g	k_d
Sediment A	1.783	10.871	3.083	0.341
Sediment B	2.304	11.142	3.217	0.353
Sediment C	3.054	11.163	3.140	0.363

2.2.4 Measurement Techniques

Several parameters were measured during the experimental studies, namely: the temporal variations of total flow and sediment discharges, sediment concentration under the three bed sediments, and length and width of the deposition pattern downstream of the debris-flow breaker.

To measure the sediment concentration, total flow, and sediment discharges, first the debris flow under the same identical conditions with the three bed sediments were generated, and then the approaching debris flows were collected into the sample boxes (from 1 to 12) as time passed at the end of the upstream flume. Second, the collected sample was then measured for the calculation of total volume and dry weight by an electronic scale in each box. A digital video camera was used to record the images for calculation of the time of capturing debris flow throughout the experiment from beginning to end. Photo 2.7 shows the process of capturing the debris flow for analysis.

To measure the thickness of deposition (the flow depth plus the deposition thickness in the final stage) accurately, the scale bar and the vernier point gauge are used in each point as shown in Photo 2.8. Currently, some researchers (Shrestha et al. 2011) have been using a scale bar for measuring the deposition process with respect to the time at the downstream flume. This method is very easy to use along with a video camera in experiments. However, when the debris flow is coming downstream, it may be interrupted in the flow direction due to the scale bar on the

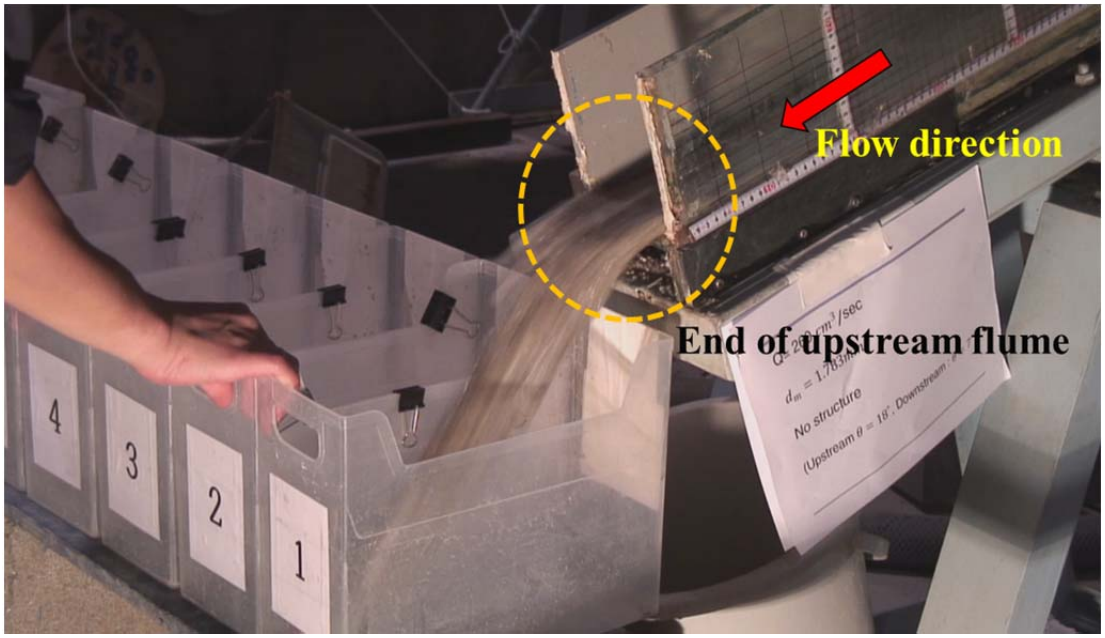

Photo 2.7 Measurement of sediment concentration and total discharge

breaker. Therefore, in these experiments, a scale bar is used to measure the time series of the deposition process and the deposition thickness at the final stage is measured using the Vernier point gauge. Figure 2.5 shows the observation points on the debris-flow breaker. The points can be classified into two categories with the X-axis (A, B, C, and D) towards across the flow direction and the Y-axis (from 1 to 11) the flow direction.

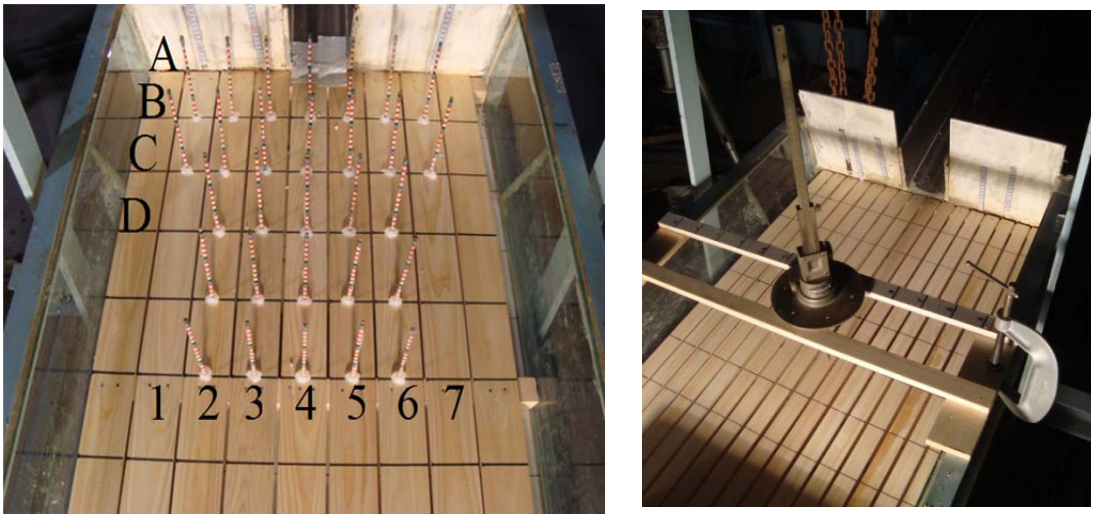

Photo 2.8 Measurement techniques of deposition thickness on the debris-flow breaker

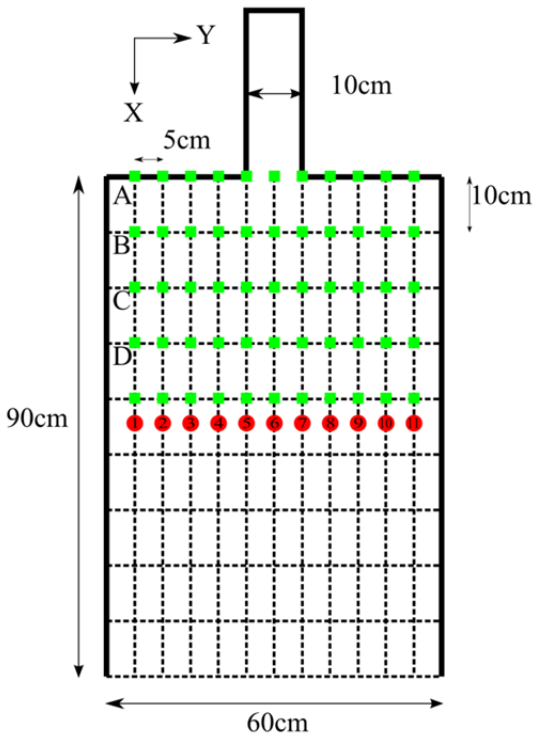

Figure 2.5 Observation points on the debris-flow breaker

The thickness of the deposited debris was measured by taking the difference of the depth measured from the reference top to the bottom of the debris-flow breaker without debris (H) and the depth to the top of the debris after the deposition occurs (h_2). Furthermore, the maximum travel length was measured directly from the end of the upstream flume to the point of the accumulated debris on the breaker at the final state of the experiment, as shown in Figure 2.6.

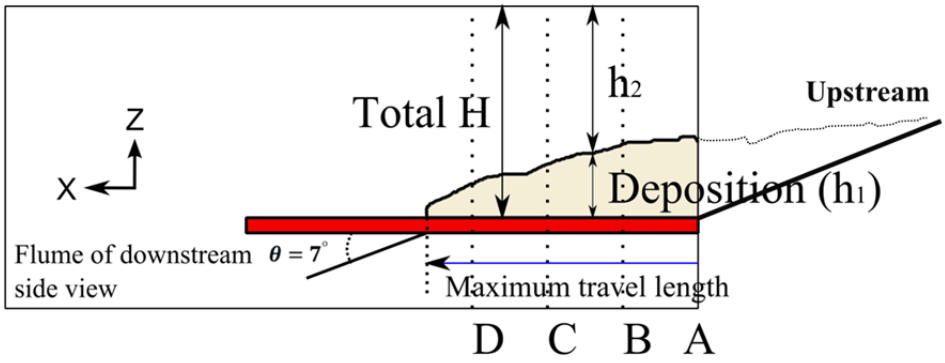

Figure 2.6 Measurement of deposition thickness

2.3 Experimental Results

Fundamental experiments were conducted to investigate debris flow to clarify the characteristics of a debris-flow breaker. The parameters, such as total discharge, flow and sediment discharges, sediment concentration, deposition thickness, deposit formation at the debris-flow breaker, and travel length will be discussed in detail using the comparison of the results of the numerical simulation in Chapter 3. Considering the quantitative and qualitative results from the experiments, the characteristics of debris-flow breakers were discussed, which are summarized below.

2.3.1 Deposition Process

The thicknesses of debris flow mass at flood basin (i.e. the part where we will put the debris-flow breaker later set at just downstream of the channel) were measured using two video cameras: cameras A and B which measures the deposition process at the flood basin. The thickness of the deposit was measured on the video image reading out the elevations of the deposit surface shown by the scale bar set on the flood basin. The vernier point gauge was used to measure thickness of deposits at the final stage of the deposition. To confirm the characteristics of the debris flow deposition at the flood basin, the experiments were conducted

under the two bed slopes of flood basin i.e. 5º and 7º in combination with upstream channel slope of 18º (which is kept constant for both cases) using sediment B only.

Figure 2.7 shows the experimental results under the combination of an 18º upstream channel slope and a 5º flood basin slope. The deposition patterns at different elapsed times after

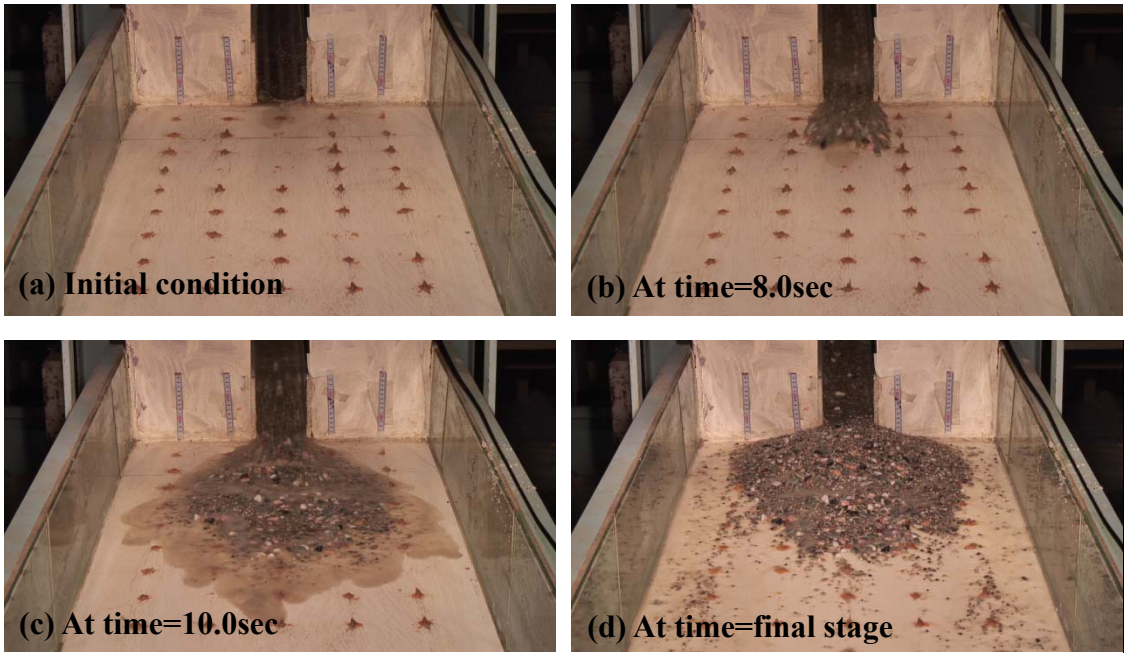

Figure 2.7 Temporal changes of shapes and thicknesses of a debris flow at 5º flood basin slope

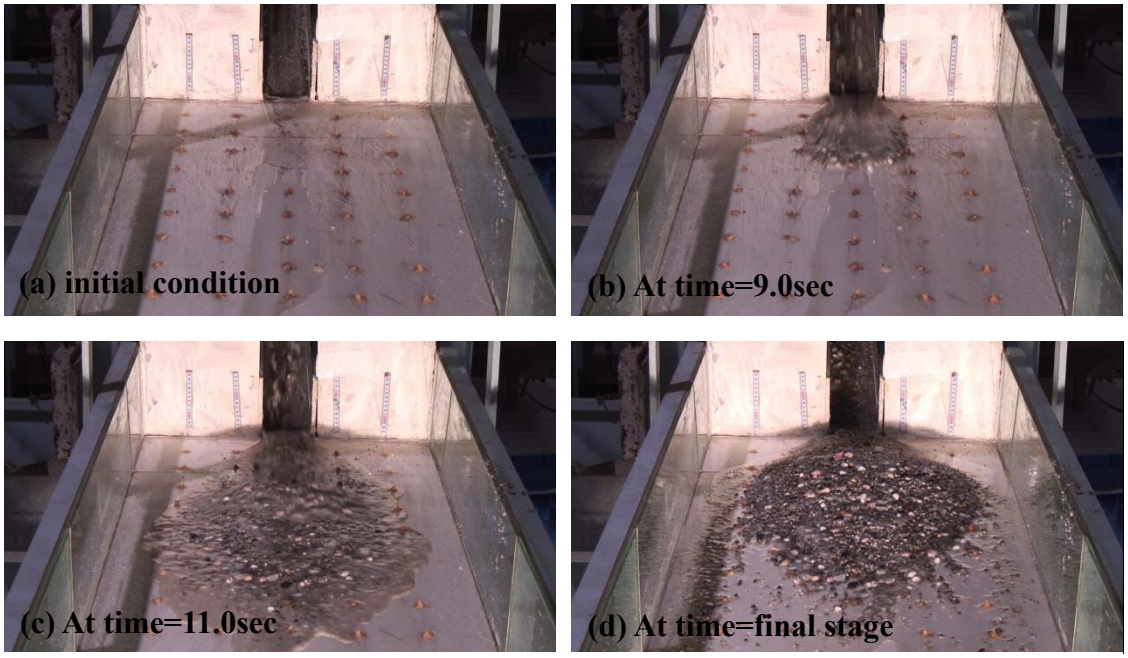

Figure 2.8 Temporal changes of shapes and thicknesses of a debris flow at 7º flood basin slope

the arrival of the flow front at the mouth of the downstream flume (the entrance of the flood basin) are shown in Figure 2.7. The figure clearly reveals that in the first stage, when the debris flow debouches onto the fan area, the path of the flow downstream from the downstream flume outlet was straight, with large boulders, sediments, and water. In the second stage, it began to deposit the sediments with the diffusion rapidly and it quickly reached its maximum travel length while the water and fine sediments detached from the original group due to the physiographic change (conditions of breaker). Finally, the debris was deposited on the fan area without water, as shown in the final stage. The results of the experiment considering a 7º flood basin slope are shown in Figure 2.8. The formation processes of debris flow occur in a similar fashion as the 5º case but the maximum travel length and the diffusion area are different (i.e. increases than the previous case).

Similarly, with debris-flow breaker (opening size 0.4 cm and blocking size 1cm) at the flood basin and sediment B, the process of deposition follow the same procedure as previously described but only difference visualized is that the separation of water with fine sediment particles occurs beneath the breaker due to opening areas at the breaker and of course, the travel length is smaller than that developed in flood basin case as shown in Figure 2.9.

Table 2.4 and Figure 2.10 show the comparison of travel length and fan area for flood basin and breaker case. The value shows the decrease in respective values, if the debris-flow breaker was installed at the flood basin. The result obtained by comparing the maximum diffusion of debris is greatly affected by the bed slope. In other words, it can reduce the diffusion of debris due to the changing bed slope.

So, analyzing above results, it can be concluded that slope of 7º will reflect the deposition and thickness process more clearly during the experiment than 5º slope case due to its wider

(a) 5º flood basin with debris-flow breaker (B) 7º flood basin with debris-flow breaker

Figure 2.9 Final stage of shape and thickness of a debris-flow at breaker

diffusion and good thickness measurability. Hence, for the analysis of hydraulic properties of debris-flow breaker analysis further, 7º slope is fixed.

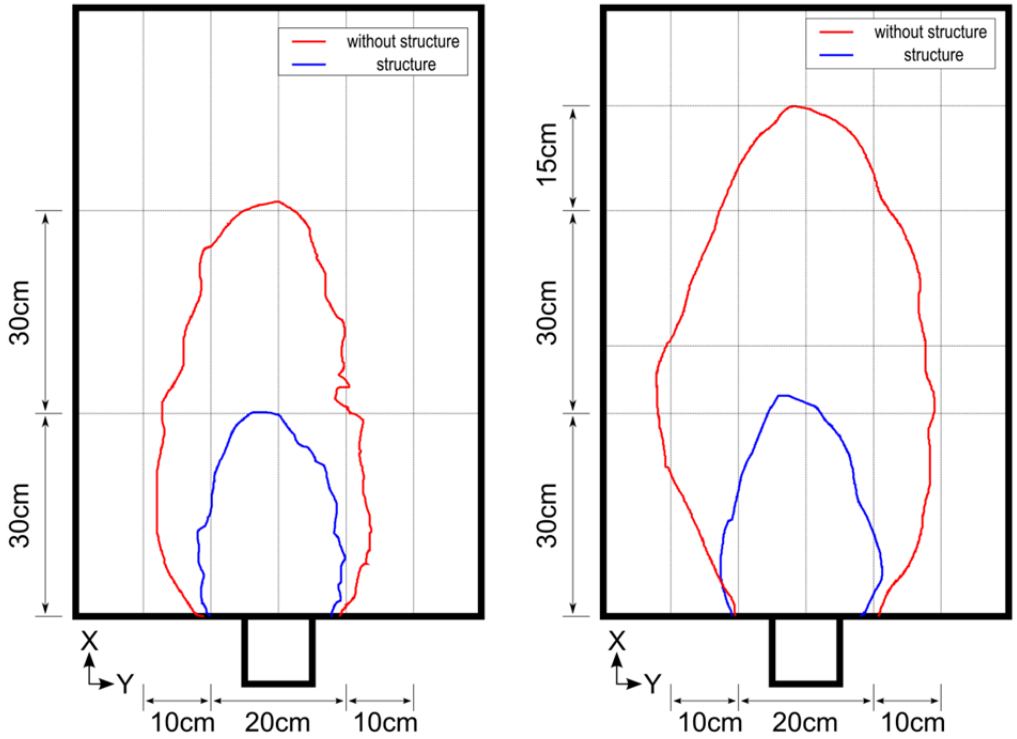

(a) 5º flood basin (b) 7º flood basin

Figure 2.10 Results of diffusion debris under the two bed slopes

Table 2.4 Results of diffusion debris (unit: cm)

	Slope	*Fan area*		*Remarks*
		Y	X	
Without breaker	5º	43.0	62.0	R (%) means reduction in Y and X comparing with and without breaker case.
Debris-flow breaker		25.0	30.0	
R (%)		(▼) 41.9	(▼) 51.6	
Without breaker	7º	46.0	75.0	
Debris-flow breaker		31.0	35.0	
R (%)		(▼) 32.6	(▼) 53.3	

2.3.2 Deposition Process for Different Configuration of Breaker

The three-dimensional phenomenon occurs in the flow separation on the breaker when the water and fine sediments curdle from the debris flow, due to separation when a debris flow passes by. Figure 2.11 shows the movement of a debris flow on the breaker due to separation (case1-0.4-B). From the figure, it can be seen that the generation of the debris flow after 8 sec occurred with the separation. Figures 2.12 ~ 2.41 show the characteristics of the deposit process of the debris flow for various conditions at the debris-flow breaker. From the experimental results, the debris-flow breaker can control effectively the velocity of the front part of a debris flow due to the simple steel frame.

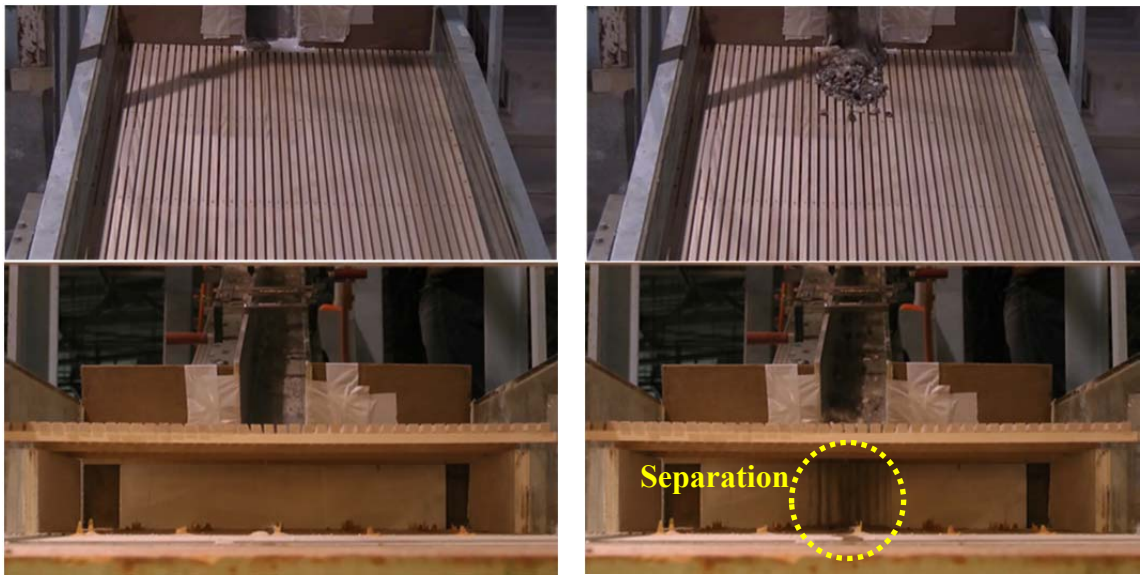

(a) Initial condition Time = 0.0 sec

(b) At time = 8.0 sec

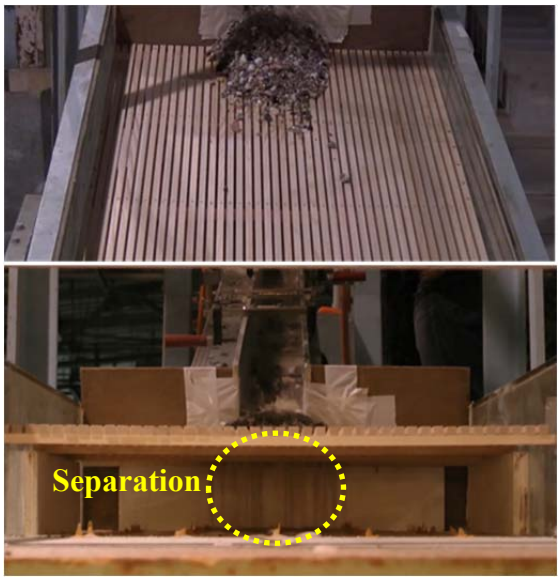

(c) At time = 10.0 sec

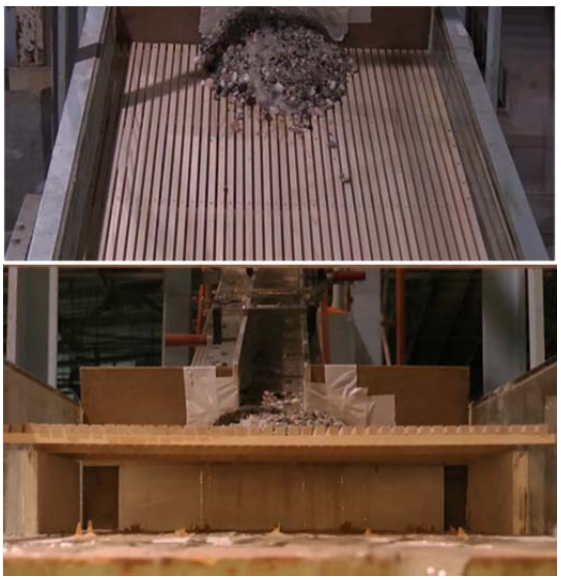

(d) At time = final stage

Figure 2.11 Movement of debris flow due to the separation (Case1-0.4-B)

[Camera A] [Camera B]

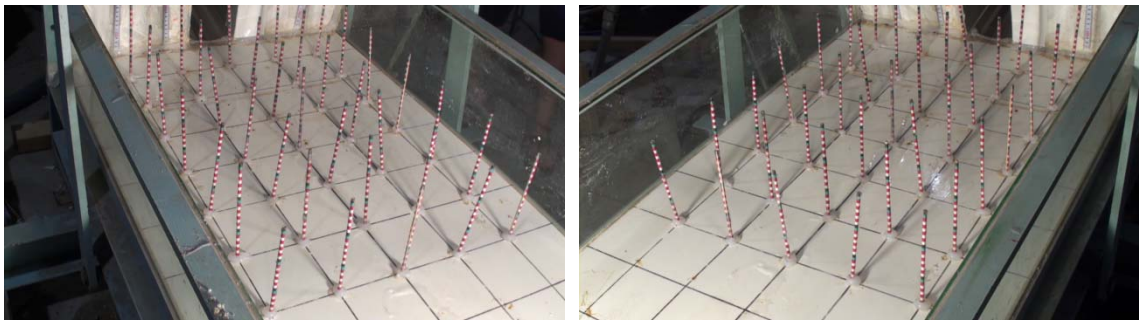

(a) Initial condition Time = 0.0sec

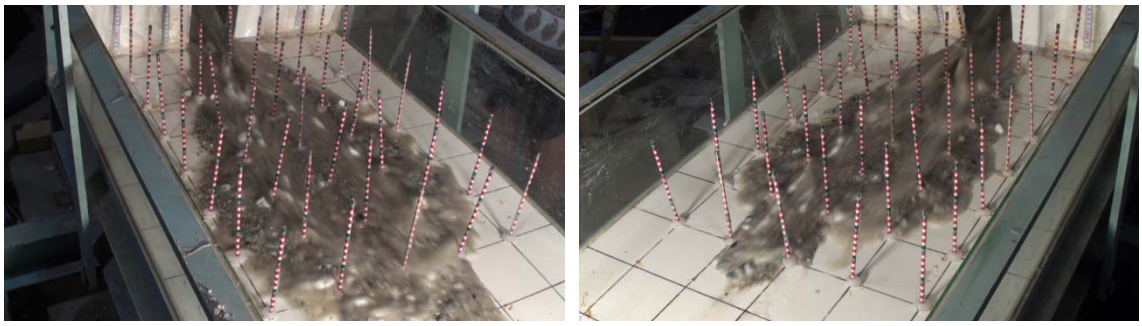

(b) At time = 8.0 sec

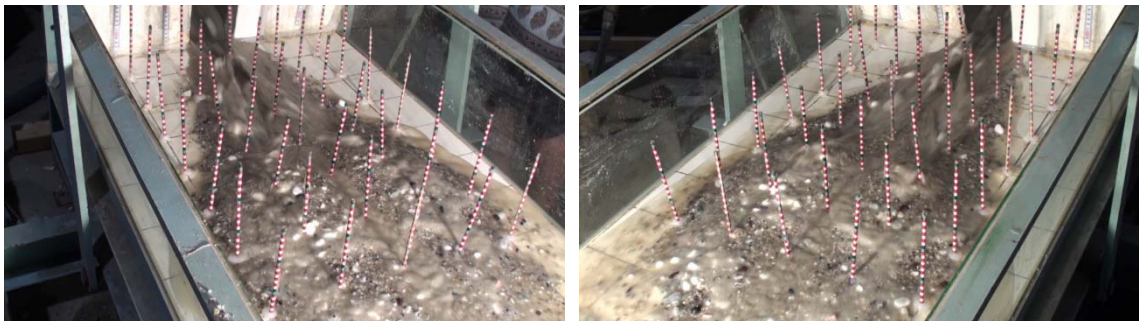

(c) At time = 10.0 sec

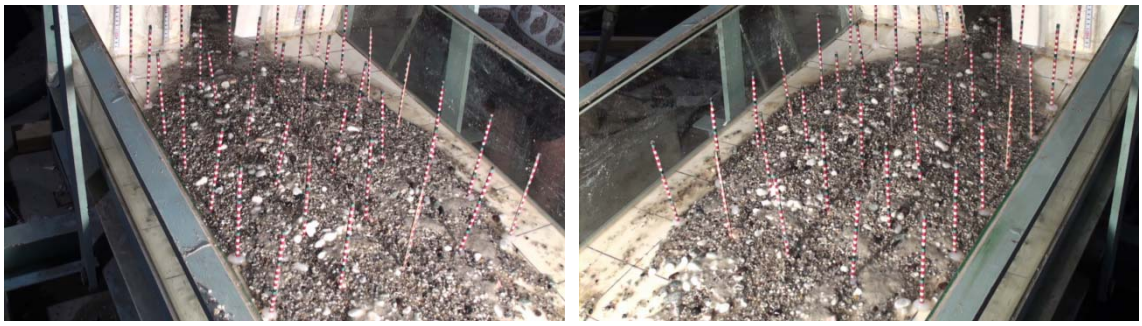

(d) At time = final stage

Figure 2.12 Movement of debris flow (Case0-0.0-A)

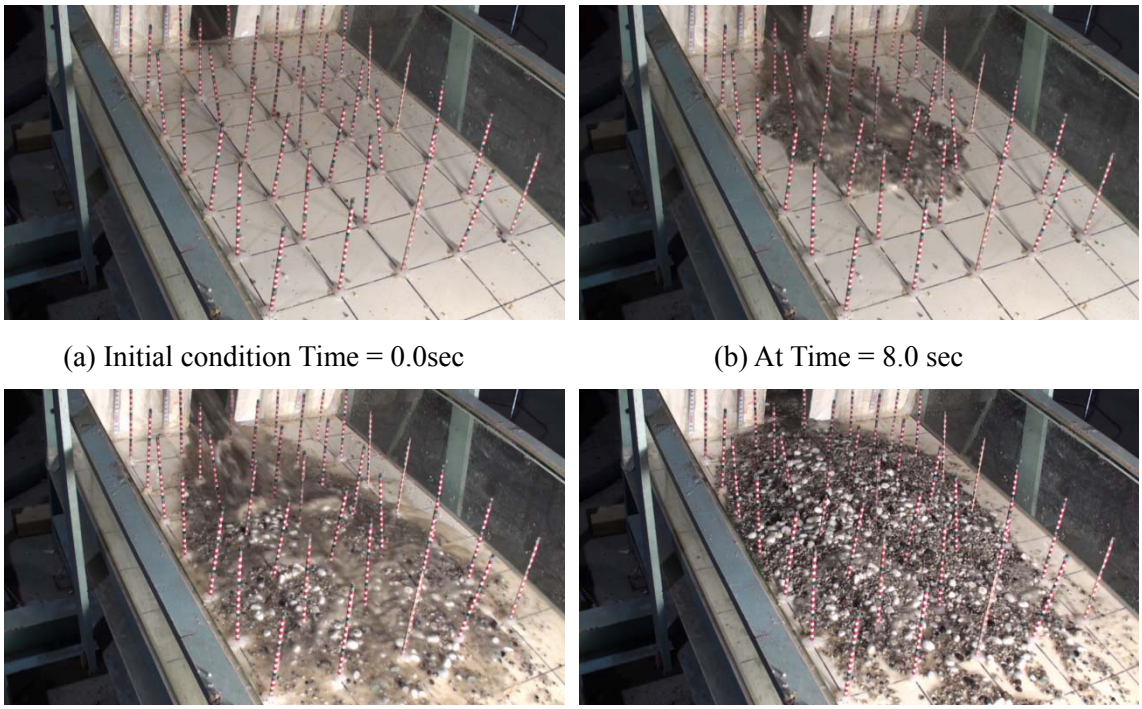

(a) Initial condition Time = 0.0sec (b) At Time = 8.0 sec

(c) At Time = 10.0sec (d) At Time = final stage

Figure 2.13 Movement of debris flow (Case0-0.0-B)

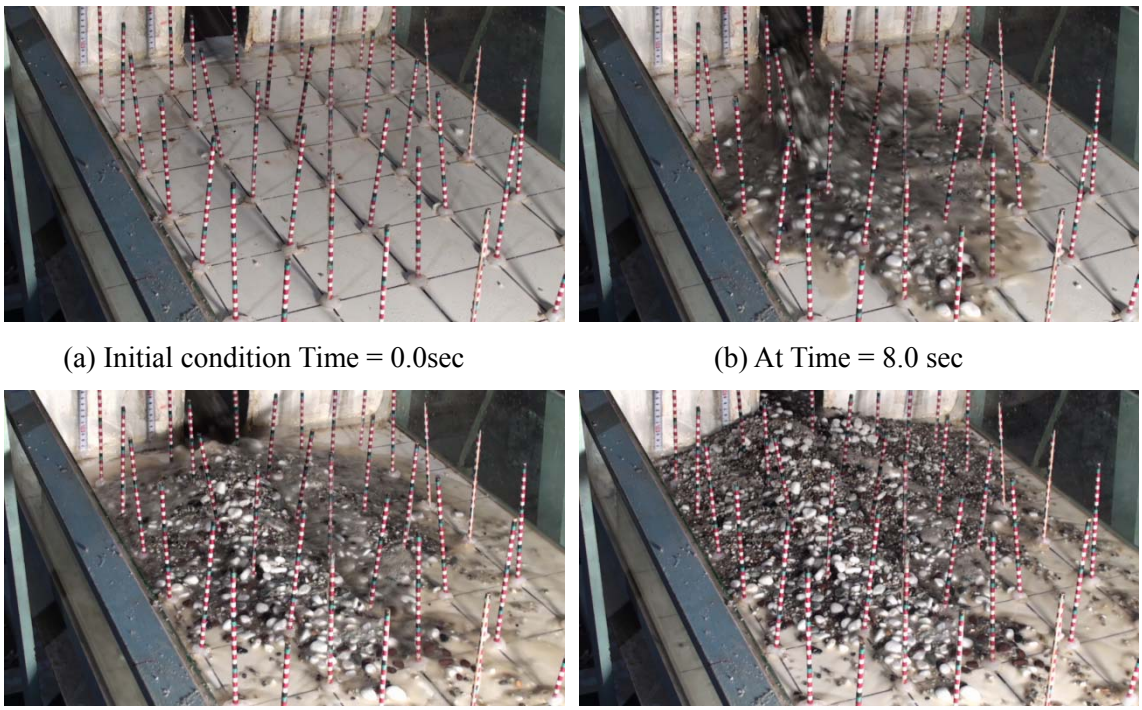

(a) Initial condition Time = 0.0sec (b) At Time = 8.0 sec

(c) At Time = 10.0sec (d) At Time = final stage

Figure 2.14 Movement of debris flow (Case0-0.0-C)

[Camera A] [Camera B]

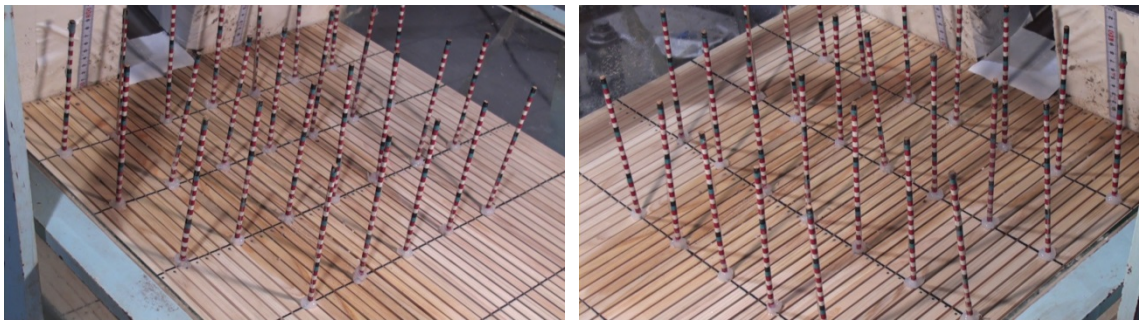

(a) Initial condition Time = 0.0sec

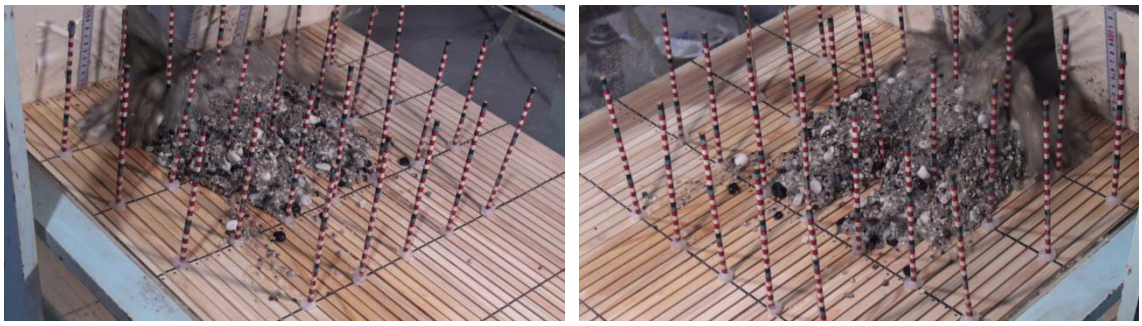

(b) At time = 8.0 sec

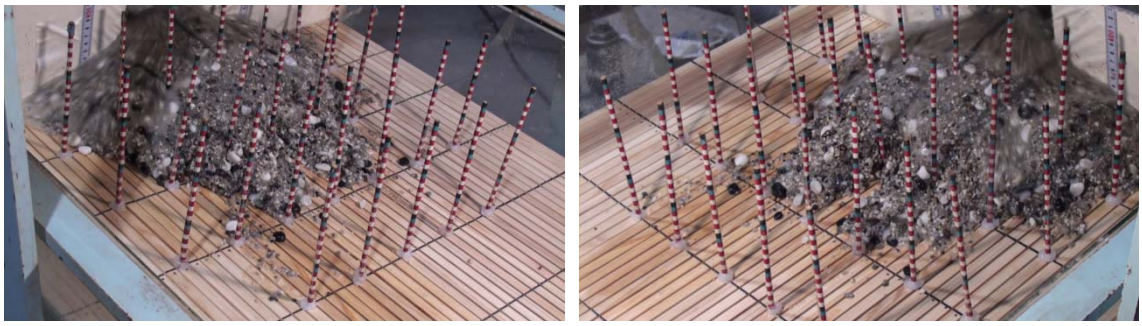

(c) At time = 10.0 sec

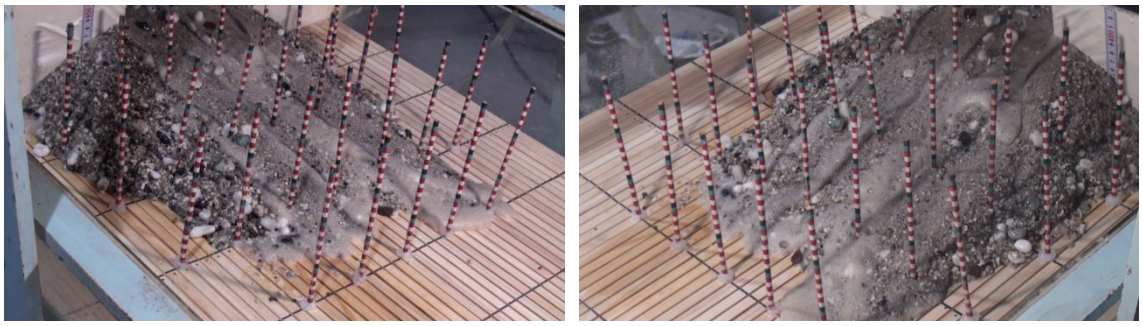

(d) At time = final stage

Figure 2.15 Movement of debris flow (Case1-0.2-A)

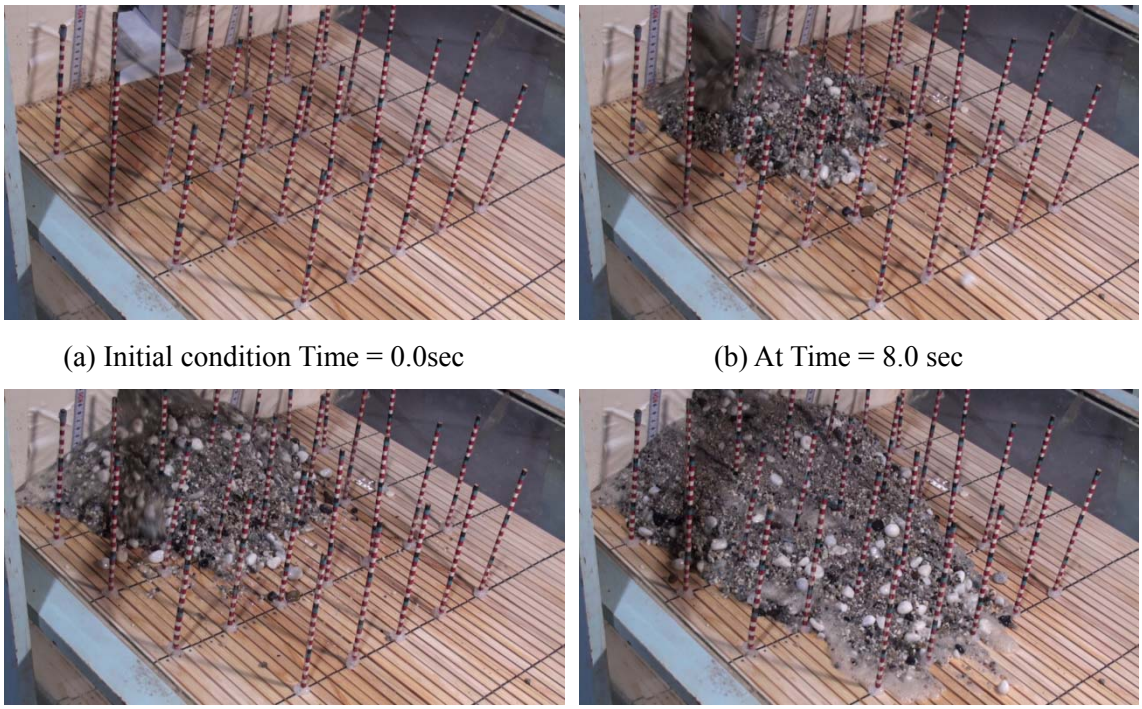

(a) Initial condition Time = 0.0sec (b) At Time = 8.0 sec

(c) At Time = 10.0sec (d) At Time = final stage

Figure 2.16 Movement of debris flow (Case1-0.2-B)

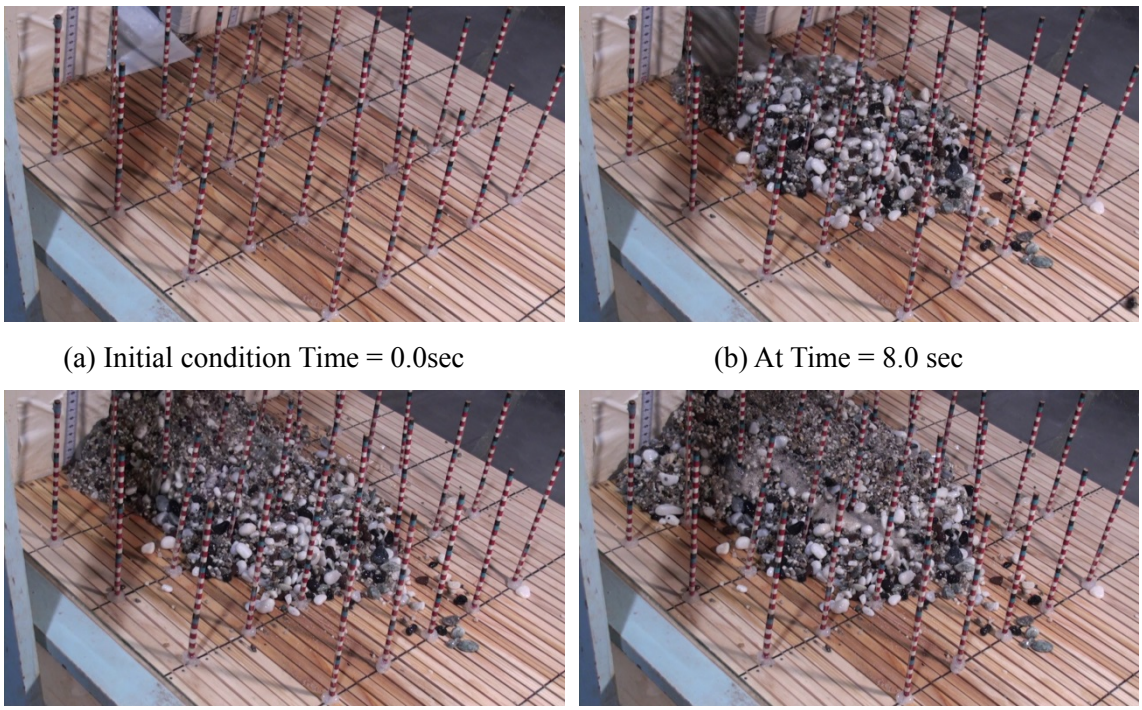

(a) Initial condition Time = 0.0sec (b) At Time = 8.0 sec

(c) At Time = 10.0sec (d) At Time = final stage

Figure 2.17 Movement of debris flow (Case1-0.2-C)

[Camera A] [Camera B]

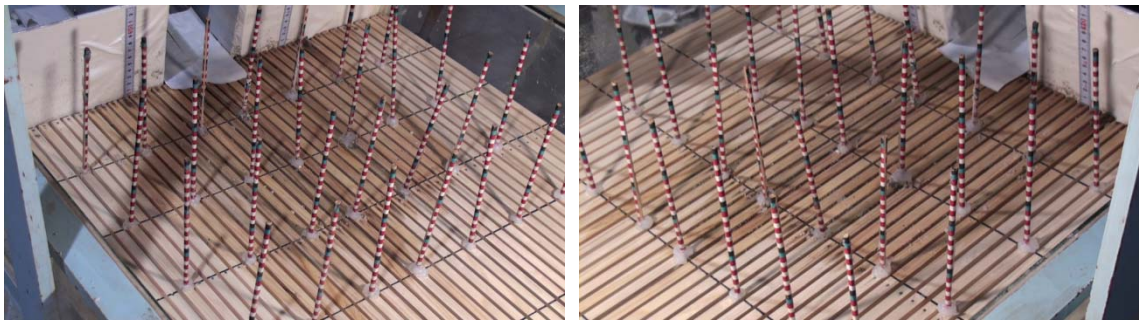

(a) Initial condition Time = 0.0sec

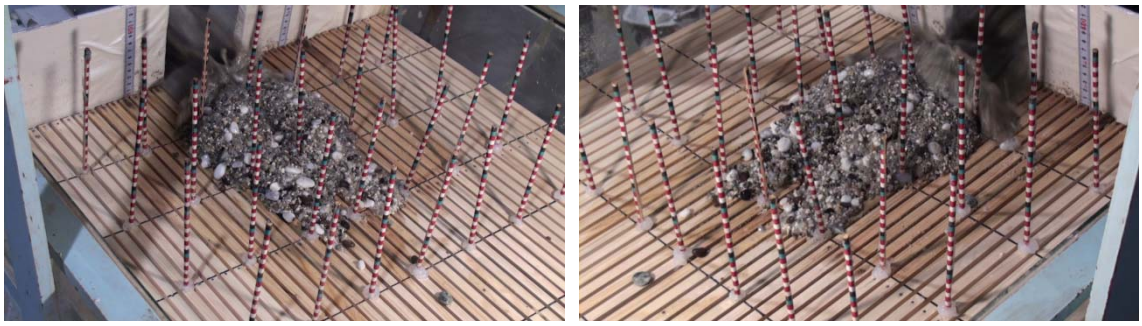

(b) At time = 8.0 sec

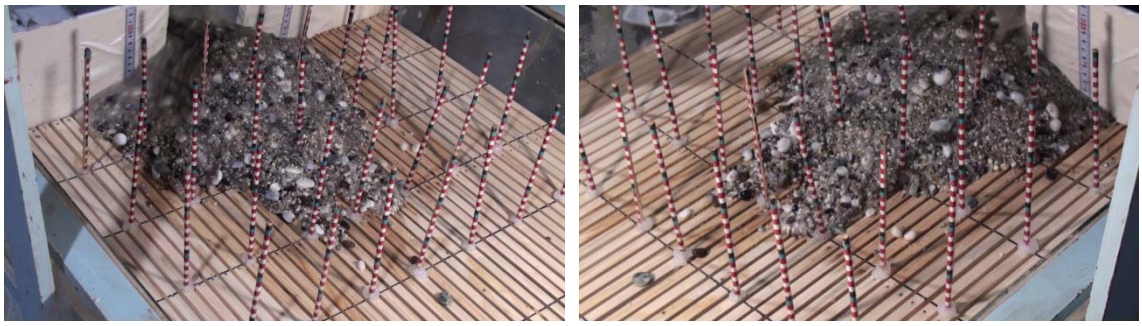

(c) At time = 10.0 sec

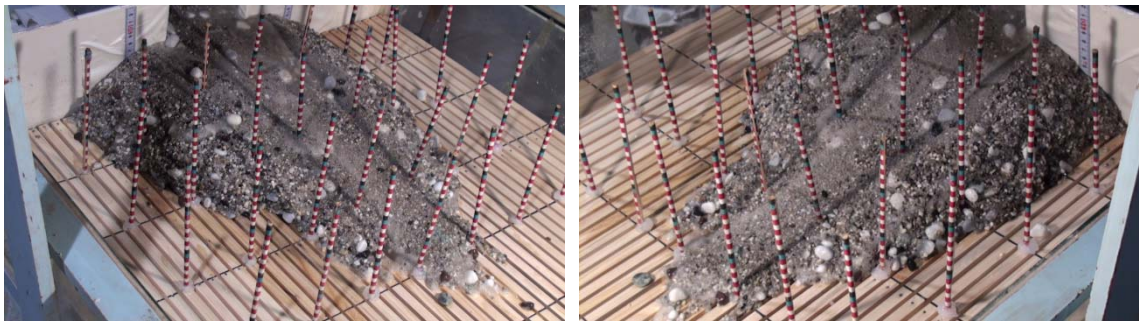

(d) At time = final stage

Figure 2.18 Movement of debris flow (Case1-0.4-A)

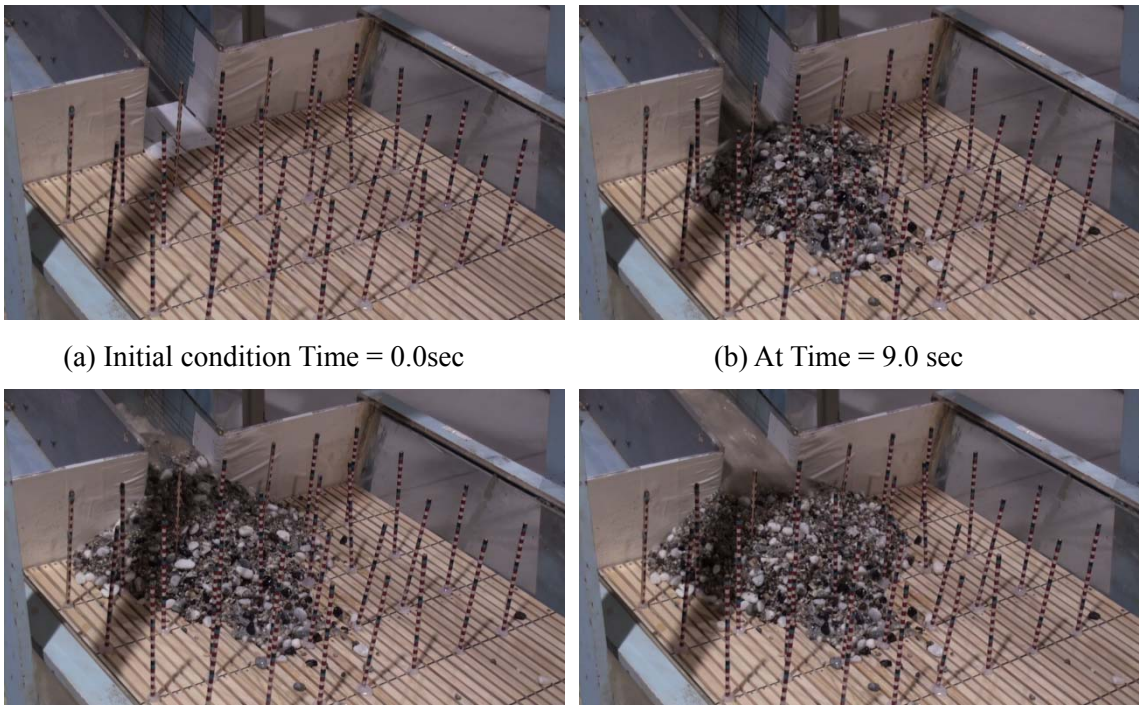

(a) Initial condition Time = 0.0sec (b) At Time = 9.0 sec

(c) At Time = 11.0sec (d) At Time = final stage

Figure 2.19 Movement of debris flow (Case1-0.4-B)

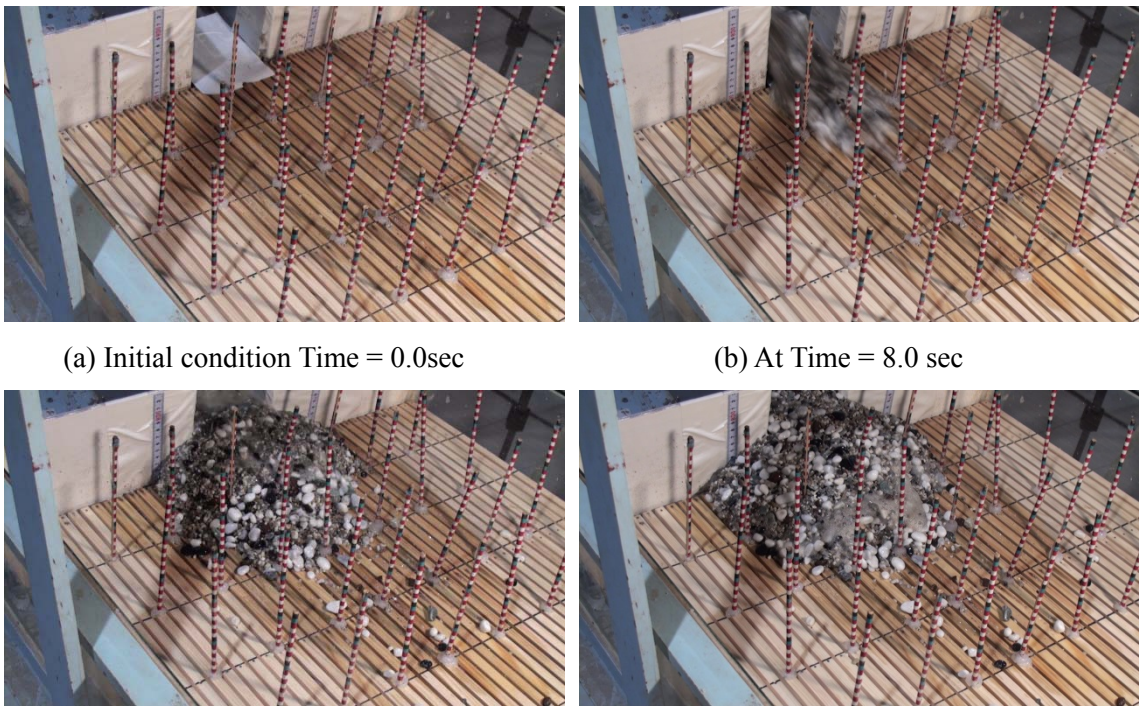

(a) Initial condition Time = 0.0sec (b) At Time = 8.0 sec

(c) At Time = 10.0sec (d) At Time = final stage

Figure 2.20 Movement of debris flow (Case1-0.4-C)

[Camera A] [Camera B]

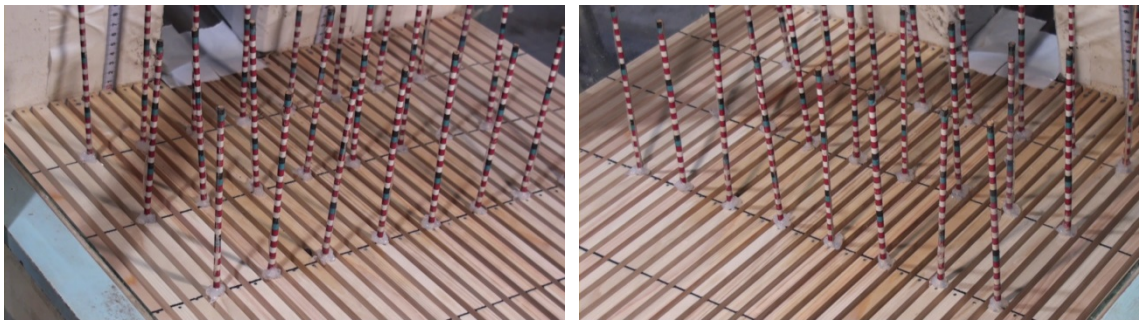

(a) Initial condition Time = 0.0sec

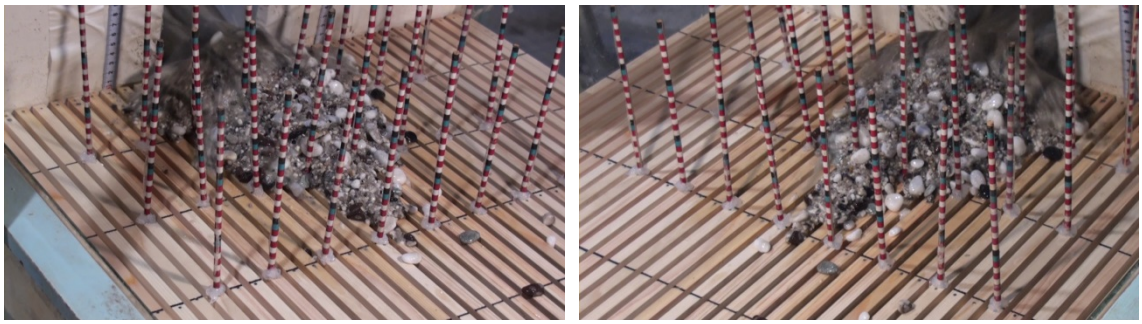

(b) At time = 8.0 sec

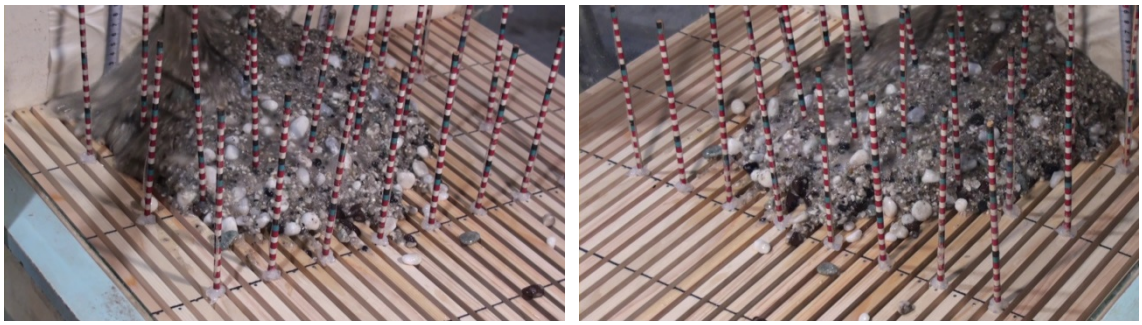

(c) At time = 10.0 sec

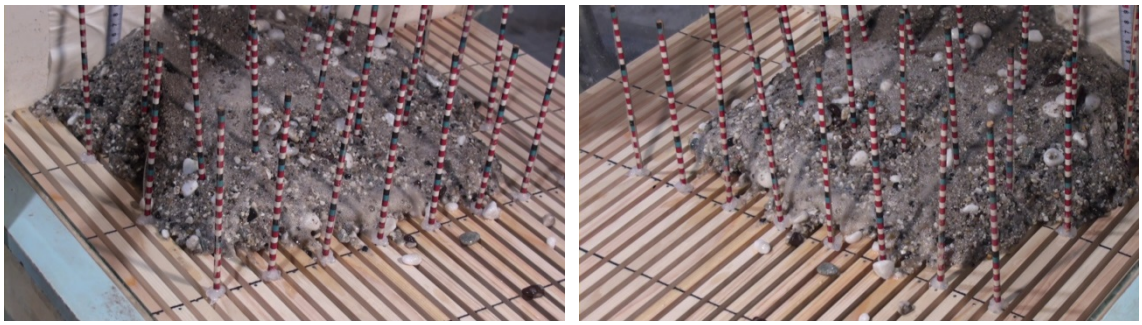

(d) At time = final stage

Figure 2.21 Movement of debris flow (Case1-0.6-A)

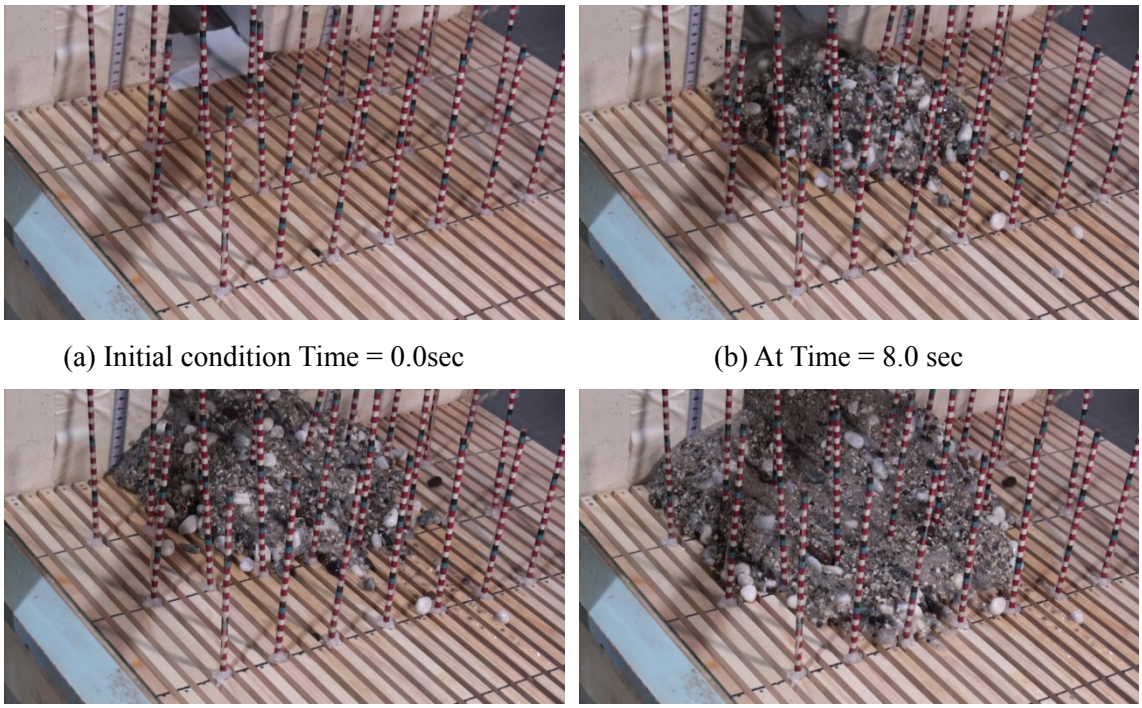

(a) Initial condition Time = 0.0sec (b) At Time = 8.0 sec

(c) At Time = 10.0sec (d) At Time = final stage

Figure 2.22 Movement of debris flow (Case1-0.6-B)

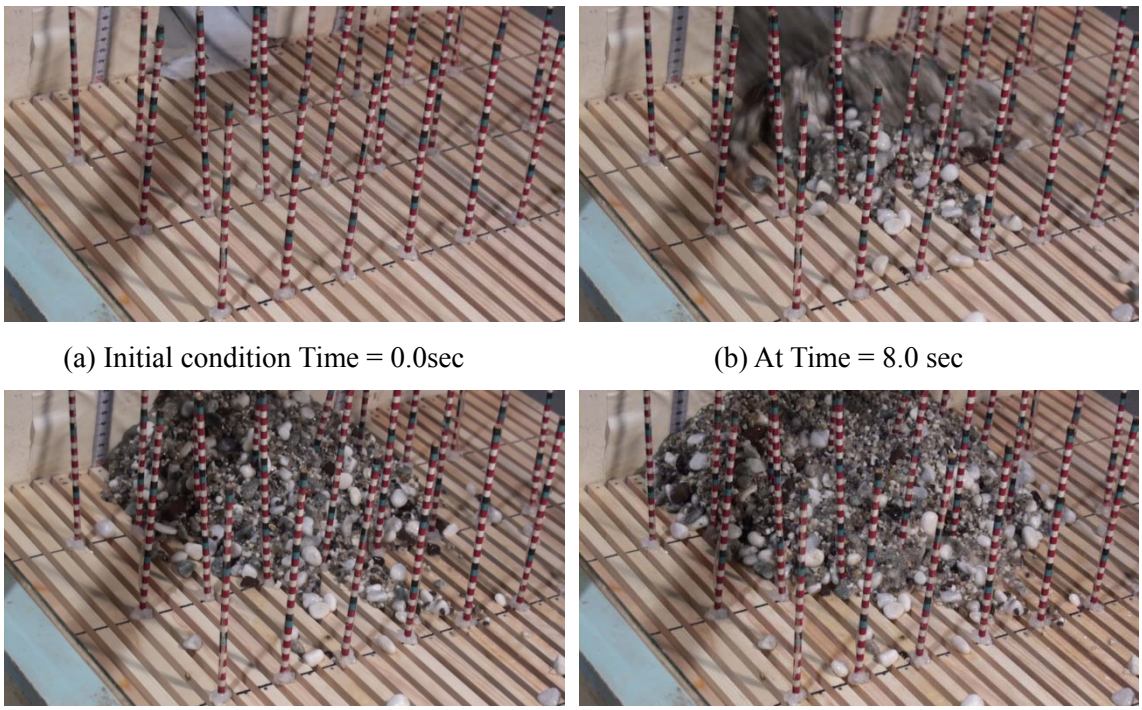

(a) Initial condition Time = 0.0sec (b) At Time = 8.0 sec

(c) At Time = 10.0sec (d) At Time = final stage

Figure 2.23 Movement of debris flow (Case1-0.6-C)

(a) Initial condition Time = 0.0sec (b) At Time = final stage

Figure 2.24 Movement of debris flow (Case3-0.2-A)

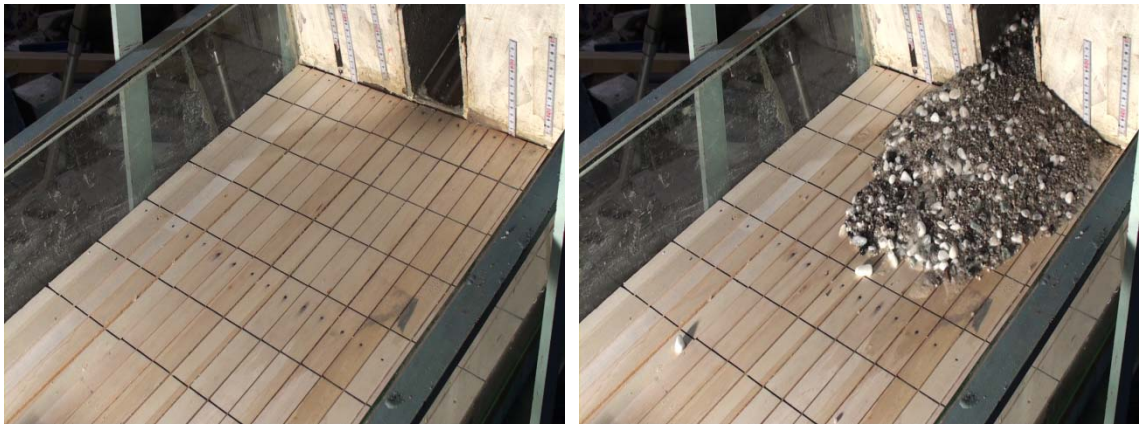

(a) Initial condition Time = 0.0sec (b) At Time = final stage

Figure 2.25 Movement of debris flow (Case3-0.2-B)

(a) Initial condition Time = 0.0sec (b) At Time = final stage

Figure 2.26 Movement of debris flow (Case3-0.2-C)

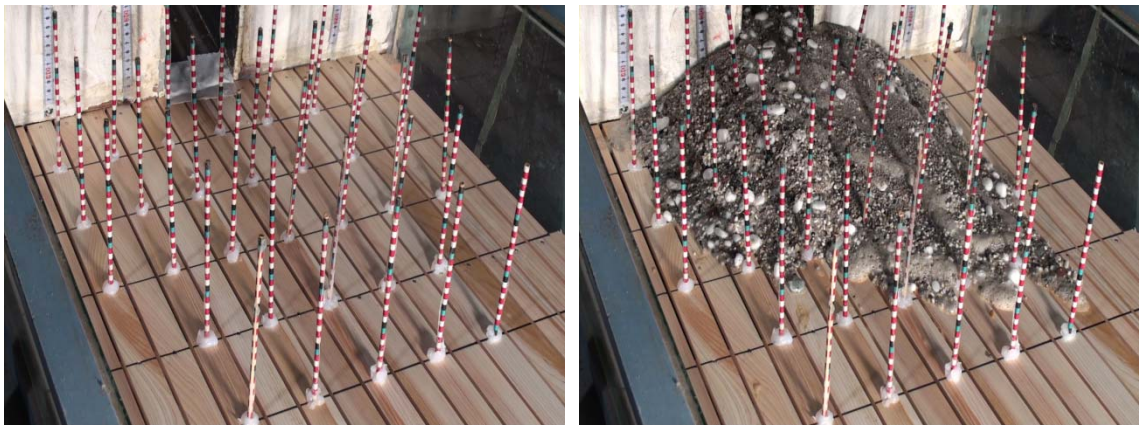

(a) Initial condition Time = 0.0sec (b) At Time = final stage

Figure 2.27 Movement of debris flow (Case3-0.4-A)

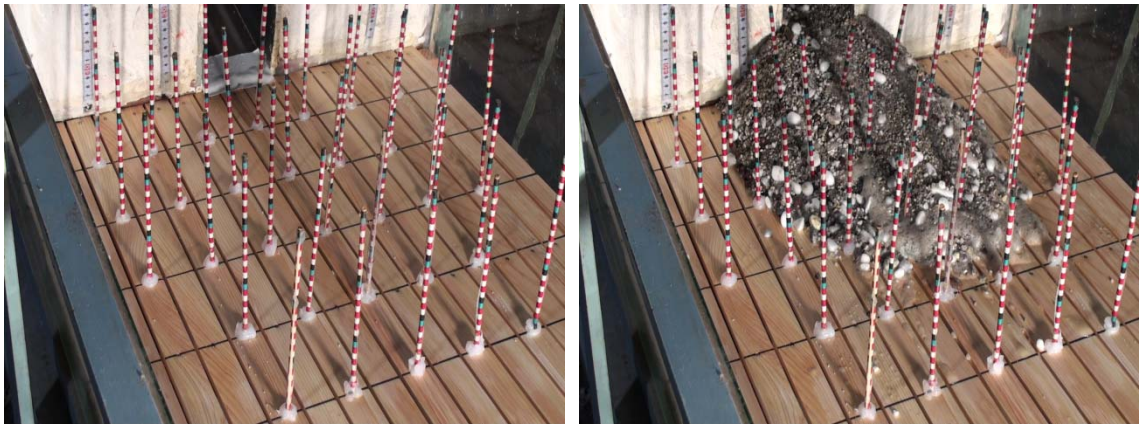

(a) Initial condition Time = 0.0sec (b) At Time = final stage

Figure 2.28 Movement of debris flow (Case3-0.4-B)

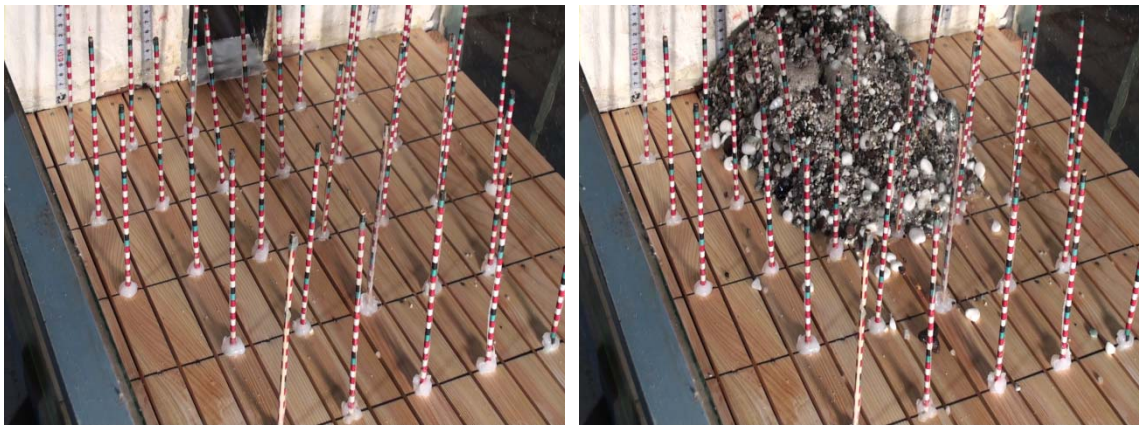

(a) Initial condition Time = 0.0sec (b) At Time = final stage

Figure 2.29 Movement of debris flow (Case3-0.4-C)

(a) Initial condition Time = 0.0sec (b) At Time = final stage

Figure 2.30 Movement of debris flow (Case3-0.6-A)

(a) Initial condition Time = 0.0sec (b) At Time = final stage

Figure 2.31 Movement of debris flow (Case3-0.6-B)

(a) Initial condition Time = 0.0sec (b) At Time = final stage

Figure 2.32 Movement of debris flow (Case3-0.6-C)

(a) Initial condition Time = 0.0sec (b) At Time = final stage

Figure 2.33 Movement of debris flow (Case6-0.2-A)

(a) Initial condition Time = 0.0sec (b) At Time = final stage

Figure 2.34 Movement of debris flow (Case6-0.2-B)

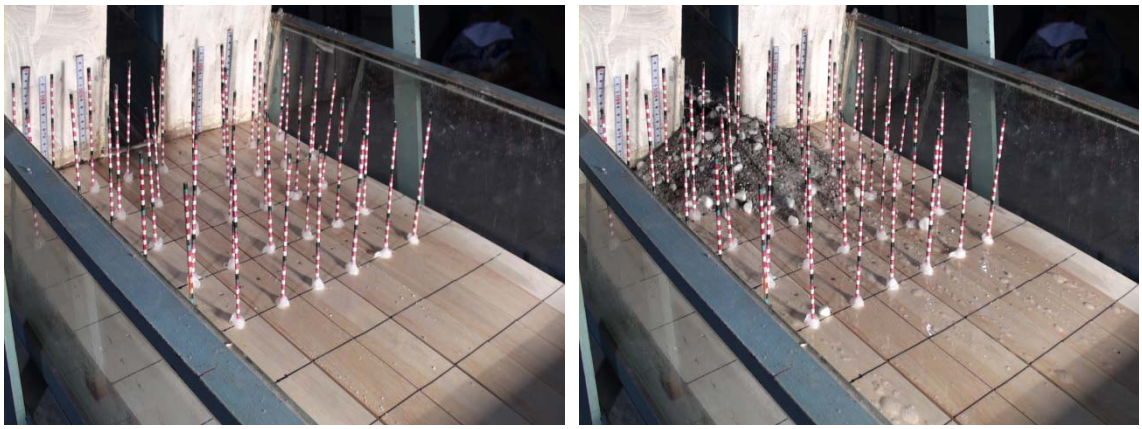

(a) Initial condition Time = 0.0sec (b) At Time = final stage

Figure 2.35 Movement of debris flow (Case6-0.2-C)

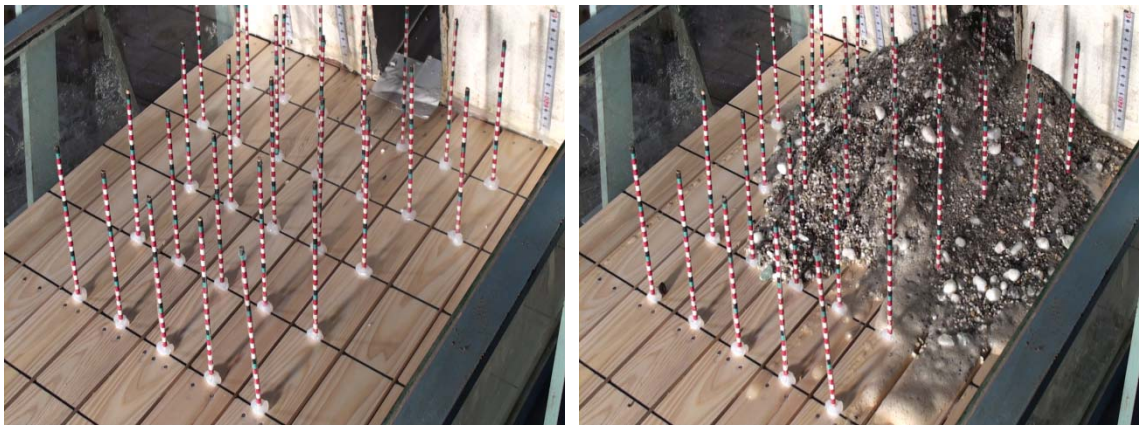

(a) Initial condition Time = 0.0sec (b) At Time = final stage

Figure 2.36 Movement of debris flow (Case6-0.4-A)

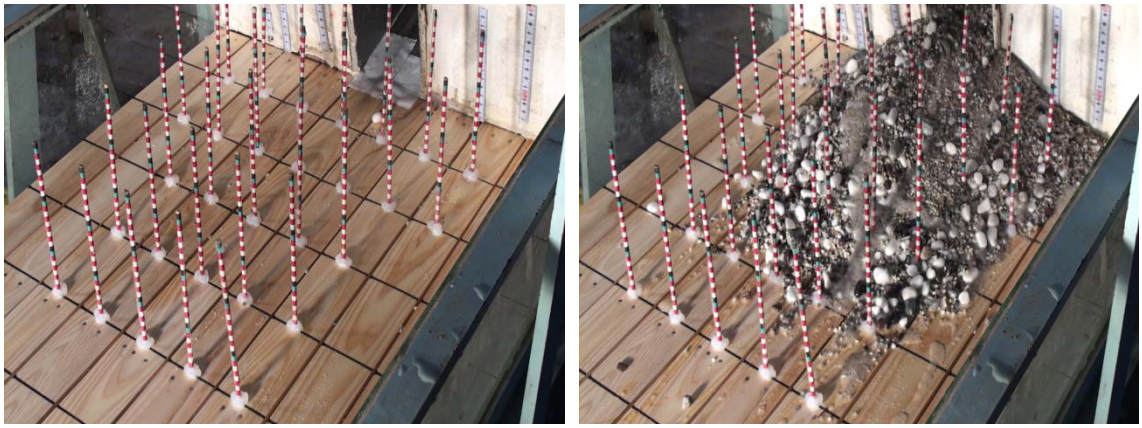

(a) Initial condition Time = 0.0sec (b) At Time = final stage

Figure 2.37 Movement of debris flow (Case6-0.4-B)

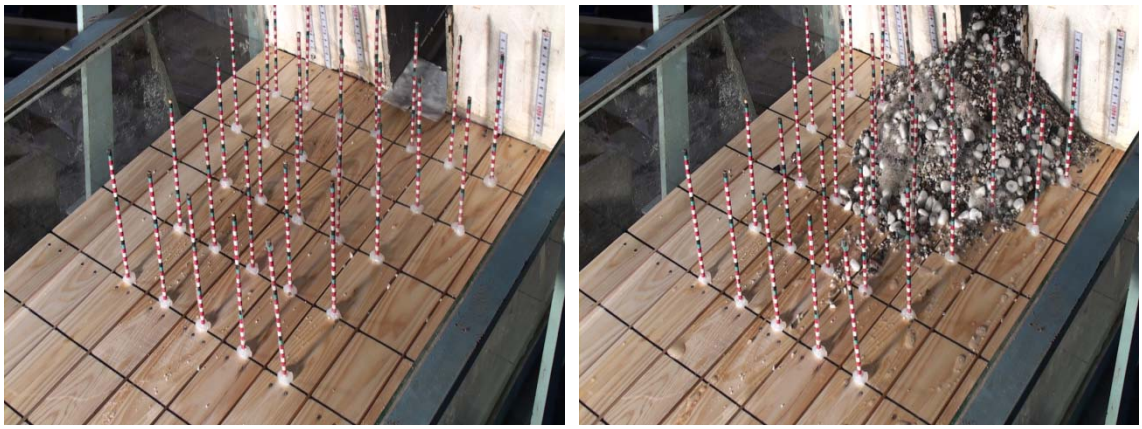

(a) Initial condition Time = 0.0sec (b) At Time = final stage

Figure 2.38 Movement of debris flow (Case6-0.4-C)

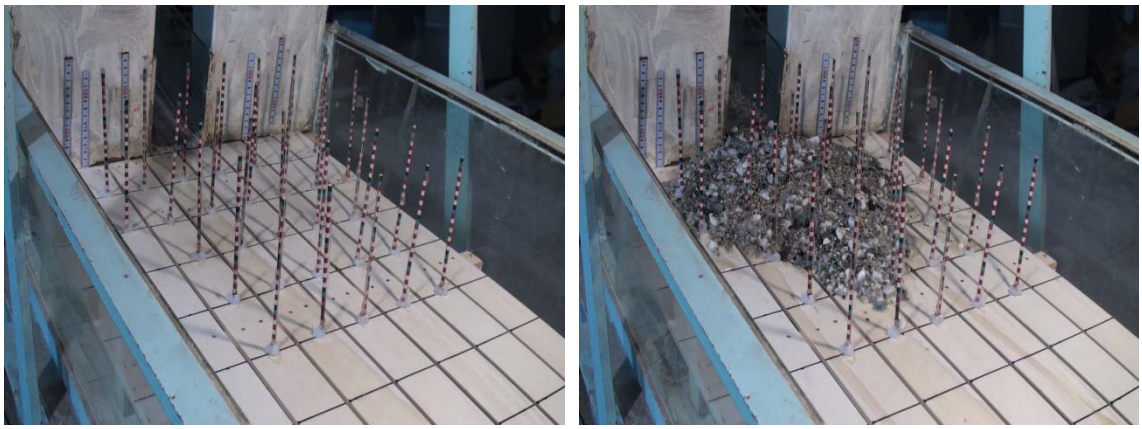

(a) Initial condition Time = 0.0sec (b) At Time = final stage

Figure 2.39 Movement of debris flow (Case6-0.6-A)

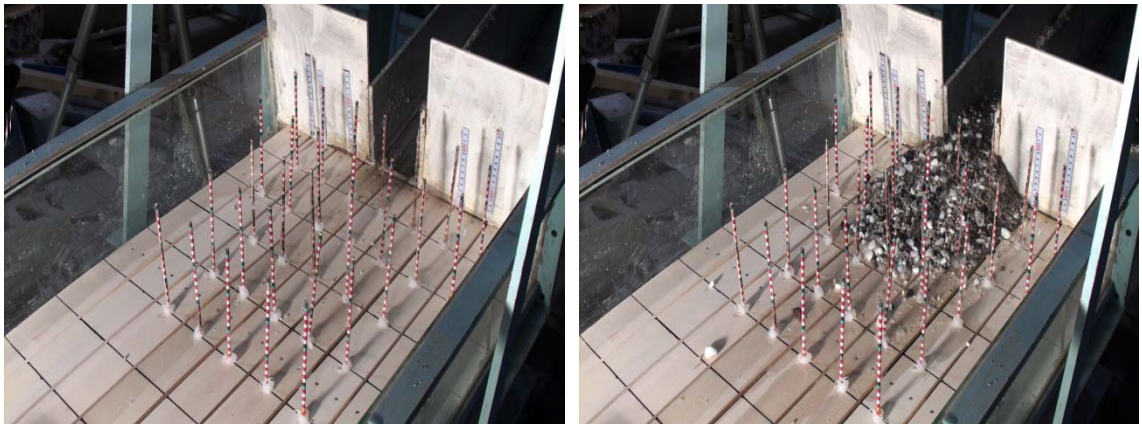

(a) Initial condition Time = 0.0sec (b) At Time = final stage

Figure 2.40 Movement of debris flow (Case6-0.6-B)

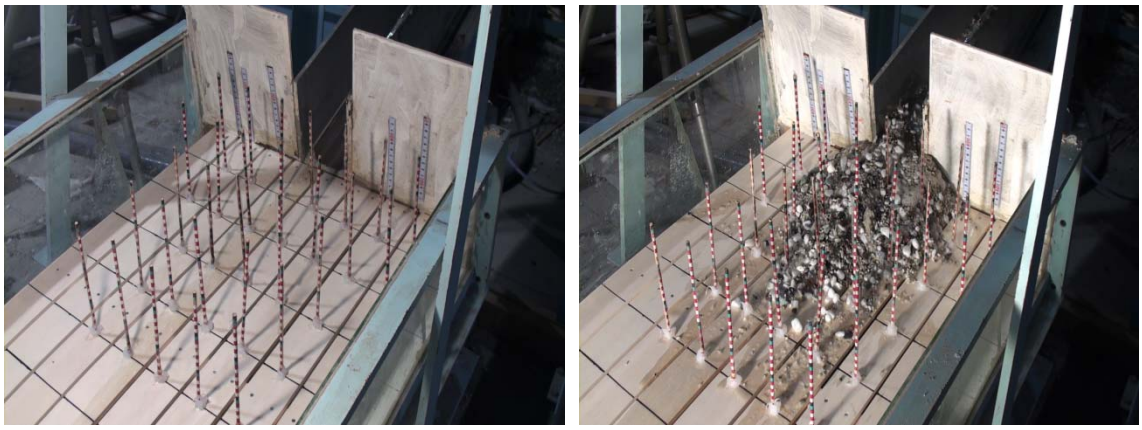

(a) Initial condition Time = 0.0sec (b) At Time = final stage

Figure 2.41 Movement of debris flow (Case6-0.6-C)

To confirm the characteristics (i.e. sedimentation of debris) of debris-flow breakers, nine types of dams were tested. The experiments were carried out for three bed sediments in order to observe the velocity dissipation phenomenon at the dam. Once the flow reaches the sabo dams, a part of the flow is detached and forms a grave travelling in a downstream direction while the other part (i.e. fine sediment and water) falls in the direction of gravity, as shown in Figure 2.11. The above results indicated that the debris-flow breaker has an advantage for effectively stopping a debris flow front.

Also, as shown in Figure 2.42, the deposition pattern upstream of breaker and flood basin was compared. The comparison here also shows that the placing of breaker will deposit more debris mass upstream than without breaker case. It means the breaker is again very much useful to reduce the transfer of debris flow volume downstream.

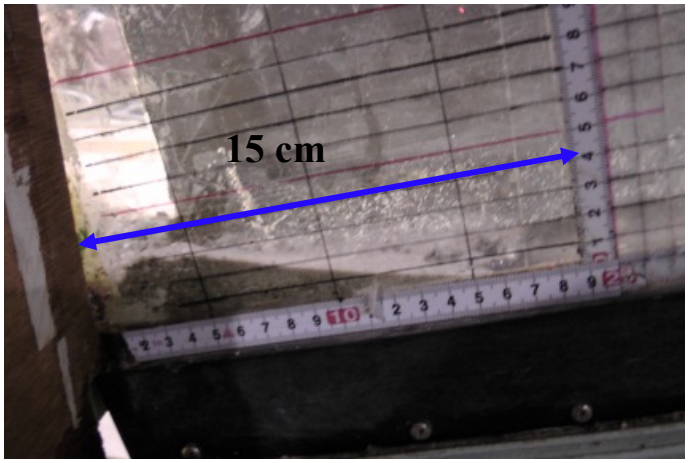

(a) 7º flood basin without breaker

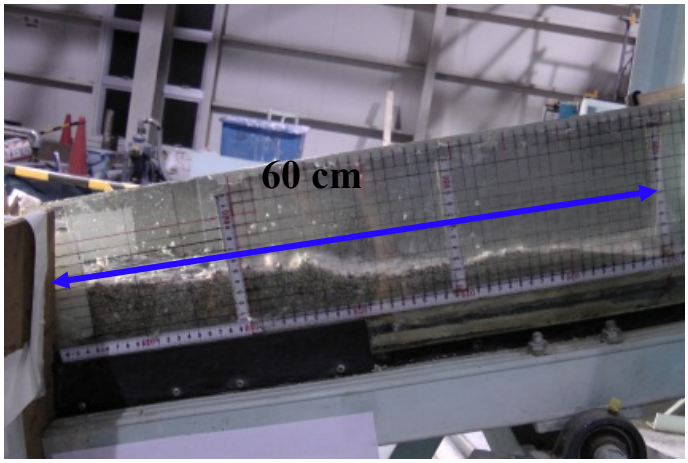

(b) 7º flood basin with debris-flow breaker

Figure 2.42 Results of deposition at the upstream in both cases

2.3.3 Travel Length

To clarify the relation between the opening and blocking sizes due to changing pore water pressure, the maximum travel length was observed during the experiment. In the experiments, the data were obtained from the three repetitions under the same hydraulic conditions. Figure 2.43 compares the test results of the average maximum travel length values. The results obtained by comparing the travel length with those without the debris-flow breaker are summarized below.

In the case of without breaker (case 0-0.0 with the three bed sediments), the maximum travel length is influenced by the conditions of the bed slope and the approaching debris flow properties (especially the approaching velocity). As a result, the maximum travel length of debris was the case of bed sediment A in comparison to other types. Other cases, including bed sediment A, moved farther away from the end of the upstream channel. In the case of the debris-flow breaker (i.e. it has opening and blocking sizes), the travel length decreased by nearly 34% ~ 62%, compared to the without breaker cases. Table 2.5 shows the results of the experiments regarding the maximum travel length.

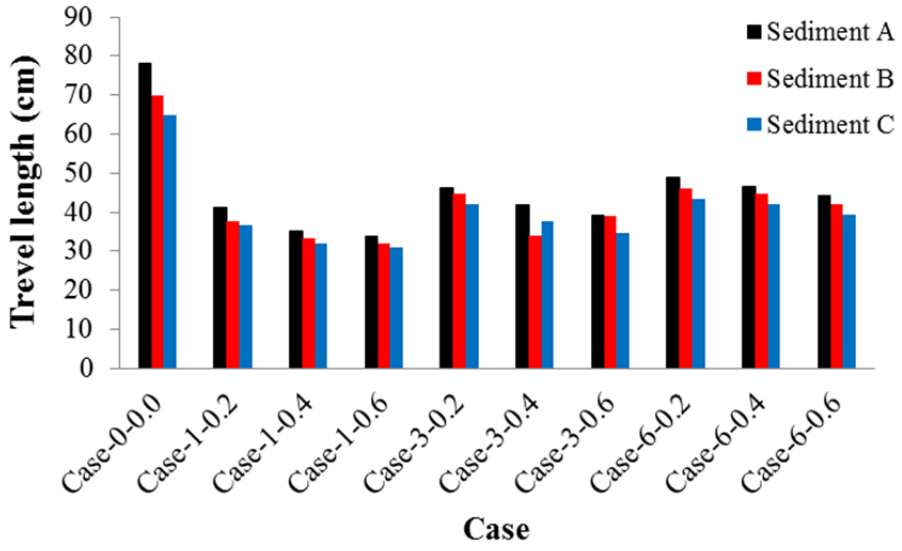

Figure 2.43 Results of the travel length under the three bed sediments

Table 2.5 Results of experiments regarding the maximum travel length (unit: cm)

Case	*Sediment*	*Blocking size*	*Opening size*	*Travel length*
Case-0-0.0-A	A	×	×	78.0
Case-1-0.2-A		1	0.2	42.0
Case-1-0.4-A			0.4	40.0
Case-1-0.6-A			0.6	30.0
Case-3-0.2-A		3	0.2	47.9
Case-3-0.4-A			0.4	42.0
Case-3-0.6-A			0.6	38.5
Case-6-0.2-A		6	0.2	51.1
Case-6-0.4-A			0.4	49.0
Case-6-0.6-A			0.6	44.1
Case-0-0.0-B	B	×	×	70.0
Case-1-0.2-B		1	0.2	39.0
Case-1-0.4-B			0.4	34.0
Case-1-0.6-B			0.6	30.0
Case-3-0.2-B		3	0.2	40.6
Case-3-0.4-B			0.4	38.0
Case-3-0.6-B			0.6	37.9
Case-6-0.2-B		6	0.2	41.0
Case-6-0.4-B			0.4	46.0
Case-6-0.6-B			0.6	42.8
Case-0-0.0-C	C	×	×	65.0
Case-1-0.2-C		1	0.2	35.0
Case-1-0.4-C			0.4	26.0
Case-1-0.6-C			0.6	28.0
Case-3-0.2-C		3	0.2	37.1
Case-3-0.4-C			0.4	32.0
Case-3-0.6-C			0.6	34.7
Case-6-0.2-C		6	0.2	41.1
Case-6-0.4-C			0.4	40.0
Case-6-0.6-C			0.6	35.2

2.3.4 Discharges and Sediment Concentration

The temporal variations of flow and sediment discharge at the downstream end of the flume for a flume slope of 18º are measured for the verification between the numerical model and the experiment. The experimental results are shown in Figure 2.44.

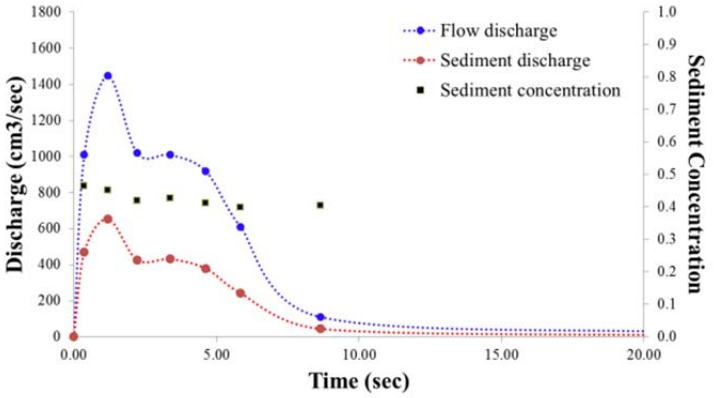

(a) Bed sediment A

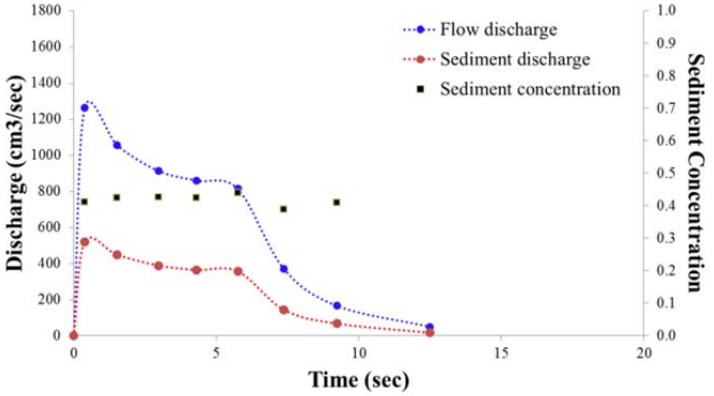

(b) Bed sediment B

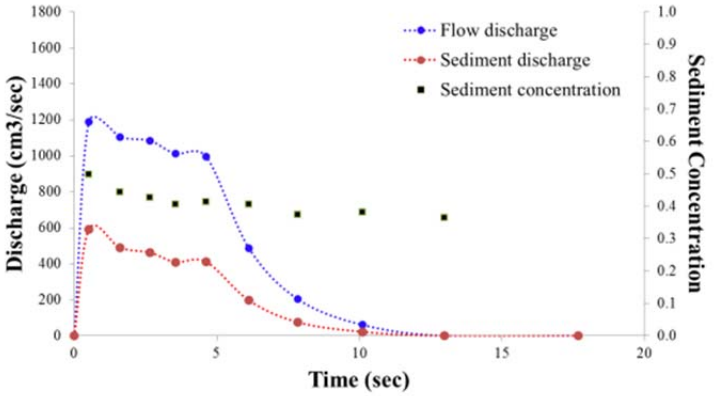

(c) Bed sediment C

Figure 2.44 Flow and sediment discharges, and sediment concentration

2.4 Summary

In summary, this chapter clearly described the experimental condition and the setup for the hydraulic model test as well as the measurement techniques considering both with and without debris-flow breaker to indicate important functions of placing the debris-flow breaker. From the experiment, the various important phenomena such as the debris flow formation process and the respective flow pattern at the breaker for two types of the bed slopes of the downstream channel and three types of sediments; thickness of the debris at the breaker and the total flow, sediment discharges and the sediment concentration, for both with and without breaker case, were measured to understand the working principle of the breaker.. Furthermore, the important characteristic of a debris-flow breaker is confirmed from the experiments. The experimental data analyses lead to the following conclusions:

1. In the case of without the debris-flow breaker, when the debris flow debouches onto the fan area, at the first stage, the flow advances from the upstream flume outlet without expanding as straight. In the second stage, it begins to deposit the sediments with rapid diffusion and quickly reaches its maximum travel length while the water and fine sediments detach from the original group due to the physiographic changes (i.e. the conditions of breaker). Finally, the debris was deposited on the fan area without water due to the bed slope.

2. In the case of the debris-flow breaker, when the debris flow debouches onto the fan area, at the first stage, as in the previous case, the flow advances from the upstream flume outlet without expanding as straight for shorter time than previous and due to the openings on the bed, the water starts to separate from the debris flow and flows through the opening. In the second stage, it begins to deposit the sediments with rapid diffusion and quickly reaches its maximum travel length. Finally, the debris mass without water was deposited on the fan due to the bed slope and infiltration.

3. The bed slope of flood basin or debris-flow breaker was chosen for further analysis as 7º based on better diffusivity and easily measurability of the deposited thickness.

4. The maximum travel length for the debris-flow breaker case is decreased by nearly 34 % ~ 62 % compared to without breaker cases. From the experimental results, it can be seen that the debris-flow breaker can decelerate effectively the velocity of the front part of a debris flow hence decreases the travel length subsequently. Also, the deposition upstream of the

breaker was increased due to installation of breaker (i.e. more capture of debris volume upstream) which shows the importance of debris-flow breaker.

It is not sufficient to generalize the mechanism of the debris-flow breakers discussed under the limited experimental conditions. In practicality, many parts cannot be studied with the results of the hydraulic model test. Therefore, Chapter 3 will discuss the results of numerical simulations in detail, to understand clearly the mechanism of deposition and the hydraulic characteristics.

References

1) Fiebiger G. 1997, Structures of debris flow countermeasures. *American Society of Civil Engineers,* pp. 596-605.
2) Gonda Y. 2009, Function of a debris-flow brake. *International Journal of Erosion Control Engineering,* Vol. 2, No. 1, pp. 15-21.
3) ICHARM. 2008, Debris-flow dewatering brakes: a promising tool for disaster management in developing countries. *International Center for Water Hazard and Risk Management Newsletter,* Vol. 3, No. 3, pp. 10.
4) Imai K., Miyamoto N. and Mizuyama T. 1989, Test of a debris-flow breaker at the Kamikamihori Valley, Mt. Yakedake (Part-2). *Journal of the Japan Society of Erosion Control Engineering,* Vol. 42, No. 2, pp. 16-20. (in Japanese)
5) Itoh T., Horiuchi S., Akanuma J.I., Kaitsuka K., Kuraoka S., Morita T., Sugiyama M., and Mizuyama T. 2011, Fundamental hydraulic flume tests focused on sediment control function using a grid-type high dam. *Italian Journal of Engineering Geology and Environment,* B-114, pp. 1051-1061.
6) Izumi I., Watanabe M., Takemura T. and Mizuyama Y. 1982, Test of a bottom infiltration screen in Ohsawa Fam, Mt. Fuji. *Journal of the Japan Society of Erosion Control Engineering,* Vol. 34, No. 3, pp. 45-50. (in Japanese)
7) Mizuyama T. 2008, Structural countermeasures for debris flow disaster. *International Journal of Erosion Control Engineering,* Vol. 1, No. 2, pp. 38-43.
8) Nisimoto H., Ishikura K., Mizuyama T. and Santosa U.B. 1994, Behavior of a debris-flow on the debris-flow breaker at Mount Yake-dake. *Journal of the Japan Society of Erosion Control Engineering,* Vol. 46, No. 6, pp. 21-24. (in Japanese)
9) Kim Y., Nakagawa H., Kawaike K. and Zhang H. 2012a, Numerical analysis of debris flow deposition on breaker structure. *Annual Journal of Japan Society of Civil Engineering, JSCE,* Vol. 68, No. 4, pp. 1-6.
10) Kim Y., Nakagawa H., Kawaike K. and Zhang H. 2012b, Numerical and experimental study on debris-flow breaker. *Annuals of the Disaster Prevention Research Institute, Kyoto University,* No. 55 B, pp. 471-481.
11) Kiyono M., Miyakoshi H., Uehara S. and Mizuyama T. 1986, Test of a debris flow breaker in Valley Kamikami, Mt. Yake-dake. *Journal of the Japan Society of Erosion Control Engineering,* Vol. 39, No. 3, pp. 15-19. (in Japanese)
12) Kurihara J., Hukujawa M. and Iwata Y. 1987, The report on mud flows occurred at Osawa River, Mt. Fuji and the function of the screen dam (prompt report). *Journal of the Japan Society of Erosion Control Engineering,* Vol. 40, No. 3, pp. 23-28. (in Japanese with English Abstract)
13) Shrestha B.B., Nakagawa H., Kawaike K., BaBa Y. and Zhang H. 2011, Numerical and experimental analysis on deposition process of debris flow with driftwood on the fan. *Journal of Hydroscience and Hydraulic Engineering,* Vol. 29, No. 1, pp. 15-32.
14) Suwa H., Okano K. and Nanno T. 2009, Behavior of debris flows monitored on test slopes of Kamikamihorizawa Creek, Mount Yakedake, Japan. *International Journal of Erosion Control Engineering,* Vol.2, No.2, pp. 33-45.
15) Watanabe M., Mizuyama T. and Uehara S. 1980, Review of debris flow countermeasure facilities. *Journal of the Japan Society of Erosion Control Engineering,* Vol. 32, No. 4, pp. 40-45. (in Japanese)

CHAPTER 3

NUMERICAL SIMULATION AND VERIFICATION ON DEBRIS-FLOW BREAKER

3.1 General

In the last decades, a number of regions worldwide have been affected by debris flows. These disasters generate an enormous amount of human and property losses every year. Although investigating past events is important in forecasting potential future debris flows, theoretical numerical modeling is necessary to understand the mechanisms and characteristics of debris flows and therefore selecting the most suitable mitigation measures to adopt. In order to mitigate these sediment-related disasters, many researchers used numerical simulations and they have tried to be as brief as possible about the mechanisms of debris flows, due to the various theories.

Numerical simulations are an effective tool for a broader analysis of the problem. Comprehensive study of the process of debris flows from the initiation stage to deposition stage via transportation and the analyses of the effect of the combination of structural and non-structural countermeasures to prevent such disasters is effectively studied only with the proper numerical simulation. The efficiency of the sediment removal system with various parameters is easily analyzed with the numerical simulation. The climate change scenarios are effectively addressed with the quick changes in the model. However, the mechanism of debris flows is very complex. From the outset, research has always concentrated on understanding the physical mechanisms that govern the triggering of debris flows along particularly steep slopes,

their mobilization and their relatively abrupt stoppage in the fan area. The matter is complex and must be tackled from various points of view; sources of continuous interest are the dynamic behavior of these particularly concentrated mixtures and given their non-Newtonian nature, the constitutive laws that govern them.

Since Bagnold (1954) presented his dilatant fluid model in 1954, a large number of other constitutive laws have been put forward. The approaches adopted for studying this matter are the traditional approach proposed by Shields (1936), which analyzes the instability of a mobile bed in streams characterized by bed-load or suspended load, through a transport mechanism that has been defined as individual particle motion as it considers the equilibrium of a single particle. It also considers that proposed by Takahashi (1981, 1991), which analyzes the stability of an entire finite and saturated granular layer, subject to a surface flow of water, and for this reason it has been defined as massive motion. The study of natural river bed changes and the deposition and erosion in natural water bodies is a difficult but important research topic. The basic principles for these studies are well established, yet a complete analytical solution is not known but for the most basic cases is not difficult to find the exact solution. The complexities of the flow movement and its interaction with its boundaries, which are deformable, have precluded the development of closed form solutions to governing equations that describe the mechanical behavior of fluid and solid-fluid mixtures. There are two types of models: the numerical model, which is based on computation techniques and the physical model, which is based on traditional laboratory techniques and equipment for experimental measurements of the necessary parameters to solve the problem. Numerical modeling has become very popular in the past decades, mainly due to the development of data processing, storage capacity and increasing availability of more powerful and affordable computing platforms.

Debris flow is a rapidly moving fluid of a mixture of sediment and water that occurs in a wide variety of environments throughout the world. To understand the formation process on the debris-flow breaker, this study (numerical simulation of debris flow) analyzes the mechanism and hydraulic characteristics of the interaction between the opening and blocking areas. For this purpose, a new 2-D numerical analysis model (Kim et al. 2012a, 2012b) will be developed to analyze debris flow based on an existing 2-D numerical model (Takahashi 1991). Chapter 3 provides a detailed description on numerical simulation, which was developed to analyze flow interactions between the opening and blocking sizes under the debris-flow breaker, as well as the characteristics of the deposition process of debris flows under the various parameters (i.e. bed sediments and various configuration conditions) and verification of numerical simulations with experimental results.

3.2 Pore Water Pressure on the Debris-Flow Breaker

The debris-flow breaker is a simple engineering structure that filters fine sediment with water and traps the course debris on a horizontal screen. It was designed to separate coarser clastic debris from water with a fine debris matrix so that the water passes through the breaker board while the coarser debris flow is trapped. When the debris flow reaches the breaker, the separation occurs rapidly which can changes the pore water pressure (γ is a coefficient of pore water pressure) as shown in Figure 3.1.

Bottom rack or bottom intake (i.e. debris-flow breaker) is a simple structure that consists of a channel on the river bottom vertical to the river flow and a screen on top of the channel, as shown in Photo 3.1. Water intakes by trash racks located on the beds of streams are often adopted in relatively small mountain rivers, where steep slopes, irregular bed configurations, intense sediment transport, and rapid floods prevent the use of gated dams (Bouvard 1992). Much research is being carried out to estimate the function of bottom racks as well to clarify the discharge ratio based on field observations, laboratory experiments, and numerical simulations.

The review of present knowledge is restricted to rectangular channels with an opening in the bottom made of racks to divert sediment and to produce an intake structure in which sediment sizes larger than the bar spacing are excluded (Brunella et al. 2003). The hydraulic behavior of bottom racks is also strongly influenced by the particular arrangement of bars forming the rack. The first hydraulic description of bottom intakes was provided by Orth et al. (1954) investigating flows on a 20% sloping channel with five different transverse rack geometries. Kuntamann and Bouvard (1954) presented the first computational approach for the free-surface profile over bottom racks by assuming constant energy at the head and a conventional orifice equation. Ract-Madoux et al. (1955) presented general experiences on bottom intakes obtained through various projects in the Savoy region of the French Alps. Their general conclusions may be summarized as follows: (1) a knowledge of the water and sediment

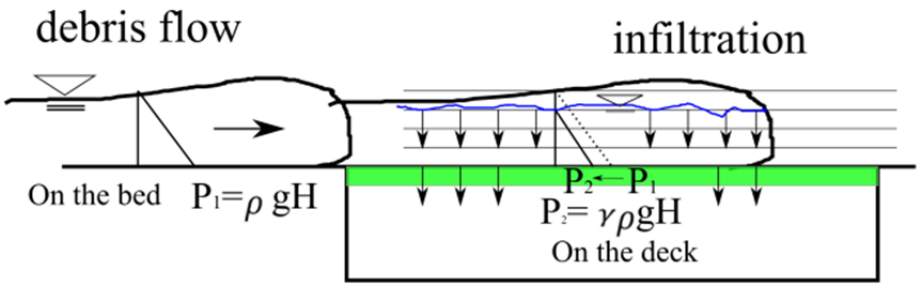

Figure 3.1 Sketch of pore water pressure distribution on the debris-flow breaker

discharge is important for design; (2) the rack should consist of rounded profiles in the direction of the stream; (3) to obtain a minimum risk of sediment clogging, the bottom slope of the rack should be more than 20%; and (4) a rack spacing of less than 0.10 m should be acceptable for mountainous regions.

A bottom rack depends on the parameters such as the configuration of the screen (length of rack, opening and blocking sizes), slope (angle at which the rack axis forms with the horizontal), flow depth, and Froude number. Generally, the rate of change of the diverted discharge per unit width is given by the relationship:

$$\frac{dq}{dx} = C_q \omega \sqrt{2gY} \tag{3.1}$$

where d_q=discharge per unit width diverted along a piece of grid length d_x, ω=void ration (i.e. the ratio of the openings area to the total area), Y=suitable value of the hydraulic head, and C_q=discharge coefficient. The latter coefficient depends on the hydraulic characteristics of the approaching flow, the geometry of the rack (length, slope, orientation), and of the bars forming the rack (form, size, spacing). Furthermore, many researchers suggested each of the parameter values. However, almost all studies were performed using clear water without sediment, while a few studies were conducted with sediment to see the rate of clogging of the breaker due to the presence of sediment. Likewise, debris flows in the latter case occurs in different phenomena on the debris-flow breaker in comparison to the clear water and the mechanism of the debris-flow breaker structure has not been well explained.

In previous studies by Mizuyama and Mizuno (1994) as well as Gonda (2009), debris-flow breakers were used to visualize debris flow phenomenon. As per Gonda (2009), it was suggested that change in pore water pressure is due to the suction by γ factor using a 1-D dynamic model, with the relationship among γ, K_s, and K_d given simply by Eq. (3.2).

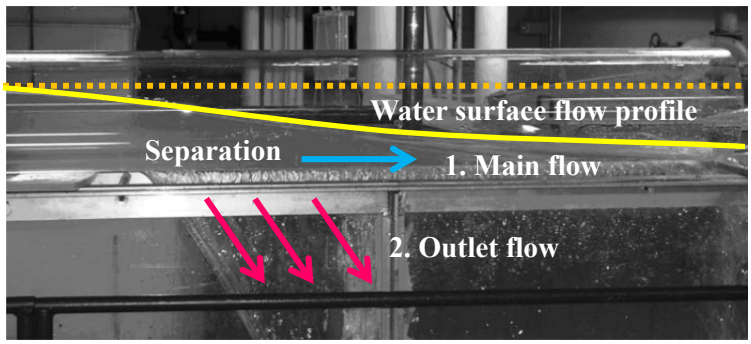

Photo 3.1 Image of flow profile over a bottom outlet slot (Lewis et al. 2011)

$$\gamma = \begin{cases} 0 & : \ (K_s \geq K_d) \\ 1-(K_s / K_d) & : \ (K_s < K_d) \end{cases} \tag{3.2}$$

K_s = the permeability of the breaker and K_d = the sediment pores near the breaker.

Gonda's (2009) study considered only the permeability of breaker and the porosity of sediment. However, we found the need to modify the previous γ coefficient of pore water pressure because the previous γ coefficient is not coherent with all cases. Specifically, in this study, results of the travel lengths, case1-0.2-B (travel length is 39.0 cm and the γ coefficient is 0.191), case3-0.2-B (travel length is 40.6 cm and the γ coefficient is 0.823), and case6-0.2-B (travel length is 37.9 cm and the γ coefficient is 0.909) are recorded around 39.2 cm as experimental data (as shown in Figure 3.2). Results of travel lengths are very similar but the γ coefficients have very different values in each case. Figure 3.2 shows that the results of the travel length and γ coefficient depend on the blocking size and opening size with sediment B (using previous the γ coefficient). Thus, in this study (Kim et al. 2012b), new γ coefficients are estimated as below:

$$\gamma = \begin{cases} 1 & : \ \text{on the bed} \\ 1-\left[\dfrac{k_s}{k_d} \times \text{Impact of loss}\right]^T & : \ \text{on the deck} \end{cases} \tag{3.3}$$

$$\begin{aligned} &\text{Impact of loss} = 1-\left(\frac{N_h}{W}\right) \\ &N_h = \left[\frac{2\left(\sum l_o \times \sum l_b\right)}{\sum l_o + \sum l_b}\right] \end{aligned} \tag{3.4}$$

Here, k_s is the permeability of debris-flow breaker, k_d is the porosity of sediment, l_o and l_b are the opening size and blocking size, W is the width in the debris-flow breaker and T is the constant coefficient (equal to 0.3). The new γ coefficient included an impact of loss factor, as in Eq. (3.4). Impact of loss factors indicates the effectiveness between the opening size and blocking size using the T-test method (Ralph et al. 2000). This analysis is appropriate whenever you want to compare the impact of two groups. Figure 3.3 shows that the proposed relation of the γ coefficient depends on the variation of the blocking size and opening size using Eq. (3.3).

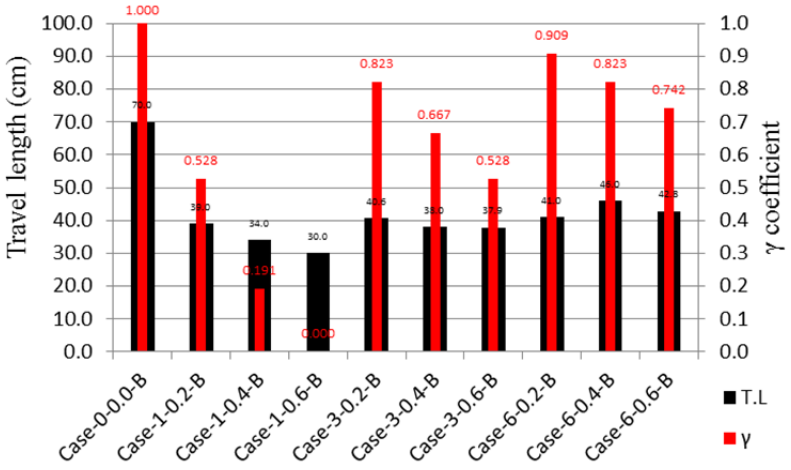

Figure 3.2 Compare to travel length and γ coefficient

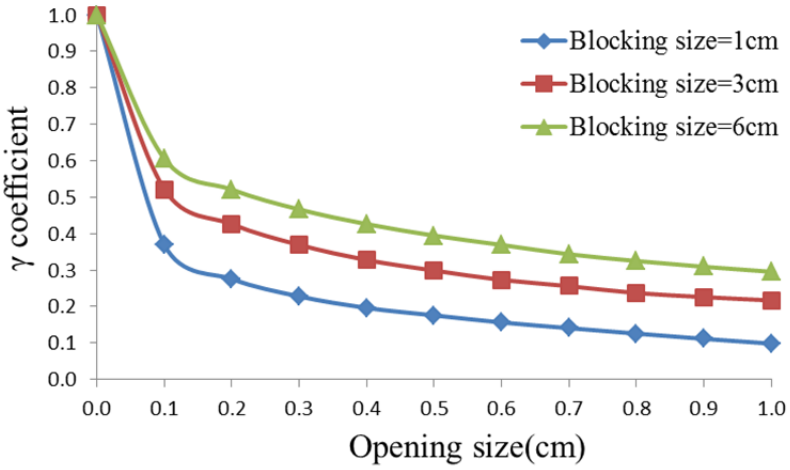

Figure 3.3 Variation of γ coefficient (in the case of sediment B)

3.3 Governing Equations

Since the numerical three-dimensional calculation is still very difficult (the mechanism of debris flow is very complex compared with the clear fluid because it was composed of many particles and water), it makes sense to reduce the Reynolds equations for calculations with simpler flow conditions. The depth-averaged two-dimensional flow equations, also called shallow water equations, provide an example. The shallow water equations are obtained, as the name suggests by averaging the Reynolds equations over the depth. Simplified Reynolds equations can be written as follows:

$$\frac{\partial u}{\partial t}+\frac{\partial uu}{\partial x}+\frac{\partial uv}{\partial y}+\frac{\partial uw}{\partial z}=F_x-\frac{\partial p}{\partial x}+\varepsilon\left(\frac{\partial^2 u}{\partial x^2}+\frac{\partial^2 u}{\partial y^2}+\frac{\partial^2 u}{\partial z^2}\right) \tag{3.5}$$

$$\frac{\partial v}{\partial t}+\frac{\partial vu}{\partial x}+\frac{\partial vv}{\partial y}+\frac{\partial vw}{\partial z}=F_y-\frac{\partial p}{\partial y}+\varepsilon\left(\frac{\partial^2 v}{\partial x^2}+\frac{\partial^2 v}{\partial y^2}+\frac{\partial^2 v}{\partial z^2}\right) \tag{3.6}$$

$$\frac{\partial w}{\partial t}+\frac{\partial wu}{\partial x}+\frac{\partial wv}{\partial y}+\frac{\partial ww}{\partial z}=F_z-\frac{\partial p}{\partial z}+\varepsilon\left(\frac{\partial^2 w}{\partial x^2}+\frac{\partial^2 w}{\partial y^2}+\frac{\partial^2 w}{\partial z^2}\right) \tag{3.7}$$

When we take *x, y* axes horizontally and the *z* axis vertically, $F_x = F_v = 0$, F_z=-*g* for the vertical direction, gravity and pressure term is significant. Thus, Eq. (3.7) is simplified as follows:

$$0=-g-\frac{1}{\rho}\frac{\partial p}{\partial z} \tag{3.8}$$

The continuity equation is

$$\frac{\partial u}{\partial x}+\frac{\partial v}{\partial y}+\frac{\partial w}{\partial z}=0 \tag{3.9}$$

where *u(t, x, y, z), v(t, x, y, z)* and *w(t, x, y, z)* are velocity components in *x, y* and *z* directions, respectively, *t*= time, *g*= gravitational force per unit mass, *p*= pressure, ε= kinetic eddy viscosity, and ρ= density of fluid.

In the case of overland flood flows, flow conditions can be characterized as shallow because the problem possesses much larger horizontal than vertical scales. These equations can be integrated over *z* direction under the assumption of hydrostatic pressure distribution. Referring the pressure term of Eq. (3.8) can be integrated by using the Leibniz rule from bed surface $z = z+z_b$ to water surface $z=\eta$ as follows:

$$\int_{z_b}^{\eta}-\frac{1}{\rho}\frac{\partial P}{\partial x}dz=-gh\frac{\partial H}{\partial x} \tag{3.10}$$

where *H* is water level, $H=\eta=h+z_b$ ($z_b=\eta_b$, elevation of bed surface from datum line). This

equation is used the boundary conditions between the bed (equal to hydrostatic pressure) and surface (equal to zero). However in the case of debris-flow breakers, the pore water pressure will change rapidly on the debris-flow breaker with the opening area. Even if the debris flow will block the opening area due to the deposition, the separation still occurs through the porosity between the sediments. Therefore, in this study, in order to consider the change in pore water pressure on the breaker, it used the two kinds of bed boundary conditions between the bed (kinetic boundary condition) and the breaker (kinetic boundary condition with Eq. (3.3) relation of γ coefficient). Using both boundary conditions, it can be rewritten as follows by substituting, $p= \rho g(\eta-z)$, $p(\eta)=0$ (at the surface), and $p(z_b)= \gamma\rho gh$ (at the debris-flow breaker).

$$
\begin{aligned}
\int_{\eta_b}^{\eta} -\frac{1}{\rho}\frac{\partial P}{\partial x}dz &= -\frac{1}{\rho}\left\{\frac{\partial}{\partial x}\int_{\eta_b}^{\eta} Pdz - P(\eta)\frac{\partial \eta}{\partial x} + P(\eta_b)\frac{\partial \eta_b}{\partial x}\right\} \\
&= -\frac{1}{\rho}\left\{\frac{\partial}{\partial x}\int_{\eta_b}^{\eta} pg(\eta - z)dz - P(\eta)\frac{\partial \eta}{\partial x} + P(\eta_b)\frac{\partial \eta_b}{\partial x}\right\} \\
&= -\frac{1}{\rho}\left\{\frac{\partial}{\partial x}\left[pg(H_z - z^2/2)\right]_{\eta_b}^{\eta} + P(\eta_b)\frac{\partial \eta_b}{\partial x}\right\} \\
&= -\left\{\frac{\partial}{\partial x} g\left(H^2/2 - H_{\eta_b} + \eta_b^{\,2}/2\right) + \frac{1}{\rho}P(\eta_b)\frac{\partial \eta_b}{\partial x}\right\} \\
&= -gh\frac{\partial H}{\partial x} + g\eta_b\frac{\partial H}{\partial x} + gH\frac{\partial \eta_b}{\partial x} - g\eta_b\frac{\partial \eta_b}{\partial x} - \frac{1}{\rho}P(\eta_b)\frac{\partial \eta_b}{\partial x} \\
&= -g\frac{\partial H}{\partial x}(H - \eta_b) + gH\frac{\partial \eta_b}{\partial x} - g\eta_b\frac{\partial \eta_b}{\partial x} - \frac{1}{\rho}P(\eta_b)\frac{\partial \eta_b}{\partial x} \\
&= -gh\frac{\partial H}{\partial x} + \left(gh - \frac{1}{\rho}P(\eta_b)\right)\frac{\partial \eta_b}{\partial x} \\
&= -gh\frac{\partial H}{\partial x} + \left(gh - \gamma gh\right)\frac{\partial \eta_b}{\partial x} \\
&= -gh\frac{\partial H}{\partial x} + \left(gh - \gamma gh\right)\frac{\partial z_b}{\partial x}
\end{aligned}
\tag{3.11}
$$

The depth-wise averaged two-dimensional debris flow model consisted of the momentum equations with constitutive equations, the total volume and the sediment particles fraction of continuity equations, the change in bed surface elevation equation, and erosion or deposition velocity equations. The developed model of composition is summarized in the following section.

3.3.1 Momentum Conservation Equations

The depth-wise averaged two-dimensional momentum equations of the debris flow for the *x*–wise (down valley) and the *y*-wise (lateral) directions are described as follows.

$$\frac{\partial M}{\partial t}+\beta\frac{\partial(uM)}{\partial x}+\beta\frac{\partial(vM)}{\partial y}=gh\sin\theta_{bx0}-gh\cos\theta_{bx0}\frac{\partial(z_b+h)}{\partial x}$$
$$-(gh-\gamma gh)(\sin\theta_{bx0}-\cos\theta_{bx0}\frac{\partial z_b}{\partial x})-\frac{\tau_{bx}}{\rho_T} \tag{3.12}$$

$$\frac{\partial N}{\partial t}+\beta\frac{\partial(uM)}{\partial x}+\beta\frac{\partial(vM)}{\partial y}=gh\sin\theta_{by0}-gh\cos\theta_{by0}\frac{\partial(z_b+h)}{\partial y}$$
$$-(gh-\gamma gh)(\sin\theta_{by0}-\cos\theta_{by0}\frac{\partial z_b}{\partial y})-\frac{\tau_{by}}{\rho_T} \tag{3.13}$$

The continuity equation of the total volume is:

$$\frac{\partial h}{\partial t}+\frac{\partial M}{\partial x}+\frac{\partial N}{\partial y}=i_b \tag{3.14}$$

The continuity equation of the coarser particle fraction that is sustained in the flow by the action of the particle encounter is:

$$\frac{\partial(C_L h)}{\partial t}+\frac{\partial(C_L M)}{\partial x}+\frac{\partial(C_L N)}{\partial y}=\begin{cases} i_b C_{*L} & (i_b\geq 0)\\ i_b C_{*DL} & (i_b<0)\end{cases} \tag{3.15}$$

The continuity equation for the fine particle fraction that is sustained in the interstitial fluid by the action of turbulences is:

$$\frac{\partial\{(1-C_L)C_F h\}}{\partial t}+\frac{\partial\{(1-C_L)C_F M\}}{\partial x}+\frac{\partial\{(1-C_L)C_F N\}}{\partial y}$$
$$=\begin{cases} i_b(1-C_{*L})C_{*F}; & (i_b\geq 0)\\ i_b(1-C_{*DL})C_F; & (i_b<0)\end{cases} \tag{3.16}$$

Here, $M=(uh)$ and $N=(vh)$ are the flow discharge per unit widths in x and y directions, u and v are the velocity components in x and y directions, h is the flow depth, z_b is erosion or deposition thickness of the bed measured from the original bed surface elevation, β is the momentum correction factor equal to 1.25 for stony debris flow (Takahashi et al. 1992) and equal to 1.0 for both an immature debris flow and a turbulent flow, i_b is the erosion (≥ 0) or deposition (< 0) velocity, g is the acceleration due to gravity, θ_{bx0} and θ_{by0} are the x and y components of the

slope of the original bed surface, τ_{bx} and τ_{by} are the bottom shear stresses in x and y directions, ρ_t the is mixture density ($\rho_t=\sigma C+(1-C)\rho$, σ is the density of the sediment particles, and ρ is the density of the water), C is the sediment concentration in the flow, C_* is the sediment concentration in the bed, C_L is the volumetric sediment concentration of the coarser fraction in the flow, C_F is the volumetric sediment concentration of the fine fraction in the interstitial fluid, C_{*L} and C_{*F} are the volumetric concentrations of the coarser and fine fractions in the original bed, and C_{*DL} is the volumetric concentration of the coarser fraction in the static bed produced by deposition of the debris flow.

The erosion or deposition thickness to calculate the change in bed surface elevation is given by:

$$\frac{\partial z_b}{\partial t} + i_b = 0 \tag{3.17}$$

3.3.2 Constitutive Equations and Bottom Shear Stress

Many researchers have proposed several constitutive equations for debris flow. A debris flow implies fluid-to-fluid, fluid-to-solid, and solid-to-solid interactions, which are generally not well understood and are not considered in most of the existing approaches to model debris flows (Koch 1998). Most of the models developed have been restricted to the one-dimensional case, with mainly three types of constitutive equations: Bingham flow, Newtonian turbulent flow, or Quasi-dilatant flow by Sharpe (1938), Varnes (1958), Takahashi (1977, 1980, 1981, 1991), Miyamoto (1985), Tsubaki et al. (1982), O'Brien and Julien (1988), Coussot (1992), Ashida (1992), Hunt (1994), and Egashira et al. (1989, 1997). In particular, Takahashi (1991) presented a detailed understanding of the mechanics of the flow of a layer of a particle-fluid mixture under simple gravity driven shear from Bagnold's (1954) grain inertial and macro viscous regimes. The model equations of the two-constituent model were eventually simplified to essentially a one-constituent model. In this study, the development of a 2-D numerical analysis model will be modified to analyze debris flows based on an existing 2-D numerical model (Takahashi 1991).

In the upstream region of a debris-flow breaker, the sediment concentration is higher than that of the equilibrium state and becomes its maximum concentration due to the existence of the debris-flow breaker. The yield stress exceeds the driving force, and then the debris flow stops and deposition occurs, before filling up the upstream of the breaker. This mechanism of deposition is incorporated in the momentum equation of the flow mixture when considering yield stress in the bottom shear stress. From a review of the mechanism of debris flows, the

space where stress occurs as Bingham fluid is independent from the space where stress occurs as a dilatant fluid; moreover, since Reynolds stress expresses the amount of momentum transport, three of them can be added to a linear type. The following formula generally holds true as the fluid equation of debris flows.

$$\tau = C_o + \tau_y + \mu\left(\frac{du}{dz}\right) + A\left(1-e^2\right)\sigma\frac{1}{b}d^2\left|\frac{du}{dz}\right|\left(\frac{du}{dz}\right) - \rho\overline{u`v`} \tag{3.18}$$

Here, τ is shear stress due to the flow, the first term C_o is the cohesive component, the second term τ_y is the shear stress yield, which is not dependent on the velocity gradient, the third term μ is the apparent coefficient of viscosity and du/dz is the velocity gradient, the fourth term is shear stress caused by the collision between the particles, and the last term is shear stress due to turbulent mixing.

The constitutive equations of Takahashi et al. (1997) for a fully stony debris flow are described in the following. The expression for the shear stress is:

$$\tau = \tau_y + a_i \sin a_i \left\{\left(\frac{C_*}{C_L}\right)^{1/3} - 1\right\}^{-2} \sigma d_m^2 \left(\frac{\partial u}{\partial z}\right)^2 \tag{3.19}$$

$$\tau_y = p_s \tan\phi \tag{3.20}$$

where α_i is the experiment constant, α_i is the collisions angle of the particle ($\alpha_i \sin\alpha_i = 0.02$) (Takahashi et al. 1992), z is the coordinate perpendicular to the bed and positive upward in the normal direction of flow (Figure 3.4) and p_s is the static pressure which can be expressed as follows (Takahashi et al. 1997).

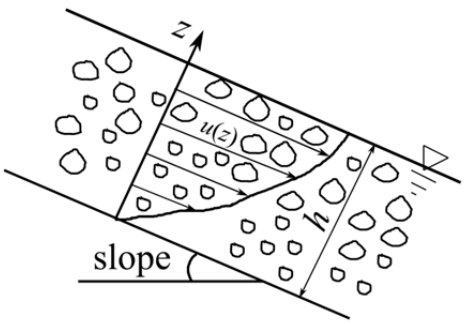

Figure 3.4 Coordinate of two-dimensional uniform debris flow

$$p_s = f(C_L)(\sigma - \rho) C_L g (h - z) \cos\theta \tag{3.21}$$

in which $f(C_L)$ is described as

$$f(C_L) = \begin{cases} \dfrac{C_L - C_3}{C_* - C_3} & ; \quad C_L > C_3 \\ 0 & ; \quad C_L \le C_3 \end{cases} \tag{3.22}$$

where C_3 is the limitative sediment concentration. Therefore, the bottom shear stress for a two-dimensional flow is described as follows.

For a fully developed stony debris flow: ($C_L > 0.4C_*$)

$$\tau_{bx} = \frac{u}{\sqrt{u^2 + v^2}} \tau_{yx} + \rho f_b u \sqrt{u^2 + v^2} \tag{3.23}$$

$$\tau_{by} = \frac{v}{\sqrt{u^2 + v^2}} \tau_{yy} + \rho f_b v \sqrt{u^2 + v^2} \tag{3.24}$$

in which τ_{yx} and τ_{yy} are the yield stresses in x and y directions, it can be expressed using the constitutive equations of Takahashi et al. (1997) as follows:

$$\tau_{yx} = f(C_L)(\sigma - \rho) C_L g h \cos\theta_x \tan\phi \tag{3.25}$$

$$\tau_{yy} = f(C_L)(\sigma - \rho) C_L g h \cos\theta_y \tan\phi \tag{3.26}$$

Here, θ_x and θ_y are the x and y components of the slope of the bed surface. C_s is the limitative sediment concentration (=0.48). The coefficient of resistance, f_b, is described below.

For an immature debris flow: ($0.02 \le C_L \le 0.4C_*$)

$$\tau_{bx} = \frac{\rho_T}{0.49} \left(\frac{d_m}{h} \right)^2 u \sqrt{u^2 + v^2} \tag{3.27}$$

$$\tau_{by} = \frac{\rho_T}{0.49}\left(\frac{d_m}{h}\right)^2 v\sqrt{u^2+v^2} \tag{3.28}$$

For a turbulent flow: $(C_L < 0.02)$;

$$\tau_{bx} = \frac{\rho g n^2 u\sqrt{u^2+v^2}}{h^{1/3}} \tag{3.29}$$

$$\tau_{by} = \frac{\rho g n^2 v\sqrt{u^2+v^2}}{h^{1/3}} \tag{3.30}$$

3.3.3 Erosion and Deposition Velocity Equations

The bed erosion or deposition velocity i_b is a source term. The dependence of this quantity with the basic set of dependent variables has to be modeled, which can be done using the model proposed by Takahashi et al. (1992). The erosion and deposition velocity are described as follows.

Erosion velocity, if $C \le C_\infty$;

$$i_b = \delta_e \frac{C_\infty - C_L}{C_* - C_\infty}\frac{\sqrt{u^2+v^2}h}{d_m} \tag{3.31}$$

Deposition velocity, if $C > C_\infty$;

$$i_b = \delta_d\left(1-\frac{\sqrt{u^2+v^2}}{pU_e}\right)\frac{C_\infty - C_L}{C_{*DL}}\sqrt{u^2+v^2} \tag{3.32}$$

where $p = (2/3)$ is a numerical constant and U_e is the equilibrium velocity at which neither erosion nor deposition takes place, as follows.

$$U_e = \frac{2}{5d_m}\left[\frac{g\sin\theta_e}{a_i\sin\alpha_i}\left\{C_L + (1-C_L)\frac{\rho_m}{\sigma}\right\}\right]^{1/2}\left\{\left(\frac{C_{*DL}}{C_L}\right)^{1/3} - 1\right\}h^{3/2} \tag{3.33}$$

where θ_e channel slope in which coarser sediment concentration is in equilibrium, which can be obtained as follows.

$$\tan\theta_e = \frac{C_L(\sigma-\rho_m)\tan\phi}{C_L(\sigma-\rho_m)+\rho_m} \tag{3.34}$$

where ϕ is the internal friction angle of sediment, δ_e (=0.0007) is the erosion coefficient, δ_d (=0.01) is the deposition coefficient, d_m is the mean diameter of the sediment, and C_∞ is the equilibrium sediment concentration, described as follows (Nakagawa et al. 2003). If $\tan\theta_w > 0.138$, a stony type debris flow occurs, and

$$C_\infty = \frac{\tan\theta_w}{(\sigma/\rho-1)(\tan\phi-\tan\theta_w)} \tag{3.35}$$

If $0.03 < \tan\theta_w \le 0.138$, an immature type debris flow occurs, and

$$C_\infty = 6.7\left\{\frac{\rho_m\tan\theta_w}{(\sigma-\rho_m)(\tan\phi-\tan\theta_w)}\right\}^2 \tag{3.36}$$

If $\tan\theta_w \le 0.03$, a turbulent water flow with bed load transport occurs, and

$$C_\infty = \frac{(1+5\tan\theta_w)\tan\theta_w}{\sigma/\rho_m-1}\left(1-\alpha_0^2\frac{\tau_{*c}}{\tau_*}\right)\left(1-\alpha_0^2\sqrt{\frac{\tau_{*c}}{\tau_*}}\right) \tag{3.37}$$

where θ_w is the water surface gradient, ρ_m is the density of the water, ϕ is the internal friction angle of the sediment, and

$$\alpha_0^2 = \frac{2\{0.425-(\sigma/\rho_T)\tan\theta_w/(\sigma/\rho_T-1)\}}{1-(\sigma/\rho_T)\tan\theta_w/(\sigma/\rho_T-1)} \tag{3.38}$$

$$\tau_{*c} = 0.04\times10^{1.72\tan\theta_w} \tag{3.39}$$

$$\tau_* = \frac{h \tan\theta_w}{(\sigma / \rho_T - 1) d_m} \tag{3.40}$$

in which τ_{*c} is the non-dimensional critical shear stress and τ_* is the non-dimensional shear stress.

The inclination of the surface of the flow to the direction of the velocity vector, which is necessary for the calculation of C_∞ using Equation (3.35), (3.36), or (3.37), is described as

$$\tan\theta_w = \frac{u \sin\theta_{bx}^{'} + v \sin\theta_{by}^{'}}{\sqrt{u^2 \cos^2\theta_{bx}^{'} + v^2 \cos^2\theta_{by}^{'}}} \tag{3.41}$$

where

$$\tan\theta_{bx}^{'} = \tan\left(\theta_{bx0} + \theta_{bzhx}\right); \quad \tan\theta_{by}^{'} = \tan\left(\theta_{by0} + \theta_{bzhy}\right) \tag{3.42}$$

$$\tan\theta_{bzhx} = \frac{-\partial\left(z_b + h\right)}{\partial x}; \quad \tan\theta_{bzhy} = \frac{-\partial\left(z_b + h\right)}{\partial y} \tag{3.43}$$

According to Takahashi (1991), the flow can be divided into three categories based on sediment concentration in the flow: (a) stony debris flow, (b) immature debris flow, and (c) turbulent flow. Different flow resistance equations are proposed for different types of flow. The flow is called stony debris flow when the volume concentration of the solids fraction in the flow (C) is more than 40% of the volume concentration in the bed (C_*) as below.

$$C > 0.4 C_* \tag{3.44}$$

The flow is called immature debris flow if the volume concentration of solids is larger than 1% but smaller than 40 % of C_*. If the volume concentration of the solid is less than 1 %, the flow is called turbulent flow and the sediment flow regime is a bed load or suspended load.

3.4 Solution Methods

This numerical analysis method is based on FDM (Finite Difference Method) and thus, grid generation should be put used first to calculate it. In grid construction, the calculation area is divided into fixed rectangular grids through a discretization procedure, considering the given physical insight, numerical stability, and accuracy. The partial differential equations of basic equations of debris flow are obtained from the methods of Nakagawa (1989) using a Leap-Frog scheme, in which an upwind scheme is adopted in the advection term and an implicit scheme is introduced in the friction term. Vector quantities, such as *M, N* and *u, v* are defined in the middle of the cell face and scalar quantities, such as *h,* C_L, and C_F are defined in the center of the cell (Figure 3.5). The arrangement of variables and the way to advance the calculations are shown in Figure 3.6. The finite difference form of Eq. (3.12) for the momentum equation in the *x* direction is as follows.

$$\begin{aligned}
&\frac{M_{i,j+1/2}^{n+2}-M_{i,j+1/2}^{n}}{2\Delta t}+\beta XDX+\beta XDY= \\
&\quad g\bar{h}\sin\theta_{bx0}-g\bar{h}\cos\theta_{bx0}\frac{\left(h+z_b\right)_{i+1/2,j+1/2}^{n+1}-\left(h+z_b\right)_{i-1/2,j+1/2}^{n+1}}{\Delta x} \\
&-\left(g\bar{h}-\gamma g\bar{h}\right)\left(\sin\theta_{bx0}-\cos\theta_{bx0}\frac{\left(z_b\right)_{i+1/2,j+1/2}^{n+1}-\left(z_b\right)_{i-1/2,j+1/2}^{n+1}}{\Delta x}\right) \\
&-\frac{u_{i,j+1/2}}{\sqrt{\left(u_{i+1/2,j}^{n}\right)^2+\left(v_{i+1/2,j}^{n}\right)^2}}\cdot\frac{f\left(\overline{C}_L\right)\left(\sigma-\rho\right)g\bar{h}\cos\theta_{bx\ i+1/2,j+1/2}^{n+1}+\cos\theta_{bx\ i-1/2,j+1/2}^{n+1}}{\overline{\rho}_T}\tan\phi \\
&-\rho\frac{1}{\overline{\rho}_T}\frac{f_{b\ i+1/2,j+1/2}^{n+1}+f_{b\ i-1/2,j+1/2}^{n+1}}{2}u_{i,j+1/2}\sqrt{\left(u_{i+1/2,j}^{n}\right)^2+\left(v_{i+1/2,j}^{n}\right)^2}
\end{aligned} \tag{3.45}$$

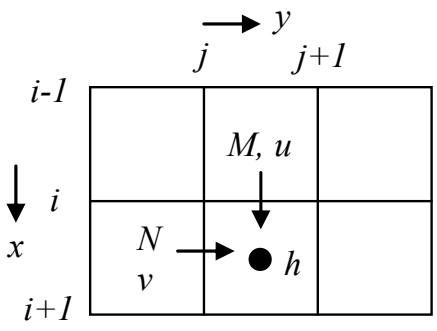

Figure 3.5 Arrangement of variables on meshes

where

$$XDX=\begin{cases}\dfrac{u^n_{i,j+1/2}M^n_{i,j+1/2}-u^n_{i-1,j+1/2}M^n_{i-1,j+1/2}}{\Delta x} & : \ u^n_{i,j+1/2}\ge 0,\quad u^n_{i-1,j+1/2}\ge 0\\ \dfrac{u^n_{i,j+1/2}M^n_{i,j+1/2}-0}{\Delta x} & : \ u^n_{i,j+1/2}\ge 0,\quad u^n_{i-1,j+1/2}< 0\\ \dfrac{u^n_{i+1,j+1/2}M^n_{i+1,j+1/2}-u^n_{i,j+1/2}M^n_{i,j+1/2}}{\Delta x} & : \ u^n_{i,j+1/2}< 0,\quad u^n_{i-1,j+1/2}< 0\\ \dfrac{0-u^n_{i,j+1/2}M^n_{i,j+1/2}}{\Delta x} & : \ u^n_{i,j+1/2}< 0,\quad u^n_{i+1,j+1/2}\ge 0\end{cases} \tag{3.46}$$

$$XDY=\begin{cases}\dfrac{\tilde{v}^n_{i,j+1/2}M^n_{i,j+1/2}-\tilde{v}^n_{i,j-1/2}M^n_{i,j-1/2}}{\Delta y} & : \ \tilde{v}^n_{i,j+1/2}\ge 0,\quad \tilde{v}^n_{i,j-1/2}\ge 0\\ \dfrac{\tilde{v}^n_{i,j+1/2}M^n_{i,j+1/2}-0}{\Delta y} & : \ \tilde{v}^n_{i,j+1/2}\ge 0,\quad \tilde{v}^n_{i,j-1/2}< 0\\ \dfrac{\tilde{v}^n_{i,j+3/2}M^n_{i,j+3/2}-\tilde{v}^n_{i,j+1/2}M^n_{i,j+1/2}}{\Delta y} & : \ \tilde{v}^n_{i,j+1/2}< 0,\quad \tilde{v}^n_{i,j+3/2}< 0\\ \dfrac{0-\tilde{v}^n_{i,j+1/2}M^n_{i,j+1/2}}{\Delta y} & : \ \tilde{v}^n_{i,j+1/2}< 0,\quad \tilde{v}^n_{i,j+3/2}\ge 0\end{cases} \tag{3.47}$$

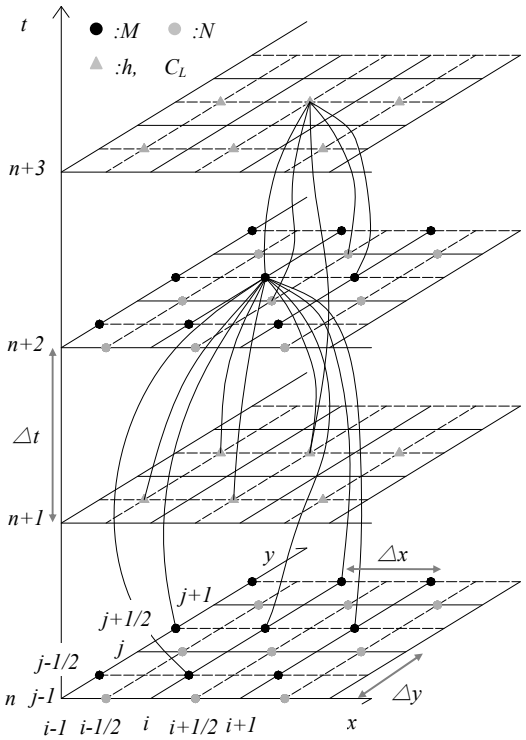

Figure 3.6 Arrangement of variables and the way of advancing the calculation

$$u_{i,j+1/2}^{n}=\frac{2M_{i,j+1/2}^{n}}{h_{i-1/2,j+1/2}^{n+1}+h_{i+1/2,j+1/2}^{n+1}},\qquad v_{i+1/2,j}^{n}=\frac{2N_{i+1/2,j}^{n}}{h_{i+1/2,j-1/2}^{n+1}+h_{i+1/2,j+1/2}^{n+1}} \tag{3.48}$$

$$\tilde{v}_{i,j+1/2}^{n}=\frac{1}{4}\left(v_{i-1/2,j}^{n}+v_{i-1/2,j+1}^{n}+v_{i+1/2,j}^{n}+v_{i+1/2,j+1}^{n}\right) \tag{3.49}$$

$$\overline{h}=\frac{h_{i-1/2,j+1/2}^{n+1}+h_{i+1/2,j+1/2}^{n+1}}{2} \tag{3.50}$$

$$\overline{\rho}_{T}=\left(\sigma-\rho\right)\overline{C}_{L}+\rho \tag{3.51}$$

$$\overline{C}_{L}=\frac{C_{Li-1/2,j+1/2}^{n+1}+C_{Li+1/2,j+1/2}^{n+1}}{2} \tag{3.52}$$

$$f(\overline{C}_{L})=\begin{cases}\dfrac{\overline{C}_{L}-C_{3}}{C_{*}-C_{3}} & ;\quad \overline{C}_{L}>C_{3}\\ 0 & ;\quad \overline{C}_{L}\le C_{3}\end{cases} \tag{3.53}$$

Similarly, we can get the finite difference form of Equation (3.13) for the momentum equation in the *y* direction. The finite difference from Equations (3.14) and (3.15) for the continuity equation of flow and coarser sediment are expressed as follows:

$$\frac{h_{i+1/2,j+1/2}^{n+3}-h_{i+1/2,j+1/2}^{n+1}}{2\Delta t}+\frac{M_{i+1,j+1/2}^{n+2}-M_{i,j+1/2}^{n+2}}{\Delta x}+\frac{N_{i+1/2,j+1}^{n+2}-N_{i+1/2,j}^{n+2}}{\Delta y}=i_{bi+1/2,j+1/2}^{n+1} \tag{3.54}$$

$$\frac{(C_{L}h)_{i+1/2,j+1/2}^{n+3}-(C_{L}h)_{i+1/2,j+1/2}^{n+1}}{2\Delta t}+\frac{Q_{Lxi+1,j+1/2}^{n+2}-Q_{Lxi,j+1/2}^{n+2}}{\Delta x}+\frac{Q_{Lyi+1/2,j+1}^{n+2}-Q_{Lyi+1/2,j}^{n+2}}{\Delta y}=i_{bi+1/2,j+1/2}^{n+1}C_{*L} \tag{3.55}$$

where

$$Q_{Lxi,j+1/2}^{n+2}=\begin{cases}M_{i,j+1/2}^{n+2}C_{Li-1/2,j+1/2}^{n+1}; & M_{i,j+1/2}^{n+2}\ge 0\\ M_{i,j+1/2}^{n+2}C_{Li+1/2,j+1/2}^{n+1}; & M_{i,j+1/2}^{n+2}<0\end{cases} \tag{3.56}$$

$$Q_{Lxi+1,j+1/2}^{n+2}=\begin{cases}M_{i+1,j+1/2}^{n+2}C_{Li-1/2,j+1/2}^{n+1}; & M_{i+1,j+1/2}^{n+2}\geq 0\\ M_{i+1,j+1/2}^{n+2}C_{Li+1/2,j+1/2}^{n+1}; & M_{i+1,j+1/2}^{n+2}<0\end{cases} \tag{3.57}$$

$$Q_{Lyi+1/2,j}^{n+2}=\begin{cases}N_{i+1/2,j}^{n+2}C_{Li+1/2,j-1/2}^{n+1}; & N_{i+1/2,j}^{n+2}\geq 0\\ N_{i+1/2,j}^{n+2}C_{Li+1/2,j+1/2}^{n+1}; & N_{i+1/2,j}^{n+2}<0\end{cases} \tag{3.58}$$

$$Q_{Lyi+1/2,j+1}^{n+2}=\begin{cases}N_{i+1/2,j+1}^{n+2}C_{Li+1/2,j-1/2}^{n+1}; & N_{i+1/2,j+1}^{n+2}\geq 0\\ N_{i+1/2,j+1}^{n+2}C_{Li+1/2,j+1/2}^{n+1}; & N_{i+1/2,j+1}^{n+2}<0\end{cases} \tag{3.59}$$

3.5 Boundary Conditions

Almost every computational fluid dynamics problem is defined under the limits of initial and boundary conditions. In order to solve a computational problem, boundary conditions are a required component of the mathematical model, and are very important. They are divided into two types of boundary conditions, Neumann and Dirichlet boundary conditions. It is generally impossible to test every possible set of inputs to an algorithm, but it should be able to prove that it works as expected by testing the boundary conditions for each set of possible inputs.

Fluids with different characteristics influence each other's flow according to the interaction. Therefore, boundary conditions are necessary to define how the site-specific model interacts with the entire flow system. The equations of motion require boundary conditions on all sides of the domain in which the solution is to be obtained. Furthermore, fluids with different characteristics influence each other's flow according to the interaction, and unknown variables in the cell center are determined as a function of the variables in the surrounding cell. If one fluid is analyzed in a numerical calculation having interface, the flow velocity and boundary condition of interface are required for smooth calculation as explained below.

- Inlet

  The values at the upstream end will be required at the stage. Variables at the inflowing boundary were defined by a Dirichlet boundary condition (fixed value). In this study, the water flow discharge is given as the input boundary condition at the upstream end of the inflow point.

- Outlet

  The outflow condition of the downstream end of the channel is used as the drop flow equation M or $N = h\sqrt{2gh}$.

- Free surface

  At the water surface, *u, v,* and *p* have zero gradient boundary conditions.

- Side-wall

  Regarding the boundary conditions at the side-wall, computation points at the boundary are deviated by half a mesh into the flow. A slip condition is applied to the side wall, although in this study, no friction on the side wall is considered.

The vector quantities, such as flow velocity and discharge, are defined in the middle of the cell, and scalar quantities such as flow depth, sediment concentration, and bed variation, are defined in the center of the cell.

3.6 Contents of Numerical Simulation

The overall calculation process of simulation by a numerical model described above can be expressed as in Figure 3.7 and can be categorized as below. Table 3.1 also shows the parameters for numerical simulation.

1) Initial conditions such as fluid condition, sediment properties (mixing sediment), incident conditions of inflow, and geometrical shape of structures with γ coefficient are entered.

2) The momentum equation is calculated to satisfy boundary conditions and the flow discharge per unit width of the next timed step is calculated.

3) By applying fluxes, which satisfy flow and sediment continuity, equations are calculated for sediment fluxes.

4) By applying fluxes, which satisfy flow and continuity, equations of the total volume

are calculated for the flow depth.

5) The inclination of the surface of the flow to the direction of the velocity vector, which is necessary for the calculation of equilibrium in the sediment concentration, is determined using the calculated gradient of flow surface.

6) The volume of the flow layer of the debris flow either increases or decreases, corresponding to its erosion or deposition.

7) It is repeated in each timed step.

Regarding the stability condition, the time interval Δt for the computation will be set to satisfy the normal CFL (Courant Friedrichs Lewy) condition as follows, but in order to proceed with the stable computation in practice, it is normally about 1/5 of this value.

$$\frac{\left|u+\sqrt{gh}\right|_{\max}\Delta t}{\Delta x}\le 1 \tag{3.60}$$

Table 3.1 Parameters for numerical simulation

Parameter	*Unit*	*Value*
Input discharge (Q_{in})	cm^3/sec	300
Supplying time	sec	10
Δx	cm	2
Δy	cm	1
Δt	sec	0.001
Calculation time (Q_{time})	sec	50
Density of a sediment particle (σ)	g/cm^3	2.65
Density of a water (ρ)	g/cm^3	1
Tangent of internal friction angle of sediment ($\tan\phi$)	-	0.7
The volumetric concentration of the solids in the bed (C_*)	-	0.65
The limitative sediment concentration (C_3)	-	0.48
Erosion coefficient (δ_e)	-	0.0018
Deposition coefficient (δ_d)	-	0.045

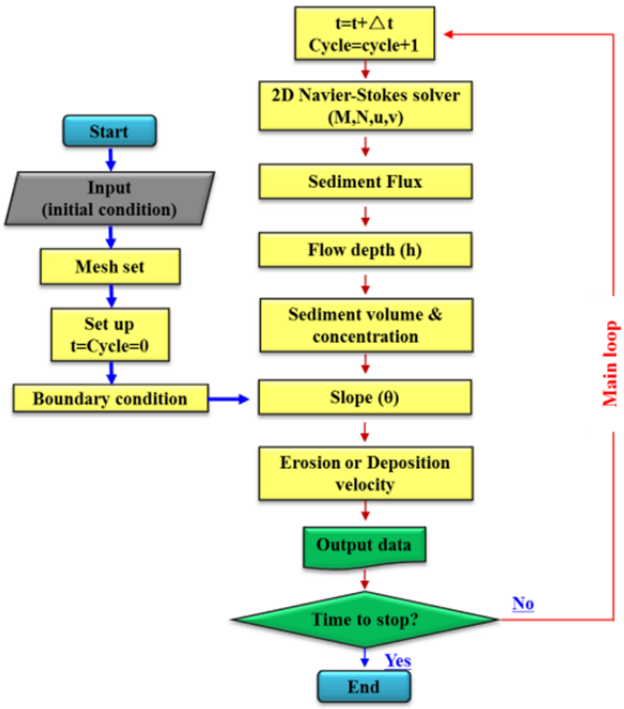

Figure 3.7 Flowchart of numerical analysis method

3.7 Numerical Results

This numerical simulation performs the study on the mechanisms and hydraulic characteristics of the debris-flow breaker, which leads to the measurement of different variables at the breaker because of changing pore water pressure that were only visualized (not measured) in the experiment. In this chapter, the results obtained from the numerical simulation are presented in detail.

3.7.1 Discharges and Sediment Concentration

The numerical simulation results of the outflow, sediment discharges, and sediment concentrations at the downstream end of the flume without a debris-flow breaker were obtained. The numerical simulations were carried out in fixed bed conditions like the experiments. The boundary conditions for the generation of debris flow are similar to the experiment with the flow of the constant water discharge of 300 cm^3/sec for 10 sec from the upstream end of the flume. The discharge hydrographs and sediment concentrations are plotted in Figure 3.8 from the numerical simulation with a flume slope of 18º.

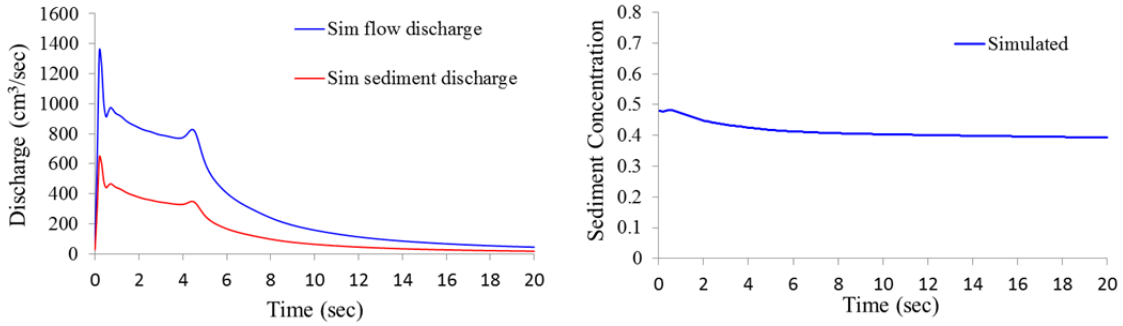

(a) Sediment A

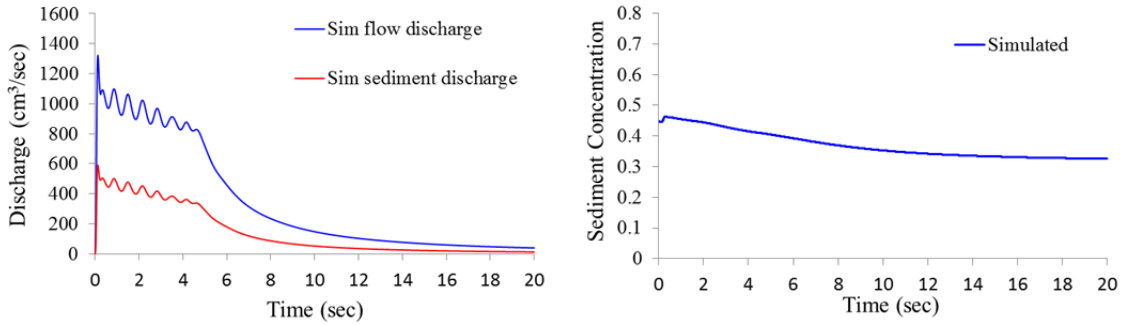

(b) Sediment B

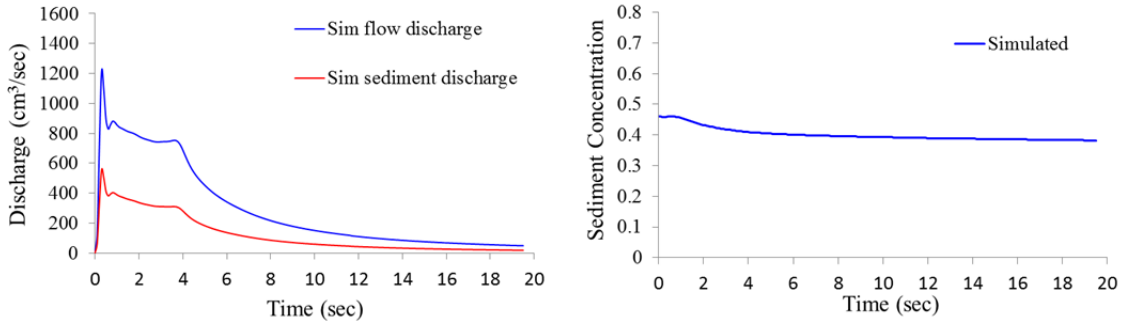

(c) Sediment C

Figure 3.8 Calculated and measured hydrographs at the downstream end of flume for bed sediment A, B, and C

3.7.2 Deposition Process (without Debris-Flow Breaker)

Figures 3.9-3.11 show the numerical results of the temporal changes of shapes and the thickness of a debris flow fan under the three different bed sediments without a debris-flow breaker.

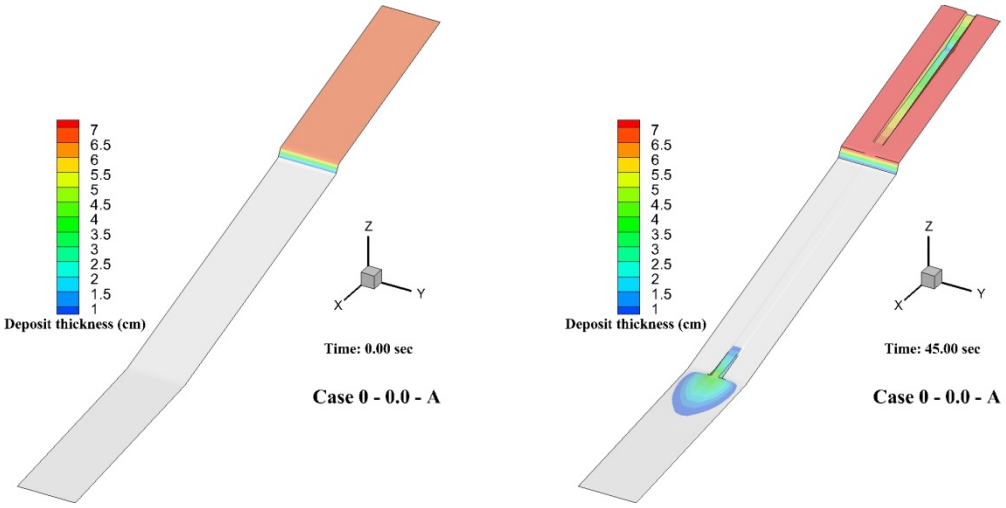

(a) Total view (without debris-flow breaker)

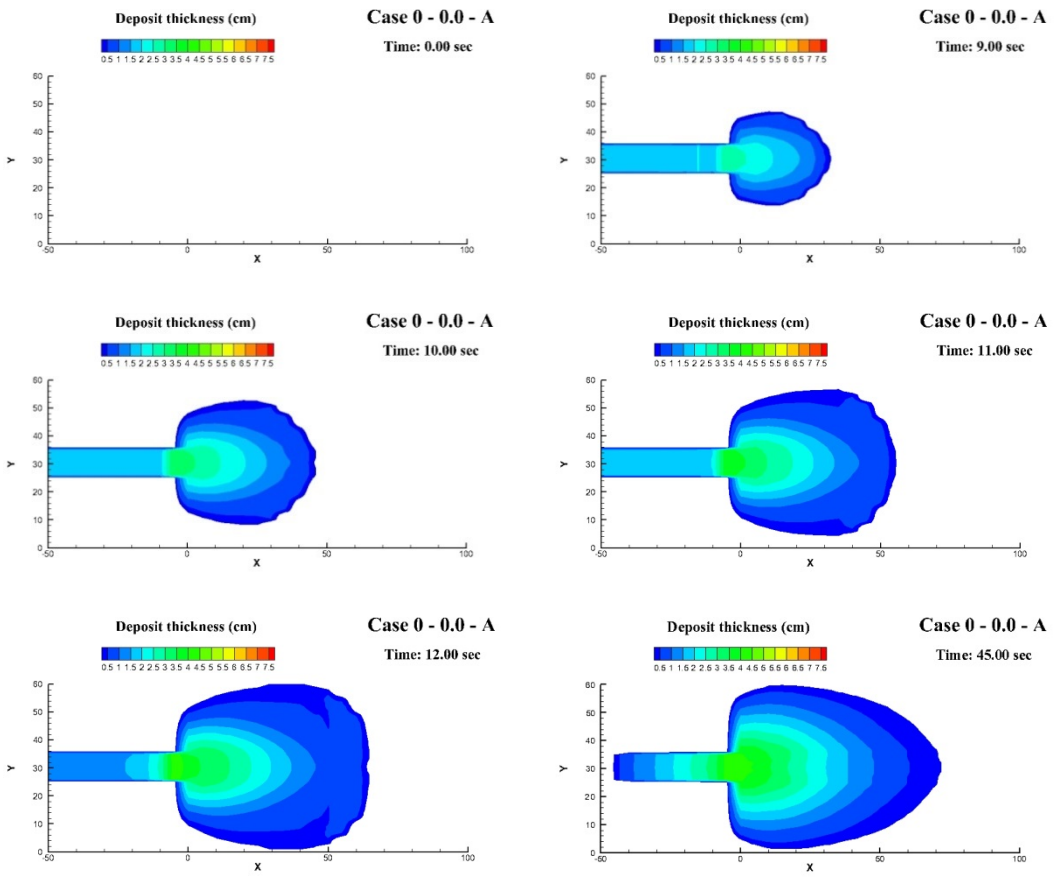

(b) Downstream view (without debris-flow breaker)

Figure 3.9 Numerical results of the movement of debris flow (Case0-0.0-A)

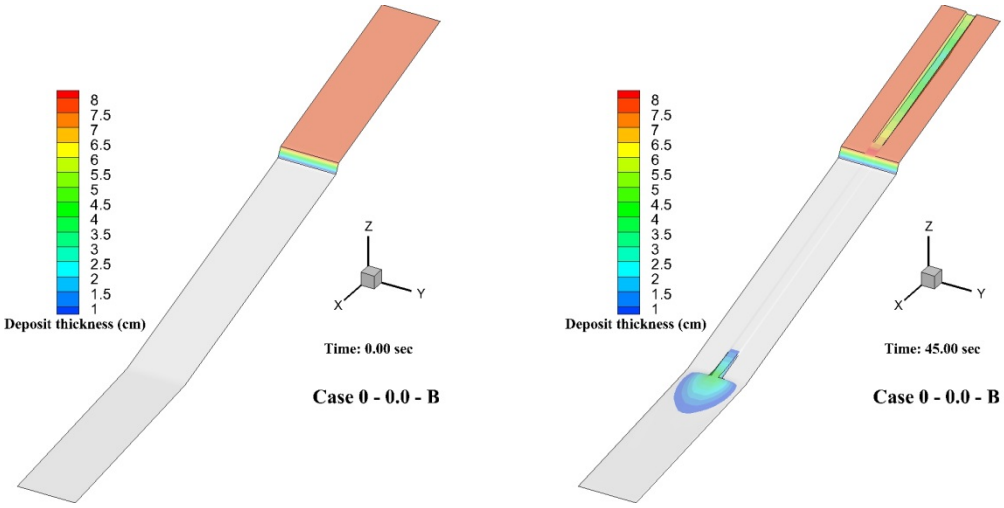

(a) Total view (without debris-flow breaker)

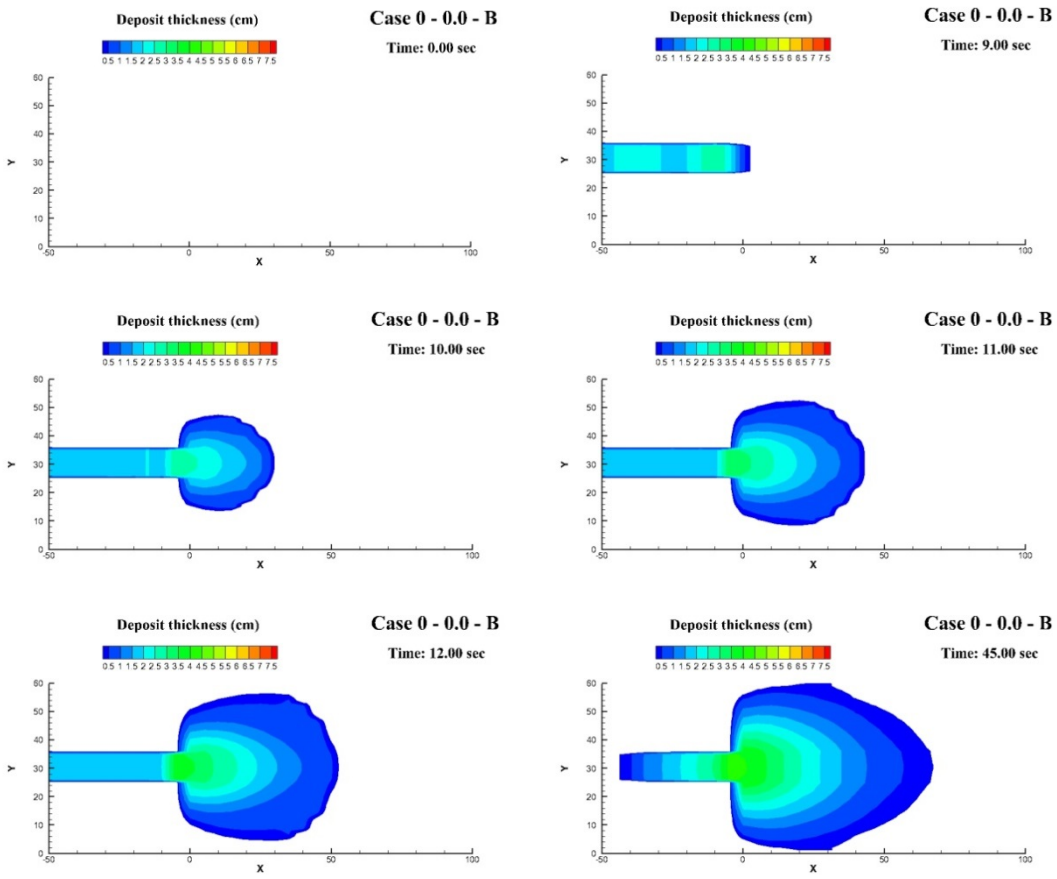

(b) Downstream view (without debris-flow breaker)

Figure 3.10 Numerical results of the movement of debris flow (Case0-0.0-B)

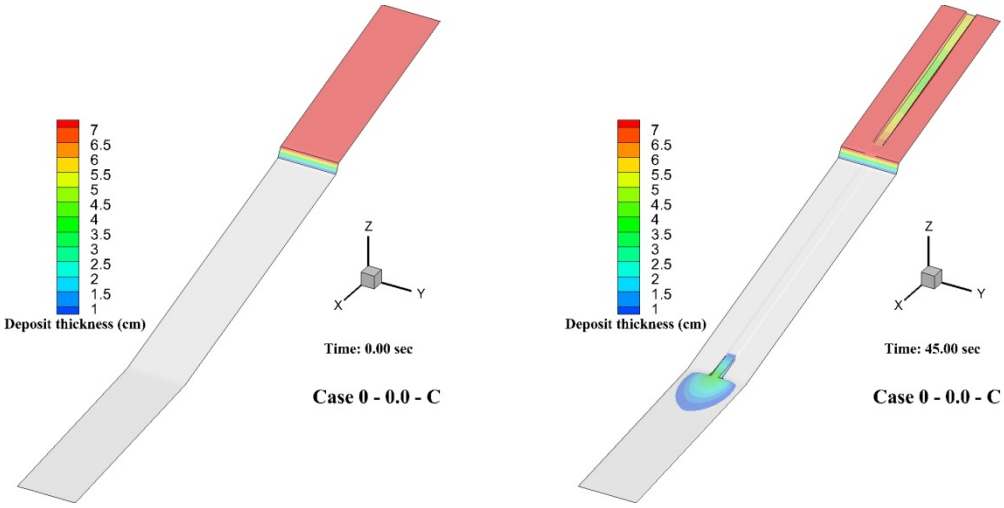

(a) Total view (without debris-flow breaker)

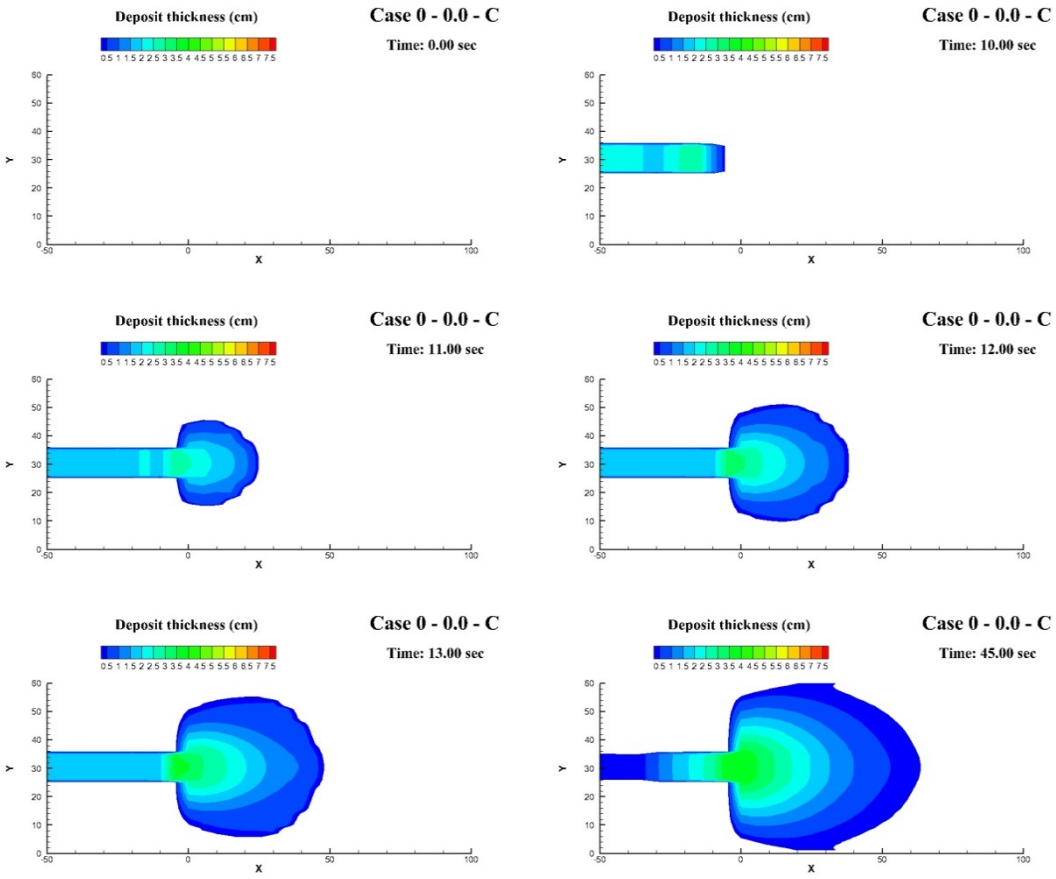

(b) Downstream view (without debris-flow breaker)

Figure 3.11 Numerical results of the movement of debris flow (Case0-0.0-C)

3.7.3 Deposition Process for Different Configurations of Breaker

Figures 3.12-3.14 show the results of the deposition pattern at the breaker with different configurations (as described in the experimental cases) under the three bed sediments.

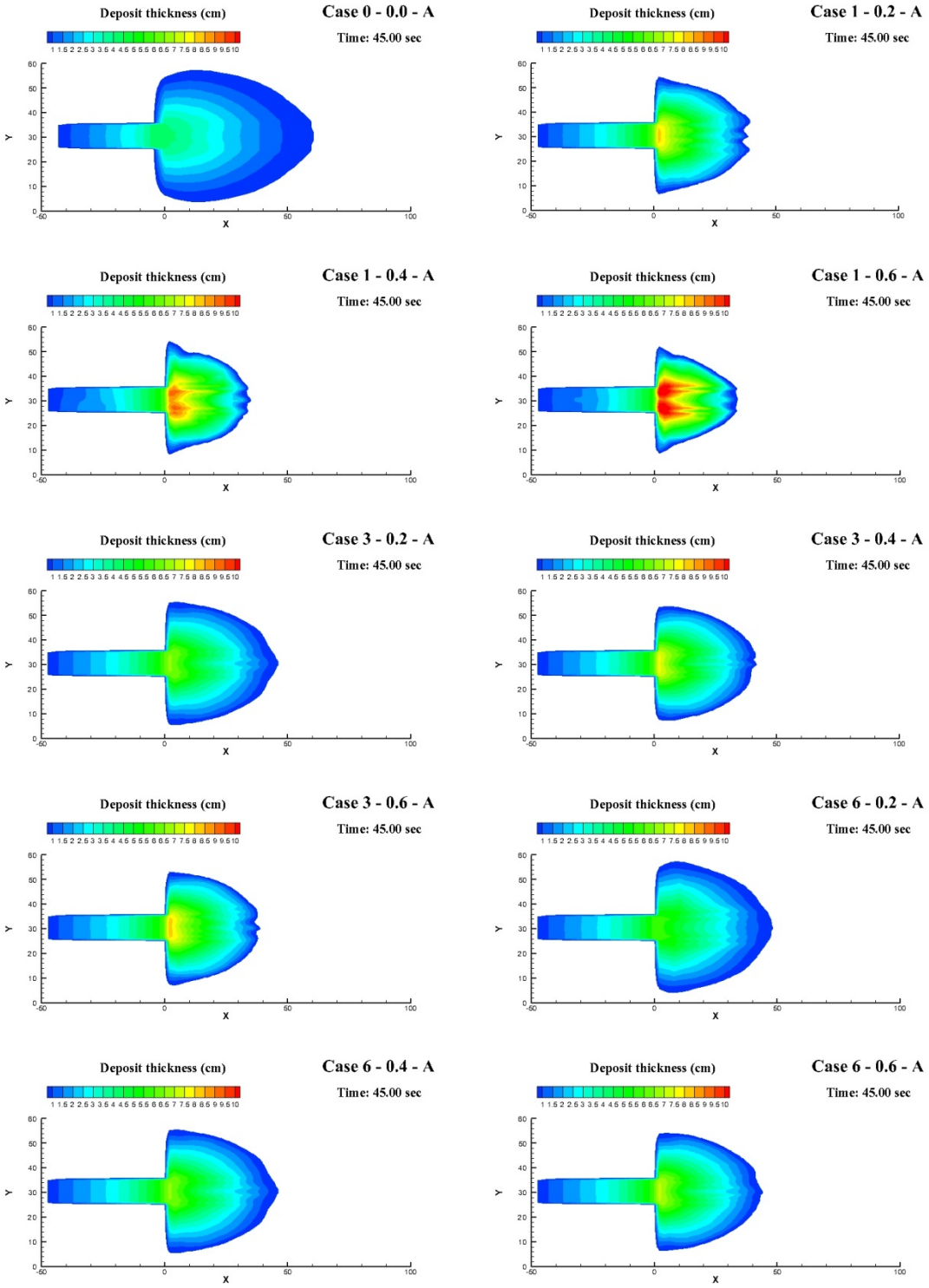

Figure 3.12 Numerical results of the deposit formation at final stage with sediment A

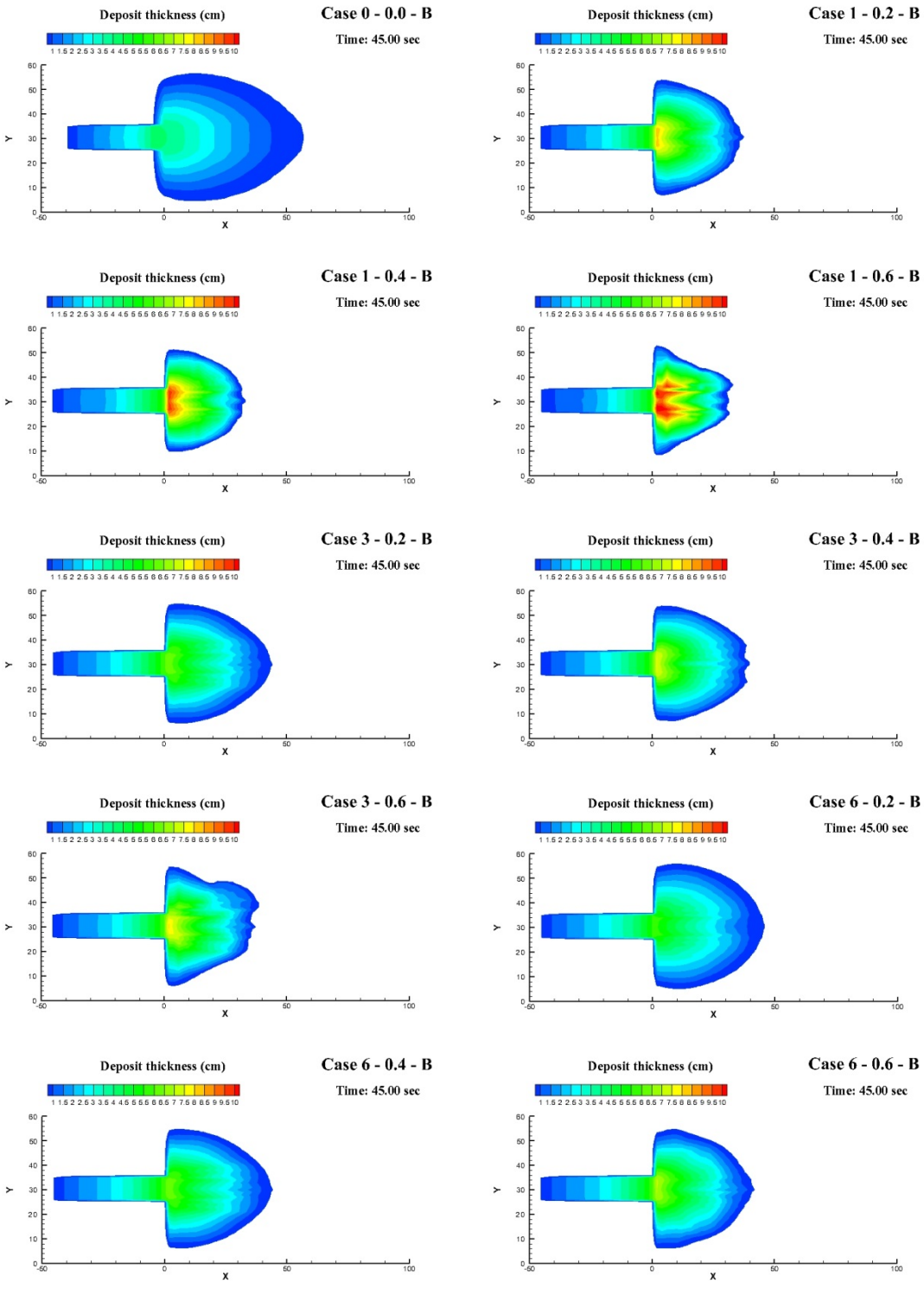

Figure 3.13 Numerical results of the deposit formation at final stage with sediment B

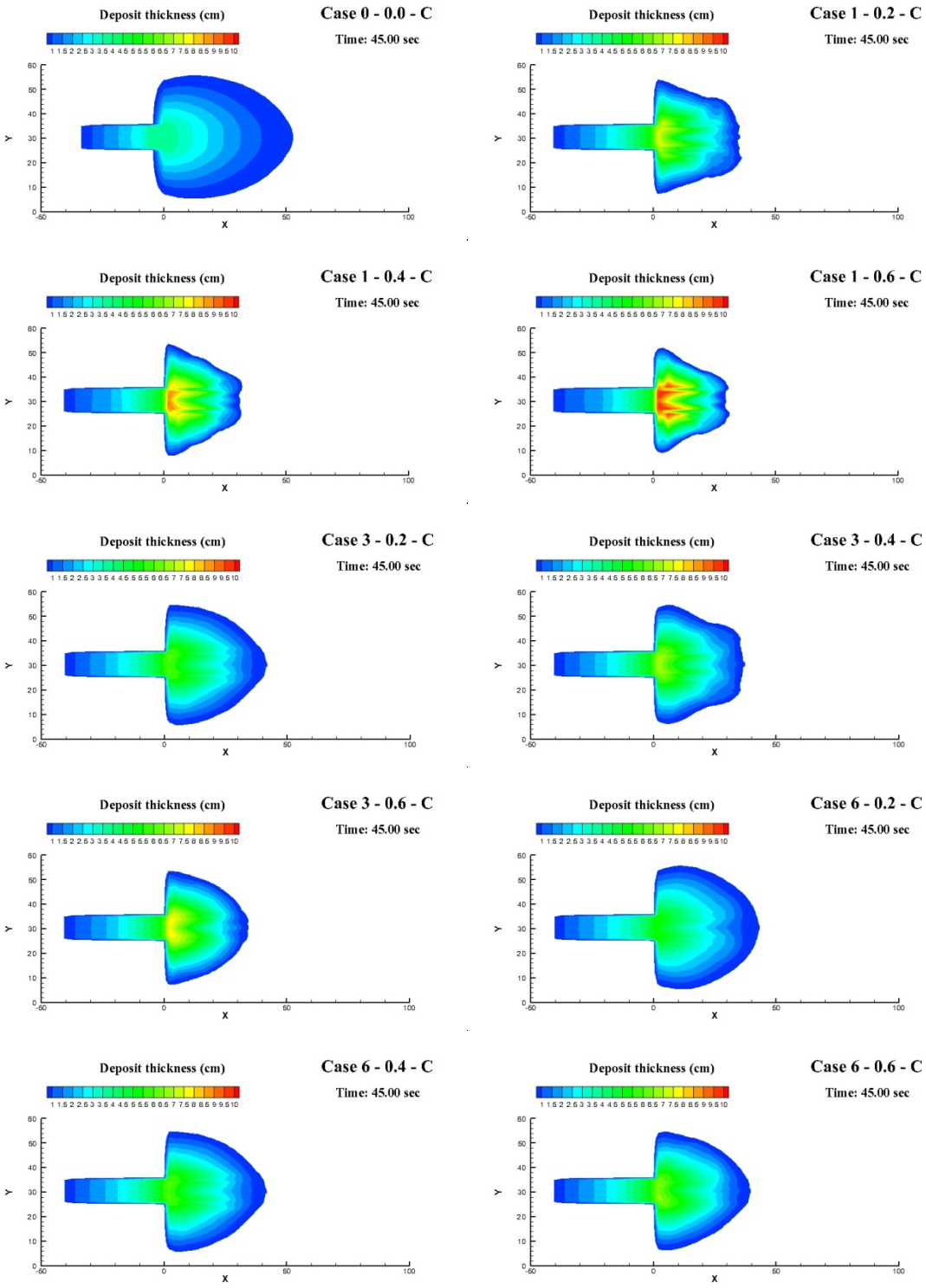

Figure 3.14 Numerical results of the deposit formation at final stage with sediment C

3.7.4 Deposit Thickness at the Debris-Flow Breaker

Figures 3.15-3.17 show the numerical results of the deposit thickness on the debris-flow breaker at the final stage (the flow depth plus the deposit thickness). The deposition pattern shows that sediment A has a higher deposition than sediment B and C.

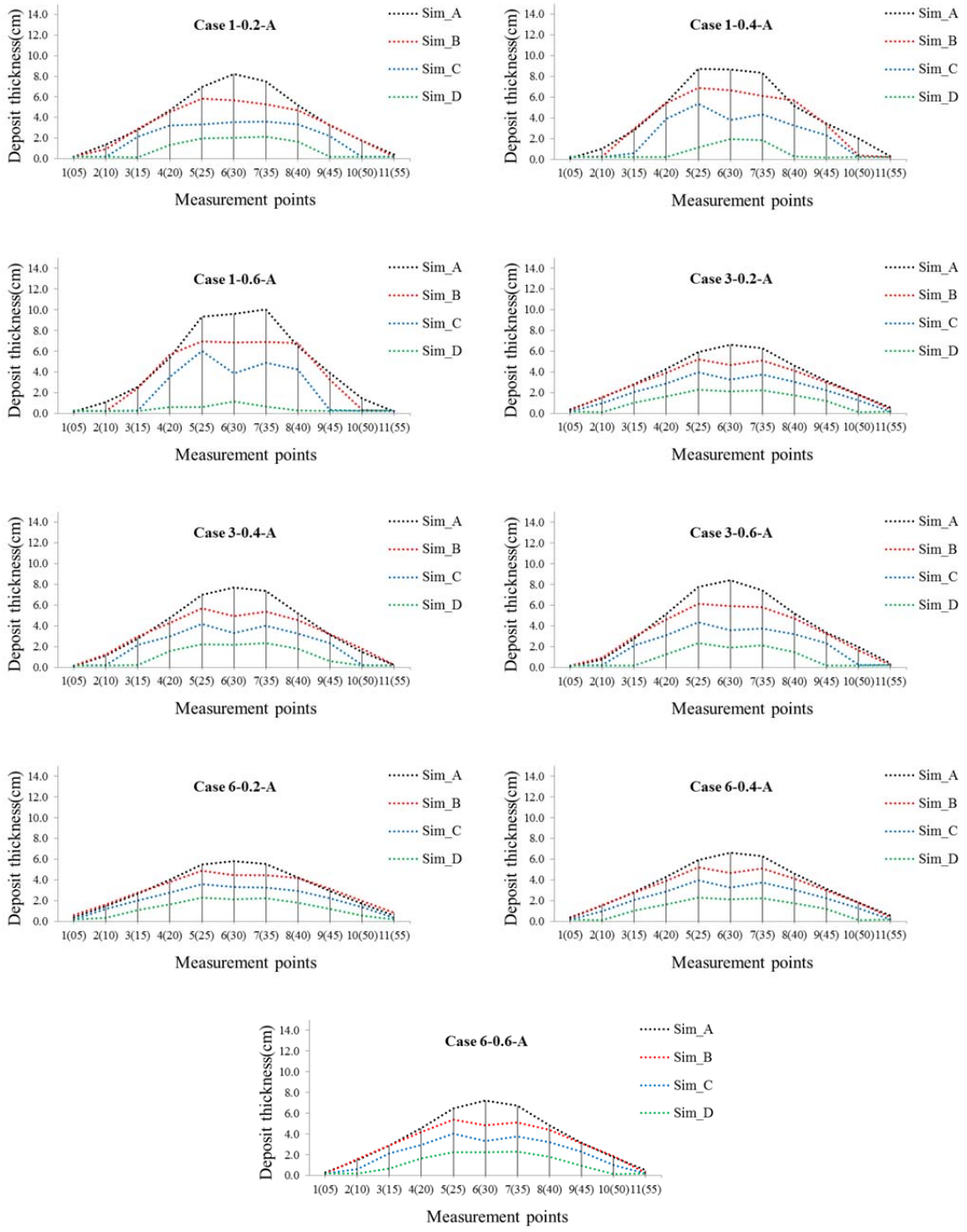

Figure 3.15 Numerical results of deposit thickness for sediment A

In the figures, the legends A, B, C and D mean the respected values of deposited thickness at cross sections A, B, C and D of the breaker as shown in Figure 2.5.

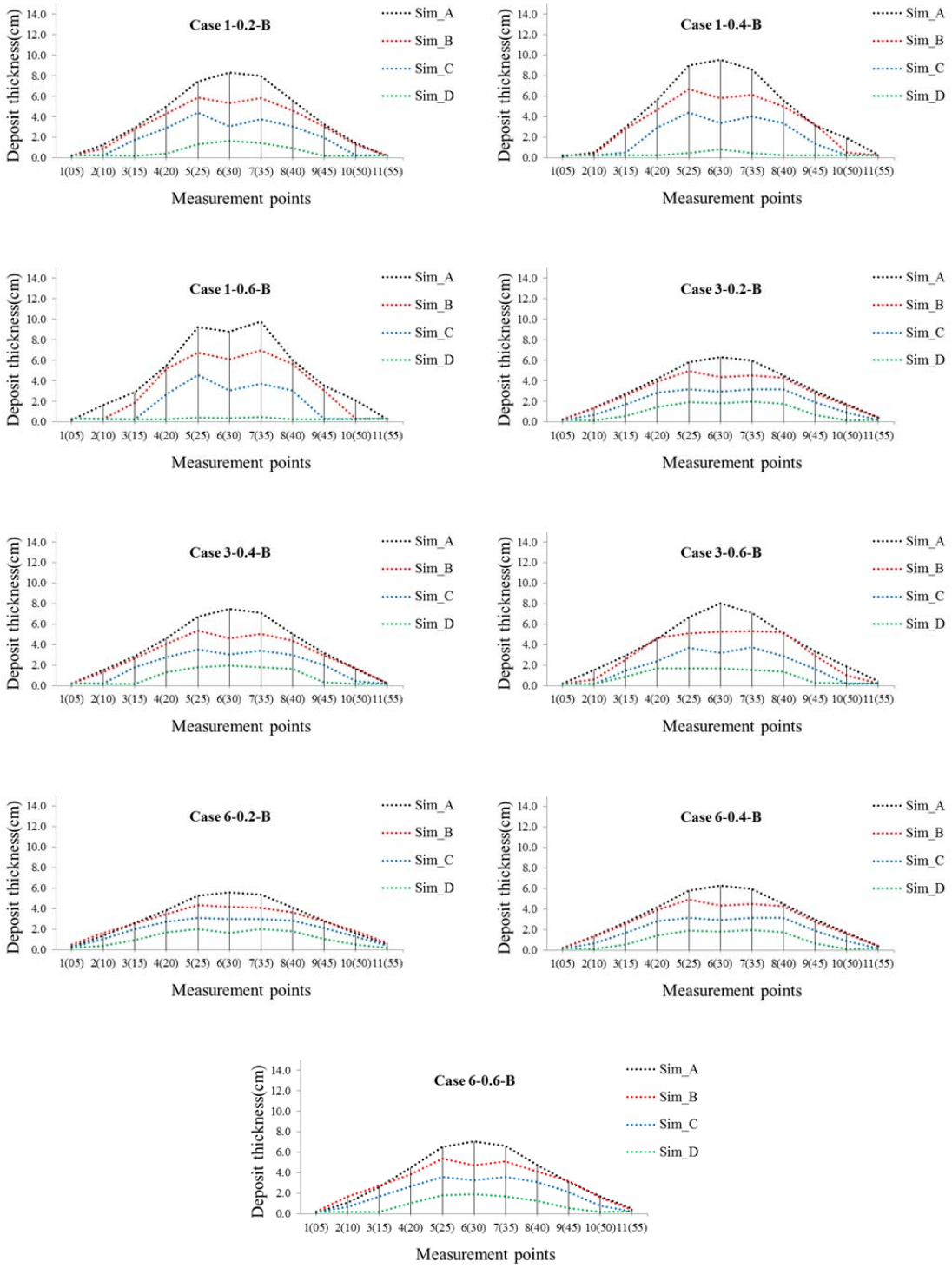

Figure 3.16 Numerical results of deposit thickness for sediment B

Also, in the figure, the values in the X-axis show the observation points and its distance from the left of the debris-flow breaker is shown inside the bracket (as shown in Figure 2.5).

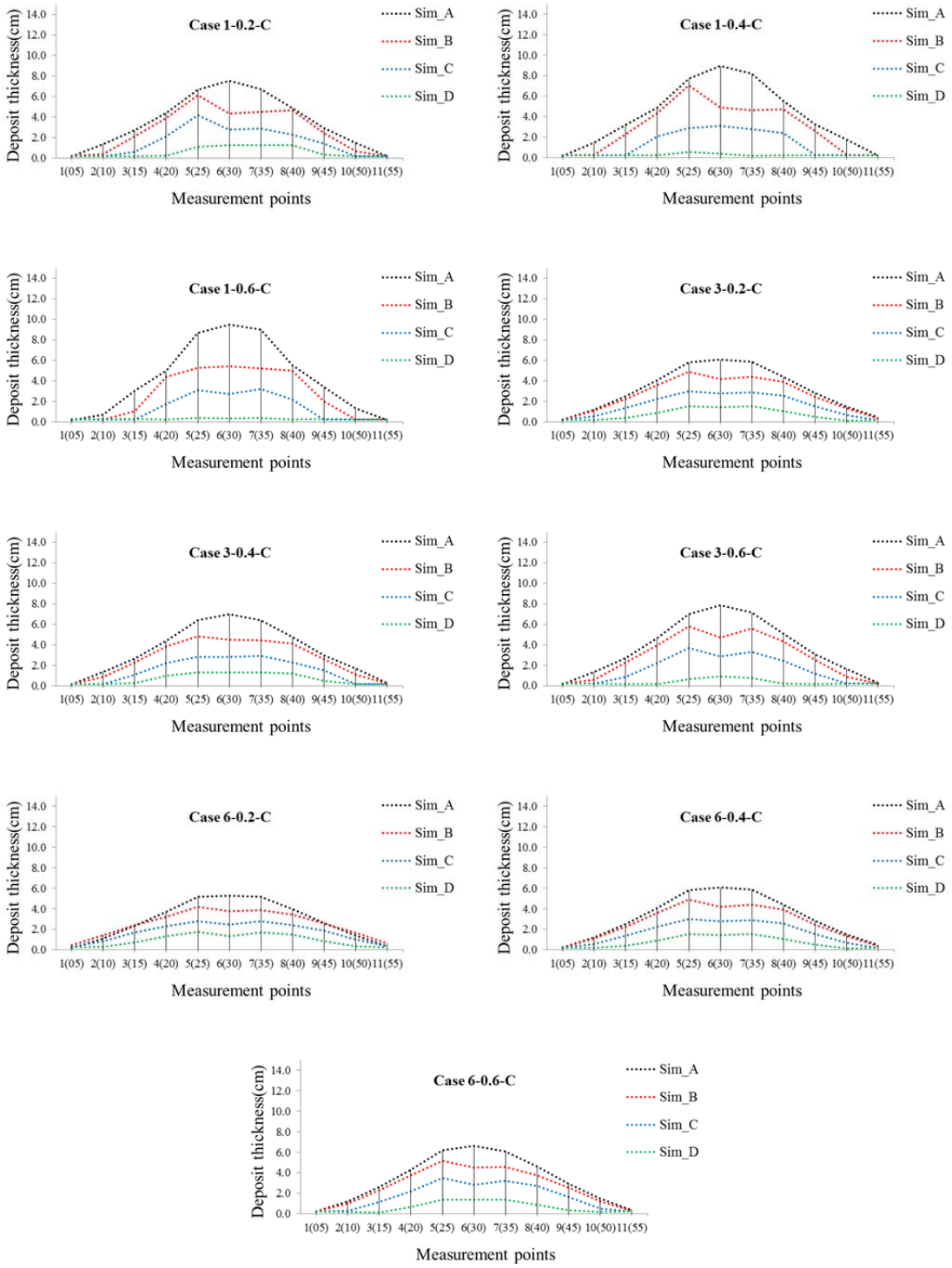

Figure 3.17 Numerical results of deposit thickness for sediment C

3.8 Verifications and Discussions for Debris-Flow Breaker

In all the experiments and the numerical simulations, the parameters, such as the flow and sediment discharges, the sediment concentration, process of deposition formation, deposit thickness on the breaker, and the maximum travel length (T.L), were measured to compare the characteristics of debris-flow breaker structures (a type of permeable dam) under the three different bed sediments. The γ factor, which is the cause of changes in pore water pressure within the debris-flow breaker, were also determined using a T-test method and compared the experimental values with the results of the numerical simulations between previous γ and proposed γ coefficients. Furthermore, the relationship between the reduction rate of travel length and various parameters, such as the width of the breaker, maximum diameter of sediment, and geometric standard deviation of sediment, were analyzed and proposed. The numerical and experimental data analyses led to the following conclusions.

3.8.1 Discharges and Sediment Concentration

To verify the model, the numerical simulation of outflow, sediment discharges, and sediment concentration at the downstream end of the flume without a debris-flow breaker were compared with the obtained experimental results.

The discharges and sediment concentrations at the downstream measuring point of the flume are measured after the debris flow reaches that point. It means that "0" at the X-axis indicates the time of measurement of the discharge and sediment concentration after the debris flow reaches the measuring point. Although the time to reach the measuring point by the debris

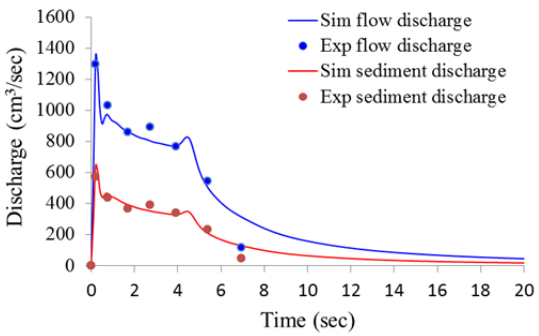

(a) Total and sediment discharges

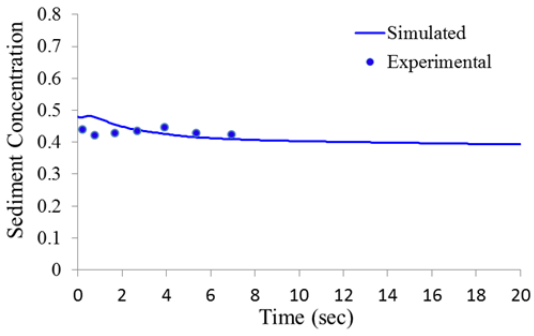

(b) Sediment concentration

Figure 3.18 Calculated and measured hydrographs at the upstream end of the flume for bed sediment A

flow is different for the various bed sediments, the main point here is to validate the numerical simulated data with the experimental data.

The results of the numerical simulations and experimental values, as shown by Figures 3.18 ~ 3.20 are in good agreement. The final result shows that the peak discharges for various bed sediments are different, indicating that sediment A has a higher discharge in comparison to sediment B and C, that is, the peak discharge from sediment A > peak discharge from B > peak discharge from C. The debris flow concentrations obtained at the downstream of the flume, from both the experimental and simulation results, as shown by Figure 3.19 (b), are about 0.4~0.5, which still satisfies the condition of a stony debris flow as given by Eq. (3.44), that is, the measured concentration of 0.4 ~ 0.5 is more than 0.4 times C_*(= 0.26). Thus, the consideration of the stony debris flow case is justified by both the experiment and the numerical simulation.

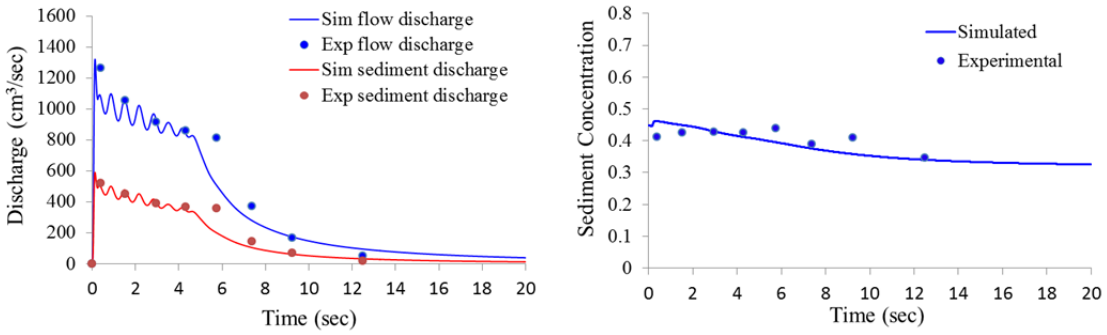

(a) Total and sediment discharges (b) Sediment concentration

Figure 3.19 Calculated and measured hydrographs at the upstream end of the flume for bed sediment B

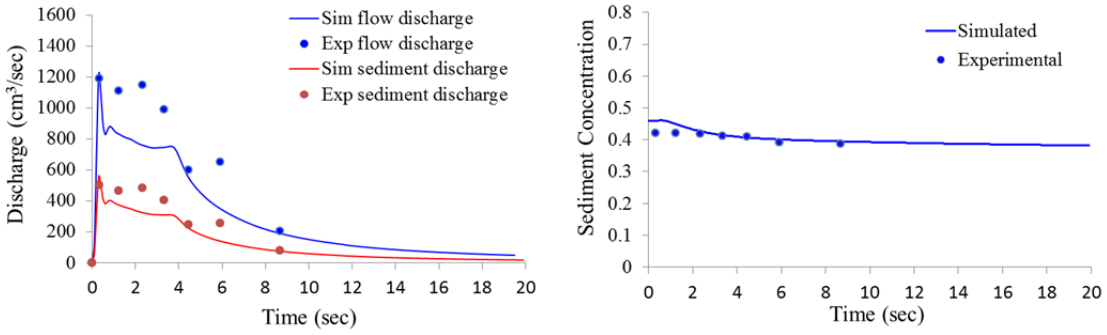

(a) Total and sediment discharges (b) Sediment concentration

Figure 3.20 Calculated and measured hydrographs at the upstream end of the flume for bed sediment C

3.8.2 Comparison of γ Coefficient

To confirm the characteristics of changing pore water pressure, various types of conditions (without and with debris-flow breakers) under the three bed sediments were tested in the experiments and numerical simulations. In order to check the change in pore water pressure, the values of the travel length were compared. Since it is very difficult to measure the change in pore water pressure in the flow directly, the changing of travel length would be considered to be caused by a change in pore water pressure at the debris-flow breaker. The results obtained by comparing the maximum travel length are summarized below.

Figure 3.21 shows the results of the γ coefficients (previous and suggested) with various conditions of the debris-flow breaker. The previous coefficients show the linear relationship with varying blocking and opening sizes. In particular, in the case of having a blocking size more than 0.6 cm, it indicates the minus value of γ coefficients, which is not possible physically. However, the suggested γ coefficients indicated the quadratic relation and did not have a minus value of the γ coefficient. Thus, the suggested γ coefficients seem more realistic and have good physical meaning than do the previous coefficients. The travel length also follows similar trend as suggested γ coefficients.

Table 3.2 shows the comparison of the travel length of different value from the experimental results with both γ coefficients, and Table 3.3 shows the results of the average difference values of travel length from the experimental results for the bed sediments. The result shows that the proposed γ coefficient revealed very good agreement and applicability with the tests than did the previous γ coefficients.

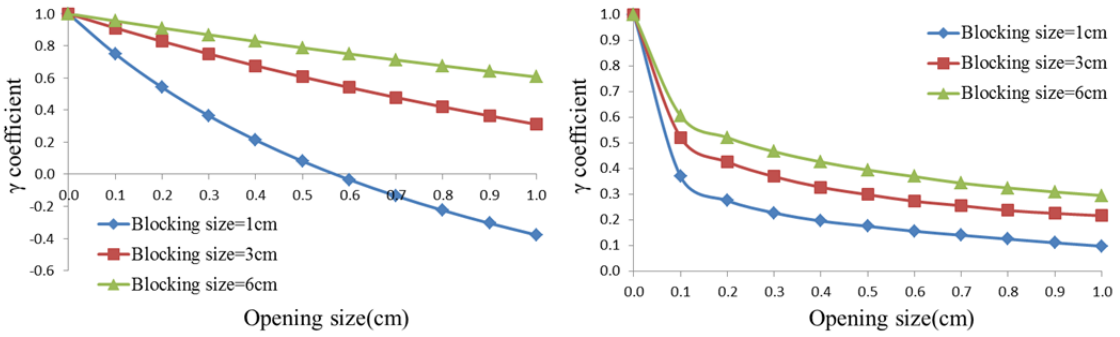

(a) Previous coefficient (b) Suggested coefficient

Figure 3.21 Results of γ coefficients with previous and suggested

Figure 3.22 shows the experimental and simulation results of the maximum travel length with both coefficients (coefficients of the previous γ and the suggested γ). This figure clearly shows the travel length has changed due to the various conditions and different bed sediments for all of the cases. However, the travel length calculations using the suggested γ coefficients have better agreement with the experimental results than using the previous γ coefficients.

Table 3.2 Comparison of travel length by previous and suggested γ coefficients (unit: cm)

Case Number	*Experiment*	*Using previous γ*	*Using new γ*
Case-1-0.2-A	42.0	(+) 6.5	(-) 0.8
Case-1-0.4-A	40.0	(-) 5.7	(-) 4.8
Case-1-0.6-A	30.0	(-) 7.0	(+) 3.8
Case-3-0.2-A	47.9	(+) 4.2	(-) 1.6
Case-3-0.4-A	42.0	(+) 8.2	0.0
Case-3-0.6-A	38.5	(+)10.0	(+) 0.8
Case-6-0.2-A	51.1	(+) 2.1	(-) 2.3
Case-6-0.4-A	49.0	(+) 3.0	(-) 2.6
Case-6-0.6-A	44.1	(+) 7.7	(+) 0.1
Case-1-0.2-B	39.0	(+) 6.6	(-) 1.3
Case-1-0.4-B	34.0	(-) 0.2	(-) 0.7
Case-1-0.6-B	30.0	(-) 9.5	(+) 1.9
Case-3-0.2-B	40.6	(+) 9.0	(+) 4.0
Case-3-0.4-B	38.0	(+)10.2	(+) 1.9
Case-3-0.6-B	37.9	(+) 7.7	(+) 1.0
Case-6-0.2-B	41.0	(+) 9.4	(+) 4.9
Case-6-0.4-B	46.0	(+) 3.5	(-) 1.4
Case-6-0.6-B	42.8	(+) 6.6	(-) 0.9
Case-1-0.2-C	35.0	(+) 9.3	(+) 1.8
Case-1-0.4-C	26.0	(+) 5.6	(+) 6.0
Case-1-0.6-C	28.0	(-) 9.8	(+) 2.8
Case-3-0.2-C	37.1	(+)11.1	(+) 4.9
Case-3-0.4-C	32.0	(+)14.2	(+) 5.5
Case-3-0.6-C	34.7	(+) 9.6	(-) 0.1
Case-6-0.2-C	41.1	(+) 7.4	(+) 2.2
Case-6-0.4-C	40.0	(+) 8.3	(+) 2.0
Case-6-0.6-C	35.2	(+)12.8	(+) 4.3

(+)/ (-) : absolute increase/ decrease in travel length obtained from the experiment.

Table 3.3 Results of average travel length from the experimental results (unit: cm)

Bed sediment	*Using previous γ*	*Using new γ*
Sediment A	(+) 3.22	(-) 0.82
Sediment B	(+) 4.86	(+) 1.04
Sediment C	(+) 7.61	(+) 3.27

(+)/ (-) : average absolute increase/ decrease in travel length obtained from the experiment.

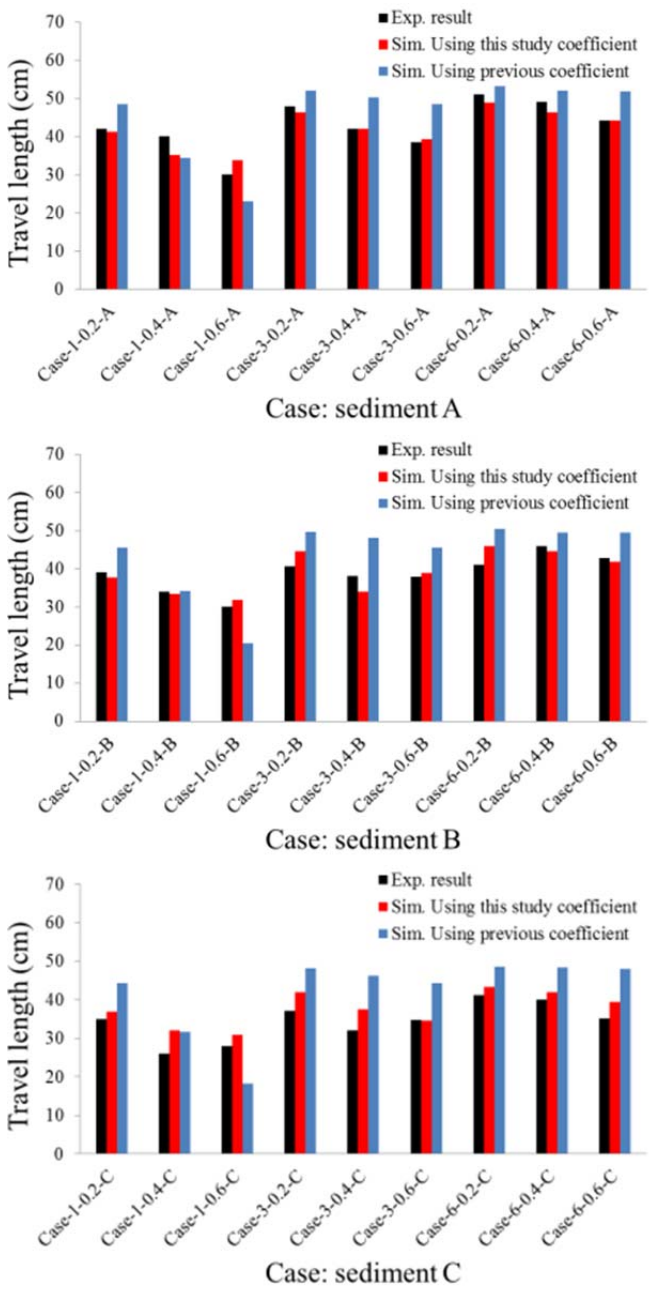

Figure 3.22 Experimental and simulation results of the maximum travel length with both coefficients

3.8.3 Deposit Thickness at the Debris-Flow Breaker

Figures 3.23~3.25 show the numerical and experimental results of the deposit thickness (the flow depth plus the deposit thickness after the final stage) at the observation points as shown in Figure 2.5 on the debris-flow breaker. Also in Figures 3.23~3.25, the values in the X-axis show the observation points and its distance from the left of the debris-flow breaker is shown inside the bracket. The experiment and simulation of the legends A, B, C and D mean the respected values of deposited thickness at cross sections A, B, C and D of the breaker as shown in Figure 2.5. The analysis of the results shows the following concluding points:

(1) The deposition pattern for all cases is the same, that is, the trend of deposition is similar. However, the deposition pattern shows that sediment A has a higher deposition thickness than sediments B and C. In summary, the maximum deposition thickness of sediment A > the maximum deposition thickness of sediment B > the maximum deposition thickness of sediment C. This is due the generated discharge from sediment A which is being higher than the others, as shown in Figures 3.18~3.20.

(2) The simulated results of the thickness of a debris flow fan are in comparatively good agreement with the experimental results (as shown in Figure 3.26). Although the correlation seems quite good, but the simulated value seems to exceed the experimental value for most of the cases. This is due to the fact that the simulation did not consider the passage of a fine fraction of deposited sediments from the pore of the debris-flow breaker.

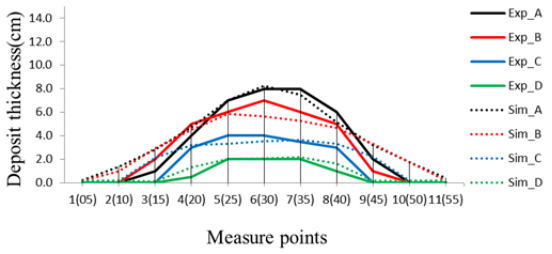

Case-1-0.2-A

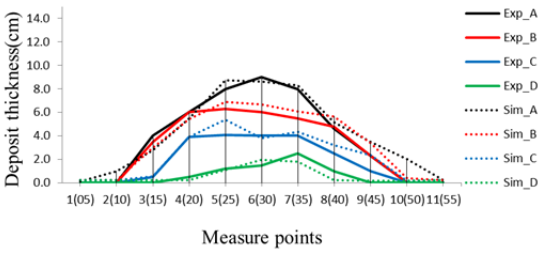

Case-1-0.4-A

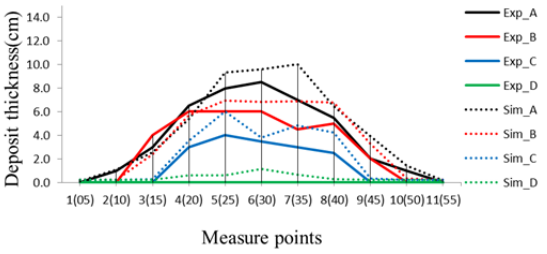

Case-1-0.6-A

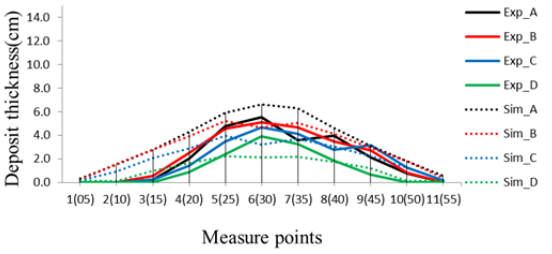

Case-3-0.2-A

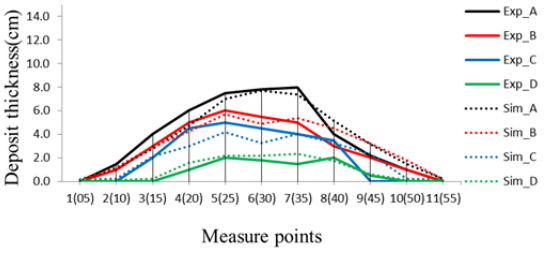

Case-3-0.4-A

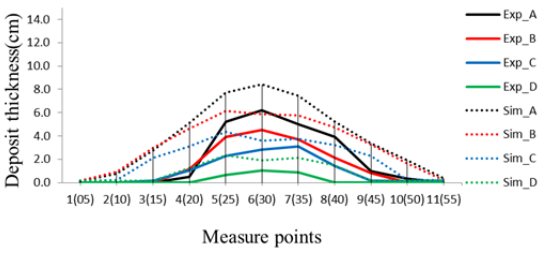

Case-3-0.6-A

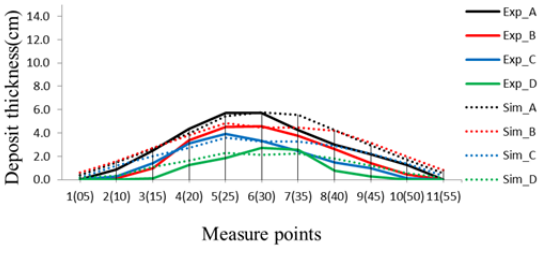

Case-6-0.2-A

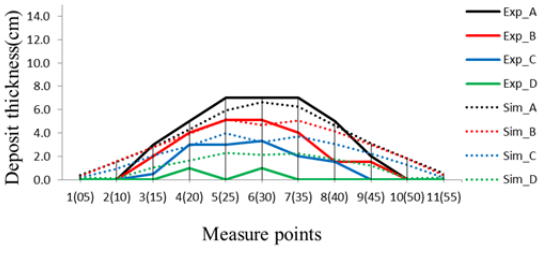

Case-6-0.4-A

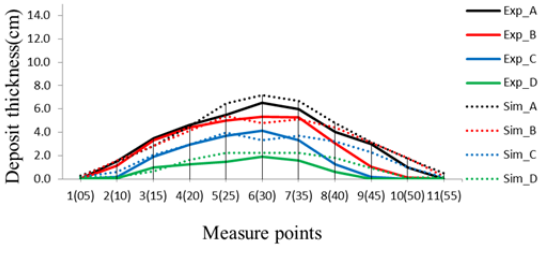

Case-6-0.6-A

Figure 3.23 Comparison of deposit thicknesses for sediment A

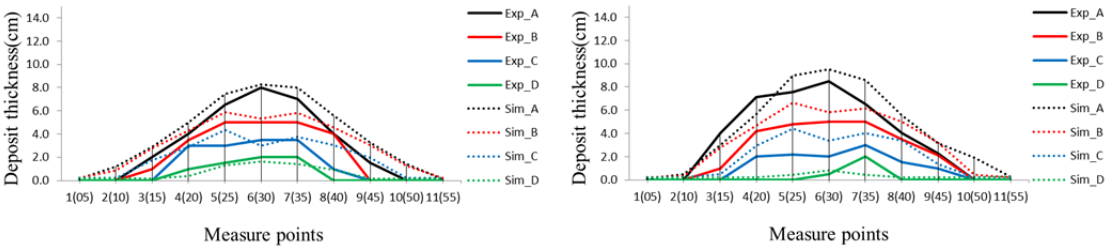

Case-1-0.2-B

Case-1-0.4-B

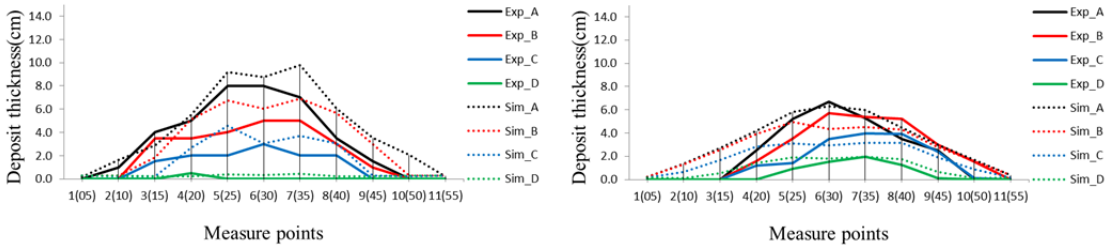

Case-1-0.6-B

Case-3-0.2-B

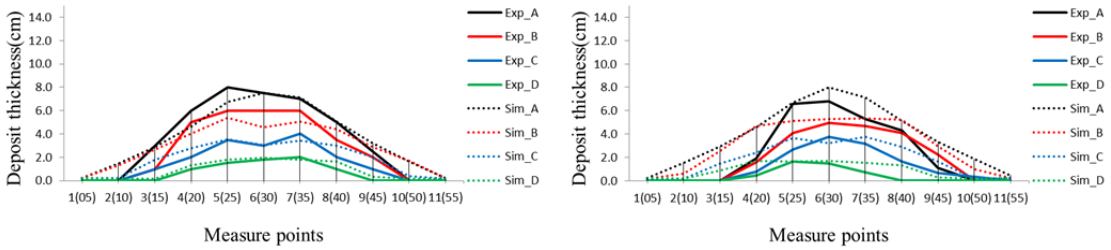

Case-3-0.4-B

Case-3-0.6-B

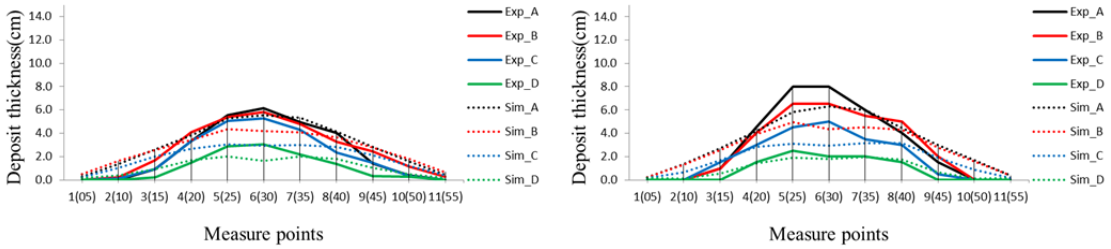

Case-6-0.2-B

Case-6-0.4-B

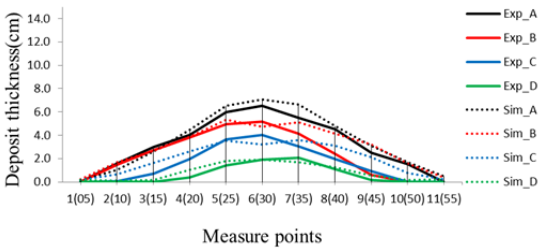

Case-6-0.6-B

Figure 3.24 Comparison of deposit thicknesses for sediment B

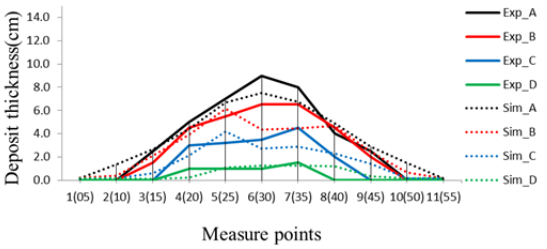

Case-1-0.2-C

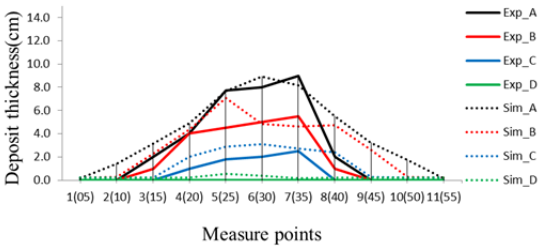

Case-1-0.4-C

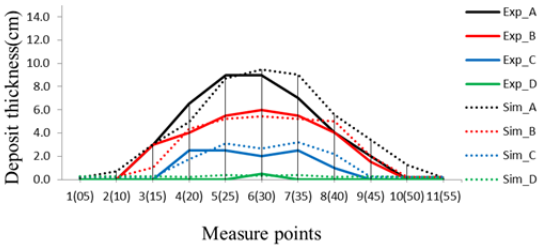

Case-1-0.6-C

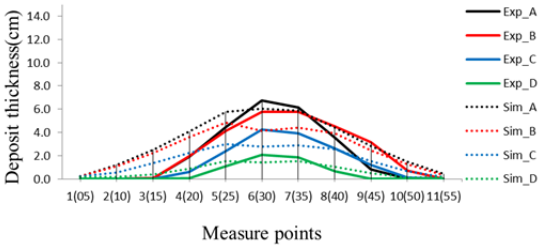

Case-3-0.2-C

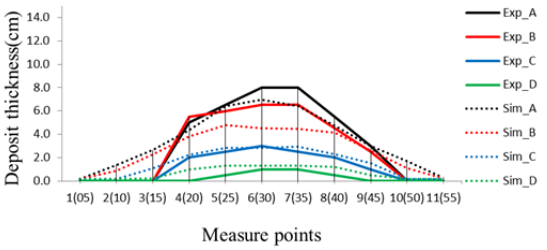

Case-3-0.4-C

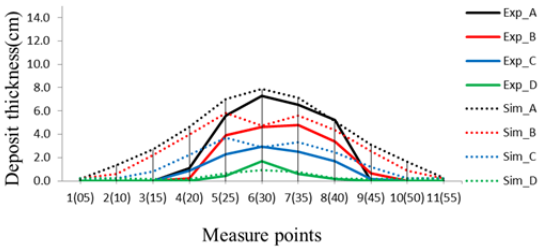

Case-3-0.6-C

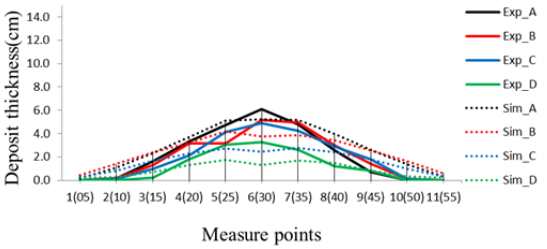

Case-6-0.2-C

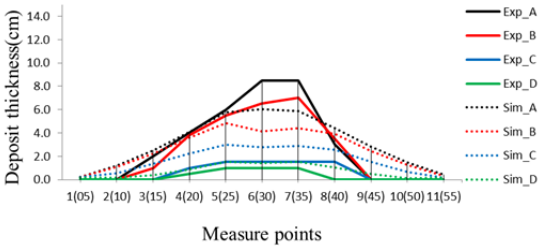

Case-6-0.4-C

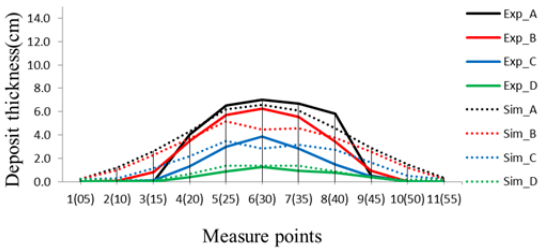

Case-6-0.6-C

Figure 3.25 Comparison of deposit thicknesses for sediment C

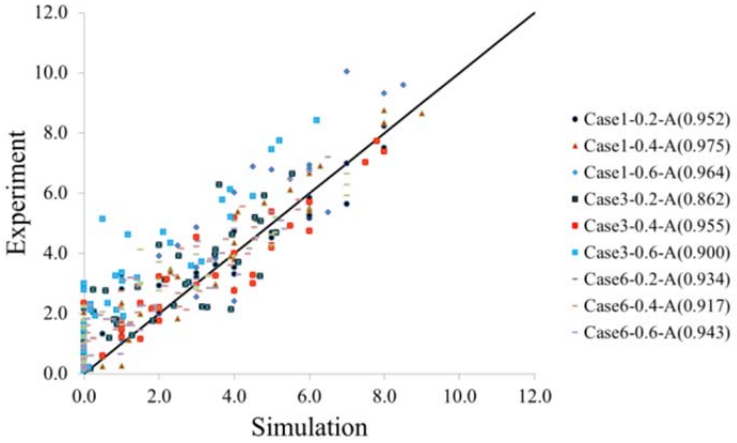

(a) Sediment A

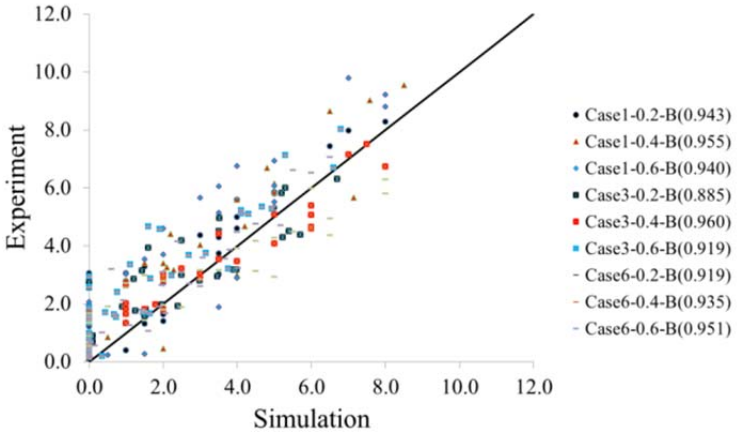

(b) Sediment B

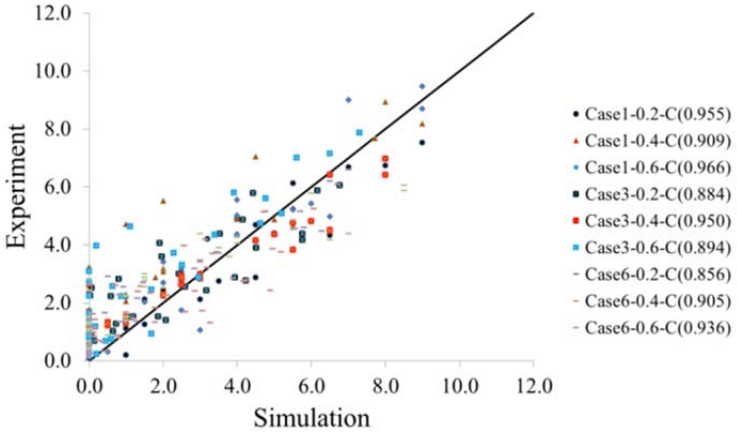

(c) Sediment C

Figure 3.26 Correlation coefficients of deposit thickness

3.8.4 Travel length

Since the maximum travel length of the debris flow is related to the total volume of runoff sediments, the bed sediment, which produces a maximum discharge, should have a maximum travel length. Figure 3.27 (a) shows the experimental results regarding the deposit formation and the maximum travel length, and Figure 3.27 (b) shows the contour maps of the debris flow fans formed with the deposit thickness in the numerical simulations under the three different bed sediments. The datum point of the X-axis is at the upstream of the mouth (start of the debris-flow breaker) and the Y-axis is the width of the debris-flow breaker. The figures clearly justify the theory that the maximum travel length is obtained from the sediments that produce higher discharges. This leads to the conclusion that the bed sediments having a small mean diameter leads to maximum sediment discharge, which further leads to maximum travel length

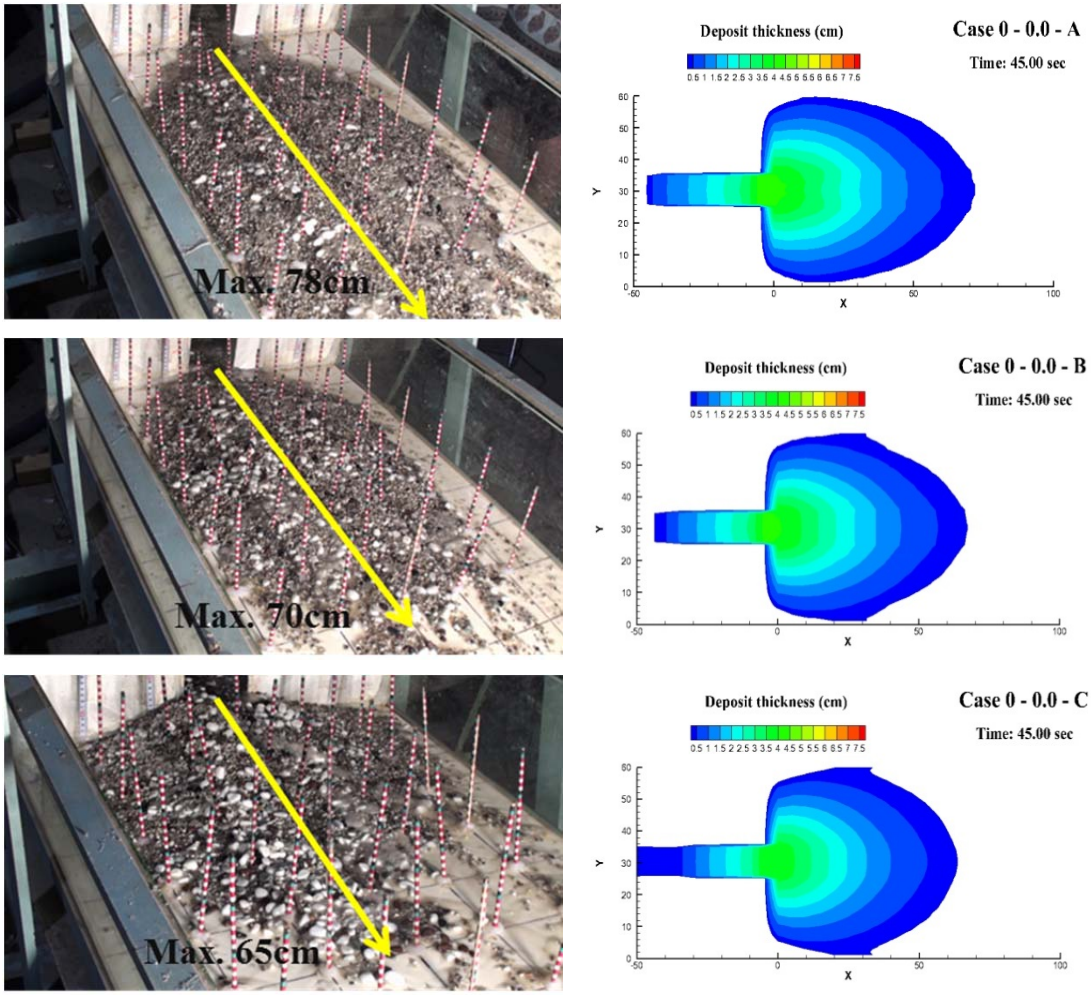

(a) Experimental results (b) Numerical results

Figure 3.27 Calculated and measured deposit formation at the debris-flow breaker for bed sediment A, B, and C (final stage)

in comparison to the sediments with a large mean diameter. As a result, the travel length calculations using the suggested γ coefficients are in better agreement with the experimental results than are the calculations using the previous γ coefficients, as shown in Table 3.4.

Table 3.4 Experimental and simulation results of the maximum travel length (unit: cm)

Case	*Sediment*	*B.S*	*O.S*	*Exp.*	*Pre. γ*	*New. γ*
Case-0-0.0-A	A	×	×	78.0	-	72
Case-1-0.2-A		1	0.2	42.0	48.5	41.2
Case-1-0.4-A			0.4	40.0	34.3	35.2
Case-1-0.6-A			0.6	30.0	23.0	33.8
Case-3-0.2-A		3	0.2	47.9	52.1	46.3
Case-3-0.4-A			0.4	42.0	50.2	42.0
Case-3-0.6-A			0.6	38.5	48.5	39.3
Case-6-0.2-A		6	0.2	51.1	53.2	48.8
Case-6-0.4-A			0.4	49.0	52.0	46.4
Case-6-0.6-A			0.6	44.1	51.8	44.2
Case-0-0.0-B	B	×	×	70.0	-	66
Case-1-0.2-B		1	0.2	39.0	45.6	37.7
Case-1-0.4-B			0.4	34.0	34.2	33.3
Case-1-0.6-B			0.6	30.0	20.5	31.9
Case-3-0.2-B		3	0.2	40.6	49.6	44.6
Case-3-0.4-B			0.4	38.0	48.2	33.9
Case-3-0.6-B			0.6	37.9	45.6	38.9
Case-6-0.2-B		6	0.2	41.0	50.4	45.9
Case-6-0.4-B			0.4	46.0	49.5	44.6
Case-6-0.6-B			0.6	42.8	49.4	41.9
Case-0-0.0-C	C	×	×	65.0	-	63
Case-1-0.2-C		1	0.2	35.0	44.3	36.8
Case-1-0.4-C			0.4	26.0	31.6	32.0
Case-1-0.6-C			0.6	28.0	18.2	30.8
Case-3-0.2-C		3	0.2	37.1	48.2	42.0
Case-3-0.4-C			0.4	32.0	46.2	37.5
Case-3-0.6-C			0.6	34.7	44.3	34.6
Case-6-0.2-C		6	0.2	41.1	48.5	43.3
Case-6-0.4-C			0.4	40.0	48.3	42.0
Case-6-0.6-C			0.6	35.2	48.0	39.5

3.8.5 Relationship of Reduction Rate

A great deal of research is being carried out to discover the optimum range of open-type sabo dams. They only considered the relative spacing factors in designing the spacing of open-type dams. Even if the debris-flow breaker is also similar to the open-type dam, the main function is different between an open-type and a breaker type. Although there are many contributing factors for the efficient design of the breaker structure but in current studies, the relationship among different parameters of breaker such as opening size, blocking size were only considered. Therefore, in order to design the debris-flow breaker, it is necessary to develop a relationship for the debris-flow breaker opening and blocking sizes.

Table 3.5 and Figure 3.28 show the comparison of maximum and minimum reductions in travel length. The reduction and reduction rate are calculated as follows.

$$\text{Reduction} = \text{T.L (without breakers)} - \text{T.L (with breakers)} \tag{3.61}$$

$$\text{Reduction Rate} = 1 - \left[\frac{\text{T.L (with breakers)}}{\text{T.L (without breakers)}} \right] \tag{3.62}$$

All of the cases for reduction of travel length were decreased due to the permeable area (opening size) compared to the cases without a debris-flow breaker. In the cases with blocking

Table 3.5 Comparison of reductions in travel length between maximum and minimum

Bed sediment	*Without (cm)*	*With breaker (cm)*	*Reduction (cm)*	*R. Rate*
Sediment A	Exp. 78.0	Min. Case 6-0.2-A : 51.1	26.9	0.34
		Max. Case 1-0.6-A : 30.0	48.0	0.62
	Sim. 72.0	Min. Case 6-0.2-A : 48.8	23.2	0.32
		Max. Case 1-0.6-A : 33.8	38.2	0.53
Sediment B	Exp. 70.0	Min. Case 6-0.4-B : 46.0	24.0	0.34
		Max. Case 1-0.6-B : 30.0	40.0	0.57
	Sim. 66.0	Min. Case 6-0.2-B : 45.9	20.1	0.30
		Max. Case 1-0.6-B : 31.9	34.1	0.52
Sediment C	Exp. 65.0	Min. Case 6-0.2-C : 41.1	23.9	0.37
		Max. Case 1-0.4-C : 26.0	39.0	0.60
	Sim. 63.0	Min. Case 6-0.2-C : 43.3	19.7	0.33
		Max. Case 1-0.6-C : 30.8	32.2	0.51

and opening sizes of 6.0 and 0.1 cm, respectively, in both cases (experimental and simulation results) there was a maximum reduction in travel length value. On the contrary of these results, in the cases of blocking and opening sizes 1.0 and 0.6 cm, respectively, there were minimum reductions in travel length values. However, it is very important to determine the suitable reduction of travel length. If it has large opening, much of the sediment and water will be separated from the debris-flow breaker. Not only this, these parameters are also dependent on the intensity of the debris flow (i.e. peak discharge hydrograph). But it is very difficult to decide the value of suitable reduction range with considering separated volume of sediments and peak discharge hydrograph due to their uncertainty. So, the current study only focuses on the development of ranges of parameters based on the reduction of maximum travel length.

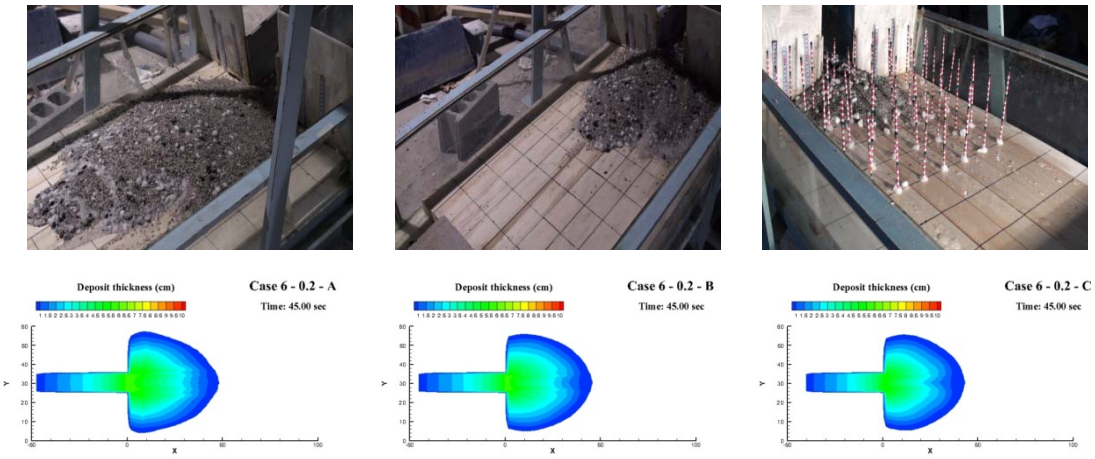

(a) Minimum reduction of travel length for debris-flow breaker

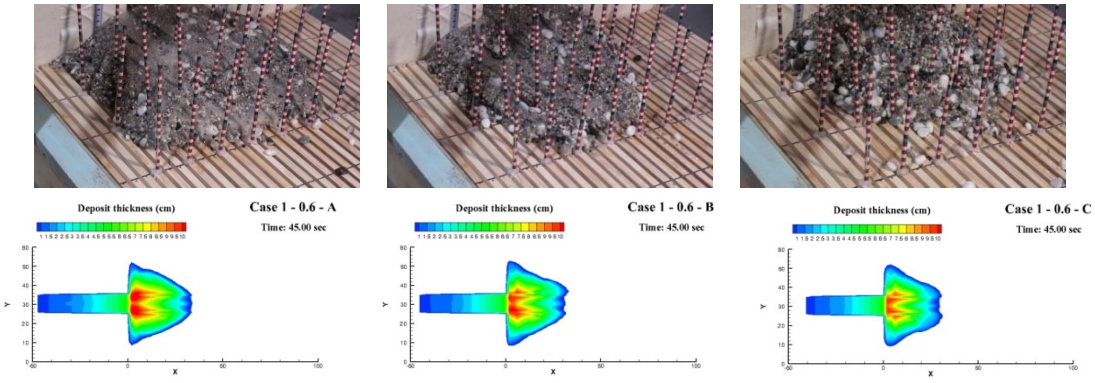

(b) Maximum reduction of travel length for debris-flow breaker

Figure 3.28 Comparisons of reduction values of travel length

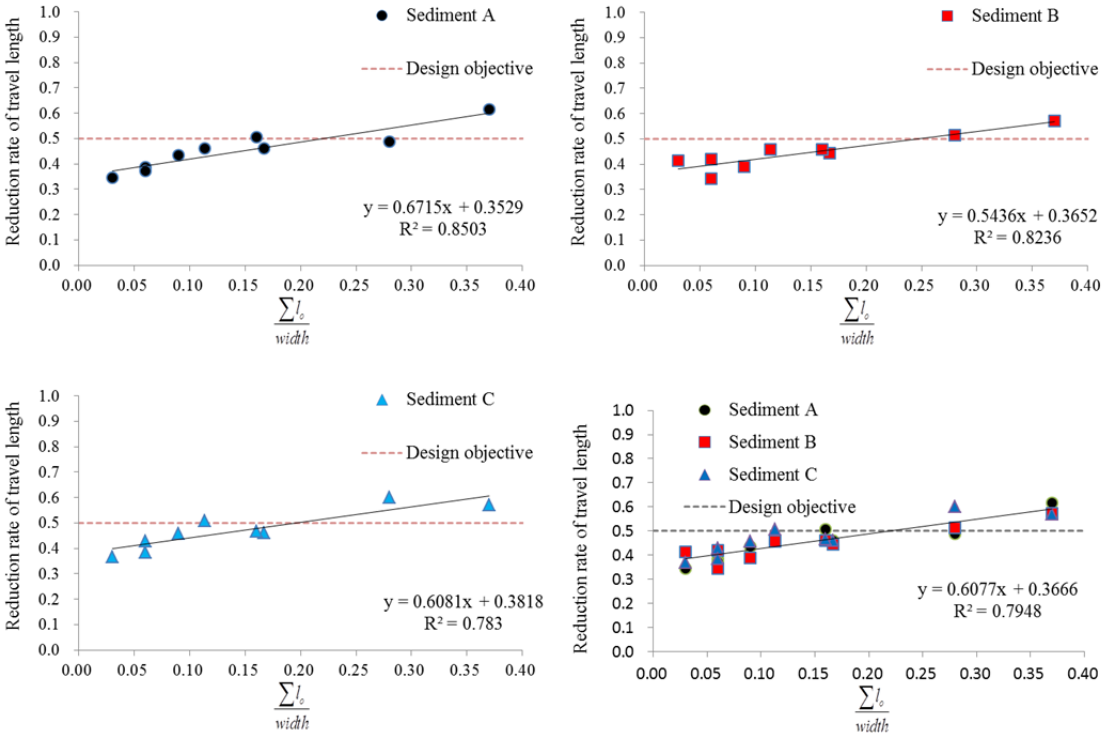

Figure 3.29 (I) Relationship of reductions rate for $\sum l_0 / width$ of breaker

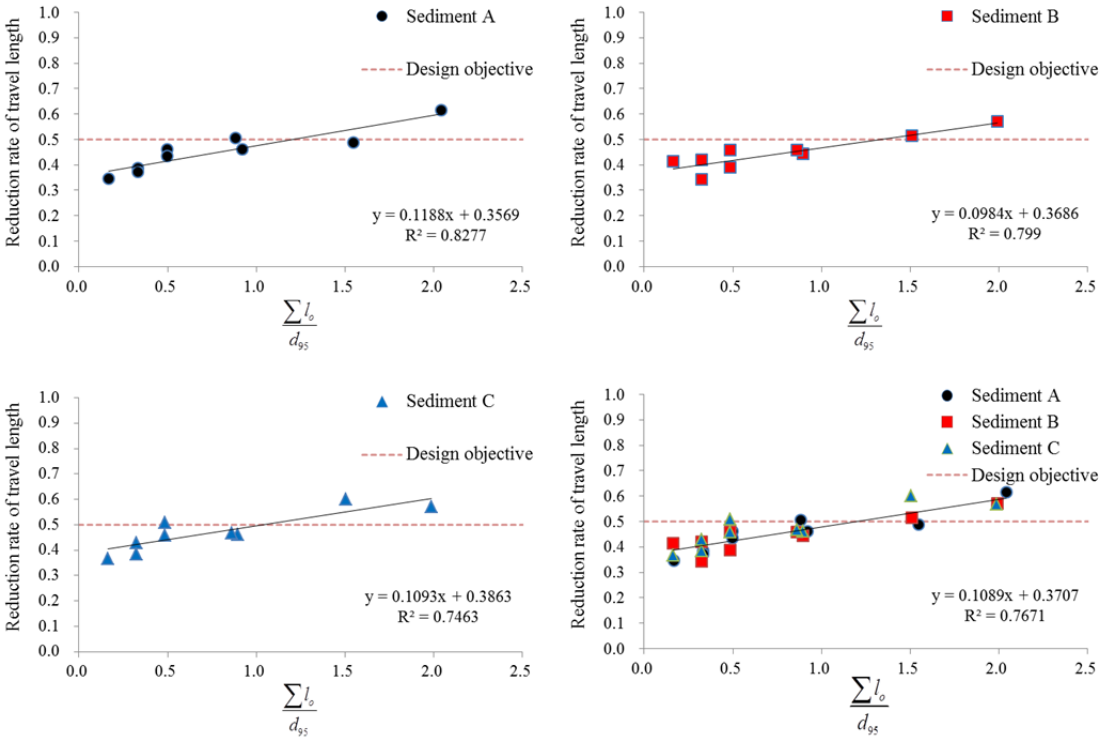

Figure 3.30 (II) Relationship of reductions rate for $\sum l_0 / d_{95}$

Figures 3.29 ~ 3.30 show the relationship of reduction rate. For the time being, 50% is being considered, but analysis can be done for different reduction rates. The relationship (I) has been shown to be effective in reducing the travel length 50% as the total opening size/width of the breaker ranges from 0.19 to 0.24 for different sediment cases (for sediment A: 0.22, for sediment B: 0.24, and for sediment C: 0.19). The relationship (II) has been shown to be effective in reducing the travel length 50% as the total opening size/maximum diameter ranges from 1.1 to 1.3 for different sediment cases (for sediment A: 1.2, for sediment B: 1.3, and for sediment C: 1.1).

3.9 Summary

To analyze the interaction between the opening and blocking sizes of debris-flow breakers under the three bed sediments, a 2-D numerical model was newly developed. To confirm the effectiveness and validity of the developed numerical model, hydraulic model test results of this research were compared and studied.

In the experiments and numerical simulations, the effects of debris-flow breakers with an emphasis as a type of permeability dam, the parameters, such as the total flow and sediment discharges, sediment concentration, travel length, and deposit thickness, were measured to compare the function of each debris-flow breaker under the three different bed sediments. The empirical γ coefficients were also proposed and compared to previous coefficients from the results of travel length. Furthermore, the relationships of reduction ratios were estimated by the various parameters of debris-flow breakers (bed sediments and various configuration conditions) according to the experimental results. The performed verifications are described below.

1. To verify the model, the numerical simulation of outflow, sediment discharges, and sediment concentration at the downstream end of the flume without a debris-flow breaker were compared with the obtained experimental results. The results of the numerical simulations and experimental values are in good agreement.

2. The peak discharges for various bed sediments are different, indicating that sediment A has a higher discharge in comparison to sediment B and C, that is, the peak discharge from sediment A > peak discharge from B > peak discharge from C. The debris flow concentrations obtained at the downstream of the flume, from both the experimental and simulation results still satisfy the condition of a stony debris flow. Thus, the consideration of the stony debris flow case is justified by both the experiment and the numerical simulation.

3. To confirm the characteristics of changing pore water pressure, two conditions (without and with debris-flow breakers) under the three bed sediments were tested in the experiments and numerical simulations. In order to check the change in pore water pressure, the values of the travel length were compared. Since it is very difficult to measure the change in pore water pressure in the flow directly, the change of travel length would be considered to be caused by the change in pore water pressure at the debris-flow breaker. The travel length

has been changed due to the various conditions and different bed sediments for all cases. However, the travel length calculations using the suggested γ coefficients have better agreement with the experimental results than do the previous γ coefficients.

4. The simulated results of the thickness of a debris flow fan are in comparatively good agreement with the experimental results. Although the correlation seems quite good, the simulated value seems to have exceeded the experimental value for most of the cases. This is due to the simulation not considering the passage of a fine fraction of deposited sediments from the pore of the debris-flow breaker.

5. The current study aimed to reduce the travel length by 50% when evaluating the relationship of range. For the time being, 50% is considered, but analysis can be done for a different reduction rate. In the relationship (I), the total opening size/width of breaker ranged from 0.19 to 0.24 for the different sediment cases, in relationship (II), the total opening size/maximum diameter ranged from 1.1 to 1.3 for the different sediment cases, and in relationship.

In summary, the experiments were carried out in the fixed bed condition, in which the debris flow depositions (due to the change in pore water pressure at the debris-flow breaker) were analyzed. In all the experiments, the configurations of a debris-flow breaker, with emphasis on the permeability dam types, and the parameters, such as the flow pattern (formation process) between the bed slopes of the flood basin, thickness of debris, total and sediment discharges, and sediment concentration were measured to compare the function of each condition of the breaker, and the phenomena of the separation flow on the debris-flow breaker under the three different bed sediments were analyzed as well.

To clarify the hydraulic characteristics of debris flows on the debris-flow breaker, a numerical simulation for debris-flow breaker was developed and analyzed the mechanism and interaction between the opening and blocking areas. The simulated results of the outflow discharge, sediment concentration, travel length, and deposit thickness are in good agreement with the experimental results. In addition, the ranges of the debris-flow breaker parameters such as opening and blocking sizes for the design of structural elements of debris-flow breaker are evaluated.

References

1) Ashida K., Egashira S., Kurita M., and Aramaki H. 1987, Debris flow control by grid dams. *Annuals of the Disaster Prevention Research Institute, Kyoto University,* No. 30 B-2, pp.441-456. (in Japanese)
2) Bagnold R.A. 1954, Experiments on a gravity-free dispersion of a large solid sphere in a Newtonian fluid under shear. *Proc. R. Soc.* London, Ser. A, 225, pp.49-63.
3) Bouvard M. 1992, Mobile barrages and intakes on sediment transporting rivers. *IAHR Monograph, Balkema,* Rotterdam, pp.1-320.
4) Brunella S., Hager W.H., and Minor H.E. 2003, Hydraulics of bottom rack intake. *Journal of hydraulic engineering,* pp. 1-448.
5) Coussot P. 1992, Rhéologie des Laves Torrentielles. *Collection Etude,* serie Montagne, Nº5, 415.
6) Egashira S., Ashida K., Yajima H., and Takahama J. 1989, Constitutive equation of debris flow. *Annuals of the Disaster Prevention Research Institute, Kyoto University,* No. 32 B2, pp.487-501. (in Japanese)
7) Egashira S., Miyamoto K., and Itoh T. 1997, Constitutive equations of debris flow and their applicability. *Proceedings of First Conference on Debris-Flow Hazards Mitigation: Mechanics, Prediction, and Assessment,* California, ASCE, pp.340-349.
8) Hunt B. 1994, Newtonian fluid mechanics treatment of debris flows and avalanches. *Journal of Hydraulic Engineering, ASCE,* Vol. 120, No. 12, pp.1350-1363.
9) Gonda Y. 2009, Function of a debris-flow brake. *International Journal of Erosion Control Engineering,* Vol. 2, No. 1, pp. 15-21.
10) Kim Y., Nakagawa H., Kawaike K. and Zhang H. 2012a, Numerical analysis of debris flow deposition on breaker structure. *Annual Journal of Japan Society of Civil Engineering, JSCE,* Vol. 68, No. 4, pp. 1-6.
11) Kim Y., Nakagawa H., Kawaike K. and Zhang H. 2012b, Numerical and experimental study on debris-flow breaker. *Annuals of the Disaster Prevention Research Institute, Kyoto University,* No. 55 B, pp. 471-481.
12) Koch T. 1998, Testing of various constitutive equations for debris flow modeling. *Hydrology, Water Resources and Ecology in Headwater, IAHS Publ.* No. 248, Merano, Italy, pp. 249-257.
13) Kuntzmann J. and Bouvard M. 1954, Etude théorique des grilles deprises d'eau du type en-dessous. La houille Blanche, 9(9/10), pp. 569-574.(in French)
14) Miyamoto K. 1985, Mechanics of grain flows in Newtonian fluid. Ph.D. Thesis, Ritsumeikan University. (in Japanese)
15) Mizuyama T. and Mizuno H. 1994, Behavior of debris flow at control structures. *Proc., IAHR Int.* Workshop on Floods and Inundations Related to Large Earth Movements, C2.1-C2.12.
16) Nakagawa H., Satofuka Y., and Kawaike K. 2003, Numerical simulation of sediment disasters caused by heavy rainfall in camuri Grande basin, Venezuela 1999. *Proceedings of the third conference on Debris-flow Hazards Mitigation: Mechanics,* Prediction and Assessment, Switzerland Rotterdam, pp. 671-682.
17) Nakagawa H. 1989, Study on risk evaluation of flood and sediment inundation disaster. *Doctoral Thesis, Kyoto University.* (in Japanese)
18) O'Brien J. S. and Julien P. Y. 1988, Laboratory analysis of mudflow properties. *Journal of Hydraulic Engineering, ASCE,* Vol. 114, No. 8, pp.877-887.
19) Orth J., Chardonnet E., and Meynardi G. 1954, Etude de grilles pour prises d'eau du type en-dessous. *La houille Blanche*, 9(6), pp. 343-351.(in French)

20) Ract-Madoux X., bouvard M., Molbert J., and Zumstein J. 1955, Quelques réalisations récentes de prises en-dessous à haute altitudeen Savoie. *La houille Blanche,* 10(6)*, pp. 852-878.*(in French)
21) Ralph L.R., Robert R., and Donald B.R. 2000, Contrasts and correlations in effect-size estimation. *A Journal of the Association for Psychological Science,* Vol. 11, No. 6, pp.446-453.
22) Sharpe C.F.S. 1938, Landslides and related phenomenon. *Cooper Square Publications Inc.,* New York.
23) Shields A. 1936, Anwendung der Ahnlichkeits-Mechanik und der Turublenzforschung auf die Geschiebebewegung. *Preussiche Versuchsantalt fur wasserbau und schiffbau,* 26, pp. 5-24.
24) Takahashi T. 1977, A mechanism of occurrence of mud-debris flows and their characteristics in motion. *Annuals of the Disaster Prevention Research Institute,* No. 20 B2, pp. 405-435. (in Japanese)
25) Takahashi T. 1980, Debris flow on prismatic open channel. *Journal of the Hydraulics Division, ASCE,* Vol. 106, No, 3, pp. 381-396.
26) Takahashi T. 1981, Debris flow, *Annual Review of Fluid Mechanics,* Vol. 13, pp. 57-77.
27) Takahashi T. 1991, Debris flow. Monograph Series of IAHR, *Balkema,* pp. 1-165.
28) Takahashi T., Nakagawa H., Harada T., and Yamashiki Y. 1992, Routing debris flows with particle segregation. *Journal of hydraulic Engineering, ASCE,* Vol. 118, No 11, pp.1490-1507.
29) Takahashi T., Satofuka Y., and Chishiro K. 1997, Dynamics of debris flows in the inertial regime. *Proceedings of First Conference on Debris-Flow Hazards Mitigation: Mechanics,* Prediction, and Assessment, California, ASCE, pp.239-248.
30) Tsubaki T.H., Hashimoto H., and Suetsugi T. 1982, Grain stresses and flow properties of debris flow. *Proceedings of 38th Annual Conference of JSCE,* No. 317, pp.79-91. (in Japanese)
31) Varnes D.J. 1958, Landslide type and process. *In landslide & Engineering Practice,* ed. E.B. Eckel, Highway Research Board, special Report 21.
32) Watanabe M., Mizuyama T. and Uehara S. 1980, Review of debris flow countermeasure facilities, *Journal of the Japan Society of Erosion Control Engineering,* Vol. 32, No. 4, pp. 40-45. (in Japanese)

CHAPTER 4

HYDRAULIC MODEL TEST ON CLOSED-TYPE SABO DAM WITH A FLAP

4.1 General

Debris flows are common in mountainous areas throughout the world, which contain various amounts of mud, sand, gravel, boulders, and water. They occur when water mobilizes large volumes of loose mud, rock, and other debris. It is generally accepted that debris flow disaster occurs in high mountainous areas far away from modern cities. Recently, this disaster simultaneously occurs in multiple locations between the high mountainous areas and the low mountainous areas in urban areas (Kim et al. 2013a, 2013b).

(a) Mt. Umeyon (Photo courtesy: PRESSian) (b) Caraballeda

Photo 4.1 Debris flow disasters

Debris flows, which contain varying amounts of mud, sand, gravel, boulders, and water, are common in mountainous areas throughout the world. As these flows cause significant morphological changes along riverbeds and mountain slopes, they are frequently reported to produce extensive property damage and loss of life (Nakagawa et al. 2002). In addition, Kim et al. (2012) reported that the incidence of occurrence of debris flow disaster is relatively very small in comparison to other sediment-related disasters, but once the debris flow occurs, the potential of damage is huge.

The debris flow disasters that occurred at Mt. Umeyon in downtown Seoul, Korea 2011 are shown in Photo 4.1 (a); photo (b) shows extensive damage to that the apartment in Caraballeda due to a passage of a debris flow front of at least 3.5m in height (Larsen et al. 2001). These disasters illustrate the destructive power of the high-velocity fluid as well as debris flow and flash floods on alluvial fans inundating coastal communities, causing severe property destruction, and resulting in a death toll estimated at 19,000 people. The debris flow disaster leads to massive property damage and casualty of life. Therefore, to estimate the disastrous effects, it is necessary to accurately understand, evaluate, quickly respond to the risks, and mitigate damage by establishing an effective measure.

Debris flow causes damage in three ways: deposition, erosion and direct impact. Impact force of a debris flow often causes structural destruction and is a key element in engineering design and risk assessment. However the impact force mechanism can be misunderstood partly due to the difficulty in measuring impact force (Hu et al. 2011). The debris flow is characterized by the front part of the flow, where large boulders accumulate, lasting for a few seconds. The following part is longer and appears like a mud flow with gradually decreasing discharge. The total force of debris flow consists of hydrostatic force, hydrodynamic force, and the impact

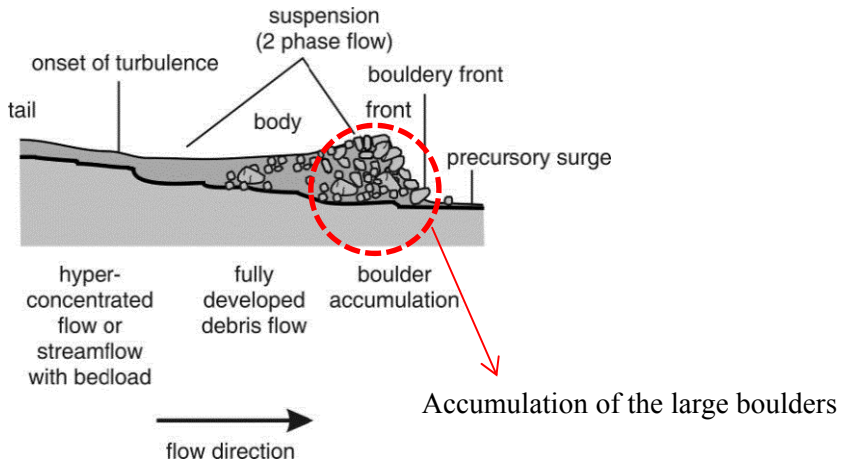

Figure 4.1 Typical feature of a debris flow longitudinal section

force due to boulders entrained in the flow. These three types of forces usually occur simultaneously so that debris flow has powerful energy.

In recent years, many researchers have experimented with the efficiency of sabo dams having a great impact on ecology and landscape. Such dams are also surcharged with the impulsive forces of the debris flow. The front part of the flow is important and complex in debris flow where large boulders accumulate. It is important to control or dampen the energy of the front part of a debris flow for the safety of the downstream area because the impact pressure of debris flow is greater than that of clear fluid. Figure 4.1 shows a typical feature of a debris flow longitudinal section (Pierson 1986).

Sabo dam (i.e. check dam) is commonly used and the most effective structural measure to protect property and loss of life from sediment-related disasters. The idea of functioning sabo dam was proposed about 70 years ago in Japan and was discussed based on qualitative recognition (Nishimoto 2011). Therefore, it is necessary to improve the function of sabo dam through advanced technology.

The proposed closed type dam consists of R (rectangular) and T (triangular) flap structures. The basic concept of this study is to propose the modification in the close-type dam i.e. as shown in Figure 4.4 (a) to form a new type of closed-type dams with a flap i.e. as shown in Figures 4.2 (b) and (c) and compare the function of each type regarding efficient energy dampening and capturing of debris (Kim et al. 2012, 2013a, 2013b, 2013c). Much research is being carried out to improve the function of sabo dams as well as to clarify the impact force of debris flow based on field observations, laboratory experiments (i.e. large and small scale), and numerical simulations.

A few field experiments have been conducted such as Okuda et al. (1978), Suwa and Okuda (1983), and Hu et al. (2011). In addition to these Hu et al. (2011) reported an in-situ test

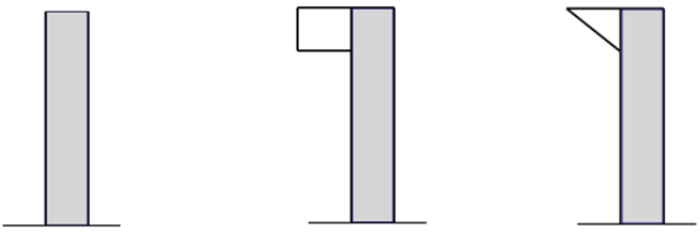

(a) Closed-type (without flap) (b) Flap-Rectangular (c) Flap-Triangle

Figure 4.2 Sketch of a sabo dams

of debris flow impact at Jiangjia Ravine, and introduced a simple approach to separate two components of the impact force into fluid pressure and grain-impact loading. In those studies, preliminary analyses were made to determine the relationships of mean velocity versus hydrodynamic pressure, and hydrodynamic pressure versus grain impact loading. Furthermore, Murakami et al. (1996) tried to modify the upper part of the sabo dam like the curved sea wall. Figure 4.3 shows the conceptual sketch of the FSS (i.e. Flaring-Shaped Seawall) (Kamikubo et al. 2002).

Many small-scale laboratory experiments have been performed in order to develop theoretical models for the calculation of impact force. Mizuyama (1979) separated the impact force of debris flow into the fluid force and impact force of boulder. According to the paper, the impact force on a sabo dam (i.e. without flap) is described with hydraulic theories and the theory of complete sphere elasticity was assumed so that the impulsive force of the boulders could be derived. Scheidl et al. (2012) analyzes the impact forces of granular and viscous debris flow and discusses the observations of single, short time impacts of large particles, significantly exceeding the peak pressure values. However, there have been very few studies that discuss how debris flow is influenced by the shape of a sabo dam. Shieh et al. (2008) designed a new form of sabo dam by changing the geometric shape of the upstream dam surface to reduce the impact force of the debris flow, with enhanced stability and reduced concrete mass being the anticipated outcomes. Their study showed that the curved dam experiences less impact force than other dams under the same debris flow condition, demonstrating the importance of curved geometry for a well-designed sabo dam. Huang et al. (2007) applied the theory of elastic collision to devise a boulder collision impact model with four types of dams. Recently, Shibuya et al. (2012) presented the load of debris flow with woody debris for an open type steel frame check dam structure. Likewise, understanding the behavior and mechanism of debris flow and the study of

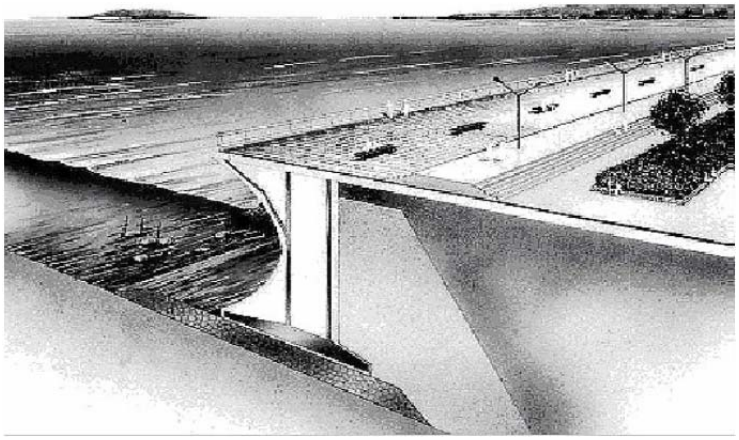

Figure 4.3 Conceptual sketch of the Flaring Shaped Seawall (FSS)

preventive measures are very important in order to manage the sediment disaster in the river basin and prevent downstream hazards. Preventive measures require the consideration of various plans and involve the evaluation of hydrological, hydraulic, grain size distribution, topographical and other parameters.

In this study, three types of closed-type dams were tested experimentally for the debris flow case and only two types, namely without and with flap-R structures, are considered for the upstream dam-break case with clear water. Experiments were conducted to investigate total pressure (combination of impact due to the collision, static and dynamic pressures) of both flows under the conditions of typical closed-type dam and that with flap. In the experiments, total pressure associated with major debris flows was recorded in real time by a system consisting of four dynamic pressure sensors (i.e. strain gages) installed at the dam. As stated above, the applied force of debris flow is usually determined by field observations, laboratory experiments and numerical simulations. But it is very difficult to estimate the applied force due to the impact collision because the debris flow is composed of many different sizes and fractions of sediment, which makes it difficult to estimate the actual contact area. So, the average value of the total pressure by the maximum value of the impact collision is determined experimentally by conducting several experiments under the same conditions.

In all the experiments, the parameters such as the flow pattern, the surface velocity between the debris flow and clear water, the total pressure, mass ratio of debris, median grain diameter of debris flow, and the uplift pressure were measured to compare the function of each s dam under the two different bed sediments. The empirical coefficients of the hydrodynamic and solid collision models were also determined and compared with the available values of those coefficients. Furthermore, observations of the load behavior of debris flow, the velocity, the average of maximum total pressures, the uplift pressure due to the impact collision, the vertical distribution of total pressure on the dams and the ability of the proposed dam to sustain such forces, are also discussed.

The objectives of this study are to analyze the working principle of the proposed closed-type dams with flap over dam without flap, to propose the best suitable type based on their characteristics, and also to determine the empirical coefficients of the hydrodynamic and solid collision model. In this chapter, the detail description of debris flow impact model, procedure of experimental set up for the experiment, experimental conditions, and measurement techniques of different parameters are incorporated. The results from experimental data are presented.

4.2 Debris Flow Impact Model

Several models have been developed to estimate the impact force of debris flow against barriers. However, it is difficult to decide the impact force due to the diversity of substances composing the debris flow (i.e. water, mixtures of granular and fine particles in water and boulders) and the conditions of dam (e.g. flexibility and properties). The impact force of debris flow has been mainly described by hydraulic and solid collision models. The hydraulic models are further separated into hydrostatic and hydrodynamic models. Based on observations and theoretical consideration, different models have been developed for estimation of the debris flow impact force.

- **Hydrostatic Model**

The hydrostatic models by Lichtenhahn (1973) and Armanini (1997) are useful because they require only the approaching depth of debris flow to calculate pressure. For simplicity, the value of Pmax is often estimated, for preliminary dam design purposes, assuming the approach depth of debris flow equal to height of dam. In general, the hydrostatic formula can be written as:

$$P_{\max} = k_p \rho_d g h \tag{4.1}$$

where P_{max} = the maximum debris flow impact pressure, k_p = the empirical factor, ρ_d = the density of debris flow, g = the acceleration of gravity and h = the depth of debris flow. The maximum impact pressure is not related to statistical considerations, but to the maximum pressure value in the load distribution on the structure (Hübl et al. 2009). Lichtenhahn (1973) proposed k_p values between 2.8 and 4.4. Armanini (1997) found a maximum static debris flow impact pressure exceeding roughly 5 times the hydrostatic pressure. Scotton and Deganutti (1997) measured the impact on an obstacle and proposed k_p values between 2.5 and 7.5 from the laboratory experiment.

- **Hydrodynamic Model**

The hydrodynamic formulas are based on the impulse theorem. The phenomenon of debris flow impact against an obstacle has been analysed in scientific literature; many empirical and non-empirical relations can be found for the calculation of the dynamic thrust.

$$P_{\max} = k_p \rho_d v^2 \tag{4.2}$$

$$F_{\max} = k_f \rho_d A v^2 \tag{4.3}$$

where P_{max} = the maximum debris flow impact pressure, k_p and k_f = the empirical factors, ρ_d = the density of debris flow, v = the velocity of debris flow, F_{max} = the modulus of the impacting force, and A = the area of the section involved in the phenomenon and whose height should be considered as the height of the debris flow front. The empirical factor value depends on the flow type. For laminar flow and fine grained material, Zhang (1993) recommends the pressure of empirical values between 3.0 and 5.0 based on field measurements at the Jiangjia Gully station. Bugnion et al. (2011) proposed that the pressure of empirical coefficient k_p approximately in the range between 0.4 and 0.8 appear to be appropriate for objects with size of the same order of magnitude as the flow heights. Canelli et al. (2012) estimated the force of empirical coefficient between 1.5 and 5.0 by a laboratory experiment with a small scale channel. Watanabe and Ikeya (1981) proposed that the force of empirical value changes with flow material; for clear water, k_f has been found to be between 1 and 2, and for bentonite, k_f = 2.0 as well as value of 1.5 by Hungr et al. (1984). Besides, when designing a sabo dam in Japan, it is usually done using Eq. (4.3) (Yamamoto et al. 1998).

- **Solid Collision Model**

Conventional contact mechanics is mainly concerned with static contact although it has been extended to approximate solutions when impact is involved. For spheroidal surfaces, Hertz theory is used to obtain the force deformation relation needed to calculate the duration of impact and the maximum indentation. According to Jackson and Do (1969), for the case of impact between two spheres of mass m_1, and m_2, investigations show that the duration of impact, i.e., the time during which the spheres remain in contact, is very long in comparison with the period

$$F = n\alpha^{3/2}$$

$$\beta = \sqrt{\frac{16 R_1 R_2}{9\pi^2 \left(k_1 + k_2\right)^2 \left(R_1 + R_2\right)}}$$

$$k_1 = \frac{1-\upsilon_1^2}{\pi E_1}, \quad k_2 = \frac{1-\upsilon_2^2}{\pi E_2} \tag{4.4}$$

$$\alpha = \left(\frac{5(v_1 + v_2)^2}{4\beta\gamma} \right)^{2/5}, \quad \gamma = \frac{m_1 + m_2}{m_1 m_2}$$

of lowest mode of vibration of the spheres. Vibrations can therefore be neglected, and it can be assumed that the force-displacement relation established for static conditions holds during impact. Where F = the compressive force (i.e. the force that acts during the period of impact between the spheres), υ_1 and υ_2 = Poisson's ratio, E_1 and E_2 = Young's moduli, v_1 and v_2 are the velocities of the colliding particles, R_1 and R_2 = the radii of spherical surfaces of the two bodies at the point of contact, and m_1 and m_2 = the mass of sphere. Mizuyama (1979) calculated the impact load between sabo structure (relates parameters with subscript 1 in above equation) and debris flow (relates parameters with subscript 2 in above equation) based on different assumed values of parameters used in equation 4. Mizuyama assumed the Young's modulus of material forming the sabo structure $E_1 = 5\times10^8$ kg/m^2 (as of concrete) and the materials forming the debris flow $E_2 = 2\times10^9$ kg/m^2 (as of stone), Poisson's ratios of sabo structure material υ_1 =1/6 (as of concrete) and material of debris flow υ_2 =1/5 (as of stone), and v_1 is equal to zero (since sabo structure is stationary) so that $v_1 + v_2$ is taken as equal to v_2 (the approaching velocity of debris flow). The impact load is rewritten using the properties of concrete (i.e. sabo dam) and large boulder as:

$$F_{\max} = k_f 48.2 v_2^{1.2} R_{\text{boulder}}^2 \tag{4.5}$$

where k_f = the control empirical factor, v_2 = the approaching velocity of debris flow, and R_{boulder} = the radius of the boulder.

4.3 Experimental Set-up for Sabo Dam with a Flap

To clarify the characteristics of debris flow in comparison with clear water as well as to compare the functions of the proposed dams with typical sabo dam (i.e. without flap), experiments were conducted in a flume located at the Ujigawa Open Laboratory (UOL) of the Disaster Prevention Research Institute (DPRI), Kyoto University, Kyoto, Japan.

4.3.1 Experiment for Hydraulic Characteristic

The experiments confirmed the characteristic of debris flow and observed the energy dissipation phenomenon near the dam as shown in Photo 4.2. Only two types of sabo dams (i.e. without and with flap-R) under the two flow conditions i.e. the clear water flow and the debris flow were tested. To clarify the characteristic of debris flow, hydraulic model tests with clear

water were performed for comparing the flow profile and total pressure in a rectangular flume that was 100 cm long, 15 cm wide, and 40 cm high. At a distance of 60 cm from its downstream end, a vertical gate was installed as shown in Figure 4.4. The walls and bottom are made of transparent smooth acrylic plank, which allows for lateral observation. At the dam section, the flume is equipped with a smooth gate that can open by hand. The flow was filmed with a digital video camera (Sony: HDR-CX560) placed on the side of the channel. The efficiency of the two types of dam with a plan-1 (without and with flap-R types) will be discussed, comparing the total pressure and flow profile near the dam.

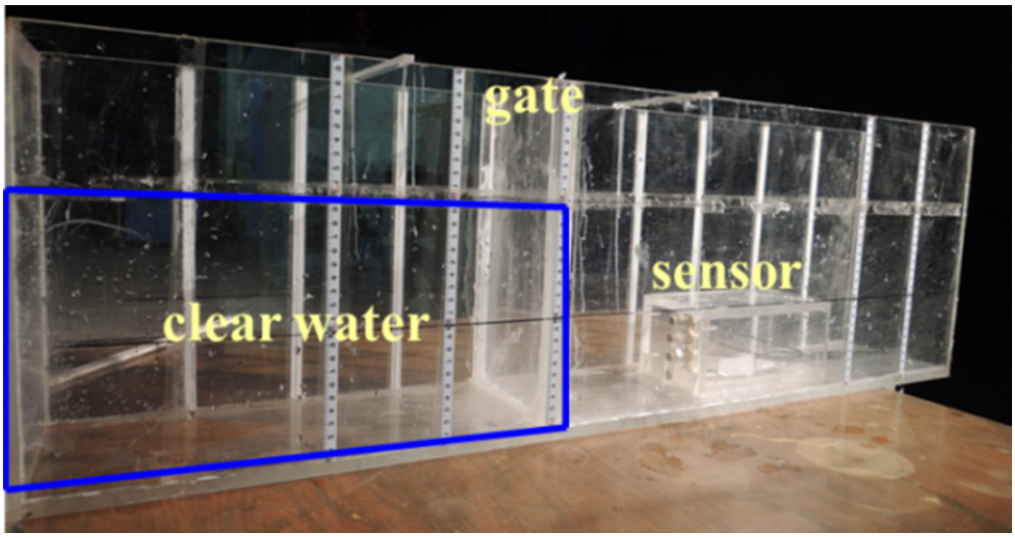

Photo 4.2 Experiment setup for dam-break upstream of the proposed dam

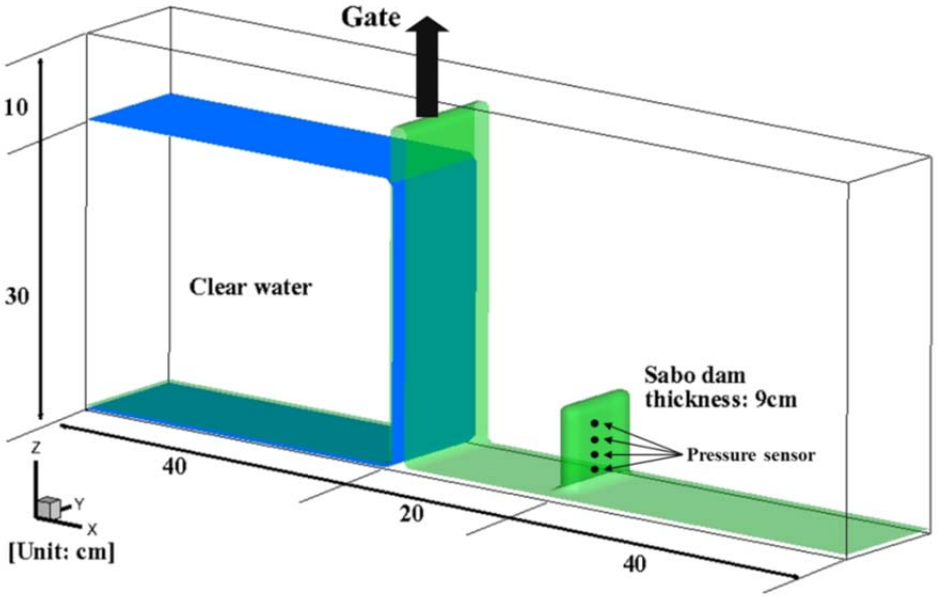

Figure 4.4 Sketch of experiment setup for upstream dam-break

4.3.2 Experiment for Debris Flow

Experimental flume for debris flow is shown in Photo 4.3. The debris flow experimental facility consists of a 5.0 m long horizontal smooth flume with a rectangular section 10cm wide and 14 cm high. One side of the walls is made of transparent glass and the other side is opaque made of PVC. The slope of the flume is set at 18 degree. The Sabo dams were built with acrylic planks of 10 mm in thickness. To generate the debris flow, a section of the flume (2.8 m upstream from the outlet) having dimensions 1.9 m long, and 7 cm deep is filled with the sediments supported at the downstream by a 7 cm high weir. The reason behind the installation of weir at the downstream of the debris flow generation section is to make the sediment pre-saturated before the debris flow generation. Then the debris flow is generated overflowing the installed weir. Debris flow is produced by supplying a constant water discharge of 300 cm^3/sec for 10 sec from the upstream end of the flume. Details of the experimental setup are shown in Figure 4.5.

Debris flow velocity, the radius of the boulder, and approaching height are very important factors to discuss in the dynamic impact force. So far, few experimental studies discuss the impact force of debris flows. Each experiment used three different generation methods. Itoh et al. (2011) explained the generation methods of debris flow as follows:

A) Type- NL: Natural landslide dam break
B) Type-U: Sediment and water is supplied steadily in the upstream end of the channel.
C) Type-QS: Bed sediment is set on the bed in an upstream reach of the channel, saturating the upstream sediment with water, and supplying the input discharge from upstream.

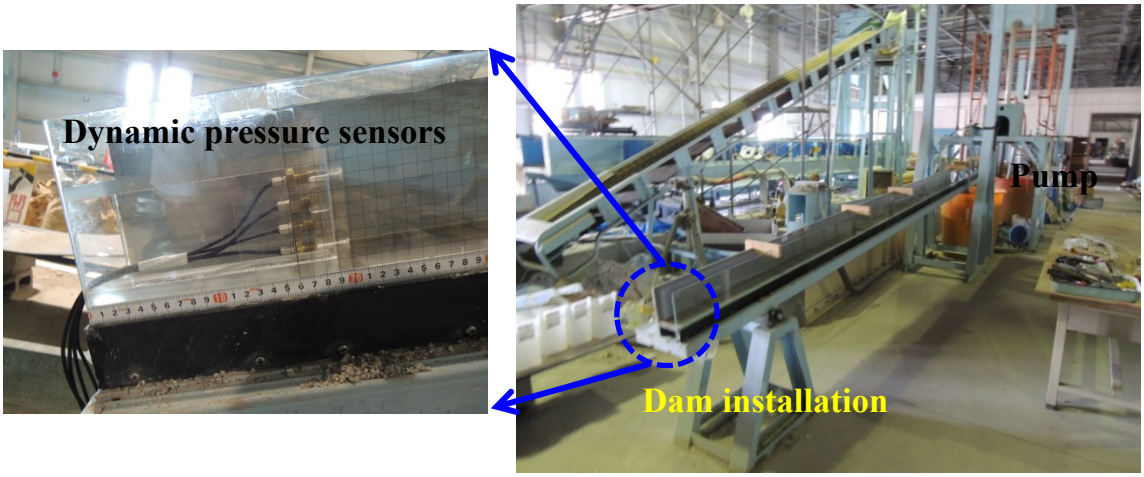

Photo 4.3 Experimental flume for debris flow

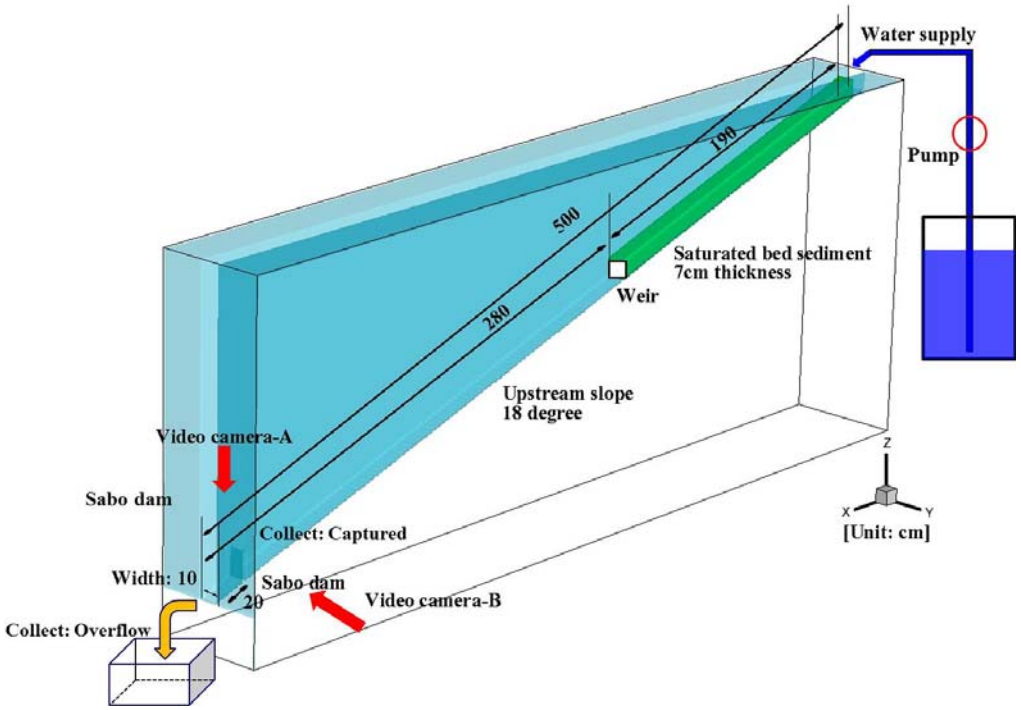

Figure 4.5 Sketch of experiment setup for debris flow

In most studies, type-U has been used for debris flow generation. In this study, the phenomenon of the debris flow is approximated by the type-QS generation method. As the generation type is QS, the sediment composition and degree of saturation might not be uniform throughout the sediment layer. In addition, the standard size of the boulder cannot be measured when a debris flow hits the obstacle. Therefore, the experiments were repeated several times under identical conditions. Debris flows produced in the experiments are the stony debris flows type and the largest particles are accumulated in the forefront. To measure the thickness of deposition (i.e. the flow depth plus the deposition thickness in the process and final stage) accurately, the graduations are marked on the side of the flume.

4.3.3 Experimental Conditions

The experiments performed two kinds of plans. The plans of sensor position are shown in Photo 4.4. First, in order to estimate the safety of flap structure, the vertical distributions of total pressure for three dams under two different bed sediments conditions are investigated by sensors positioned vertically (i.e. plan-1). To estimate the impact pressure, the same level of total pressure (i.e. 1 cm from bottom) for three dams under two different bed sediments conditions are investigated by sensors positioned horizontally (i.e. plan-2). Since plan-2 (i.e. horizontal direction) consists of the sensor installation at the bottom part only, the results are irrelevant to

the shapes of the dam, but the values are directly connected to the bed sediments. Therefore, this experiment can obtain four values of the total pressure per one case, and averages of observed maximum values are used for data analysis.

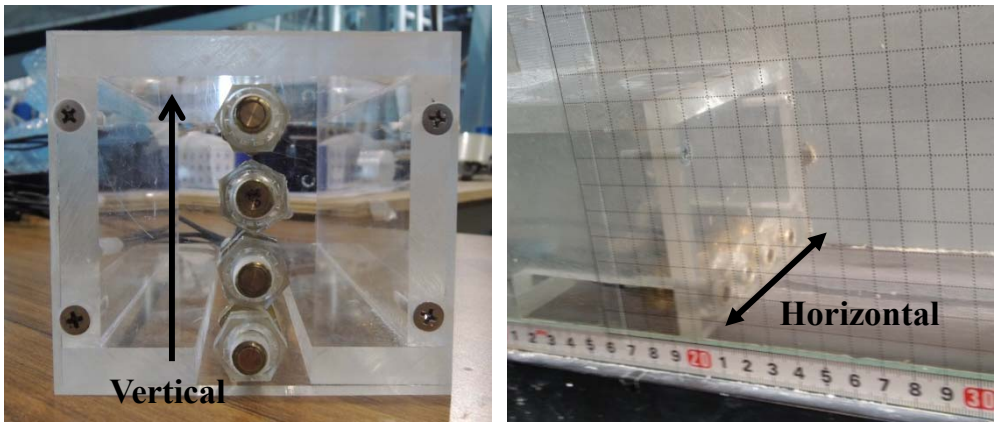

(a) Vertical direction (b) Horizontal direction

Photo 4.4 Plans of sensor position

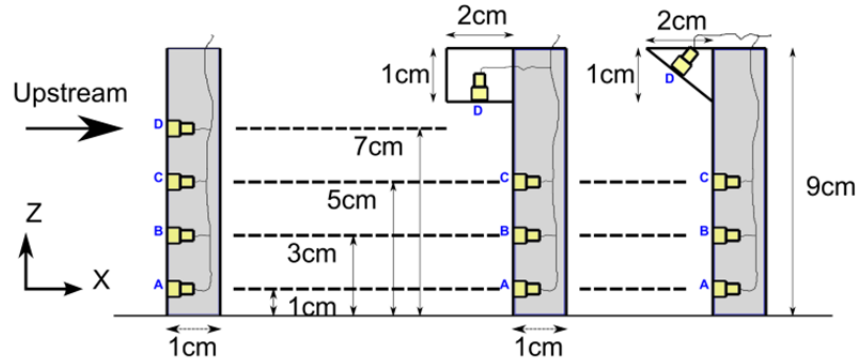

(a) plan-1: without flap with flap-R with flap-T

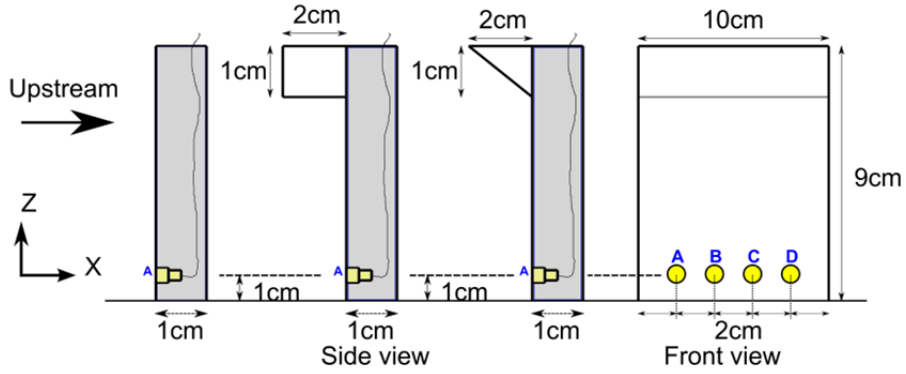

(b) plan-2: without flap with flap-R with flap-T

Figure 4.6 Sketch of diagram of three closed dams

The schematic diagrams of the three dams with different plans are shown in Figure 4.6. The total pressure associated with major debris flows was recorded in real time by a system consisting of four sensors installed at two different plans. The sensors were installed vertically along the flow depths (plan-1), and horizontally at the same flow depth (plan-2). The uplift pressure and vertical distribution of total pressures were measured by plan-1 and the total pressure due to impact collision was measured by plan-2. The pressures data were sampled at frequency rates of 500 Hz converted via an interface board and recorded on a hard disk file. The installation of the dam in the flume with plan-1 is shown in Figure 4.7. Furthermore, Table 4.1 and Table 4.2 show the experimental condition with both plans.

(a) Without flap

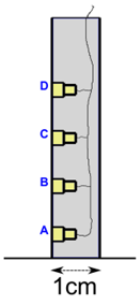

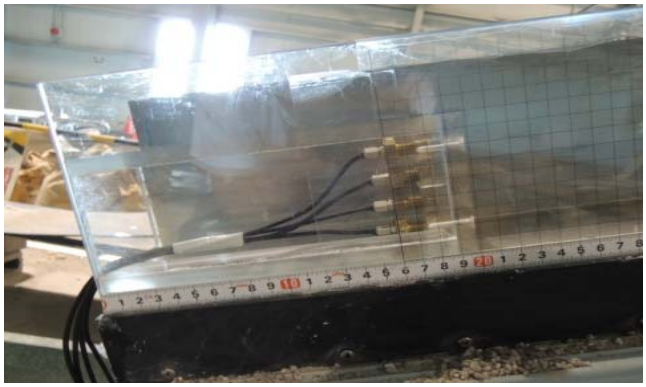

(b) With flap-R

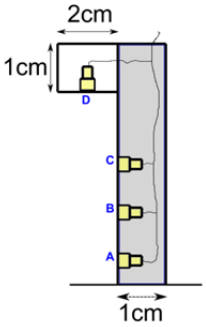

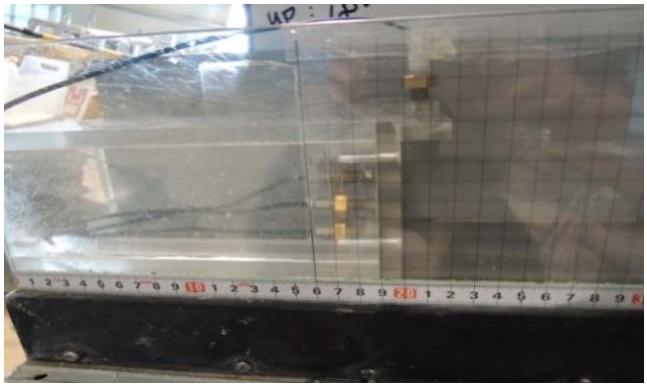

(c)With flap-T

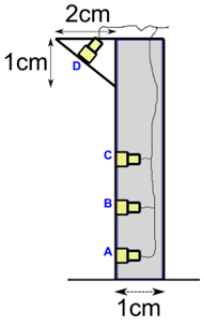

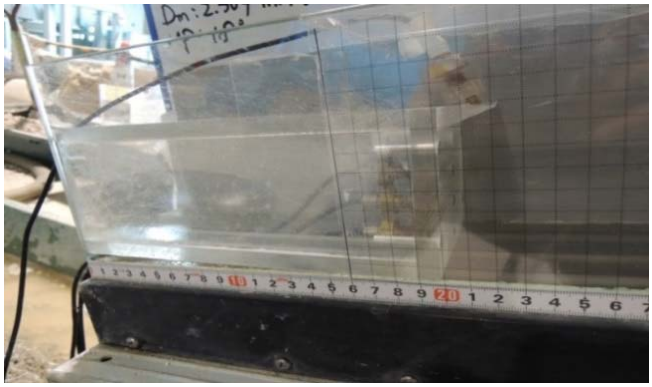

Figure 4.7 Installation of dam

Table 4.1 Experimental conditions for horizontal pressure

Bed Sediment	*Sensor installation*	*Measurement*	*Repetition*
A	Plan-2	Total pressure, velocity, depth	10 times
B	Plan-2	Total pressure, velocity, depth	10 times

Table 4.2 Experimental conditions for vertical pressure

Type	*Bed sediment*	*Sensor installation*	*Measurement*	*Repetition*
Without flap	A and B	Plan-1	Total pressure	10 times
Flap-R dam	A and B	Plan-1	Total pressure	10 times
Flap-T dam	A and B	Plan-1	Total pressure	10 times

In order to analyse the dynamic pressure accurately and clearly, the data obtained from the experiments are analysed by using the data filtering technique (i.e. boxplot method using Minitab software). A boxplot is a device used to represent the median of data, the upper and lower quartiles, and any data points that are possibly outside (outlier) values. It is also useful for summarising a data set.

4.3.4 Sediment Properties

To generate the stony debris flow, various materials can be used to mix sediment with gravel and silica sands. As for the sediment used in the experiments, silica sands (S1, S2, S3, S4, S5, S6) and gravel (G1) are mixed in equal proportion by weight to prepare the bed sediment-A. Silica sand (S1, S2, S3, S4, S5, S6) in proportion (1.6, 1.5, 1, 1, 1, 0.7) and gravel (G1) in (1.7) by weight are mixed to prepare the bed sediment-B. Figure 4.8 shows particle size distributions

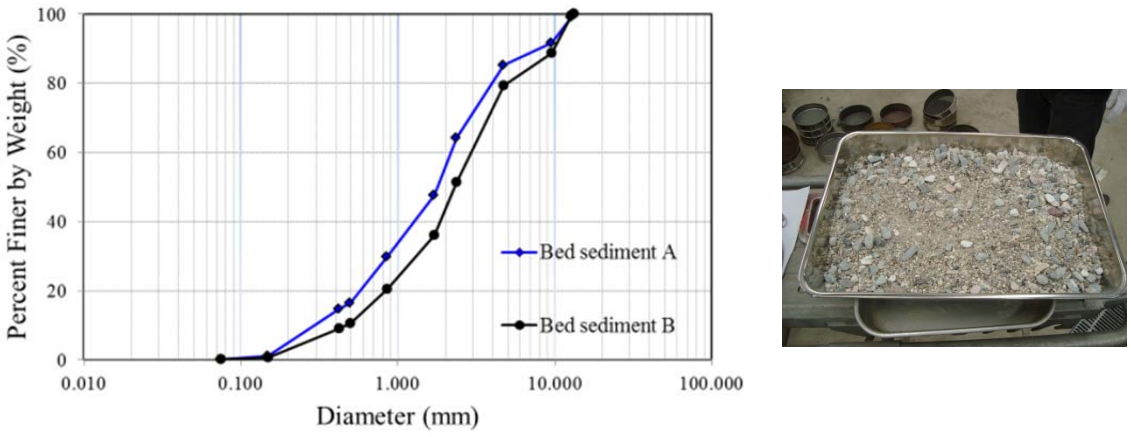

Figure 4.8 Particle size distribution curve

of the prepared material for bed sediment-A and bed sediment-B. Table 4.3 shows the diameters of sediment of median grain and mixing ratio. Properties of sediment material are shown in Table 4.4. The bed sediments have an angle of repose, tanϕ=0.7 and sediment density σ=2.65 g/cm^3 and are saturated with water. Besides, in order to estimate the median grain diameter from the sieve analysis was used by a vibration sieve machine under the 12 types of sieve.

Table 4.3 Mixing ratio of bed sediment material

Type		*Gravel*	*S1*	*S2*	*S3*	*S4*	*S5*	*S6*
D_{50} (mm)		10.00	4.26	2.56	1.85	0.94	0.67	0.29
S-A	Ratio	1	1	1	1	1	1	1
S-B		1.7	1.6	1.5	1	1	1	0.7

Table 4.4 Properties of bed sediment material

	D_{50} *(mm)*	D_{95} *(mm)*	σ_g	k_d
Sediment A	1.783	10.871	3.083	0.341
Sediment B	2.304	11.142	3.217	0.353

4.3.5 Measurement Techniques

The dynamic pressure measurement system is produced by a Japanese company, Kyowa as shown in Photo 4.5. The measuring system was composed of four dynamic pressure sensors (diaphragm type), sensor Interface (PCD-300B), and four channels of Adaptor and Note-PC by the dynamic data acquisition software (DCS-100A) as shown in Photo 4.6. These sensor transducers have a bridge of strain gages inside, achieving ultra-thin compact structure. Kyowa strain gages are available for the measurement of various types of strain, from static to dynamic

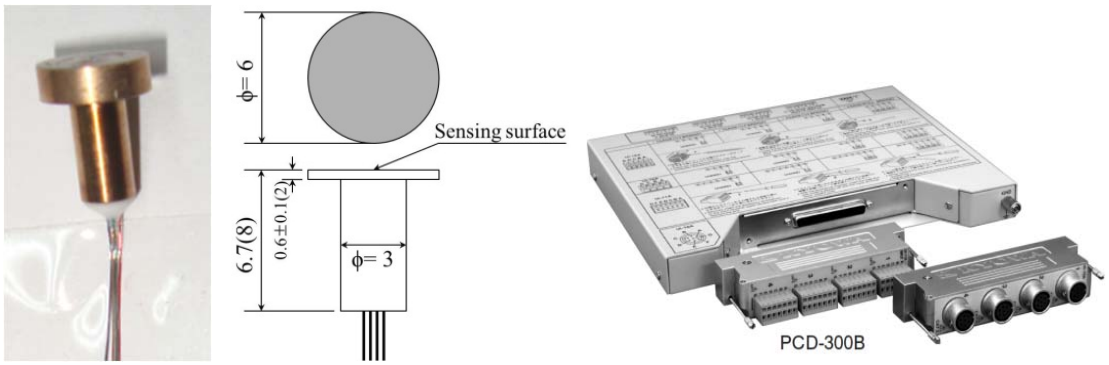

Photo 4.5 Dynamic pressure sensor and interface with four channels

strain and impact-initiated strain. Strain gages are used not only for stress measurement but also as sensing elements for various transducers owing to their excellent repeatability and linearity. Dynamic strain is a strain whose magnitude changes as time passes or which is initiated by vibration or impact. Since ever-changing strain cannot be read out on analog and digital indicators, a data recorder was used to obtain the detected data. Table 4.5 shows the specification of the sensors. Kyowa performs various tests using testing facilities completely equipped in accordance with the National Aeronautics and Space Administration Standard (NAS-942) and the German Standards (VDI/VDE2635). These pressure sensors are measuring devices that produce an output signal proportional to the applied dynamic pressure and the total pressure is calculated by the following relation as proposed by the company, Kyowa.

$$Pressure(\mathrm{Pa}) = \frac{\left(Strain\ \ ampifier's\ \ output,\ \ \varepsilon \times 10^{-6}\right)}{\left(Rated\ \ output\ \ on\ \ label,\ \ \mathrm{mV/V}\right)} \times \frac{Capacity(\mathrm{Pa})}{\left(2000 \times 10^{-6}\ /\ \mathrm{mV/V}\right)} \tag{4.6}$$

Table 4.5 Specification of the sensor

	Sensor-A	*Sensor-B*	*Sensor-C*	*Sensor-D*
Capacity	200 kPa (2.039 kgf/cm^2)			
Rated output	1mV/V (2000×10^6 strain) ±20 %			
Safe excitation	3V			
Input & output	350Ω ±10 %			
Sensitivity	0.718 mV/V ±1 %		0.748 mV/V ±1 %	

*Note: 1mV/V corresponds to 2000×10^{-6} equivalent strain

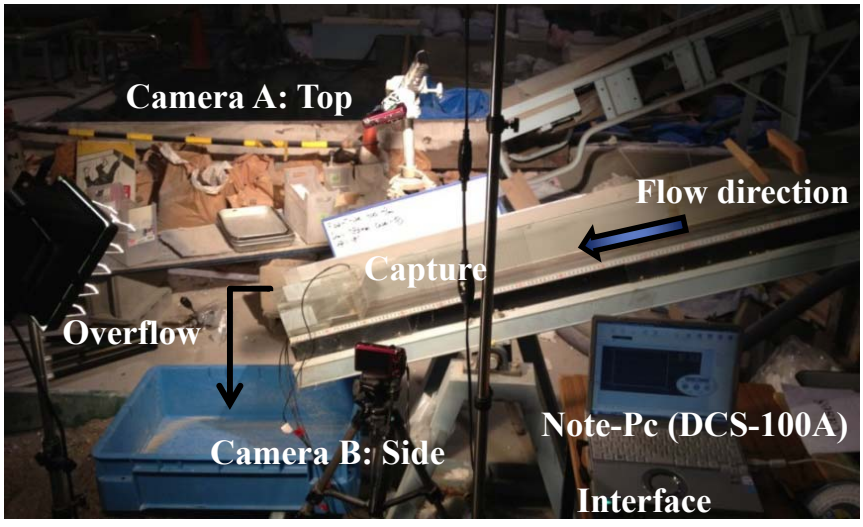

Photo 4.6 Measuring system

A high-speed camera measured the velocity of debris flow in this study. The flow was filmed with the high-speed camera (Casio: EX-ZR300) placed on the side and on top of the channel. A powerful imaging technique is exploited to measure the tracer velocities and flow patterns. At the chosen video rate of 480 frames per second, the digital images have a resolution of 224×160 pixels. All velocities were estimated by a Lagrangian particle method at the front of the dam site.

Compression pressure values measured the positive force along a single axis. The information from the sensor monitor transferred to a recorded or other computerized data collection system. Sampling frequency (f_{scan}) adopted in the experiments is 500 Hz base on the Nyquist-Shannon sampling theorem as shown in Equation (4.7). The frequency is able to how the dynamic variation within every 0.002 s.

$$f_{scan} = 2f_{max} \quad \left(f_{max} = \frac{v_{avg}}{d_{max}} \right) \tag{4.7}$$

where v_{avg} is the average surface velocity of debris flow and d_{max} is the maximum grain diameter.

Prior to the performance of experiments, sensors would confirm the response due to the external force. Even though the verification of sensors has been accomplished by Kyowa, the simple experiment is carried out to check the response of sensor. The comparison of hydrostatic pressure and sensor outputs against standard test loads before measurement produced the calibration curve. The results were desirable between hydrostatic pressure and measuring data. The mechanism of the measuring system and the calibration curve are shown in Figure 4.9, respectively.

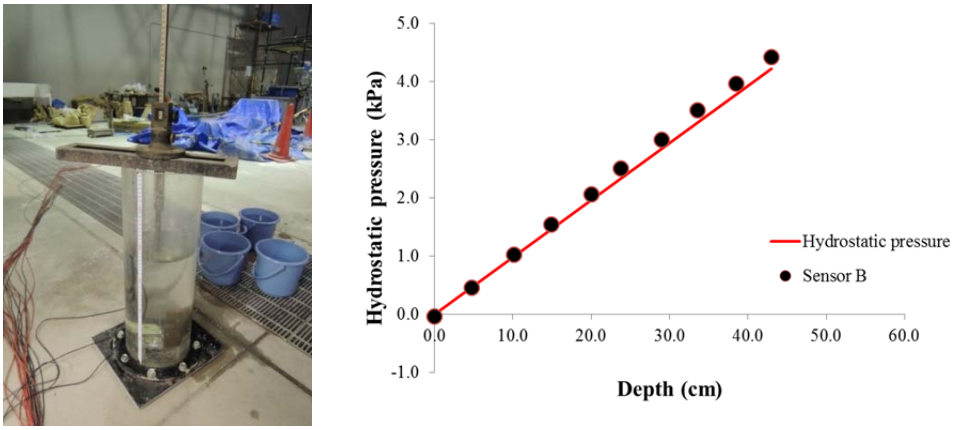

Figure 4.9 Measuring system and typical calibration curve

4.4 Results and Discussions

Fundamental experiments were conducted to investigate dam-break and debris-flow for the improvement of functions of the sabo structure. Considering quantitative and qualitative results from the experiments, the characteristics of proposed closed dams were discussed and summarized as follows:

4.4.1 Comparison of Flow Profile near the Dam

To confirm the characteristics of flow profile and total pressure, two types of closed dams (without and with flap-R) under the two flow conditions (i.e. the clear water flow and the debris flow) were tested with plan-1. The experiments were carried out for both flow conditions in order to observe the energy dissipation phenomenon near the dam. In the case of dam without flap, after suddenly opening of the gate, the flow hit the dam body and whole flow move vertically upward and then some flows overtopped the dam while rest falls down upstream. But in the case of dam with flap, after hitting the dam surface by the flow, the flow moves towards the below part of the flap vertically. Then, the flap reflect back the flow upstream which looks like a bore traveling toward the upstream direction. The flow pattern with debris flow was observed without considering the flap structure. In such case, the flow pattern is similar to clear water case but due to the mixture of different size of sediments in the debris flow, we observed that some portion of the debris flow overflows carrying large sediments while rest of the flow remains upstream depositing remaining particles at the bottom part of the dam. In contrast, if we consider the flap structure, frontal part of the debris flow which consists mostly coarser particles were captured and deposited upstream of dam due to the reflection from the flap.

Table 4.6 shows the average values of the surface velocities measured for different flow conditions (i.e. clear water and debris flows) in front of dam by a high-speed camera. Although the flow pattern and the approaching surface velocity are very similar, the total pressure is entirely different in both flow cases as shown in Figure 4.10. This is due to the fact that the debris flow has a huge energy in the front part of the flow that is much greater than clear fluid flow because of the accumulation of large boulders at the front.

Table 4.6 Results of surface velocity in both flows

Flow type	*Surface velocity (m/sec)*
Clear water	1.176
Debris flow with sediment A	1.218
Debris flow with sediment B	1.244

Figure 4.11 shows the test results of flow pattern for two different types of dam in the case of clear water. The flow pattern in the case of clear water flow is shown in Figure 4.11 (a) for the dam without flap and the Figure 4.11 (b) for the dam with flap-R. Furthermore Figure 4.12 shows the test results of flow pattern for two different types of dam in the case of debris flow whilst Figure 4.12 (a) and Figure 4.12 (b) correspond to the debris flow condition for both types of the dam. An important point is that each flow pattern is very different for different types of dam, but the pattern is the same in both flow cases. The flap-R dam generated a larger volume of spray than the dam without flap downstream in both cases. The comparison of the total pressures due to the impact collision (i.e. the value is taken as the average of all measured maximum value of pressure for each sensor in the number of experiments) reveals the following:

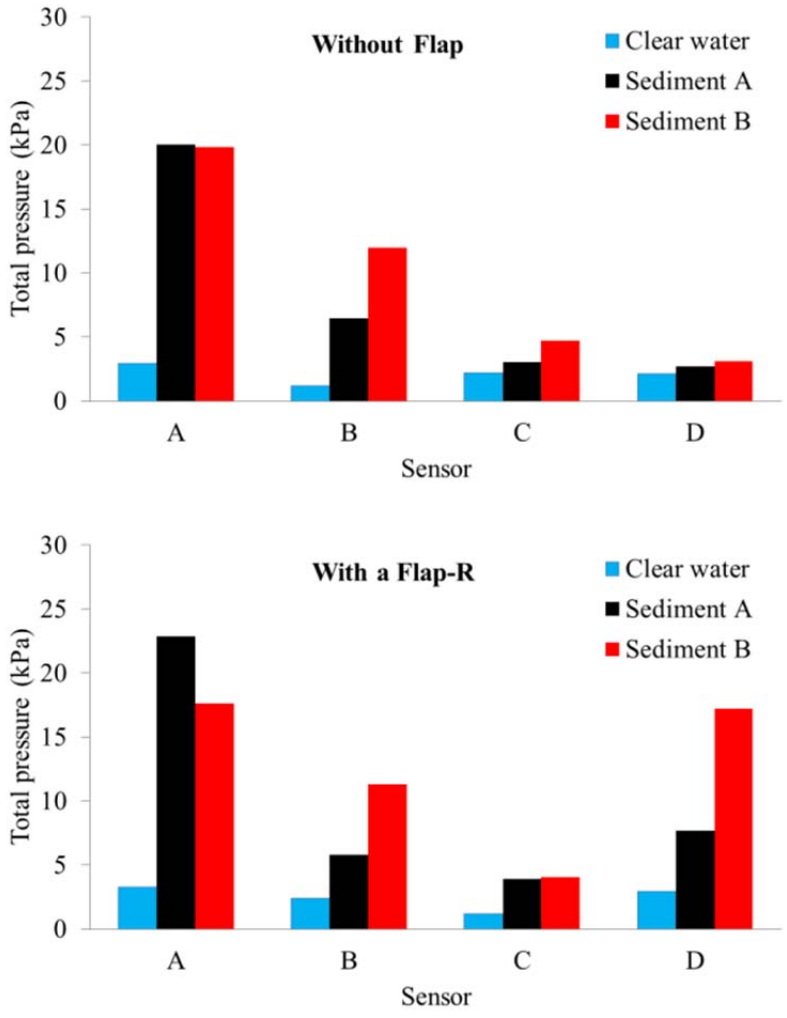

Figure 4.10 Results of the total pressure due to clear water and debris flow

(1) The sensor D indicated nearly similar total pressure in both types of flow for the dam without flap (as shown in Figure 4.10). The reason for this similarity is that, in both the flow cases, the movement of flow at the top of the dam (where sensor D located) is vertical i.e. most of the forces are uplift (due to the vertical nature of flow at the top as shown in Figure 4.11 (a) and Figure 4.12 (a)) and the dam without flap has no capability to absorb the uplift force since it has no flap. But the total pressures in the case of sensor A with debris flow have increased nearly 7 times in comparison to other types because at the bottom part of the dam (where sensor A is located) the debris flow has more impact force due to the sediments than the clear water since the flow here is not completely vertical as in sensor D as shown by Figure 4.11 (b) and Figure 4.12 (b).

(2) In the case of the dam with flap-R, the values of sensor D with bed sediment B indicated that the total pressure increased by nearly 6 times in comparison to clear water type, and the sensor

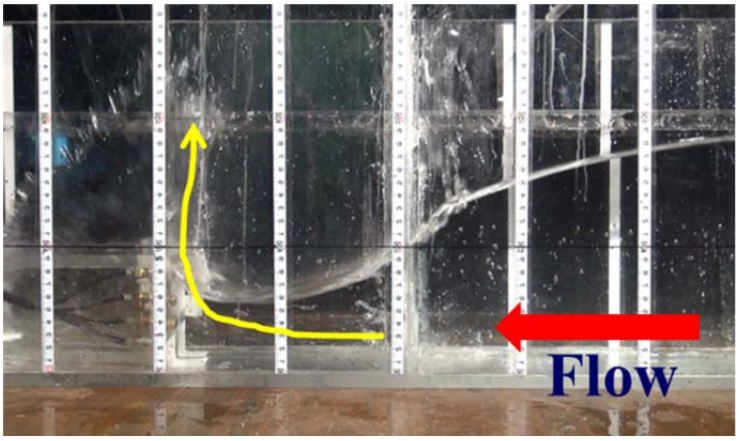

(a) Clear water case without flap

(b) Clear water case with flap-R

Figure 4.11 Results of the flow pattern for two different type dams due to clear flow

A showed a 5 times increase in the value of total pressure. The reason for this increase in value is that the flap structure for debris flow absorbed higher uplift pressure than the clear water, and the bottom part did not change significantly than the point (1).

The above result shows that the dam with flap-R can reduce the quantity of spray transportation more efficiently than the dam without flap due to the flow profile so that the reduction in energy and overtopping time occurs. This experiment should also help us better understand the energy dissipation process involved in the flow weakening. Even if the flap structure was shocked by the uplift pressure, it shows that the newly designed check dam with flap has the advantage of changing the total pressure compared to the dam without flap due to generation of the reflected flow. Furthermore, this result shows that the dynamic force of debris flow due to the impact collision is much greater than the clear fluid of dynamic force in comparison to the total pressure in the flow due to the average of maximum total pressure.

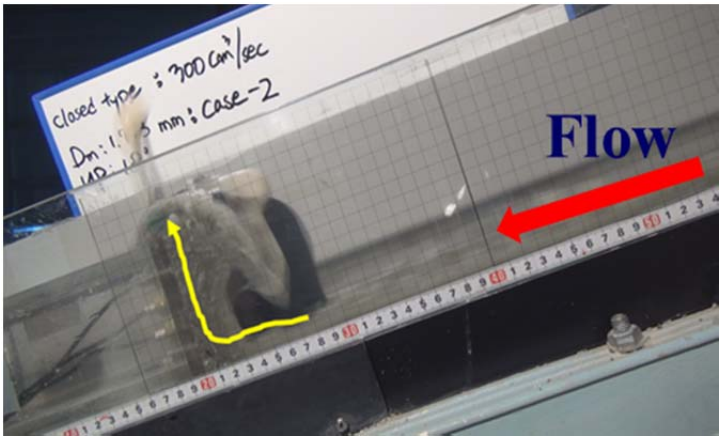

(a) Debris flow case without flap

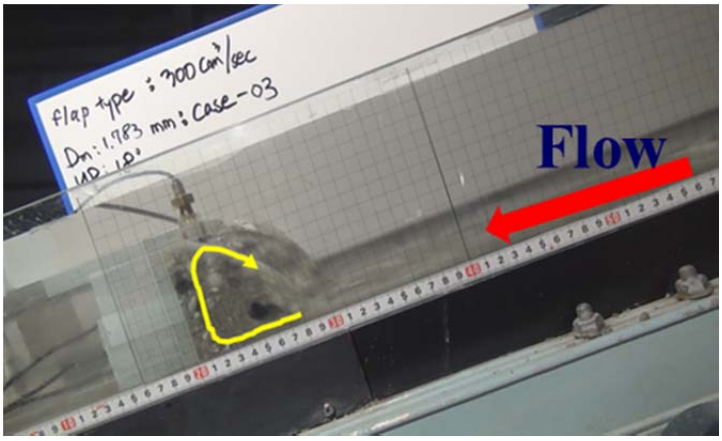

(b) Debris flow case with flap-R

Figure 4.12 Results of the flow pattern for two different type dams due to debris flow

4.4.2 Flow Pattern

Figures 4.13 ~ 4.15 show the characteristics of debris flow of all three types of dam in consideration (i.e. dams of without flap, with flap-R, and with flap-T) at different time steps. The figures clearly reveals that, in the case of a dam without flap, the large particles are seen to overflow whereas in other two types of dam such particles are seen to be captured. This leads to the conclusion that flap-T and flap-R types are more efficient regarding the capturing of large debris mass. This is because the flap structure is more efficient in capturing the large particles. The flow patterns of the proposed dams obtained by the experiments are described briefly as follows:

(1) In the case of a dam without flap: the flow pattern is influenced by the characteristic of debris flow (especially the approaching flow depth and velocity). First the dam was immensely shocked by the impact collision; secondly flow uprush occurred vertically with large boulders due to the uplift pressure quickly and finally the debris flow separated into two flows at the top of the dam: some debris flow is transformed as an overflow with few large boulders, and other debris is dropped by gravity from the top of the dam. A dead zone is developed at the bottom of the dam by the incoming debris flow simultaneously with the above process. Due to those processes, now the channel bed will rise upstream of the dam because of the captured debris mass.

(2) In the case of the proposed dams (i.e. flap-R and flap-T dams), when debris flow occurs in front of the dam, the impact collision and the vertical lift of the debris mass occur in similar fashion as in the case of the dam without flap but there will be no overflow of the debris mass and all the debris mass is captured upstream of the dam due to the generation of the reflected flow as shown in Figure 4.14 (b) and Figure 4.15 (b). But later after deposition above the dam height the overflow of debris mass may occur. Therefore, it is inferred from this process that the proposed dam type will capture more large boulders than the other types of dam and also the proposed type will reduce the overflow time (which is not quick enough like the dam without flap) and reduce the impact energy on the dam from the incoming debris flow due to the deposited mass before the dam.

Although the figures show that the final stage of the debris flow pattern is similar in all three types of dam, it should be understood that the process to reach the final stage is different for each type of dam as shown by the research.

(a) Without flap: Initial condition, at t = 0.0sec

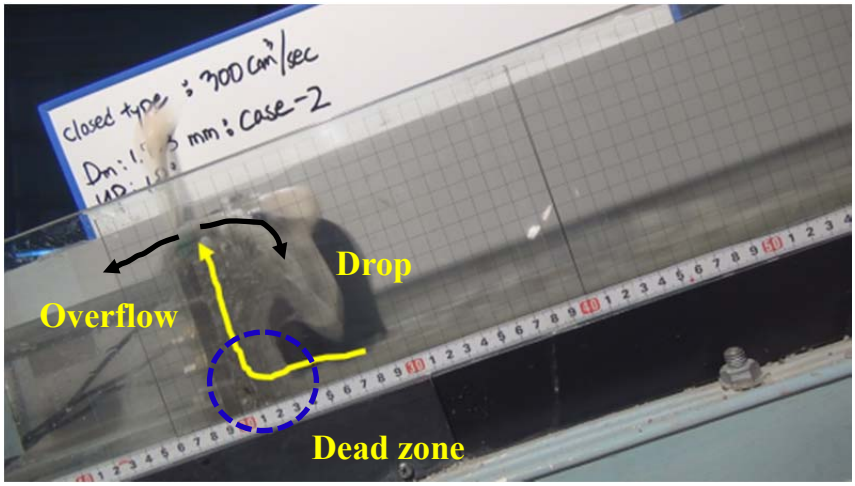

(b) At time = 6.67sec

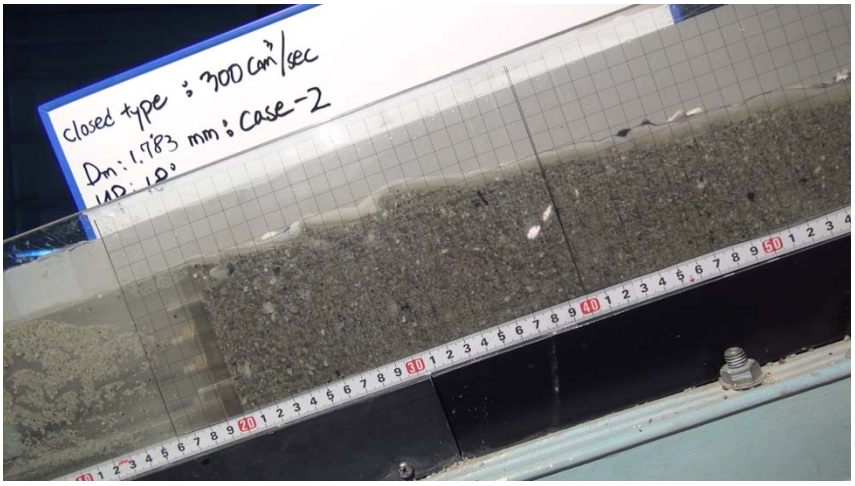

(c) At time = final sec

Figure 4.13 Movement of debris flow at different time step: sediment A for dam without flap

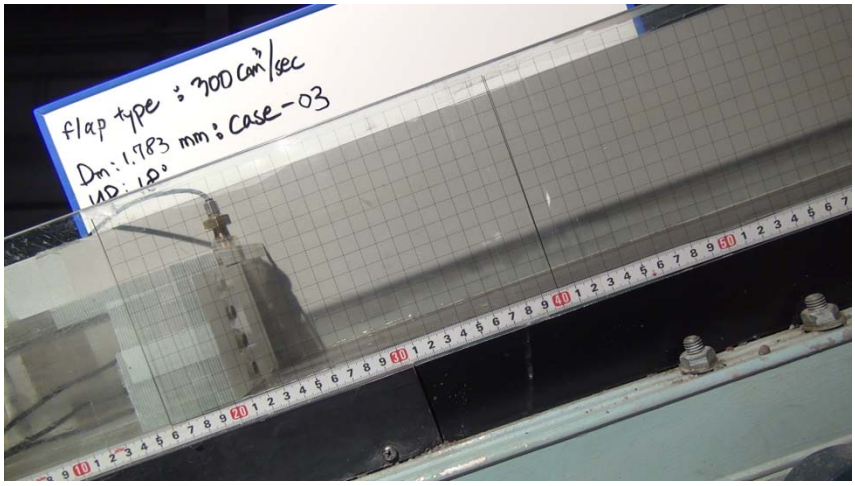

(a) With flap-R: Initial condition, at t = 0.0sec

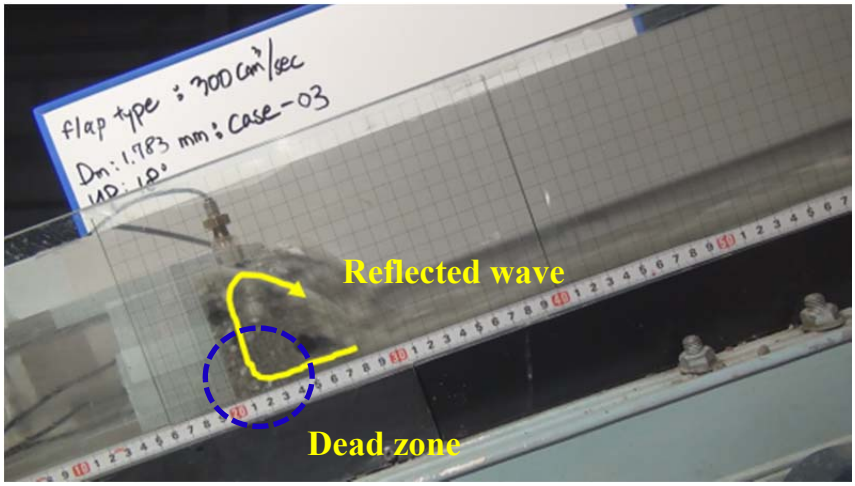

(b) At time = 7.43sec

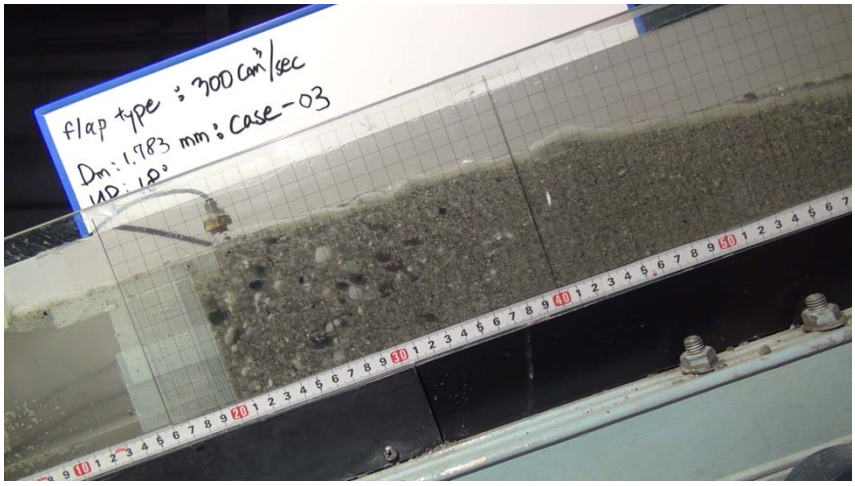

(c) At time = final sec

Figure 4.14 Movement of debris flow at different time step: sediment A for dam with flap-R

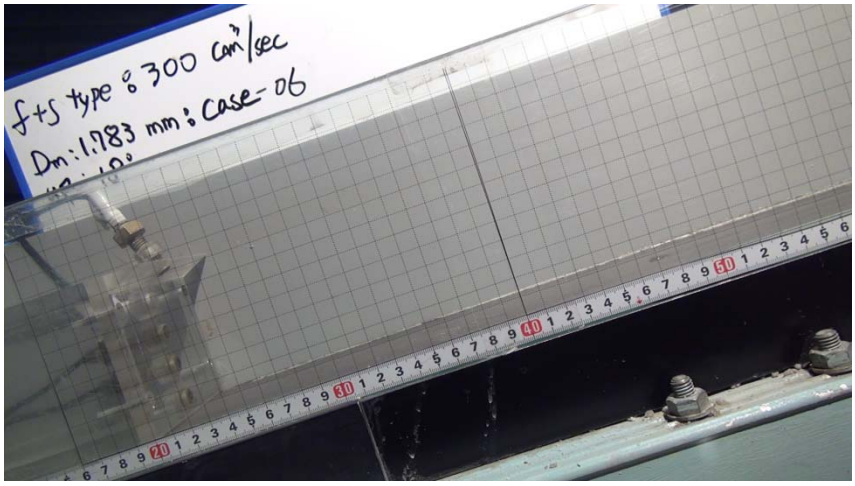

(a) With flap-T dam: Initial condition, at t = 0.0sec

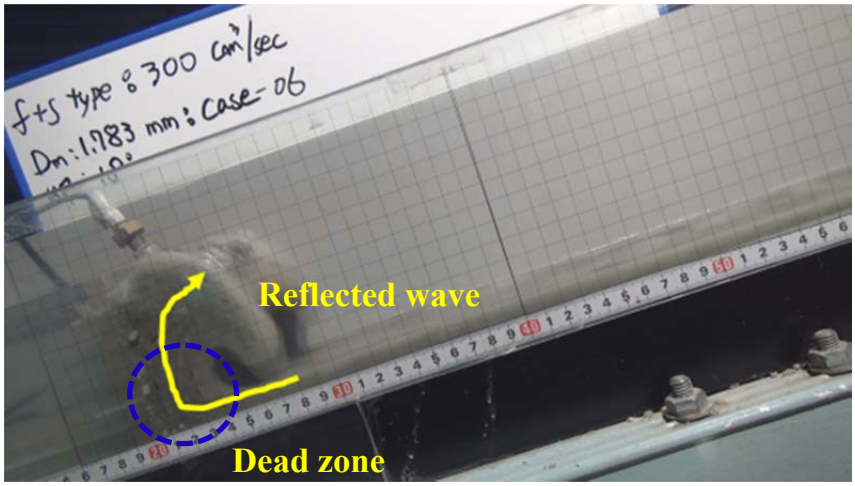

(b) At time = 6.30sec

(c) At time = final sec

Figure 4.15 Movement of debris flow at different time step: sediment A for dam with flap-T

4.4.3 Mass Ratio and Median Grain Diameter

To clarify the function of flap structures, the debris flow mass captured by and overflowed through the dam and the respective median grain diameters between two types of dams (i.e. dam without flap structure and dam with T- type flap) under the two different sediment conditions were observed and compared. The results of the mass and grain size distribution in the experiment were taken as the average value of 5 observations under the identical conditions.

Referring to Figure 4.16, initially (V), 23 kg of the sediment (density of 2.65 g/cm^3 and porosity of 0.35) was placed in the flume as a rectangular bed (sizes 190 cm×10 cm×7 cm) for the generation of debris flow (Type-QS) at the upstream of channel. Then 300 cm^3/sec of water was poured into the sediment bed for 10 sec and the debris flow was generated. During the experiment, not all the input sediments were developed into the debris flow during 10 sec but some sediment remains (IV) in the bed at the channel upstream (as shown in Figure 4.16). After the experiment, the mass of debris (i.e. the (I) overflowed and (II) captured) were measured directly with an electronic scale by collecting mass at the measurement boxes. In both cases of sediment A and B; the initial generation of debris flow mass (III) was calculated for dam both

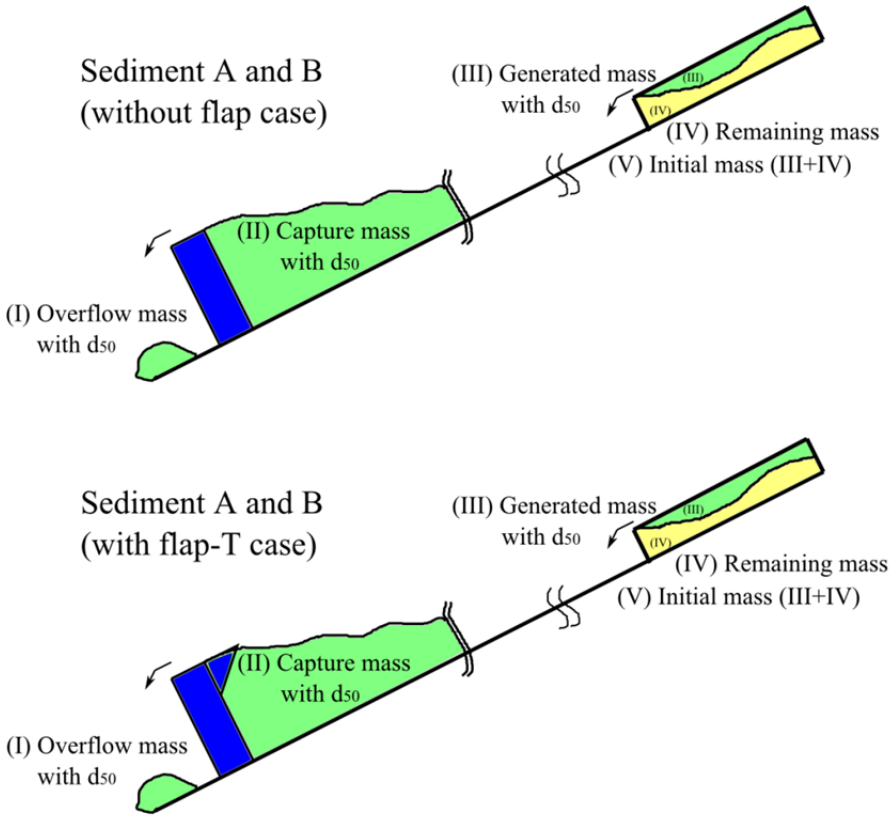

Figure 4.16 Experimental observations of the process and measurement techniques (not in scale)

without flap and with flap-T cases by summing up the captured (II) and overflow mass (I) of debris flow. The same collected mass was taken as a sample for the grain size distribution to find out D_{50} by sieve analysis method.

Table 4.7 and Table 4.8 compare the test results of the debris ration of mass with D_{50} (i.e. (III) generated, (I) overflow, and (II) captured) for two dams. Out of total 23 kg mass for generation of debris flow, the actual generation of debris flow as measured by summing of the captured and overflow debris flow mass was found to be 37.60 % of the total input sediments (i.e. 8.648 kg) for sediment A and 39.62 % of total input sediments (i.e. 9.114 kg) for sediment

Table 4.7 Results of the mass ratio of debris with D_{50} – Sediment A

	Without flap		*Flap-T*	
	Mass (kg)	*D_{50} (mm)*	*Mass (kg)*	*D_{50} (mm)*
Generated(III)	8.648	1.992	8.769	1.733
Overflow (I)	2.116	2.201	2.570	1.658
Captured (II)	6.532	1.931	6.119	1.789
CR1	-	(+) 10.5	-	(-) 4.3
CR2	-	(-) 3.1	-	(+)3.2
Remarks		+:increase in overflow d_{50} -: decrease in captured d_{50}		-: decrease in overflow d_{50} +: increase in captured d_{50}

CR1 = % change in overflow value with reference to generated value.

CR2 =% change in captured value with reference to generated value.

Table 4.8 Results of the mass ratio of debris with D_{50} – Sediment B

	Without flap		*Flap-T*	
	Mass (kg)	*D_{50} (mm)*	*Mass (kg)*	*D_{50} (mm)*
Generated(III)	9.114	2.857	8.269	2.707
Overflow (I)	1.245	3.330	1.397	2.853
Captured (II)	7.868	2.764	6.872	2.669
CR1	-	(+) 16.6	-	(+) 5.4
CR2	-	(-) 3.3	-	(-) 1.4
Remarks		+:increase in overflow d_{50} -: decrease in captured d_{50}		+:increase in overflow d_{50} -: decrease in captured d_{50}

CR1 = % change in overflow value with reference to generated value.

CR2 =% change in captured value with reference to generated value.

B for the dam without flap case. The results indicate that a similar quantity of debris flow was generated during the experiment. Similarly, for the flap-T type, the recorded values of actual generation of debris flow were 38.13 % and 35.95 % of the total input sediments for sediment A and sediment B cases, respectively. These results conclude that the experiments revealed very good reproducibility of the tests, supporting the results obtained by the applied generation method of debris flow.

Table 4.7 and Table 4.8 show the comparison of the median grain diameter in the case of the two dams (without flap and with flap-T) under two different sediment sizes. The results obtained by comparing the median grain diameters of generated, captured and overflowed debris with two different check dams (without flap and with flap-T) are summarized below:

(1) In the case of bed sediment A: for the dam with no flap structure, the median size of particles (d_{50}) of overflow debris mass increased by nearly 11 % compared to median grain size of the generated debris flow. But, in the case of the dam with flap-T, nearly 4 % decreases in median size were observed. These results conclude that the introduction of flap structure reduced the quantity of coarser particles in the overflowed debris flow mass whereas the dam without flap shows increase in coarser particles in the overflowed mass which is undesirable for the impact on the downstream. Also, for the dam with no flap structure, the median size of particles (d_{50}) of captured debris mass decreased by nearly 3 % compared to median grain size of the generated debris flow. But, in the case of the dam with flap-T, nearly 3 % increases in median size were observed. The decrease in captured median size of particles for the dam with no flap showed capturing finer particles and let the coarser particles through the overflow mass whereas increase in captured median grain diameter in the case of flap-T dam revealed capturing coarser particles and let the finer particles through the overflowed mass. In summary, the above results shows that the flap-T type is more efficient in capturing coarser particles of debris flow than the dam with no flap which reflects a very important characteristics and reason behind the introduction of flap structure.

(2) In the case of bed sediment B: for the dam with both no flap and with flap, the median size of particles (d_{50}) of overflow debris mass increased by nearly 17 % and 5 % compared to median grain size of the generated debris flow. Even though, in both cases, the increase in median grain diameters were observed but still we can conclude that the flap structure will let pass through less coarser particles as overflow mass than the dam with no flap case. It means that, still the flap structure is more efficient in capturing coarser particles. Also, for the dam with both no flap and with flap structure, the median size of particles (d_{50}) of captured debris mass

decreased by nearly 3 % and 1.5 % respectively compared to median grain size of the generated debris flow. Although, In both the cases, the decrease in median grain diameters were observed but the decrease in the value for the flap structure clearly shows that still the flap structure capture more coarser particles whereas the dam without flap structure captures more finer particles. In summary, the above results again show the supremacy of the dam with flap in comparison to dam without flap.

4.4.4 Vertical Distribution of Total Pressure

To estimate the safety of flap structure, the vertical distributions of total pressure for three dams under the two different bed sediments condition are investigated. Table 4.1 shows the experimental conditions and is taken as plan-1 for vertical distribution of total pressure.

Table 4.9 compares the test results on the average of maximum total pressure values by plan-1. Proposed closed dams are the extension of a typical dam with flap installed at the top. But, this might be vulnerable to accidental bumps due to the uplift pressure. In order to check the uplift pressure, sensor D was installed within the flap. The results obtained by comparing the total pressure and uplift pressure are summarized as below:

(1) In the case of sediment A: the uplift pressure of the flap-R dam has increased by nearly 3 times in comparison to other types. The reason for this increase is that the rectangular type has to absorb all of the uplift pressure directly while the flap-T type has more smooth control due to its shape and the typical type has no flap at all.

(2) In the case of sediment B: even if the main total pressures due to the impact collision are very similar by the value of sensor A, the values of uplift pressure for the flap-R type have increased by nearly 35 times in comparison to other types. So the flap-T type is still efficient in comparison to the flap-R type regarding uplift pressure. Therefore, the flap-T type can more

Table 4.9 Results of total pressure without outlier data (unit: kPa)

	Sediment A			*Sediment B*		
Sensor	Without	Flap-R	Flap-T	Without	Flap-R	Flap-T
A	20.014	22.880	16.090	19.850	17.614	19.397
B	6.478	5.764	9.749	11.985	11.317	7.728
C	3.003	3.891	4.128	4.704	4.055	6.596
D	2.689	7.645	2.611	3.120	17.199	0.492

effectively control the uplift pressure than the flap-R type due to generation of the reflected flow. Even if both flap types were shocked by the uplift pressure, it shows that the newly designed check dam with flap has the advantage of changing the dynamic pressure compared to the dam without flap due to generation of the reflected flow.

Figure 4.17 shows the trend line of vertical distribution of total pressure using the average of maximum values for the three dams (as shown in dotted line) and the trend line (as shown in black line) without the uplift pressure for both dams (i.e. flap-R and flap-T dams by the sensor D) are estimated by following relation:

$$x = Me^{Ny} \tag{4.8}$$

where x: total pressure, y: height of dam, and M and N are constant coefficients. The results obtained by comparing the trend line of vertical distributions are summarized below:

In the case of sediment A and B, all dam types show a similar trend of vertical distribution of total pressure. However, the flap-R dam shows two patterns regarding the vertical distribution of total pressure (i.e. the first pattern is decrease from bottom to below the flap part; the second pattern is rapid increase at the flap part due to the uplift pressure). This is because the flap-R type has to absorb all of the uplift pressure directly. So, it shows the effectiveness of adding the rectangular flap to the conventional dam. But the flap-T shows a similar trend to the dam without flap due to the fact that it has a smooth control of the pressure because of its shape. So, the pressure calculation while designing the sabo dam with flap-T does not require any different approach to that of the without flap dam but the flap-R does require a different approach for the consideration of uplift force.

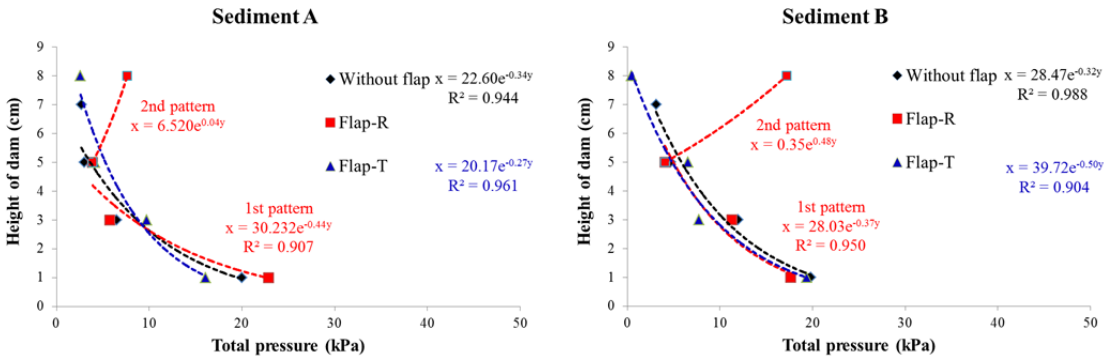

Figure 4.17 Vertical distribution of total pressure for three dams

4.4.5 Force Behaviour of Debris Flow

The force behaviour of debris flow can be classified into three stages. The maximum total pressure will occur due to the impact force (by the collision) when debris flow just reaches the sabo dam at first. Secondly, both the dynamic and static applying condition will occur due to moving debris flow. Finally, the static applying condition will occur due to the static pressure when debris flow is deposited on the front of the sabo dam. Photo 4.7 as the case of the flap-R dam shows the movement of debris flow due to the main forces for each stage condition.

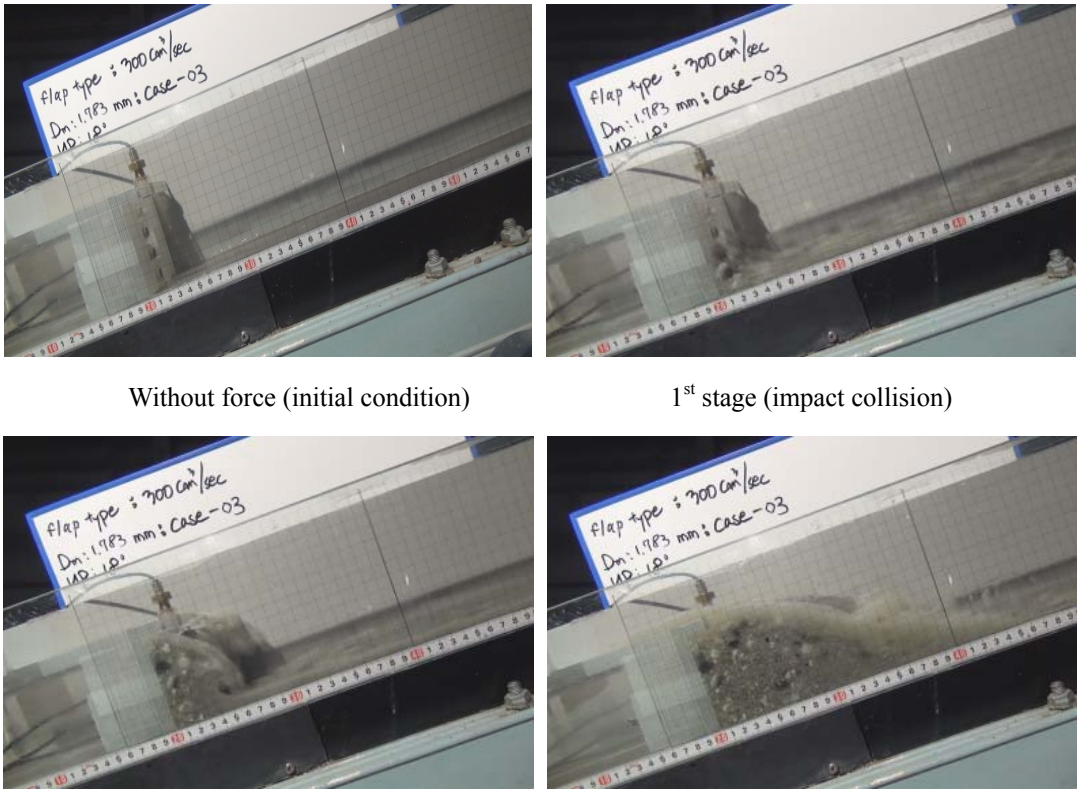

Without force (initial condition) — 1st stage (impact collision)

2nd stage (dynamic and static) — 3rd stage (static)

Photo 4.7 Movement of debris flow due to main forces with bed sediment B (Flap-R dam)

Figure 4.18 shows the variation of total pressure due to the main applying force with time. The debris flow in front of the dams became strongly turbulent due to the impact (1st stage), dynamic (2nd stage) and static (3rd stage) forces that are shown by the sharp increase in the value in the graph shown in the figure. After the debris flow stopped, the static pressure was the main force since the debris mass has deposited in front of the dams and the depth of water has increased.

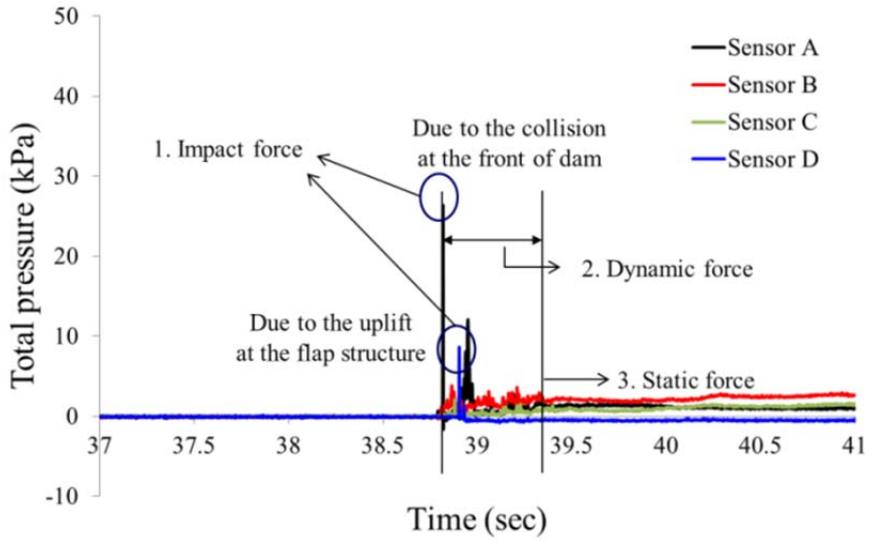

Figure 4.18 Variation of total pressure due to the main forces with bed sediment B

4.4.6 Impact Pressure and Velocity

To clarify the impact pressure due to the impact collision, parameters such as total pressure, approaching velocity and depth are observed during experiment. In the experiments, the data were obtained from the 10 times repeated experiments under the same hydraulic conditions with plan-2 (Table 4.1 shows the experimental conditions).

Since plan-2 consists of sensor installation at the bottom part only, the results are extraneous as to dam shape but the values are directly connected to the bed sediments.

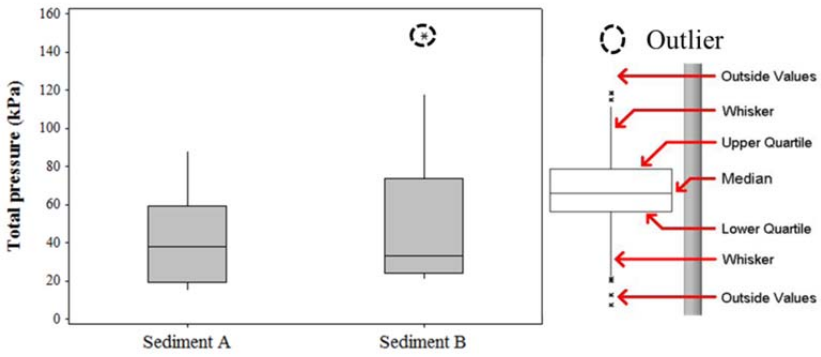

*lower quartile: split lowest 25% of data (= 25th percentile)

*upper quartile: splits highest 25% of data, or lowest 75% (=75th percentile)

Figure 4.19 Results of the boxplot under the two bed sediments

Therefore, this experiment can obtain four values of the total pressure per one case and averages of the maximum values observed are used for the data analysis. Also, the box plot method of data analysis is performed as shown in Figure 4.19.

Table 4.10 shows the test results for the averaged total pressure and surface velocity of debris flow under the two bed sediments. It shows that there are almost similar values of the average total pressures and velocities in the case of both bed sediments. However, in the case of bed sediment B, the maximum total pressure value has increased by nearly 1.3 times and Q1 (lower quartile) and Q3 (upper quartile) values have also increased by 1.2 times in comparison to sediment A. This should not be ignored. The reason for this increase is that the amount of large particles in the composition of sediment B is more than that of sediment A and maximum pressure is the result of sudden impact by the large particles. From this result, it is concluded that the maximum total pressure generated by debris flow is not proportional to the amount of debris flow, but strongly depends on the particle size distribution of debris flow. In addition, the results reveal that the colliding total pressure is different in all three types of dam although all the influencing parameters as described by Hu et al. (2011) such as generation pattern, initial sediment size, properties and volume, impact angle etc. are similar. The reason for this is due to the contact area of the sediment particles with the sensor. So the contact area of the different particles should be one of the important parameters when deciding impact pressure on the dam.

Table 4.10 Results of the total pressure and surface velocity

	Sediment A		*Sediment B*	
	Total pressure (kPa)	Surface velocity (m/sec)	Total pressure (kPa)	Surface velocity (m/sec)
Q1	19.176	1.151	23.940	1.130
Median	37.621	1.231	33.011	1.231
Q3	59.136	1.272	73.477	1.338
IQ range	39.961	0.120	49.538	0.208
Average	42.415	1.218	43.512	1.244
Max	88.255	1.333	117.644	1.548

*Q1: Lower quartile

*Q3: Upper quartile

*IQ Range: Range of Q1~Q3

4.4.7 Impact Model of Debris Flow

Pressure is the force on an object that is spread over a surface area. The equation for pressure is the force divided by the area where the force is applied. Although this measurement is straightforward when a solid is pushing on a solid, the case of a solid pushing on a liquid or gas requires that the fluid be confined in a container. The force can also be created by the weight of an object. When we apply a force to a solid object, the pressure is defined as the applied force divided by the area of application. The equation for pressure is:

$$P = \frac{F}{A} \tag{4.9}$$

where P = the total pressure, F = the applied force, and A = the surface area where the force is applied. In this experiment, the total pressure from debris flow was measured by the dynamic pressure sensor. To calculate the applied force (i.e. impact force due to the collision) by Eq. (4.9), we have to estimate the actual contact area. But it is very difficult to obtain the actual contact area. So, in this study, the sensor area is considered as the actual contact area (A = 0.2826 cm^2). Likewise, Scheidl et al. (2012) also estimated the peak forces by multiplying measured pressure by the sensor contact area. To calculate the force of debris flow by Eqs. (4.3) and (4.5), various parameters such as the density of debris flow, the approaching surface velocity of debris flow, the flow depth, the discharge of debris flow, and the radius of the boulder are required. The approaching surface velocity of debris flow is obtained from the experiments by measurement from the high-speed camera. However, the flow depth is taken as average of 10 values of measurement of flow depth (= 2.0 cm), the radius of the boulder is obtained from the value of d_{max} from particle size distribution curves of gravel, and the discharge of debris flow was calculated from the channel geometry, approaching surface velocity, and depth of debris flow. Since the exact size of the colliding particles of debris flow (since it consists of variety of particle sizes) changes with time and the debris flow is accumulated with the large boulders at the front part of the flow, so for simplicity the maximum size of the particle is adopted for the calculations (i.e. 0.5 cm for sediment A and 0.6 cm for sediment B, refer Table 4.4). Finally, the density of debris flow is very difficult to measure in the flow through the experiment. So, the density of debris flow is calculated using an equilibrium sediment concentration equation. The equilibrium sediment concentration (Eq. 4.10) and the mixture density of debris flow (Eq. 4.11) are described as follows: According to Nakagawa et al. 2003, if a stony debris flow occurs ($\tan\theta_w > 0.138$), then

$$C_{\infty} = \frac{\rho \tan\theta_w}{(\sigma/\rho - 1)(\tan\phi - \tan\theta_w)} \tag{4.10}$$

$$\rho_d = \sigma C + \rho(1 - C) \tag{4.11}$$

where ρ = the density of water, θ_w = the water surface slope, σ = the density of sediment particle, ϕ = the internal friction angle of the sediment, ρ_d = the mixture density of debris flow, and C = the sediment concentration of debris flow. The equilibrium sediment concentration is taken as 1.866 g/cm^3 calculated by Eq. (4.10) using the value of the density of sediment particles and water as 2.65 and 1 g/cm^3, respectively. The water surface slope is taken as 18º equivalent to the flume slope, and the angle of internal friction of the sediment is assumed as 35º. The results of impact force calculated using equations (4.3), (4.5) and (4.9) are shown in Table 4.11. This table shows the calculated applied force (i.e. due to the impact collision) of debris flow with different impact models for bed sediments A and B. The parameters of the equations are measured from the experiments under the same hydraulic conditions with plan-2 performing experiment 10 times. The maximum, minimum and average values for equations (4.3) and (4.5) in the table means the impact force is calculated using maximum, minimum and average flow velocities in 10 experiments while for equation (4.9) those values are calculated using maximum, minimum and average measured total pressure.

Furthermore, Table 12 shows a comparison of the empirical coefficients (i.e. pressure and force) used in both hydrodynamic and solid collision models with the experimentally obtained value from this study. The result shows the new range of values regarding the use of the equations of both models (i.e. hydrodynamic and solid collision model). The result from the experiment reveals that the values of k_p (i.e. coefficient of impact pressure) as proposed by other researchers are relatively smaller for the hydrodynamic model, but the values of k_f (i.e.

Table 4.11 Results of the impact force with three theory (unit: N)

	Sediment A			*Sediment B*		
	Eq. (4.3)	Eq. (4.5)	Eq. (4.9)	Eq. (4.3)	Eq. (4.5)	Eq. (4.9)
Max.	6.632	1.701	2.494	8.944	2.931	3.325
Min.	4.649	1.375	0.425	3.891	1.779	0.591
Avg.	5.560	1.528	1.199	5.860	2.259	1.230
Parameters	ρ_d, v, Q	v, R	A	ρ_d, v, Q	v, R	A

coefficient of impact force) as proposed by other researchers are comparatively higher for both the hydrodynamic and solid collision models.

Table 4.12 Comparison of empirical coefficients

Empirical coefficient			*Sediment A*	*Sediment B*
Hydrodynamic model	k_p by Eq. (4.2)	In this study	0.1~0.2	0.1~0.2
		Bugnion et al. (2001)	0.4~0.8	
	k_f by Eq. (4.3)	In this study	5.5* (1.9~11.8)	6.5* (1.8~12.6)
		Yamamoto et al. (1998)	1.0	
Solid collision model	k_f by Eq. (4.5)	In this study	1.8* (0.6~4.0)	2.5* (0.7~4.4)
		Mizuyama (1979)	1.0	

( ): Range value from experimental data

*: Average value

4.5 Summary

In all the experiments, the effects of sabo structures, with emphasis in the sabo dams, the parameters such as the flow pattern, the surface velocity between the debris flow and clear water, the total pressure and the uplift pressure, mass ratio of debris, and median grain diameter were measured to compare the function of each sabo dam under the two different bed sediments. The empirical coefficients of the hydrodynamic and solid collision models are also determined and compared with available values of those coefficients. Furthermore, the characteristic of debris flow and proposed dams are confirmed due to the experiments. The experimental data analyses lead to the following conclusions:

1. From the experimental results, although the flow pattern and the approaching velocity are very similar, the total pressure is entirely different in both flow cases. This is due to the fact that the debris flow has high energy in the front part of the flow, more than clear fluid flow because of large boulders accumulation at the front.

2. The proposed closed-type sabo dams with flap structure can reduce the quantity of spray transportation more efficiently than the dam without flap (i.e. typical type).

3. Flap-T type (triangle type) can control the uplift pressure more effectively than flap-R type (rectangular type) due to the generated reflected flow and is more efficient to capture large debris mass than the dam without flap (i.e. typical type). Even if both flap types were shocked by the uplift pressure, it was shown that the newly designed check dam with flap has the advantage of changing the dynamic pressure compared to the dam without flap due to reflection. Moreover, the triangular flap shows a similar trend like the dam without flap because it has smooth control of the pressure due to its shape. So, the pressure calculation while designing the sabo dam with flap-T does not require any different approach to that of the without flap dam but the flap-R does require a different approach for the consideration of uplift force. Therefore, the triangular flap structure is more suitable than the rectangular shape for actual application.

4. The results of mass ratio of debris indicate that the similar quantity of debris flow was generated during the experiment. For the dams of without flap and with flap-T, the recorded values of the actual generation of debris flow were 38 % for sediment A and sediment B cases, respectively. From this result, it is concluded that the experiments revealed very good reproducibility of the tests, giving confidence in the results obtained by the applied generation method of debris flow.

5. From the results of the median grain diameter, it is concluded that, in the case of sediment A for the dam with no flap structure, the median size of particles (d_{50}) of overflow debris mass increased by nearly 11 % compared to median grain size of the generated debris flow. But, for the dam with flap-T, nearly 4 % decreases in median size were observed. These results reveal that the introduction of flap structure reduced the quantity of coarser particles in the overflowed debris flow mass whereas the dam without flap shows increase in coarser particles in the overflowed mass which is undesirable for the impact on the downstream. Therefore the flap-T type is more efficient in capturing coarser particles of debris flow than the dam with no flap which reflects a very important characteristics and reason behind the introduction of flap structure.

6. The force behaviour of debris flow can be classified into the three steps due to the main applied force (i.e. impact force, dynamic and static force, and static force).

7. The empirical coefficients were estimated by the hydrodynamic and the solid collision models from the experimental results. The result from the experiment reveals that the values of k_p (i.e. coefficient of impact pressure) as proposed by other researchers are

relatively smaller value for the hydrodynamic model but the value of k_f (i.e. coefficient of impact force) is comparatively higher for both the hydrodynamic and solid collision models.

8. The maximum of total pressure generated by debris flow is not proportional to the amount of debris flow, but depends strongly on the particle size distribution of debris flow. Besides, the contact area of the different particles should be one of the important parameters when deciding impact pressure to the dam.

This study was carried out with the stony debris flow, but the case of mud debris flow proves equally applicable. The reason is that the mud debris flow is easy to generate and does not consist of larger particles compared to the stony debris flow. Also, the flap structure should build monolithically with main dam structure to correlate this research results.

References

1) Armanini A. 1997, On the dynamic impact of debris flows. *In: Armanini A, Masanori M (eds) Recent developments on debris flows,* lecture notes in earth sciences, Springer, Berlin, pp. 208-226.
2) Bugnion L., McArdell B.W., Bartelt P., and Wendeler C., 2011, Measurements of hillslope debris flow impact pressure on obstacles. *Landsildes (2012)* 9, pp. 179-187.
3) Canelli L., Ferrero A.M., Migliazza M., and Segalini A. 2012, Debris flow risk mitigation by the means of rigid and flexible barriers-experimental tests and impact analysis. *Nat. Hazards Earth Syst. Sci.,* 12, pp. 1693-1699.
4) Hu K., Wei F., and Li Y. 2011, Real-time measurement and preliminary analysis of debris-flow impact force at Jiangjia ravine, China. *Earth Surface Process and Landforms* 36, pp. 1268-1278.
5) Huang H.P., Yang K.C., and Lai S.W. 2007, Impact force of debris flow on filter dam. *Geophysical Research European Geosciences Union,* Vol. 9, 03218.
6) Hübl J., Suda J., Proske D., Kaitna R., and Scheidl C. 2009, Debris flow impact estimation. *In: Popovska C, Jovanovski M (eds) Eleventh international symposium on water management and hydraulic Engineering,* Vol. 1, pp. 137-148.
7) Hungr O., Morgan G.C., and Kellerhals R. 1984, Quantitative analysis of debris torrent hazards for design of remedial measures. *Canadian Geotech. J.,* 21, pp. 663-677.
8) Itoh T., Horiuchi S., Akanuma J.I., Kaitsuka K., Kuraoka S., Morita T., Sugiyama M., and Mizuyama T. 2011, Fundamental hydraulic flume tests focused on sediment control function using a grid-type high dam. *Italian Journal of Engineering Geology and Environment,* B-114, pp. 1051-1061.
9) Kamikabo Y., Murakami K., Irie I., and Hamasaki Y., 2002, Transportation of water spray on non-wave overtopping type seawall, *International Offshore and Polar Engineering Conference Kitakyushu, Japan,* May 26–31.
10) Kim Y., Nakagawa H., Kawaike K., and Zhang H. 2012, An experimental study on impact force for verification of 3D debris flow model. *31st Japan Society for Natural Disaster Science annual meeting*, pp.159-160.
11) Kim Y., Nakagawa H., Kawaike K., and Zhang H. 2013a, Study on the function of closed-type sabo dam with a flap by debris flow. *12th international Symposium on River Sedimentation, ISRS2013.* (In printing)
12) Kim Y., Nakagawa H., Kawaike K. and Zhang H. 2013b, Study on characteristic analysis of closed-type sabo dam with a flap due to dynamic force of debris flow. *Annuals of the Disaster Prevention Research Institute, Kyoto University,* No. 56 B. (In printing)
13) Kim, Y., Nakagawa, H., Kawaike, K., and Zhang, H. 2013c, Study on impact force of debris flow due to variable of check dam shape. *Journal of Disaster Research,* Vol.8, No.1, pp.195-196.
14) Larsen M.C., Wieczorek G.G., Eaton L.S., and Torres-Sierra H. 2001, The rainfall-triggered landslide and flash flood disaster in northern Venezuela, December 1999. *Proceedings of the Seventh Federal Interagency Sedimentation Conference,* pp. IV9-16.
15) Mizuyama T. 1979, Computational method and some considerations on impulsive force of debris flow acting on sabo dams. *Journal of the Japan Society of Erosion Control Engineering,* 112, pp. 40-43 (in Japanese)
16) Murakami K., Irie I., and Kamikubo Y., 1996, Experiments on a non-wave overtopping Type Seawall, *Proc. 24th Int. Conf. Coastal. Eng., ASCE,* pp.1840-1851.
17) Lichtenhahn C. 1973, Die Berechnung von Sperren in Beton und Eisenbeton. *In: Kolloquium über Wildbachsperren, Mitteilungen der Forstlichen Bundesanstalt Wien,* Vol. 102, pp. 91-127.

18) Nakagawa H., Satofuka Y., and Kawaike K. 2003, Numerical simulation of sediment disasters caused by heavy rainfall in camuri Grande basin, Venezuela 1999. *Proceedings of the third conference on Debris-flow Hazards Mitigation: Mechanics,* Prediction and Assessment, Switzerland Rotterdam, pp. 671-682.
19) Nishimoto H. 2011, Discussion on the transition of idea about sediment control effect functioned by check dam. *Journal of the Japan Society of Erosion Control Engineering,* Vol.64, No.4, pp. 46-51. (in Japanese with English Abstract)
20) Okuda S, Suwa H, Okunishi K, Yokoyama K, Nakano M, Ogawa K, and Hamana S. 1978, Synthetic observation on debris flow (part 4) observation in 1977, *Disaster Prevention Research Institute Annals 21,* Vol. 1, pp. 277-296 (in Japanese with English synopsis).
21) Pierson T.C. 1986, Flow behavior of channelized debris flows, Mount St. Helens, Washington. *In: A. D. Abrahams (ed.),* Hillslope Processes, pp. 269-296 (Allen & Unwin, Boston).
22) Scheidl C., Chiari M., Kaitna R., Müllegger M., Karawtschuk A., Zimmermann T., and Proske D. 2012, Analysisng Debris-Flow Impact Models, Based on a Small Scale Modelling Approach. *Surv Geophys (2013) 34,* pp. 121-140.
23) Scotton P., and Deganutti A. 1997, Phreatic line and dynamic impact in laboratory debris flow experiments. *In: Chen C (ed) Proceedings of the 1st. international conference on debris-flow hazards mitigation: mechanics,* prediction and assessment, American Society of Civil Engineers, New York, pp. 777- 786.
24) Shibuya H., Katsuki S., KokuryoH., Ohsumi H., and Ishikawa N. 2012, Experimental study of load for steel frame check dam caused by debris flow with woody debris. *Journal of the Japan Society of Erosion Control Engineering,* Vol. 65, No. 1, pp. 54-61 (in Japanese with English Abstract)
25) Shieh C.L., Ting C.H., and Pan H.W. 2008, Impulsive force of debris flow on a curved dam. *International Journal of Sediment Research 23,* pp. 149-158.
26) Suwa H., and Okuda S. 1983, Deposition of debris flow on a fan surface, Mt. Yakedake, *Japan. Z. Geo-morph,* Vol. 46, pp. 79-101.
27) Varnes D.J, 1984, Landslide hazard zonation: a review of principles and practice. *Commission of Landslides of the IAEG, UNESCO, Natural Hazards* No. 3, pp. 61.
28) Watanabe M., and Ikeya H. 1981, Investigation and analysis of volcanic mud flows on Mt Sakurajima, Japan. *Erosion and Sediment Transport Measurement (Proceedings of the Florence Symposium). IAHS Publ.* No. 133, pp. 245-256.
29) Yamamoto A., Yamamoto S., Toriihara M., and Hirama K. 1998, Impact Load on Sabo Dam due to Debris flow. *Journal of the Japan Society of Erosion Control Engineering,* Vo1. 51, No. 2, pp. 22-30. (in Japanese with English Abstract)
30) Zhang S. 1993, A Comprehensive Approach to the Observation and Prevention of Debris flow in China. *Natural Hazards 7,* pp. 1-23.

CHAPTER 5

GENERAL CONCLUSIONS AND RECOMMENDATIONS

5.1 General

Sediment-related disasters caused by localized torrential downpours, earthquakes, volcanic eruptions, and so on occur frequently every year, and they account for nearly half of the total human casualties from natural disasters. A sediment disaster is not as large as an earthquake, flood, storm surge or tsunami, but its threat to human lives is very high because it can occur in multiple locations simultaneously. Therefore, it is important to mitigate damage by establishing effective structural and non-structural measures.

In this study, the most effective and available methods to reduce sediment-related disasters caused by a debris flow were investigated using numerical simulation and experimental approaches. First, as the existing structure (debris-flow breaker), a numerical model was developed to simulate the debris-flow breaker. In addition, to clarify the hydrodynamic characteristics of debris-flow breakers where erosion and deposition coexists which has not been defined by existing research, the interaction considering the change in pore water pressure was conducted by both the experimental and numerical simulation. Second, as the new type of sabo dams, a closed-type sabo dam with a flap structure is proposed to clarify the characteristics of proposed dams in comparison with the typical dam as well as reveal their functions. The conclusions based on the studied cases are to be interpreted within this context. These conclusions are summarized in the following section. The final section gives some recommendations for implementation and future research.

5.2 Conclusions

The results of the present study have been extensively assessed and have been discussed in the previous chapters. In the following, the most important conclusions are summarized.

5.2.1 Debris-Flow Breaker

The main function of a debris-flow breaker is effectively stopping the front part of a debris flow. These structures have the advantage not only to dampen the energy of the frontal part of a debris flow, but also to create a suitable narrow or wider area, cost-efficient, simply designed, easily repaired, and maintained structure. Likewise, these structures have many features. However, the mechanism of the debris-flow breaker has not been explained. Therefore, in this research, fundamental experiments and numerical simulations were conducted to investigate the mechanism of the debris-flow breaker.

To judge the optimal parameters of the debris-flow breaker, the understanding of the behavior and mechanisms of the debris flow were needed. Since the characteristics of debris flows would be changed due to the geographic environment of the occurrence area and various contributing factors, but for the current study, the mechanism between the opening size and blocking size (an influencing physical factor) under the different bed sediments were analyzed to understand clearly the hydraulic characteristics of the debris-flow breaker.

The experiments were carried out in the fixed bed condition, in which the debris flow depositions (due to the change in pore water pressure at the debris-flow breaker) were analyzed. In all the experiments, the configurations of a debris-flow breaker, with emphasis on the permeability dam types, and the parameters, such as the flow pattern (formation process) between the bed slopes of the flood basin, thickness of debris, total and sediment discharges, and sediment concentration were measured to compare the function of each condition of the breaker, and the phenomena of the separation flow on the debris-flow breaker under the three different bed sediments were analyzed as well.

To clarify the hydraulic characteristics of debris flows on the debris-flow breaker, a numerical simulation for debris-flow breaker was developed and analyzed the mechanism and interaction between the opening and blocking areas. The simulated results of the outflow discharge, sediment concentration, travel length, and deposit thickness are in good agreement with the experimental results. In addition, the ranges of the debris-flow breaker parameters such as opening and blocking sizes for the design of structural elements of debris-flow breaker are

evaluated.

5.2.2 Closed-Type Sabo Dam with a Flap

The objectives of this study are to analyze the working principle of the proposed closed-type dams with a flap over dams without a flap, to propose the best suitable type based on their characteristics, and to determine the empirical coefficients of the hydrodynamic and solid collision model. Three types of closed-type dams were tested experimentally for the debris flow case and only two types (without and with flap-R structures) were considered for the upstream dam-break case with clear water. Experiments were conducted to investigate the total pressure (combination of impact due to the collision, static, and dynamic pressures) of both flows under the conditions of typical closed-type dams and those with a flap. Furthermore, observations of the load behavior of debris flows, the velocity, the average of the maximum total pressures, the uplift pressure due to the impact collision, the vertical distribution of the total pressure on the dams and the ability of the proposed dam to sustain such forces, were also discussed.

From the experimental results, although the flow pattern and the approaching velocity were very similar, the total pressure was entirely different in both flow cases. This is due to the debris flow having a higher energy in the front part of the flow, with more than clear fluid in the flow because of large boulders accumulating at the front. The proposed closed-type sabo dams with a flap structure can reduce the quantity of spray transportation more efficiently than the dam without a flap (typical type). Flap-T types (triangle type) can control the uplift pressure more effectively than flap-R types (rectangular type) due to the generated reflected flow and are more efficient at capturing large coarser particles than the dams without a flap (typical type). Moreover, the flap-T type shows a trend similar to the dam without a flap because it has smooth control of the pressure due to its shape. Thus, the pressure calculation while designing the sabo dam with a flap-T does not require any different approach than that without a flap, but the flap-R does require a different approach for the consideration of uplift force. Therefore, the triangular flap structure is more suitable than the rectangular shape for actual application. Furthermore, the force behavior of debris flows can be classified into the three steps due to the main applied force (impact force, dynamic and static force, and static force), and the empirical coefficients were estimated by the hydrodynamic and the solid collision models from the experimental results. The proposed dam can be used to investigate the preventive measures of debris flow disasters by combining structural and non-structural countermeasures.

5.3 Recommendations for Future researches

Future work is required to improve the performance of the model. The recommendations for future researches are discussed as follows:

1. The verification and calibration of the numerical models are of crucial importance before the models can be used to solve problems in actual fields. In the dissertation, the main function of the models has been verified within a limited field and laboratory data. More verifications and calibrations are suggested, including: (a) Verification of the debris flow model with the debris-flow breaker; (b) Verification of the 3-D morphological model with both passage of a fine fraction of deposited sediments and outflow discharge from the pore of the debris-flow breaker; and (c) Verification of the deposition process with separation at the debris-flow breaker.

2. Although the proposed model of the debris-flow breaker is duly verified with the experimental results. But the application of the model to real field cases needs to be conducted to examine the applicability of this model. It is also necessary to investigate the effectiveness of proposed sabo dams for debris flow control in a river basin scale.

3. A two-dimensional numerical model of debris flow was developed with the combination of two boundary conditions (surface and bottom boundary on the bed and on the debris-flow breaker). In particular, in this study, type-QS was used for debris flow generation. The experimental event of debris flow will be finished in a short time due to the generation method of type-QS. However, the reality of the situation is that the events of debris flows have continuous flow conditions. Therefore, it is also necessary to check the applicability of the model with actual field cases. Thus, in the present study, the similarity of the debris flow to the actual one is not considered, which will be necessary to investigate.

4. The simulated value seems to exceed the experimental value for most of the cases of the debris-flow breaker model. This is due to the fact that the simulations were not considering the passage of a fine fraction of deposited sediments from the pore of the debris-flow breaker. Therefore, by considering the effect of the passage of a fine fraction of deposited sediments, we can get better results than the current results. So, the model should be modified considering separation at debris-flow breaker.

5. In this study for the analysis of functions of debris flow breaker, the static change in pore water pressure was considered for simplicity but the dynamic nature of pore water pressure should also be considered for future studies.

6. From the experimental and numerical results, the relationships of the reduction rates were estimated by several parameters, but these relationships are limited for the experimental conditions and few diverse conditions only. Therefore, it is necessary to develop more diverse conditions to refine the suggested parameters of the debris-flow breakers for realistic analysis.

7. Proposed new type sabo dam with a flap, in the experiments for calibration of the sensor were conducted in comparison with hydrostatic pressure only although the company claims the instrument is well suited for dynamic case, but actual debris flows are a dynamic flow condition and need to be verified. In addition, the sensor needs to be calibrated for various sediment particles because of the nature of debris flows i.e., it is composed of various sediment particles.

8. In addition, the flap structure, in this study, is treated as monolithic with the main dam structure and the results are found with this assumption, but there will be the possibility to perform more studies without considering monolithic assumptions between the flaps and the main dam body.

9. Although the present studies mainly focused on only one proposed sabo dam with flap structure but future researches should be performed on series of such dams to analyses the hydraulic phenomena associated with the new arrangement. In the real world also only one sabo dam is not sufficient or more than one sabo dam is installed in most vulnerable areas. The new analysis for series of dam and the associated numerical model will be good new research topics for future researchers.

10. The three-dimensional numerical calculation is still very difficult since the mechanism of debris flow is very complex in comparison with the clear fluid due to the composition of various particle sizes and water. Till now, many researchers used the depth-averaged models. In order to establish more effectively the structural measures to mitigate the sediment-related disasters, it will require the development of a 3-D numerical model.

List of Figures

Figure 1.1	Number of sediment-related disasters (Data source: MLIT, Japan)	6
Figure 1.2	Death toll due to sediment-related disasters (Data source: MLIT, Japan)	6
Figure 1.3	Functions of a sabo dam	12
Figure 1.4	Warning and evacuation system (MLIT, Japan)	13
Figure 1.5	Designation of hazard areas and preventive measures (MLIT, Japan)	14
Figure 2.1	Sketch of experimental setup	33
Figure 2.2	Definition of breaker properties	36
Figure 2.3	Particle size distributions of silica sands and gravels	37
Figure 2.4	Particle size distributions of bed sediments	38
Figure 2.5	Observation points on the debris-flow breaker	40
Figure 2.6	Measurement of deposition thickness	41
Figure 2.7	Temporal changes of shapes and thicknesses of a debris flow at 5º flood basin slope	42
Figure 2.8	Temporal changes of shapes and thicknesses of a debris flow at 7º flood basin slope	42
Figure 2.9	Final stage of shape and thickness of a debris-flow at breaker	43
Figure 2.10	Results of diffusion debris under the two bed slopes	44
Figure 2.11	Movement of debris flow due to the separation (Case1-0.4-B)	45
Figure 2.12	Movement of debris flow (Case0-0.0-A)	46
Figure 2.13	Movement of debris flow (Case0-0.0-B)	47
Figure 2.14	Movement of debris flow (Case0-0.0-C)	47
Figure 2.15	Movement of debris flow (Case1-0.2-A)	48

Figure 2.16 Movement of debris flow (Case1-0.2-B) 49

Figure 2.17 Movement of debris flow (Case1-0.2-C) 49

Figure 2.18 Movement of debris flow (Case1-0.4-A) 50

Figure 2.19 Movement of debris flow (Case1-0.4-B) 51

Figure 2.20 Movement of debris flow (Case1-0.4-C) 51

Figure 2.21 Movement of debris flow (Case1-0.6-A) 52

Figure 2.22 Movement of debris flow (Case1-0.6-B) 53

Figure 2.23 Movement of debris flow (Case1-0.6-C) 53

Figure 2.24 Movement of debris flow (Case3-0.2-A) 54

Figure 2.25 Movement of debris flow (Case3-0.2-B) 54

Figure 2.26 Movement of debris flow (Case3-0.2-C) 54

Figure 2.27 Movement of debris flow (Case3-0.4-A) 55

Figure 2.28 Movement of debris flow (Case3-0.4-B) 55

Figure 2.29 Movement of debris flow (Case3-0.4-C) 55

Figure 2.30 Movement of debris flow (Case3-0.6-A) 56

Figure 2.31 Movement of debris flow (Case3-0.6-B) 56

Figure 2.32 Movement of debris flow (Case3-0.6-C) 56

Figure 2.33 Movement of debris flow (Case6-0.2-A) 57

Figure 2.34 Movement of debris flow (Case6-0.2-B) 57

Figure 2.35 Movement of debris flow (Case6-0.2-C) 57

Figure 2.36 Movement of debris flow (Case6-0.4-A) 58

Figure 2.37 Movement of debris flow (Case6-0.4-B) 58

Figure 2.38 Movement of debris flow (Case6-0.4-C) 58

Figure 2.39 Movement of debris flow (Case6-0.6-A) 59

Figure 2.40	Movement of debris flow (Case6-0.6-B)	59
Figure 2.41	Movement of debris flow (Case6-0.6-C)	59
Figure 2.42	Results of deposition at the upstream in both cases	60
Figure 2.43	Results of the travel length under the three bed sediments	61
Figure 2.44	Flow and sediment discharges, and sediment concentration	63
Figure 3.1	Sketch of pore water pressure distribution on the debris-flow breaker	69
Figure 3.2	Compare to travel length and γ coefficient	72
Figure 3.3	Variation of γ coefficient (in the case of sediment B)	72
Figure 3.4	Coordinate of two-dimensional uniform debris flow	77
Figure 3.5	Arrangement of variables on meshes	82
Figure 3.6	Arrangement of variables and the way of advancing the calculation	83
Figure 3.7	Flowchart of numerical analysis method	88
Figure 3.8	Calculated and measured hydrographs at the downstream end of flume for bed sediment A,B, and C	89
Figure 3.9	Numerical results of the movement of debris flow (Case0-0.0-A)	90
Figure 3.10	Numerical results of the movement of debris flow (Case0-0.0-B)	91
Figure 3.11	Numerical results of the movement of debris flow (Case0-0.0-C)	92
Figure 3.12	Numerical results of the deposit formation at final stage with sediment A	93
Figure 3.13	Numerical results of the deposit formation at final stage with sediment B	94
Figure 3.14	Numerical results of the deposit formation at final stage with sediment C	95
Figure 3.15	Numerical results of deposit thickness for sediment A	96
Figure 3.16	Numerical results of deposit thickness for sediment B	97
Figure 3.17	Numerical results of deposit thickness for sediment C	98

Figure 3.18	Calculated and measured hydrographs at the upstream end of flume for bed sediment A	99
Figure 3.19	Calculated and measured hydrographs at the upstream end of flume for bed sediment B	100
Figure 3.20	Calculated and measured hydrographs at the upstream end of flume for bed sediment C	100
Figure 3.21	Results of γ coefficients with previous and suggested	101
Figure 3.22	Experimental and simulation results of the maximum travel length with both coefficients	103
Figure 3.23	Comparison of deposit thicknesses for sediment A	105
Figure 3.24	Comparison of deposit thicknesses for sediment B	106
Figure 3.25	Comparison of deposit thicknesses for sediment C	107
Figure 3.26	Correlation coefficients of deposit thickness	108
Figure 3.27	Calculated and measured deposit formation at the debris-flow breaker for bed sediment A, B, and C (final stage)	109
Figure 3.28	Comparisons of reduction values of travel length	112
Figure 3.29	(I) Relationship of reductions rate for $\sum l_0$ / *width of breaker*	113
Figure 3.30	(II) Relationship of reductions rate for $\sum l_0 / d_{95}$	113
Figure 4.1	Typical feature of a debris flow longitudinal section	120
Figure 4.2	Sketch of a sabo dams	121
Figure 4.3	Conceptual sketch of the Flaring Shaped Seawall (FSS)	122
Figure 4.4	Sketch of experiment setup for upstream dam-break	127
Figure 4.5	Sketch of experiment setup for debris flow	129
Figure 4.6	Sketch of diagram of three closed dams	130

Figure 4.7	Installation of dam	131
Figure 4.8	Particle size distribution curve	132
Figure 4.9	Measuring system and typical calibration curve	135
Figure 4.10	Results of the total pressure due to clear water and debris flow	137
Figure 4.11	Results of the flow pattern for two different type dams due to clear flow	138
Figure 4.12	Results of the flow pattern for two different type dams due to debris flow	139
Figure 4.13	Movement of debris flow at different time step: sediment A for dam without flap	141
Figure 4.14	Movement of debris flow at different time step: sediment A for dam with flap-R	142
Figure 4.15	Movement of debris flow at different time step: sediment A for dam with flap-T	143
Figure 4.16	Experimental observations of the process and measurement techniques (not in scale)	144
Figure 4.17	Vertical distribution of total pressure for three dams	148
Figure 4.18	Variation of total pressure due to the main forces with bed sediment B	150
Figure 4.19	Results of the boxplot under the two bed sediments	150

List of Photos

Photo 1.1	Debris flow event in Caraballeda, Venezuela	2
Photo 1.2	Slope failure event in Minamata, Kumamoto prefecture, Japan	3
Photo 1.3	Deep-seated Landslide event in Mt. Akatani, Nara prefecture, Japan	3
Photo 1.4	Types of debris flow	4
Photo 1.5	Debris flow disaster event at Mt. Umeyon in downtown Seoul	5
Photo 1.6	Effectiveness of sabo structure	8
Photo 1.7	Closed dam	9
Photo 1.8	Slit dam (open type) at Mt. Fuji, Japan	10
Photo 1.9	Grid (permeable structure) dams	10
Photo 1.10	Drain-off structure	11
Photo 1.11	Series of sabo dams (Combination type)	11
Photo 2.1	Debris-flow breaker (Suwa et al. 2009)	29
Photo 2.2	Debris flow breaker stopping the front portion of a debris flow	30
Photo 2.3	Advantages of debris-flow breaker	31
Photo 2.4	Experimental flume	34
Photo 2.5	Experimental flume for generation of debris flow	35
Photo 2.6	Installation of debris-flow breaker	35
Photo 2.7	Measurement of sediment concentration and total discharge	39
Photo 2.8	Measurement techniques of deposition thickness on the debris-flow breaker	40
Photo 3.1	Image of flow profile over a bottom outlet slot (Lewis et al. 2011)	70
Photo 4.1	Debris flow disasters	119

Photo 4.2	Experiment setup for dam-break upstream of the proposed dam	127
Photo 4.3	Experimental flume for debris flow	128
Photo 4.4	Plans of sensor position	130
Photo 4.5	Dynamic pressure sensor and interface with four channels	133
Photo 4.6	Measuring system	134
Photo 4.7	Movement of debris flow due to main forces with bed sediment B (Flap-R dam)	149

List of Tables

Table 2.1	Properties of bed sediment material (size unit: cm)	36
Table 2.2	Mixing ratio of bed sediment material	37
Table 2.3	Properties of bed sediment material	38
Table 2.4	Results of diffusion debris (unit: cm)	44
Table 2.5	Results of experiments regarding the maximum travel length (unit: cm)	62
Table 3.1	Parameters for numerical simulation	87
Table 3.2	Comparison of travel length by previous and suggested γ coefficients (unit: cm)	102
Table 3.3	Results of average travel length from the experimental results (unit: cm)	103
Table 3.4	Experimental and simulation results of the maximum travel length (unit: cm)	110
Table 3.5	Comparison of reductions in travel length between maximum and minimum	111
Table 4.1	Experimental conditions for horizontal pressure	132
Table 4.2	Experimental conditions for vertical pressure	132
Table 4.3	Mixing ratio of bed sediment material	133
Table 4.4	Properties of bed sediment material	133
Table 4.5	Specification of the sensor	134
Table 4.6	Results of surface velocity in both flows	136
Table 4.7	Results of the mass ratio of debris with D_{50} – Sediment A	145
Table 4.8	Results of the mass ratio of debris with D_{50} – Sediment B	145
Table 4.9	Results of total pressure without outlier data (unit: kPa)	147

Table 4.10 Results of the total pressure and surface velocity 151

Table 4.11 Results of the impact force with three theory (unit: N) 153

Table 4.12 Comparison of empirical coefficients 154

IMFORMATION OF AUTHOR

PERSONAL DATA

Name	: Yeonjoong KIM
Sex	: Male
Date of Birth	: January 09, 1980
Nationality	: Republic of Korea
Languages	: Korean, Japanese, and English
Home Address	: 196-13 Saman-ro, Gimhae-si, Gyeongsangnam-Do, 621-909, Republic of Korea
Mailing Address	: (Gimhae Campus) 197 Inje-ro, Gimhae-si, Gyeongsangnam-Do, 621-749, Korea E-003, Coastal Eng. Lab.
E-mail	: kimanyseason@gmail.com
Telephone Number	: +82-55-326-5768

SPECIALISM

Major	: Civil and Earth Resources Engineering
Concentration	: Sediment-related Disaster
Area of study	: Debris flow, Numerical Modeling, Experiment, Sabo structures

EDUCATION

B.S	: Dept. of Civil-Engineering., Inje Univ., Korea, 2007
M.S.	: Dept. of Civil-Engineering., Inje Univ., Korea, 2009
Ph.D.	: Dept. of Civil and Earth Resources Engineering., Kyoto Univ., Japan, 2013

REFEREED JOURNAL ARTICLES

International Journal:

[1] KIM, Y., Nakawawa, H., Kawaike, K., and Zhang, H. (2013): Performance study of sabo dam with a flap structure in the case of debris flow. *International Journal of Sediment Research*. (In submitted)

Peer-reviewed Papers:

[1] KIM, Y., Nakagawa, H., Kawaike, K., and Zhang, H. (2013): Study on the function of a closed-type sabo dam with a flap for debris flow. *The 12th International Symposium on River Sedimentation.* (In printing)

[2] KIM, Y., Nakagawa, H., Kawaike, K., and Zhang, H. (2012): Numerical analysis of debris flow deposition on breaker structure. *Annual Journal of Hydraulic Engineering, JSCE,* Vol.68, No. 4, pp.I_1-I_6.

[3] KIM, Y., Kim M., and Yoon J. (2010): Study of formation and development of oxygen deficient water mass, using ecosystem model in Jinhae · Masan bay. *J. Ocean Eng. And Tech., KSOE,* Vol.24, No. 6, pp41-50. (In Korean with English Abstract)

[4] KIM, Y. and Yoon J. (2009): A study on the behavior of floating debris and fresh water diffusion according to discharge of Namgang dam. *J. Ocean Eng. And Tech., KSOE, Vol.23,* No. 2, pp37-46. (In Korean with English Abstract)

Papers:

[1] KIM, Y., Nakagawa, H., Kawaike, K., and Zhang, H. (2013): Study on impact force of debris flow due to variable of check dam shape. *Journal of Disaster Research.* Vol.8, No.1, pp.195-196.

[2] KIM, Y., Nakagawa, H., Kawaike, K., and Zhang, H. (2013): Study on characteristic analysis of closed-type sabo dam with a flap due to dynamic force of debris flow. *Annuals of Disas. Prev. Res. Inst., Kyoto Univ*., No. 56 B. (In printing)

[3] KIM, Y., Nakagawa, H., Kawaike, K. and Zhang, H. (2012): Numerical and experimental study on debris flow breaker. *Annuals of Disas. Prev. Res. Inst., Kyoto Univ.,* No. 55 B, pp.471-481.

[4] KIM, Y., Nakagawa, H., Kawaike, K., and Zhang, H. (2012): An experimental study on impact force for verification of 3D debris flow model. *31st Japan Society for Natural Disaster Science* annual meeting, pp.159-160.

[5] KIM, Y., Cho S., and Yoon J. (2007): A study on the influence caused by coastal region waste in water quality environment according to discharge of Namgang dam. *Korea Society of Civil Eng. Conf., and Civil Expo, KSCE*, pp. 598-601.

International Conference

[1] KIM, Y., Nakagawa, H., Kawaike, K., and Zhang, H. (2013): Study on the function of a closed-type sabo dam with a flap for debris flow. *The 12th International Symposium on River Sedimentation,* (Finish peer-reviewed and Oral)

[2] KIM, Y., Nakagawa, H., Kawaike, K., and Zhang, H. (2012): Study on impact force of debris flow due to variable of check dam shape. *International Symposium on Sustainability/Survivability Science for a Resilient Society Adaptable to Extreme Weather Conditions, Kyoto University,* Oct. (Poster)

Conference

[1] KIM, Y., Nakagawa, H., Kawaike, K., and Zhang, H. (2013): *S*tudy on characteristic analysis of closed-type sabo dam with a flap due to dynamic force of debris flow. *Annuals of Disas. Prev. Res. Inst., Kyoto Univ*., B-16, Feb. (Oral)

[2] KIM, Y., Nakagawa, H., Kawaike, K., and Zhang, H.: An experimental study on impact force for verification of 3D debris flow model. *Japan Society for Natural Disaster Science* annual meeting, Sep. (Oral)

[3] KIM, Y., Nakagawa, H., Kawaike, K., and Zhang, H.: Numerical and experimental study on debris flow breaker, *Annuals of Disas. Prev. Res. Inst., Kyoto Univ*., C-17, Feb. (Oral)

[4] KIM, Y., Cho S., and Yoon J. (2007): A study on the influence caused by coastal region waste in water quality environment according to discharge of Namgang dam. *Korea Society of Civil Eng. Conf., and Civil Expo, KSCE,* Oct. (Oral)